GAMMA-RAY BURST HOST GALAXIES AT HIGH RESOLUTION

CHRISTINA CARINA THÖNE

Dissertation
Submitted for the Degree

PHILOSOPHIÆ DOCTOR

Dark Cosmology Centre
Niels Bohr Institut
Det Naturvidenskabelige Fakultet
Københavns Universitet

Submission: *July 4th, 2008*
Defence: *October 3rd, 2008*

Supervisor: *Assoc. Prof. Johan P. U. Fynbo*
Opponents: *Prof. Max Pettini*
Dr. Chryssa Kouveliotou

Cover art:

Going observing brings you not only scientific images, sometimes, there is also time to do pretty pictures, either with the telescope itself or with your own camera. This cover joins both. The panorama at the bottom was taken in a very cold full moon night in August 2008 on La Silla after a thunderstorm and fresh snow in the Cordillera Central. The pictures were taken in raw format and dark- and bias-subtracted before joining them to a panorama. Thanks to Antonio for making this nice panorama from the raw files taken with my small, but apparently not so crappy Olympus. The telescope at the right side of the back cover shows UT1 of the VLT telescopes, taken a few days before under nearly full moon, this time with Antonios camera and a tripod. The dome to the left belongs to one of the two Keck telescopes on Mauna Kea.

The main image of the cover is a mosaic of the nebula around η Carinae, a massive luminous blue variable but likely never becoming a GRB, created by its violent outbursts and mass losses over the last 100 years with the star itself hiding behind the dark dust clouds. The mosaic consists of 8 panels taken in V, R and I filters with the Danish 1.54m telescope in February 2006. Thanks to Robert Gendler for processing and merging the images. The little "cosmic explosion" in the upper left of the back cover is a picture of our own sun taken during the solar eclipse 2006 which I watched from a hotel near Antalya/Turkey during a GRB workshop. It marks the end of the eclipse when the sun is shining through the valleys at the edge of the moon creating the diamond ring effect. It is also a symbol for the background picture I had on my mobile phone used for GRB triggering over the last years which showed a picture of the moon with some artistic rays around but which I could not get in high resolution. The cover was put together in Photoshop, thanks to Ana Lucía for helping with various problems in Photoshop.

The titlepage of Part I of the thesis is a color composite of the starburst galaxy M82 taken with ALFOSC at the NOT in B, V and Hα filters and symbolizes the absorption lines likely caused by starburst winds from GRB hosts that we detected in the spectra of GRB 030329 and GRB 060206. Thanks to Johan for making the color image. The title of Part II shows a part of the η Carinae mosaic and a color composite of a galaxy whose name I forgot. It was taken at the Brorfelde observatory west of Copenhagen when Chloé and I were training for going observing the first time back in October 2005. The two pictures are a symbol for the resolved host galaxies of GRB 060505 and SN 2008D and for the fact that we were interested in the progenitors of GRBs/SNe in that part of the thesis.

CONTENTS

ACRONYMS

AOD	Apparent Optical Depth
BAT	Burst Alert Telescope (on *Swift*)
CoG	Curve of Growth
DLA	Damped Lyman Alpha system
DSS	Digital Sky Survey
EW	Equivalent Width
FOV	Field of View
GAIA	Graphical Astronomy and Image Analysis (reduction and analysis software)
GCN	Gamma-ray Burst Coordinates Network
GRB	Gamma-ray Burst
HIRES	High-resolution Echelle Spectrograph (at Keck)
HST	Hubble Space Telescope
IDL	Interactive Data Language (programming language)
IPN	Interplanetary Network
IRAF	Image Reduction and Analysis Facility (reduction and analysis software)
LBG	Lyman Break Galaxy
LBV	Luminous Blue Variable (e.g. η Carinae)
LLS	Lyman Limit System
MIDAS	Munich Image Data Analysis System (reduction and analysis software)
OT	Optical Transient
QSO	Quasi-stellar Object
RRM	Rapid Response Mode (even faster than ToO)
SED	Spectral Energy Distribution
SFR	Star formation rate
SSFR	Specific star formation rate
SN	Supernova
SNR	Supernova rate
ToO	Target-of-Opportunity (proposal type/fast observation mode)
UVES	Ultraviolet and Visual Echelle Spectrograph (at the VLT)
UVOT	Ultraviolet and Optical Telescope (on *Swift*)
VLA	Very Large Array (New Mexico)
VLT	Very Large Telescope (Paranal/Chile)
WHT	William Herschel Telescope (La Palma)
WR	Wolf-Rayet (star)
XRF	X-ray flash (a "weak" GRB)
XRT	X-ray telescope (on *Swift*)

LIST OF FIGURES

LIST OF TABLES

ACKNOWLEDGMENTS

Three years - or, two years, nine months and one day to be precise - are a long time and again they are not. Time did fly very fast, but so much happened in these three years that it is hard to judge in the end if the time felt long or short. I think, it did both. The reason why I came to Denmark is Norway, though this might sound funny. When I spent a year in Norway back in 2002/2003, I fell in love with Scandinavia and thought Denmark might be a good substitute, until I realized that Denmark is not Norway, but another universe. Still I managed somehow to come through the three years and life was not always bad. If the future is more promising than the current situation, I doubt it, but I would be happy if I'm wrong. After all, I come out from these three years as a different person than I was before, even though in a different way than I thought. In the end, it was worth it. Since I was a child I wanted to become a scientist and an astronomer and I could have never imagined myself being anything else. And so it happend.

These years, I fortunately did not have to spend alone and the list of people to whom I have to be grateful is long. First of all, I should thank my supervisor Johan who has definitely not been anything like the typical picture of a PhD supervisor. You left me the freedom I needed and wanted to pursue my own research and to work on the things I found interesting. If I was stuck and you could help, you were always eager to do so and I never felt I was your "working slave" (occasionally, it might have actually been the other way round). I think you did not see me as your student but more like a fellow researcher which I truly appreciated. You also supported me going observing and traveling to conferences and let it always up to me to work when and how and how much I wanted even though that meant we had only a small overlap between our working hours. And you are definitely the master of the shortest emails (and sms) in the world! Thank you for everything!

When I came to Denmark, I thought now I would have the chance to travel in Scandinavia more often, but instead, I started to see the world. Chile, Peru, Australia, the US, Easter Island, Hawaii, La Palma, Turkey, back and forth in Europe, I am sometimes thinking I might have been the PhD student who travelled the most ever. I have not counted the distance, but it adds up to 106 takeoffs and landings (yes, I did count that), fortunately, I'm not too concerned about climate change. I also got the chance to go observing at the Danish 1.54 on La Silla and to the NOT on La Palma and La Silla became my favorite place on this planet after Norway. These experiences and different views about the world and science in the last three years I owe to DARK and the almost unlimited travel funding plus the attitude that working means not necessarily sitting in the office.

All this traveling might seem a bit like an escape and it sometimes was indeed. Still, DARK is a special place and a group that really feels like a group. I am truly impressed by how Jens built up this center out of almost nothing within a very short time and how he wants to make this a nice working place for everyone. Here, I also want to thank Josh Bloom and the Berkeley

crowd, Enrico Ramirez-Ruiz and Xavier Prochaska for inviting me over to California to work there for one summer and allowing me to play around with the largest telescope in the world. It was an interesting experience and it showed me, that even “elite” universities only cook with water. Not that this means they are not doing excellent work, but Europe does not have to hide behind them. I also thank the organisers of various conferences, workshops and summer schools that I was able to attend and that always gave me a lot of inspiration, opened new collaborations and were the start of some of my most precious friendships. At last, I want to thank the telescope staff helping with the frequent ToO observations and all the observers who were willing to give some of their precious time to “those annoying GRB people”, without you, this thesis would not have been possible.

Career, traveling and the money, however, is not everything, life would be very lonely without the people I could share all this. The work done in this thesis would not have been possible without the scientific and personal support by all my colleagues, collaborators and observing mates and many of them became my friends. Most of them are distributed all over the world and that is why I first have to thank the inventors of skype, iChat, msn messenger, email and the internet itself, which allows us to stay in contact even if we probably only meet once a year. One that I have to mention here in particular is Alex Kann, not only a good collaborator, but a true friend. I think, our skype history must fill an entire server and a diary would not be a better record of my life than this.

I’m also thankful to all my colleagues here at DARK for help, support and a lot of fun at and outside work: Daniele, with whom I started a similar skype excess until he came to DARK and talking in person is better anyway, José María (I hope I got the accents right), my first officemate and still my friend, Christa, the long awaited other German speaking girl (well, mother of two kids....), Paul (Pablito), the Dutch sailor who did not make it to cross the Atlantic with his boat (yet), Chloé, my French trainer, observing mate and travel companion in Peru, Danka, always up for a party, Árdís, who is as well but just hides it better, Giorgos, who thinks football and candles don’t go together and Michał, a true collaborator on the last rushed paper. I’m also indebted to Brian for managing our computers, fixing stupid problems of even more stupid users and for the advice that saved me a year of work: "You should make a backup before you leave the mountain!" (that was while I was observing on La Silla, one week before my harddrive decided to become a chaos of 1s and 0s).

Except my colleagues at DARK, there is this growing crowd out there in the world that I only get the chance to meet occasionally but many of them became more than just scientific collaborators if not even very good friends. A few I want to mention in particular are Gabe in Los Alamos, the best travelmate for the Southwest, a frequent iChat chatter and an American of the kind that lets me hope life in Boston will not be too bad. Antonio, who I had in principle known for years but since a few months became one of my closest friends, Klaas, another close collaborator, observing mate and the best gossip source in the GRB world, Jouni, the not so strange Finnish, Lise, who I possibly owe my VIMOS proposals and who I might finally meet this summer, Javier, one of the few astronomers who can dance, Annalisa, Palli, Jesper, Jan-Erik, Andreas, Cédric, Göran, Rhaana, Massimo, Stefano and all those who have helped me with various problems at various times and/or just had a lot of fun with, I’m sure I forgot someone but it is not on purpose. And finally, I want to thank all my non astronomy friends back home in Germany, my sorority in Munich where I was always very welcome, Klaus, Toni and my Norwegian friends Gunn Marit and Tone Luise.

Above all, I want to thank Patrick for sharing now already nearly eight years of good and bad days and for endless support every day. I could and I would not want to imagine life without you. And last, I want to thank my mom back home in Bavaria, who 28 years ago would probably never have thought I would get a PhD one day, but who supported me every day in my life and my career. Thank you also for taking care of our cats and for giving me a place in this world I can call home.
Thank you all!

Christina Thöne
Copenhagen
July 4th 2008
Independence Day

In contrast to the date chosen for the defence (the German National Day), the day for the submission of this thesis was not chosen because of a special devotion to the US (quite the contrary), but in a more figurative sense.

Addendum: After handing in the thesis, I could start to follow my passion for travelling again and so I did, even though this meant missing another Danish summer. After a very nice, but cold week on the Færøer, I spent one very nice month in Chile at ESO. For this, I want to thank Antonio, Lise and Diego for hosting me in Santiago and for taking care of me as a visitor as it could not have been nicer. I think we all enjoyed being together and have fun. I also want to thank ESO for hosting me, paying part of the stay and for allowing me (and financing) a visit to Paranal in order to finally see the telescopes and instruments I was getting most of the data for this thesis from. And finally, I had two very funny weeks on La Silla (the 5th time!) thanks to Uffe sending me as an observing "teacher", to the people from the Swiss telescope, Didier, Francesco and Michel, their cheese fondue and fully equipped kitchen and Gaspare, the support astronomer with endless funny stories to tell. But, watch out for heaters in the parking lot!!

Life is not too short to be wasted, life is too long to be wasted.
Nick Cox, PhD propositions

ABSTRACT

GRBs are the most powerful explosions in the universe and a very interesting phenomenon in themselves. Even though they are the brightest objects detected, they are nevertheless only stellar explosions or mergers of compact objects. Since their discovery in 1967, a lot of progress has been made in identifying them as high redshift events, investigating their high energy and afterglow properties, dividing them into subgroups of long and short duration GRBs with likely different origins and studying their host galaxies. As more and better sampled data become available, notably since the launch of the *Swift* satellite (Nov. 2004), explanations for what actually happens in the explosion start to be more complicated and more questions are raised than answered.

The following thesis does not deal with the GRB phenomenon itself but it is studying their environment and host galaxies through optical spectroscopy and using them as lightsources in the distant universe. The work is divided in three parts.

The first Chapter gives in introduction to the **history** of the GRB discovery and research, explains the processes involved in producing a **GRB and its afterglow radiation** and the different **progenitor models** for GRBs. It also summarizes the properties of its **host galaxies** and the differences between **short and long GRB hosts**. Finally, an overview is given over the **fast follow-up observing** strategies for GRB afterglows, the special type of proposals needed, and some examples are mentionied in which the author of this thesis was involved in.

Part II presents three examples of using GRBs as **powerful lightsources that allow to study the high redshift universe with low and high resolution spectrosocpy**. An introduction to the methods of how to observe the high redshift universe is given, what information can be obtained from high resolution spectra and what they tell us about the environment and host galaxy of a GRB.

For the first case, **GRB 060526**, follow-up observations from a large range of telescopes were put together in order to study its afterglow properties. This luminous GRB also allowed us to obtain a dataset of low to medium resolution spectra with FORS 1 at the VLT. A range of UV restframe metal absorption lines are detected of which we determine the column densitiy with the CoG method and subsequently the metallicity.

The next Chapter presents **high resolution spectra of the afterglow of GRB 030329** that has both resolved absorption and emission lines, which was possible due to the low redshift of the GRB of z=0.1686. The absorption lines split up in different components with a range of 230 km/s blueshifted compared to the host. We argue that they likely originate from a starburst wind outflow as observed in some nearby starburst galaxies, e.g. M 82.

The last Chapter finally presents a large range of resonant and finestructure transitions detected in the **medium resolution spectra of z=4.048 GRB 060206**. Those also split up in different

components spanning a range of ~ 400 km/s by both the resonant and finestructure absorption lines where the latter trace the resonant lines. This has never been observed so far in a GRB afterglow spectrum. The ratio between finestructure and resonant transitions allow us to determine the properties in the different absorbing system and to get a rough estimate on their distance from the GRB. Finally, we reinvestigate the claim of variability in an intervening system at z=1.45 in another series of spectra of this GRB by Hao et al. (2007) with our and new data from the Subaru archive which disprove this claim.

Part III deals with the **low redshift universe** where we can study the host galaxies of GRBs in detail with **spatially resolved emission line spectroscopy**. Both events studied here, GRB 060505 and SN 2008D, caused some debate in the GRB community. GRB 060505 was the first presumably long GRB not connected to a SN and its nature is therefore highly controversial. Type Ib SN 2008D was connected to an X-ray flash which had never been observed so far for a SN. The introduction to this part therefore gives an overview over the GRB-SN connection, the SN nondetection and the properties of SN 2008D. Furthermore, the different techniques on how to study low redshift galaxies and HII regions with emission line diagnostics are explained and an example for a study using an integral field unit investigating the host of GRB 980425, the first SN-associated GRB, is given.

The first chapter then presents a rough long-slit **spatially resolved study of the host of GRB 060505** seen nearly face on. The slit covers the major axis of the galaxy and the GRB region and our study reveals that the properties of the HII region where the GRB took place is different from the rest of the galaxy, esp. in terms of metallicity and SFR. These results argue in favour of the theory that GRB 060505 came from the collapse of a massive star. We also investigate part of the galaxy with high resolution spectroscopy, fit a rotation curve and study the kinematics.

The second chapter does a similar study of the **host of SN 2008D, NGC 2770**, covering the SN site, the major axis and the site of two other Ib SNe in this galaxy with four longslit spectra. While the SFR at the SN Ib sites is not especially high, the metallicity lies inbetween the one of broadline Ic SNe and GRB connected Ic SNe. We further compare the properties of all galaxies with at least 3 SNe detected to those of NGC 2770. While some galaxies seem to favour a specific type of SN, also reflected in their global properties, this is not the case for NGC 2770. From this and statistical considerations we conclude that the occurence of three Ib SNe (and no other SN type) was likely just a coincidence.

With the observational progress made in the last years with faster follow-up and better datasets, GRBs have shown their capability as probes of the high redshift universe in great detail. Some fortunate low redshift GRBs allow us to have a closer look to their places of origin in order to get more insights in the progenitor properties and to compare it with progenitors e.g. SNe. The sample is still small and the generally high redhift prohibits such studies for a larger sample, but surprises and a very low redshift case might come every day.

SAMMENFATNING

Gammaglimt er de kraftigste explosioner i universet og et meget interessant fænomen i sig selv. Men selv om de er de mest lysstærke objekter i universet er de forbundet med forskellige typer af stellare eksplosioner eller sammenstød. Siden de blev opdaget i 1967 er der gjort store fremskridt og de er nu identifiseret som hændelser primært ved høje rødforskydninger. Vi har undersøgt deres egenskaper ved høj energi og deres efterglød ved lavere energier, vi har indelt dem i undergrupper af lange og korte gammaglimt som sandsynligvis har forskellig oprindelse og studeret deres værtsgalakser. Flere og bedre data er tilgængelige, især siden *Swift* satelliten blev opsendt (November 2004), forklaringen på, hvad der egentlig sker i disse eksplosioner er blevet mere og mere kompliseret og flere spørgsmål bliver stillet end besvaret.

Denne PhD afhandling beskæftiger sig ikke med selve gammaglimt-fænomenet, men studerer deres omgivelser og værtsgalakser gennem optisk spektroskopi og bruger dem som fyr- tårne i det fjerne univers. Opgaven er indelt i tre dele.

Den første del giver en indføring i **historien** om og udforskningen af gammaglimt. Det bliver forklaret, hvilke processer der er involvert i at producere en **GRB og dens efterglød** og de forskellige **forgængerobjekter for gammaglimt**. Den sammenfatter også egenskaberne af gammaglimtenes **værtsgalakser** og forskellen mellem værtsgalakser for **lange og korte gammaglimt**. Til slut gives en kort oversigt over observationsstrategier for **hurtig efterfølgning af gammaglimternes efterglød** og det bliver nævnt nogle eksempler på sådanne observationer, hvori forfatteren af denne afhandling selv var involveret.

Anden del af afhandlingen indeholder tre eksempler på brugen af **gammaglimt som fyrtårn** som tillader at **studere universet ved høje rødforskyninger med lav- og højopløsningsspektroskopi**. F o rst gives en indføring i metoderne med hvilke man studerer det fjerne univers, hvilken information vi kan uddrage fra højopløsningsspektrokopi af gammaglimt eftergløder og hvad de fortæller os om gammaglimtets omgivelser og værtsgalakse.

For det første eksempel som blir præsenteret her, **GRB 060526**, blev efterglødsobservationer fra mange teleskoper fordelt over hele kloden analyseret for at studere efterglødens egenskaber. Vi fik også indsamlet et datasæt bestående af lavopløsningsspektre af eftergløden med instrumentet FORS1 på VLT, i hvilket vi måler en række absorptionslinjer rødforskudt fra UV området til optiske bølgelængder (rødforskydning z=3.221). Udfra disse målinger bestemmer vi søjletætheden af disse elementer og dermed metalliciteten af værtsgalaksen.

Det næste afsnit præsenterer **højopløsningsspektrer af eftergløden af GRB 030329** som har både absorptions- og emissionslinjer detekteret, hvilket er muligt på grund af glimtets lave rødforskydning (z=0.1686). Absoptionslinjerne er splittet op i forskellige hastighedskomponenter som strækker sig ud over 230 km/s of som er blåforskudt i forhold til værtsgalaksens systemiske rødforskydning. Vi konkluderer at de mest sandsynlig bliver dannet i en starburst vind som vi

kender eksempler på fra nære galakser, for eksempel M 82.

Det sidste afsnit præsenterer en lang række af resonante og finstruktur absorptionslinjer detektert i **mediumopløsningsspektrer af GRB 060206** ved z=4.048. Disse linjer splitter sig også op i forskællige komponenter som fordeler sig over 400 km/s i både resonante- og finstrukturlinjer. Finstrukturlinjerne er ved samme hastigheder som de resonante overgange, hvilket ikke tidligere er observert i gammaglimt. Forholdet mellem finstruktur og de resonante overgange fortæller os noget om egenskaberne i det interstellare medium i de forskællige hastighedskomponenter. Ud fra dem kan vi også anslå deres afstand til selve gammaglimtet. Til slut tilføjes en nye analyse af et system i foregrunden ved z=1.45, for hvilket ændringer i absorptionsstyrken over tiden er blevet hævdet. Dette kan vi ikke bekræfte ud fra vores data og data fra Subarutelekopets arkiv.

Tredje del beskæftiger sig med **universet ved lav rødforskydning**, hvor vi kan studere gammaglimtenes værtsgalakser i detalje med **rumlig opløst spektroskopi**. Begge begivenheder studeret her, GRB 060505 og SN 2008D, var ophav til nogen debat i gammaglimtsforskningskredse. Den første var det første nære, lange gammaglimt som ikke havde en associeret supernova og dens ophav er derfor stærkt omstridt. SN 2008D var af type Ib og blev detekteret ved et røntgenudbrud som sansynligvis markerede starten på selve eksplosionen - noget som aldrig var blevet observert før for en supernova. Indføringen til denne del af afhandlingen giver et overblik over forbindelsen mellem lange gammaglimt og supernovae, gammaglimt som ikke havde nogen associeret supernova samt egenskaberne af SN 2008D. Det bliver også givet en forklaring på de forskellige metoder til at studere det nære univers og HII områder med emissionslinjer. Til slut er det det første eksempel på en værtsgalakse som er blevet studert med 2D spektroskopi ved at bruge en såkaldt "integral field unit". Det er værtsgalaksen for GRB 980425, det første gammaglimt som blev forbundet med en supernova explosion.

Det næste afsnit præsenterer et groft **rumlig opløst studie af værtsgalaksen for GRB 060505** ved brug af longslit-spektroskopi af galaksen som vi ses nær vinkelret på synslinjen (eng. face-on). Slitten går gennem den store halvakse og stedet hvor gammaglimtet eksploderede. Vores undersøgelse viser, at stedet hvor gammglimtet fandt sted er forskellig fra resten af galaksen især hvis man ser på metalliciteten og stjernedannelsesintensiteten. De to sidste afsnit i dette kapitel præsenterer et rumlig opløst højopløsningsspektrum af værtsgalaksen som vi bruger til at fitte en rotationskurve og hvor vi undersøger kinematikken i selve galaksen og hvor vi også undersøger værtsgalaksens omgivelser. Vi argumenterer for, at GRB 060505 faktisk var et gammglimt som kom fra kollapset af en tunge stjerne. Hvorfor vi ikke observerede en supernova er stadigvæk uklart, men det findes teorier, der forudsiger sådanne begivenheder.

Det sidste kapitel indeholder en lignende **rumlig opløst undersøgelse af værtsgalaksen for SN 2008D, NGC 2770**. Vi undersøger omgivelsen af SN 2008D og to andre Ib supernovae, SN 1999eh og SN 2007uy, i samme galakse med fire longslit spektre. Mens stjernedannelsesintensiteten ved de tre supernovalokaliteter ikke er særlig høj ligger metalliciteten mellem den for broadline Ic supernovae og den for broadline Ic supernovae som er forbundet med gammaglimt. Vi sammenligner egenskaberne af NGC 2770 med andre galakser som har haft mindst tre supernovae detekteret. Mens nogle galakser synes at give ophav til en speciel type supernova hvilket som oftest reflekteres i dens egenskaber er NGC 2770 ikke nogen speciel galakse. Ud fra dette og nogle statistiske betragtninger konkluderer vi, at det sandsynligvis bare var et tilfælde, at man har fundet tre SN Ib (og ikke nogen anden type) i denne galakse på ti år.

Fremskridtet i observationerne i de seneste år, observationer med kortere forsinkelse i forhold til glimtene og bedre data har vist, at gammaglimt kan bruges til at studere universet ved høj rødforskydning i stor detalje. Nogle gammaglimt ved lav rødforskydning muliggør, at vi kan få en mere detaljeret indsigt i naturen af omgivelserne, hvor gammaglimt finder sted og så til at finde ud hvilke objekter, der giver ophav til gammaglimt. Hidtil har der ikke været mange gammaglimt ved lav rødforskydning, men en ny overraskelse ved lav rødforskydning kan komme hver dag det skal være.

ZUSAMMENFASSUNG

Gamma-ray bursts (GRBs) sind die gewaltigsten Explosionen im Universum und für sich alleine bereits ein interessantes Phänomen. Obwohl sie die hellsten beobachteten Objekte sind, stammen sie dennoch nur von der Explosion eines Sterns oder dem Zusammenstoß zweier kompakter Objekte. Seit ihrer Entdeckung im Jahre 1967 hat ihre Erforschung große Fortschritte gemacht. GRBs sind Ereignisse im fernen Universum bei teilweise sehr hoher Rotverschiebung, ihr Verhalten im Hochenergiebereich wurde ausführlich untersucht und ihr Nachglühen bei höheren Wellenlängen studiert. Ferner gelangte man zur Schlußfolgerung, daß sie in zwei Gruppen eingeteilt werden können je nach der Dauer ihrer γ Emission. Zu guter letzt wurden auch die Hostgalaxien der GRBs näher unter die Lupe genommen. Je mehr und je bessere Daten verfügbar sind, insbesondere seit der designierte GRB-Satellit *Swift* gestartet ist, desto komplizierter werden die Erklärungen und Theorien was sich eigentlich bei einer solchen Explosion abspielt. Wie überall in der Wissenschaft werden immer mehr Fragen aufgeworfen als beantwortet.

Die folgende Dissertation beschäftigt sich nicht mit GRBs als solches sondern studiert ihre unmittelbare Umgebung und ihre Hostgalaxien mit optischer Spektroskopie, insbesondere hochaufgelöster optischer Spektroskopie.
Das erste Kapitel beinhaltet eine Einleitung zur Geschichte und grundlegenden Ergebnisse der GRB Forschung. Es werden die Prozesse erläutert, die in einem GRB ablaufen und welche den Afterglow produzieren, sowie die verschiedenen Modelle und Vorläufersterne für lange und kurze GRBs vorgestellt. Danach folgt eine Zusammenfassung über die verschiedenen Eigenschaften der Hostgalaxien von langen und kurzen Bursts. Zuletzt werden die verschiedenen Strategien erläutert, um den Afterglow so schnell wie möglich zu beobachten, sowie einige Beispiele für erfolgreiche Beobachtungskampagnen vorgestellt, an denen die Autorin dieser Arbeit selbst beteiligt war.

Teil II präsentiert drei Beispiele, in denen **GRBs als helle Lichtquellen zum Studium des hochrot- verschobenen Universums** verwendet werden. Die Einleitung zu Teil II beschreibt verschiedene Methoden, die dazu dienen können das ferne Universum zu beobachten, ferner, welche besonderen Informationen von hochaufgelösten Spektren gewonnen werden können und was sie uns über die Umgebung und die Hostgalaxien von GRBs erzählen.

Im ersten Fall, **GRB 060526**, wurden Beobachtungen des Afterglows von einer großen Zahl von Teleskopen, die über die ganze Welt verteilt sind, zusammengetragen, um die Eigenschaften des Afterglows zu studieren. Unsere Gruppe erhielt ausserdem Spektren dieses GRBs vom FORS1 Instrument am VLT mit niedriger Auflösung. Diese beinhalten eine Reihe von metallischen Absorptionslinien, die sich normalerweise im ultravioletten Wellelängenbereich befinden, die jedoch bei einer Rotverschiebung von z=3.221 in den optischen Bereich verschoben sind.

Von diesen bestimmen wir die Säulendichten und daraus die Metallizität des interstellaren Mediums in der Hostgalaxies.

Das nächste Kapitel präsentiert **hochaufgelöste Spektren des Afterglows von GRB 030329**, der nur eine Rotverschiebung von z=0.1686 hatte. Dies erlaubte die Detektion von sowohl Absorptions- als auch Emissionslinien von der Hostgalaxie, die dem Afterglowspektrum überlagert waren. Die Absorptionslinien spalten sich auf in verschiedene Geschwindigkeitskomponenten über eine Spanne von 230 km/s, die blauverschoben sind gegenüber den Emissionslinien der Hostgalaxie. Diese Komponenten stammen wahrscheinlich von einem galaktischen Superwind, der einen Materiefluß aus Sternentstehungsgebieten in der Galaxie verursacht. Solche Superwinde wurden in nahen Galaxien beobachtet mit dem berühmtesten Beispiel M82.

Das letzte Kapitel dieses Teils präsentiert ein weiteres **hochaufgelöstes Spektrum mit mehreren Geschwindigkeitskomponenten** in den Absorptionslinien, die sich über insgesamt 400 km/s verteilen. Die hohe Rotveschiebung von z=4.048 ermöglichte es eine Reihe von resonanten Übergängen zu messen, aber auch Feinstrukturlinien von manchen dieser resonanten Absorptionslinien. Überraschenderweise weisen sowohl resonante als auch Feinstrukturlinien dieselben Geschwindigkeitskomponenten auf, was noch nie zuvor in GRB Afterglowspektren beobachtet worden war. Das Verhältnis von Feinstruktur- zu resonanter Säulendichte erlaubt Informationen über den Zustand der interstellaren Materie in der Hostgalaxie und eine grobe Abschätzung der Entfernung des absorbierenden Materials vom GRB. Zuletzt untersuchen wir noch die von einer anderen Gruppe aufgestellte Behauptung, die Stärke eines Absorptionssytem bei geringerer Rotveschiebung in der Sichtlinie dieses GRBs hätte sich mit der Zeit verändert. Unsere Daten zusammen mit Daten aus dem Archiv des Subaru Teleskops widerlegen diese Behauptung.

Teil III beschäftigt sich dagegen mit dem relativ **nahen Universum** wo wir mit viel Glück die Hostgalaxien mit räumlich aufgelöster Spektroskopie detaillierter untersuchen können. Dies wiederum erlaubt Hinweise auf das Vorläuferobjekt eines GRBs. Die beiden Ereignisse, die hier vorgestellt werden, GRB 060505 und SN 2008D, erweckten einiges Aufsehen in der GRB Welt. GRB 060505 war der erste lange GRB, der offenbar von keiner Supernova begleitet wurde und dessen Ursprung deshalb heftig debattiert wurde. Die Typ Ib Supernova 2008D hingegen wurde von einem Röntgenflash begleitet, was zwar Theorien vorhergesagt hatten, aber bisher nie beobachtet worden war und manche meinten sogar, diese Röntgenstrahlung käme von einer Art schwachem GRB. Die Einleitung zum dritten Teil gibt einen kurzen Überblick über die Verbindung von GRBs und SNe, die fehlende Detektion einer Supernova für zwei GRBs bei niedriger Rotverschiebung und die Eigenschaften von SN 2008D. Weiterhin werden die verschiedenen Methoden präsentiert, mit denen aus Emissionslinien Eigenschaften des interstellaren Mediums abgeleitet werden können, z. B. Metallzität, Sternentstehungsrate, Extinktion und Alter der Sternenpopulation. Zuletzt wird eine erste Studie eines nahen GRB hosts, GRB 980425, mit einer "Integral Field Unit" vorgestellt, die es erlaubt, zweidimensionale Spektren der Hostgalaxie zu erhalten.

Das erste Kapitel dieses Teils präsentiert einen ersten Versuch die **räumlich aufgelösten Eigenschaften der Hostgalaxie von GRB 060505** mit Longslit-Spektroskopie zu studieren. Der Slit wurde über der Halbachse der Galaxie platziert und schließt die Stelle, an der der GRB stattfand, mit ein. Es stellt sich heraus, dass das Sternentstehungsgebiet um den GRB deutlich andere Eigenschaften aufweist als der Rest der Galaxie, insbesondere eine niedrigere Metallizität und eine höhere Sternentstehungsrate. Dies führt uns zu dem Schluß daß GRB 060505 wohl den Kollaps eines massiven Sterns ankündigte. Warum keine Supernova detektiert wurde, ist

weiterhin unbekannt. Hochaufgelöste räumliche Spektren eines Teils dieser Galaxie erlauben uns auch die Rotationskurve und andere kinematische Eigenschaften der Hostgalaxie zu bestimmen.

Das zweite Kapitel dieses Teils wendet dieselbe Methode mit Longslit-Spektroskopie auf den **Host von SN 2008D** an, NGC 2770, der mit 4 verschiedenen Slitpositionen untersucht wurde. Die Slits beinhalten auch die Umgebung von SN 2008D sowie zwei weiteren Ib SNe, SN 1999eh und SN 2007uy in derselben Galaxie. Die Sternentstehungsrate an allen Supernovaumgebungen ist überraschenderweise relativ niedrig, wohingegen die Metalliztät zwischen der von broadline Ic Supernovae, die zusätzlich einen GRB produziert hatten, und broadline Ic Supernovae ohne GRB liegen. Dies entspräche den Sternmodellen wonach hohe Metallizität zu höherem Massenverlust und damit zu Ic statt Ib Supernovae führen. Modelle für die Erzeugung eines GRBs fordern hingegen einen hohen Drehimplus, der nur bei niedriger Metallizität aufrechterhalten werden kann. Danach vergleichen wir die globalen Eigenschaften von NGC 2770 mit denen anderer Galaxien, die mindestens drei Supernovae detektiert hatten, und stellen fest daß NGC 2770 keine besonders prädestinierte Galaxie ist um besonders viele Ib Supernovae zu produzieren. Aus diesen Überlegungen heraus und einigen statistischen Untersuchungen über die Wahrscheinlichkeit eine Galaxie mit drei Ib Supernovae zu entdecken schließen wir, daß die hohe Rate von beobachteten Ib Supernovae wohl eher dem Zufall zuzuschreiben ist.

Der Fortschritt in den letzten Jahren mit schnelleren Nachbeobachtungen und besseren Datensätzen haben gezeigt, daß GRBs ein geeignetes Mittel sind um das frühe Universum zu beobachten. Ein paar wenige glückliche Zufälle von GRBs bei niedriger Rotverschiebung erlauben es uns einen genaueren Blick auf deren Hostgalaxien und die direkte Umgebung des GRBs zu werfen um diese beispielsweise mit den Sternpopulationen aus denen Supernovae entstehen zu vergleichen. Bisher sind es noch recht wenige GRBs, die nahe genug waren solche Studien zu ermöglichen, aber die nächste Überraschung kann schon morgen passieren.

To Alice, Rosalita and Luisa
who were the joy of my life
but had to leave this world way too early

The breath of Armageddon

Nature is cruel.

A star glitters in the full glory of its life. A clear, shining beacon of light and warmth. Then suddenly, it is over. Its time has run out. The star is in its death throes. Armageddon is a Valhalla compared with what happens here. In a fraction of a second the star collapses in on itself. Trillions of tons of hot gas disappear forever through the one-way door of a black hole. Space becomes distorted, time ceases to have meaning, and matter is thrown into a frenzy. The star devours itself from the inside out. In a last agonizing scream the disappearing nucleus of the star spews out two jets of boiling, roiling matter as a desperate lifeline to the trusting world out of which it has been thrust.

With a speed of a billion kilometers an hour the two jets make their way to the outside. They bore burning tunnels through the outer layers of the star, which has no idea of the drama that has come to pass in its dark depths. But the star cannot continue to exist in the face of this cosmic violence. It explodes, spitting out an incredible quantity of energy that comes free from its inside. The destruction is complete. The heavens rip open. A scorching, ball-shaped curtain of searing, glowing energy and expelled matter rushes with the speed of light to the outside. What remains is a barren, abandoned battlefield, a desolate cosmic landscape of a dark void.

The cosmos does not trouble itself with the death of one star. Birth and death are the order of the day in the universe. The cosmos is still young and restless, everything is in a uproar. The Milky Way is just beginning to assume its form, not yet a trance of the sun and the earth. The present is still in the future. Billions of years during which countless stars will live and die, where matter is continually shaped and reshaped by the fundamental forces of nature, and where there will come life, intelligence, consciousness and a wonderful curiosity that will be capable of observing the very cosmos itself.

And even though the catastrophic death of the star quickly becomes history, its history is engraved in the legend of the universe far in the future. Within those few seconds that it took for the star to disappear from the stage, a gigantic rush of gamma radiation was blown into space, spread with the speed of light through the universe. Although the star is long forgotten, the announcement of its death is delivered to every corner of the cosmos and the message of the disaster is carried far into the future.

On its trip to the ends of the universe the photons pass by untold numbers of galaxies and in between there is a measureless void, the deep black sea in the cosmic ocean separating those little islands of light. When the storming wave front has traversed half the distance to our Milky Way, our sun gets born on the outer rim of one of the spiral arms. While the sun forms out of a rotating cloud of gas and matter, small cold cinders remain that circle the sun as cooled globes of gas or dark stony clumps, caught forever in the grip of gravity. On one of these cinders there are oceans of liquid water and drops of organic molecules that came down out of interplanetary space. As the cosmic message comes relentlessly closer the first multi-cellular organisms are in the oceans of the earth. By the time the photons reach the Local Supercluster, the reign of voracious dinosaurs holds say upon the earth. When in the far distance, our Milky Way becomes visible as a hazy smudge of light against the black starry sky, the earth's savannas are peopled with the first predecessors of humans.

People begin for the first time to look in wonderment at the night sky and the stars above their heads. Green philosophers deliberate over the god-like perfection of the cosmos and a Polish canon contends that the earth is not the center of the universe. Now things really start moving. Galileo Galilei, Isaac Newton, the industrial revolution, the detection of the expanding universe, the first timorous steps on the way to space travel. As the gamma rays leave the bright star Cappella behind, the first scientific satellites are launched and astronomers begin to study the cosmos through the use of invisible wavelengths. The speeding gamma ray flash rooms past Alpha Centauri, the ten billion year trip is almost at its end and at the Kennedy Space Center in Florida preparations are underway for launching Vela 4, a military satellite equipped with gamma ray detectors.

On Sunday, the 2nd of July, 1967, a shower of gamma radiation blows through the solar system unseen and unheard, photons from billions of years ago and billions of light years away. The greatest portion streams unhindered between the planets, and races on with the speed of light further into the dark heavens. At last, a scant handful of gamma ray photons penetrate the detectors on the Vela satellite. The first detection of a cosmic gamma ray burst is now a fact. The mystery for man is just beginning.

From the prologue to "Flash! The hunt for the biggest explosions in the Universe", Govert Schilling, abridged

1

INTRODUCTION

1.1 A SERENDIPITOUS DISCOVERY

1.1.1 ONCE UPON A TIME...

... there was the cold war and the number of nuclear weapons growing at a considerable rate. However, mankind was also on its way to space, the first satellites launched and people seriously thought nuclear bombs might be tested in space or behind the moon without ever being noticed. Before this could happen, the Nuclear Test Ban Treaty signed in 1965, forbid all tests inside and outside the Earth's atmosphere as well as under water. But as the saying goes, trust is good, control is better, the US government told scientists in Los Alamos to design a space mission which could look for traces of a nuclear explosion. They constructed several instruments to put on a satellite of which one would measure the γ radiation from the decay of radioactive material produced in the blastwave from the explosion.

The program started in 1965 with two satellites with primitive scintillator detectors made of cesium iodide and a time resolution of only 20s. The detectors were improved and new satellite pairs started, Vela 5a and b, launched in May 1969 shorty before Apollo 11, had alread a resolution of 0.2s. Nothing, however, was detected that resembled the unlawful testing of a nuclear bomb. But in the data of July 2nd 1967, Ray Klebesadel and Roy Olsen discovered a double peaked spike that occured in both instruments and, as they found out later, was also picked up by Vela 4. This was the detection of the first gamma-ray burst, GRB 670702 [1] From the time difference of the arrival times at the different instruments, they could exclude an origin from the Sun or Earth. The signal was clearly was not from a nuclear bomb but they were lacking a conclusive explanation and therefore it took 4 years and many more of the burst detected until they published their results in 1973 (Klebesadel et al., 1973). After the publication, it became clear that actually several other satellities had detected similar signals but no one had payed attention to them.

1.1.2 BETTER LOCALIZATION - THE IPN

Nothing was known about the origin of those burst and first of all, a better localization was needed. As the first γ-ray detectors did not allow any directional information of the incoming γ photon, this had to be done by triangulation. Detectors are put at different positions far away from each other and from the time difference between the arrival of the signal the position can be

[1] GRBs are named according to their discovery date, followed by letters in case of several burst detections per day.

determined. For this purpose, Kevin Hurley created the Interplanetary Network (IPN) in 1977 (Hurley et al., 2006, for the more or less current description of IPN 3 see) and γ-ray detectors were put on a number of satellites such as Helios–2 [2], Pioneer-Venus Orbiter and Venera 11 and 12 [3]. It provided an errorbox of several arcminutes, which would have been small enough for some optical telescopes to look for a theoretically predicted optical counterpart (Paczyński & Rhoads, 1993; Meszaros & Rees, 1997). However, there was a large time delay of many days to download and processed the data, as we know today, only a handful of bursts would then still be visible and only with 4–8m telescopes not available by that time.

The IPN is still active today and the IPN3 has been founded in 1990. The main contributers today are instruments onboard 2001 Mars Odyssee [4], Konus-Wind [5], Messenger [6], RHESSI [7] and other current GRB missions, but follow-up of those bursts is still challenging. Around the turn of the century, Ulysses which had an orbit perpendicular to the ecliptic and NEAR provided errorboxes of a few tens of arcminutes which can be imaged with wide field cameras or covered with a few pointings. Today, most IPN satellites are around the Earth and errorboxes have grown to the order of several degrees again.

1.1.3 CGRO

The first large project specifically dedicated to study GRBs was the Compton Gamma Ray Observatory (CGRO) with the GRB instrument BATSE (Fishman et al., 1989) onboared among a range of other γ-ray detectors. BATSE consisted of 8 detectors at the 8 corners of the spacecraft divided into a large area detector for high sensitivity and directional information and a spectrometer. However, the position of the GRB could still only be determined down to a few degrees. Over the years, BATSE detected several thousand GRBs. Furthermore, the high energy instrument EGRET detected very high energy emission (18 GeV) from one burst, GRB 940217 (Hurley et al., 1994), whose origin is still unknown and which will now be studied further with the GLAST mission.

In addition to a large number of γ-ray lightcurves and spectra, two major results came out of the BATSE mission. First, the GRBs were uniformly distributed over the entire sky which was a clear indication for their cosmological origin (see Fig. 1.1) (e.g. Briggs et al., 1996). But even though the distribution on the sky as well as the lack of detected very faint bursts pointed to a cosmological origin, there was still a number of people that attributed the GRB phenomenon to the local universe. In 1995 the famous "great debate" was held between Donald Lamb (galactic origin) and Bohdan Paczýnski (cosmological origin) in the Smithonian Natural Museum commemorating and inspired by the great debate about the extragalacitic origin of "nebulae" (later shown to be galaxies) in 1930. The second important observation made with this huge sample was the discovery that GRBs seemed to be distributed in two main "groups" in time and spectral ratio (Kouveliotou et al., 1993) which were subsequently named short and long duration GRBs are are thought to have different progenitors.

[2] German-US project to study the sun
[3] Russian Venus lander missions
[4] Orbiter around Mars to communicate with the lander Phoenix on the Mars surface
[5] Satellite studying the solar wind, interplanetary plasma and solar flares, varying orbit around L1 and 2 and Earth
[6] Mercury mission, currently in a slightly excentric orbit around the sun, in orbit around Mercury in 2011
[7] X-ray probe to study solar flares, Earth orbit

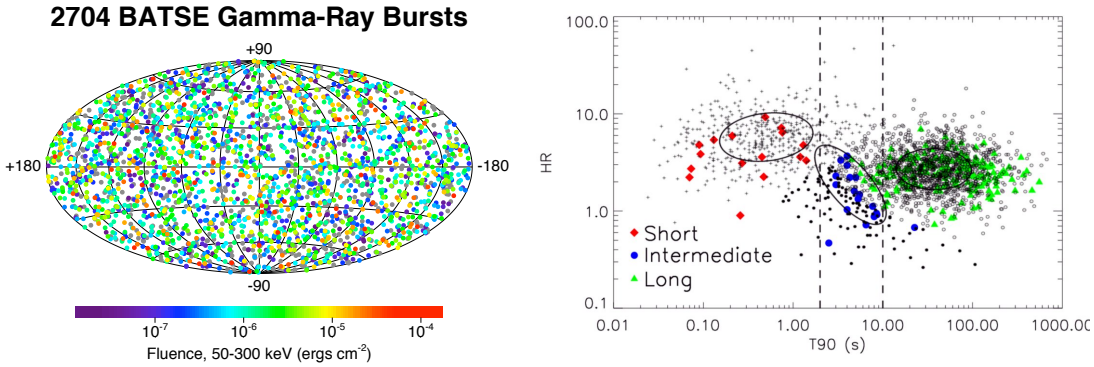

Figure 1.1: *Left panel: BATSE GRB distribution on the sky. Right panel: Division of GRBs into two subgroups according to duration and hardness, T_{90} is the time in which 90% of the γ-ray fluence is detected, the hardness is derived from the ratio of the BATSE channels HR(100–300 keV)/(50–100 keV). The colored points indicate Swift bursts, a possible intermediate group is also shown.*

1.1.4 THE FIRST AFTERGLOWS - BEPPO SAX AND HETE

As it became clear that only the identification of a lower energy counterpart and hopefully the determination of a redshift could solve the great debate, an even better localization was needed. In order to achieve that, the Americans started to develop the HETE satellite which would have a gamma-ray monitor, an X-ray widefield and an X-ray camera. Independently, the Italians were constructing an X-ray satellite called BeppoSAX (Boella et al., 1997) which finally was upgraded with a burst monitor using simply the shielding of the X-ray detectors. Both missions suffered from some trouble, BeppoSAX was delayed for many years and took finally off in 1996. HETE-Is launch failed as it could not be decoupled from the other satellite that it was launched together with. Even though it was quickly decided that HETE-II would be built and finally launched in 2000, the big credit in the field went to BeppoSAX.

On Feb. 28, 1997, BeppoSAX detected a GRB which was found to have a counterpart in X-rays detected and localized with the WFC (Costa et al., 1997). The quick distribution of the position (which also lead to a few political issues) enabled optical and radio follow-up with the Willam-Herschel-Telescope (WHT) on La Palma, the Westerbork radio telescope in the Netherlands and the Very Large Array (VLA) in New Mexico. While the radio observations revealed no new source, comparison images taken with the WHT a week later (see Fig. 1.2) showed that one of the objects not present in the Digital Sky Survey (DSS) had disappeared (van Paradijs et al., 1997). A host galaxy was discovered later and a spectrum showed a redshift of 0.695 (Kulkarni et al., 1998) [8].

The question of the cosmological origin of GRBs was then also resolved quickly. For GRB 970508, afterglow spectra taken with LRIS at Keck showed Mg II and Fe II absorption lines at a redshift of 0.835 (Metzger et al., 1997). The great debate had come to an end. In addition, GRB 970508 had also the first detected radio afterglow (Frail et al., 1997). BeppoSAX also discovered GRB 980425 in the spiral arm of a galaxy at z=0.0085 which later on showed a SN at the same position as the GRB and is considered as the first evidence of the connection between long-duration GRBs and supernovae (SNe) (Galama et al., 1998). BeppoSAX discovered 55 GRBs in total before its reentry in 2002. Even though HETE-II was launched long after these most

[8] This observations had the honour to be the first notice of the Gamma-Ray burst Circular Network (GCN) described in Chapter 1.4.1 and funnily got the number "–4" due to a mistake in the counting that was introduced later.

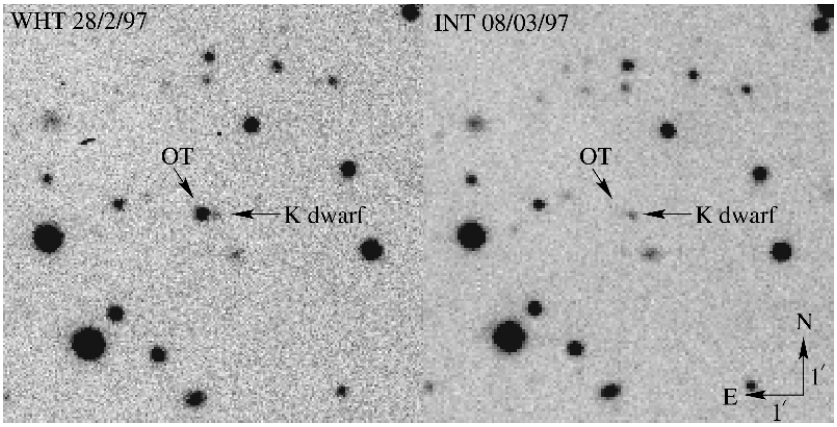

Figure 1.2: *Image of the first detection of an afterglow for GRB 970228 the night after the burst (left panel) and one week later (right panel) when it had faded. (from van Paradijs et al., 1997)*

exciting discoveries, some other important bursts go on the account of HETE-II. To mention here is the famous GRB 030329 at z=0.1685 (see also Chapter 4), the first GRB clearly linked to a SN (Hjorth et al., 2003; Matheson et al., 2003; Stanek et al., 2003) and still one of the best studied bursts ever in the entire wavelength range. GRB 050709 then finally lead to the first afterglow detection of a short burst (Hjorth et al., 2005b).

1.1.5 THE *Swift* ERA

Now that the most important issues were settled, it was time to get a larger sample of afterglows observed in the entire wavelength range. In order to achieve that, the *Swift* satellite (Gehrels et al., 2004) was designed purely for GRB detection and follow up and was launched on Nov. 20, 2004. It consists of three instruments, the burst alert telescope (BAT) with an errorbox of 1–4 arcmin, the X-ray telescope (XRT) that can slew within a few seconds to the burst position providing an errorbox of 1–4 arcsec and the UV telescope (UVOT) with 3 UV and 3 optical filters (UB and V band) with a range from 1700 to 6000 Å to detect the optical counterpart.

The ability of the telescope to slew rapidly and detect the X-ray and optical counterparts within minutes has lead to the detection of about 100 bursts/yr of which $\sim$ 60 % have a detected optical counterpart and redshifts could be determined for $\sim$ 40 %. The small errorbox of BAT allows robotic telescopes to observe within $<$1 min after the onset of the burst which enabled the observations of prompt optical emission and the very early afterglow evolution. Its larger sensitivity allows fainter bursts to be detected and subsequently, the average redshift of *Swift* bursts is higher (Jakobsson et al., 2005). It also holds the record for detecting the largest redshift burst at z=6.4, GRB 050904 (Kawai et al., 2006), the brightest afterglow, GRB 080319B (Racusin et al., 2008) and the highest number of burst per day which happened on the exactly this date, there was a GRB 080319A, B, C and D. And, finally, it has brought up possibly more new enigmas than it solved with the discovery of long GRBs without SNe (see Chapter 6), short bursts with plateaus (GRB 060313 Roming et al., 2006, Hjorth et al. in prep.) and complicated afterglow behaviour (see Chapter 1.2.1 and 3) and an X-ray flash connected to a normal SN (see Chapter 6).

Instrument	FOV	E. range [keV]	t res.	source loc.	years	GRBs
Vela 5	4π sr	3–750	0.2s	—	1969-1979	—
CGRO - BATSE	4π sr	20–1000	0.064-1s	$\sim 2^\circ$	1991–2000	2700
BeppoSAX GRBM	37 sr	60–600	0.48ms	—	1996-2002	55
WFC	$2\times 20^\circ \times 20^\circ$	2–30	0.25s	$5'$	—	—
HETE-II FREGATE	3 sr	6–400	10ms	—	2000-?	—
WXM	1.6 sr	2-25	1ms	3–$5'$	—	80
SXC	0.91 sr	0.5–14	1.2s	$30''$	—	—
INTEGRAL SPI	16°	20–8,000	50ms (ACS)	$\sim 30'$	2002–?	(ACS)290/yr
IBIS	$9^\circ \times 9^\circ$	15–10,000	61μs	$1'$	—	1/month
Swift BAT	1.4 sr	15–150	100μs	$1'$-$4'$	2004-?	100/yr
XRT	$24'\times 24'$	0.2–10	0.002–2s	$1''$-$4''$	—	—
Super-AGILE	0.8 sr	10–40	4 μs	$1'$-$3'$	2007-?	20/yr
AGILE MCAL	3 sr	300–300,000	3μs	—	2007-?	1/week
Konus Wind	4π sr	20–10,000	2ms	—	1994-?	50/yr
Suzaku WAM	2π sr	50–5,000	0.01–0.5 s	—	2005-?	50/yr
GLAST GBM	8.6	8–30,000	0.06	$15'$	2008-?	200/yr

Table 1.1: *Summary of the properties of different historic and current missions detecting GRBs*

1.1.6 GLAST AND THE FUTURE

While *Swift* will hopefully provide the community with a growing sample of rapidly localized GRBs for still a while, the other end of the spectrum, the very high energy emission, will now be investigated further. During the writing of this thesis, the Gamma-Ray large area telescope (GLAST) was finally successfully launched on June 11, 2008, 12:05 UT [9]. It consists of two instruments, the large area telescope (LAT) with a sensitivity from 20 MeV to 300 GeV and the Gamma-ray burst monitor (GBM) with a larger FOV than LAT and a sensitivity similar to BATSE, but a position accuracy of down to a few arcmin. It will detect $\sim$ 200 GRBs per year and follow up 2 bursts per month with the high energy detector LAT.

The current situation for the GRB community looks very well, GRBs are detected at such a rate that robotic telescopes are crucial and follow-up groups take shifts in order not to spend the entire time on GRB follow-up. A number of other satellites provide occisionally GRB localizations. INTEGRAL has no onboard GRB trigger, but a burst alert system IBAS (Mereghetti et al., 2003) on ground provides GRB detection alerts collected from different instruments and anticoincidence detectors. INTEGRAL, however, observes most of the time towards the galactic plane due to its main scientific goals and detected GRBs usually have a high foreground extinction. Super-AGILE and the Microcalorimeter onboard the Italian AGILE satellite (Tavani & et al., 2004) also occasionally observes GRBs and has the potential of a high time resolution for bright bursts. The Suzaku anticoincidence shield WAM (Yamaoka et al., 2006) also detects GRBs in 4 energy bands and reaches higher energies than *Swift* which allows to determine the peak energy of a GRB usually above the energy range provided by BAT. Currently, there are no plans for the time after *Swift* but its lifetime might hopefully extent to 2015–2020.

A summary of the properties of all major GRB missions is given in Table 1.1.6. Fig. 1.3 shows pictures or drawing of the missions mentioned above. Finally, Fig. 1.4 shows lightcurves of some of the historically important GRBs.

In the end, sadly, it was a project with military purpose that discovered the phenomenon

[9] Conveniently at the early afternoon MEST, the author watched the launch on NASA TV available via internet, while writing on the text of the intro of part II. Addendum: At the final print of this thesis, GLAST had started successfully operating and GBM and LAT are already delivering GRB positions.

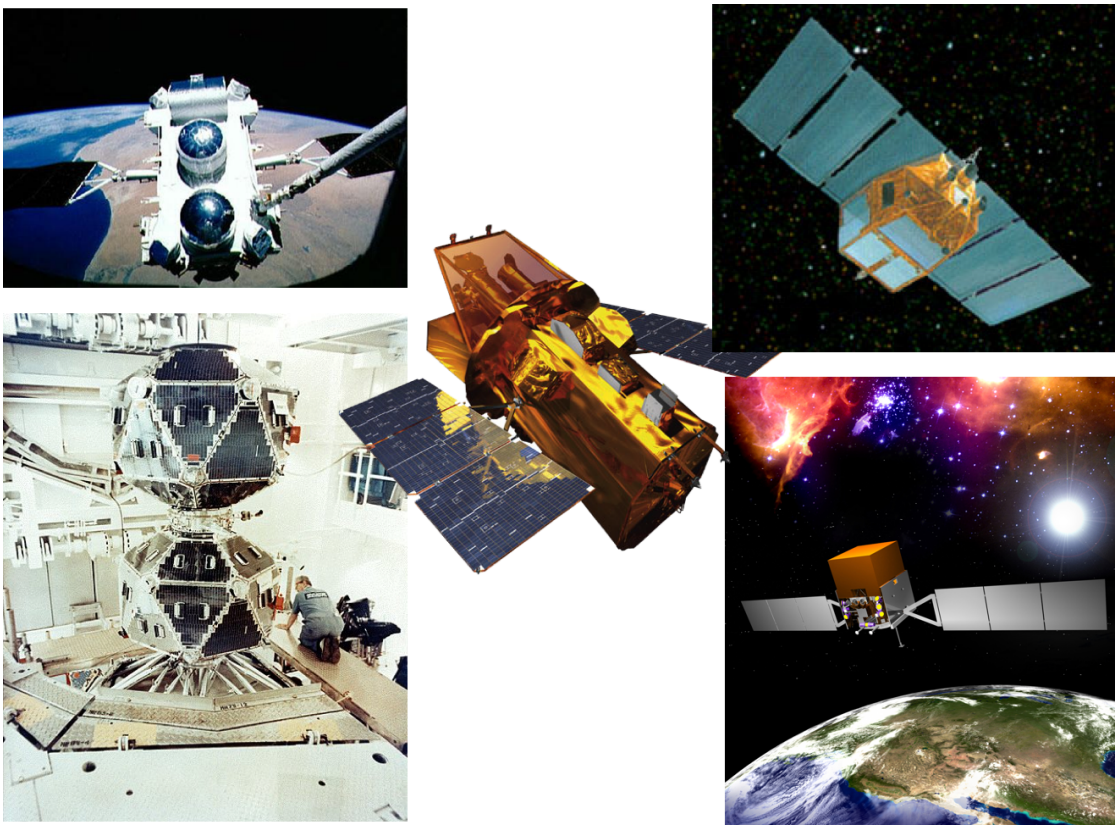

Figure 1.3: *Chart with the main satellites responsible for the discovery and study of GRBs. Upper left: the Compton Gamma Ray observatory in the bay of the Spaceshuttle, lower left: Vela 5a and b in the assembly hall, upper and lower right: drawings of BeppoSAX and GLAST, middle: Swift.*

which lead to the entirely peaceful (at least most of the time) research that became one of the important fields in extragalactic astronomy today. Interestingly, someone suggested a few months ago to revert this path as he wanted to use one of the old remaining detectors from the CGRO to detect gamma ray radiation from radioactive material that terrorist could carry around unseen. It is also interesting to note that the processes in a nuclear bomb explosion and what happens when a star explode are the same. The military had also discovered this and now sponsors research on the simulation of supernova explosions as those results are also important for simulating nuclear bomb explosions now that any test is completely forbidden. It is all physics after all and physics does not know about morality and righteousness, the universe is just happening without judging. Morality came with intelligence and the need of intelligent creatures to live together. Whether you use your knowledge for studying how the universe is happening or to make the life of your neighbour a misery is your decision, science itself is not responsible for it.

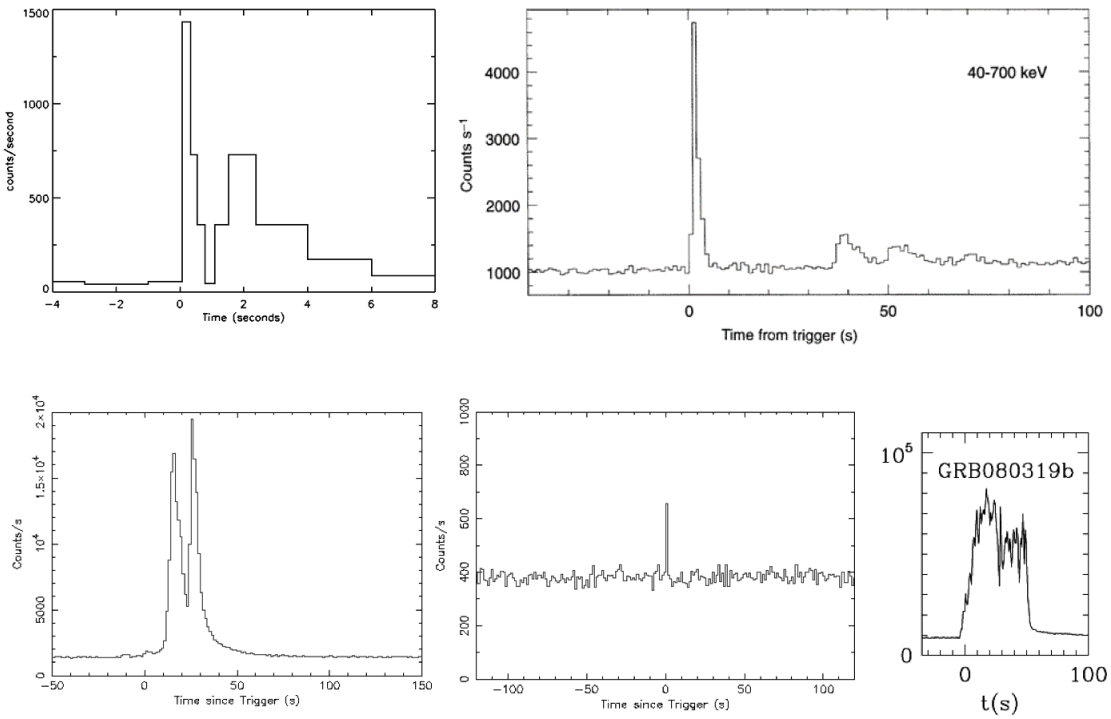

Figure 1.4: *Gamma ray lightcurves of some historically important GRBs: GRB 670702, the first detected GRB, GRB 970228, the first GRB with a detected afterglow, GRB 030329, a highly studied low-z GRB, GRB 050709, the first short burst with a detected optical afterglow and GRB 080319B, the GRB with the brightest optical afterglow.*

1.2 THE MOST POWERFULL EXPLOSIONS IN THE UNIVERSE

1.2.1 PROMPT EMISSION - THE FIREBALL MODEL

40 years of GRB observations have created a theoretical framework for the origin of the electromagnetic radiation from GRBs, the so-called the "standard fireball model". Most of the energy created by the collapse or the merger is actually released in form of thermal neutrinos with energies of 10–30 MeV and gravitational waves which are so far undetected. Even future gravitational wave detectors will only be able to detect stellar collapses out to 30 Mpc and binary mergers out to 200 Mpc (Meszaros, 2006). Neutrino detectors are likely still not sensitive enough to detect individual ν from GRBs but searches for correlations with GRB signals are ongoing.

A small fraction then goes into a highly relativistic fireball consisting of $e^{\pm}$, γ rays and baryons. Most of the baryons remain close to the central engine, otherwise the fireball could not reach relativistic velocities (this is called the baryon loading problem). High Lorentz factors, however, are required as γ rays beyond the threshold for pair production $m_e c^2$=0.511 MeV are observed for which the fireball would be optically thick (compactness problem). Infact, from the observed variability of the γ-ray lightcurve $\delta T \sim 0.1s$ we can estimate the source size $R \sim c\delta T \sim 3 \times 10^9$cm. If we assume an energy release of $\sim 10^{52}$erg in 1 MeV photons, we get N=10^{56} photons and an optical depth of $\tau \sim \sigma_T \frac{N}{4\pi R^2} \sim 3 \times 10^{11} \gg 1$. If the expanding fireball is relativistic, the photon energy in the restframe gets lower by a factor γ and the source size is reduced by γ^2 which together leads to a reduction of τ by $\gamma^{6.5}$ and $\tau \sim 1$ for $\gamma \sim 100$.

The kinetic energy transported in this flow is about 10^{52} erg and has to be transformed into radiation in order to produce the observed gamma-ray flash. This happens with shocks that

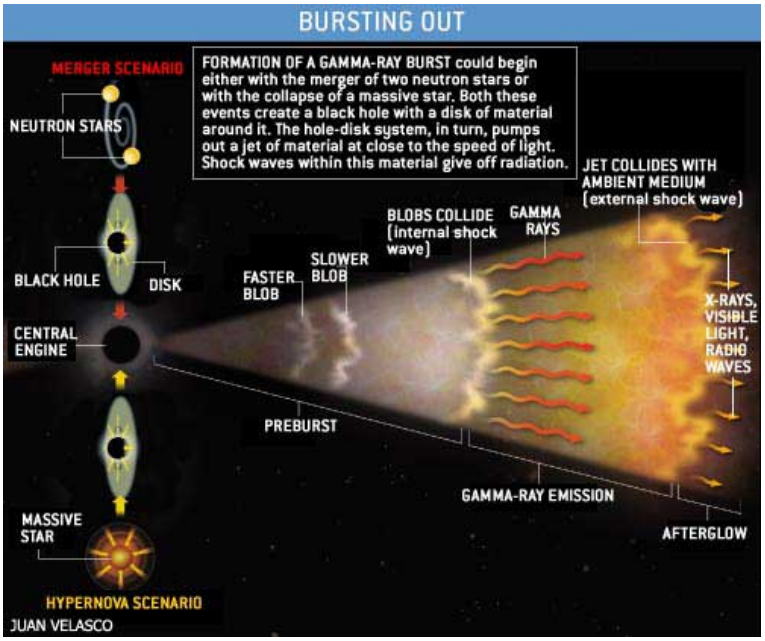

Figure 1.5: *The canonic fireball model, credit: N. Gehrels, L. Piro, P. Leonard, Scientific American Dec. 2002*

slow down the material and the remaining energy is radiated in photons. The widely accepted scenario is the model of internal shocks that arrise from colliding shells that have been sent out by the central engine with different Lorentz factors. The larger the ratio between the Lorentz factors, the more energy is released in this internal shock and a fraction $\sqrt{\gamma_1/\gamma_2}$ is tranformed into radiation.

When GRBs were discovered, one of the arguments against a cosmological origin was the extremely high energy release those distances would require, which would be of the order of a solar rest mass $M_\odot c^2 = 2\times10^{54}$ erg, about 10^3 times higher than the energy released in a supernova (SN). This problem can be solved if the radation is not emitted isotropically, but only in a very narrow jet with an opening angle of a few degrees ($\theta_0 = 1/\gamma$). This beaming would then reduce the isotropic energy release $E_{\rm iso} = 4\pi D^2 F$ (fluence F, distance $D = d_L/\sqrt{1+z}$, d_L luminosity distance) into the true energy $E = \theta_0 D^2 F$ with θ the solid angle of the jet. Observational evidence for beamed emission into a jet comes from the observations of breaks in the afterglow lightcurve.

The observed γ-ray pulses have durations between ms and 1000s and vary greatly in shape and duration. Some of them show a single peak called FRED (fast rise exponential decay), others highly variable curves with several peaks and sometimes substructure in the order of ms. Some bursts also have softer and weaker emission spanning out over longer times. For a few bursts, prompt optical emission could also be observed, coincident with the γ-ray emission (GRB 990123, GRB 060111B, GRB 041219a) and sometimes following the same structure as the gamma emission.

The observed spectrum follows the so-called Band-function (Band et al., 1993) with

$$N_E(E) \propto \begin{cases} E^\alpha e^{-E(\alpha+2)/E_{pk}} & \text{if } E \leq E_{pk}(\alpha-\beta)/(\alpha+2), \\ E^\beta & \text{if } E > E_{pk}(\alpha-\beta)/(\alpha+2). \end{cases}$$

and the typical peak energies E_{pk} range from about 100 keV to 1 MeV. Short burst usually have higher peak energies, lower fluences and a harder spectrum whereas long bursts have a soft spectrum and lower peak energies but higher fluences. Long bursts also often show a time delay between features in the high and low energies the so-called "spectral lag" (Norris, 2002) which has never been observed in short burst, that sometimes even have negative lags.

The afterglow

Once the jet collides with the interstellar medium (ISM) around the burst or clumps from the wind and mass losses of the progenitor, it also looses energy in the form of external shocks. Afterglow emission was theoretically predicted long before its discovery (e.g. Paczyński & Rhoads, 1993; Meszaros & Rees, 1997). The shock again produces a power-law for the energy distribution of the electrons as the Lorentz factors are described by a power law $N(\gamma_e) \propto \gamma_e^{-p}$ with p the electron energy index.

There are three characteristic frequencies that describe the afterglow evolution, ν_m, ν_c and ν_a. ν_m is the frequency of the electron with the minimum energy and Lorentz factor γ_m, ν_c is the cooling frequency and ν_a the frequency below which the flux is self-absorbed. These frequencies evolve with time as a powerlaw and also the flux inbetween each of these frequencies decays like a powerlaw $F(\nu) \propto \nu^{-\beta} t^{-\alpha}$. For $\nu_m < \nu < \nu_c$ the following relations yield: $\alpha_1 = 3(p-1)4, \beta_1 = (p-1)/2$ and $\alpha_1 = 3\beta_1/2$ and for $\nu > \nu_c$ $\alpha_1 = (3p-2)/4, \beta_1 = p/2$ and $\alpha_1 = 3\beta_1/2 - 1/2$ (Sari et al., 1999). For an plot of the lightcurve and spectral energy distribution of an afterglow with these frequencies see Fig. 1.6

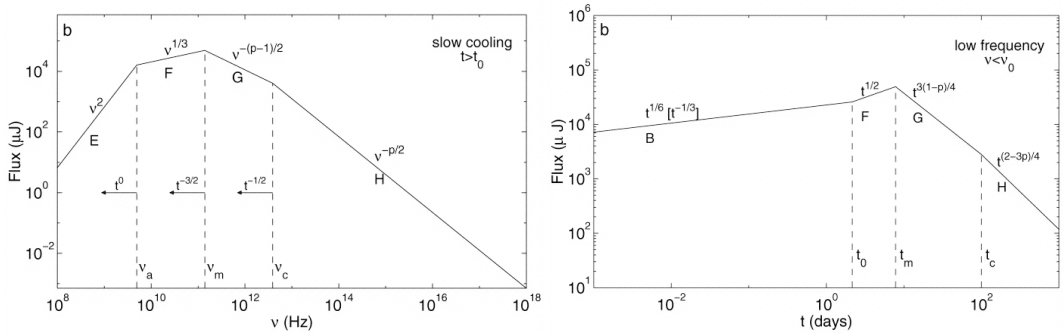

Figure 1.6: *Model afterglow spectrum and lightcurve for late times (slow cooling) and low frequencies (from Sari et al., 1999).*

The large energy release now suggests that the outflow is collimated into a jet with angle θ_0. Due to the high Lorentz factors, the radiation from the outflow is furthermore confined to a narrower cone of $1/\gamma$ in the observer frame due to the relativistic beaming. When the material slows down to lower Lorentz factors, the relativistic beaming angle at some point becomes wider than the jet and the observer does not see the entire emitting surface any more when $1/\gamma = \theta_0$. The flux therefore drops and this can be observed as another break, the so-called jet-break, which is expected to occure in all frequencies at the same time (achromatic break, in contrast to the other breaks due to the synchrotron emission which are chromatic breaks).

The break occurres at t_b=6.2 hr(1+z)$(E_{52}/n_1)^{1/3}(\theta_0/0.1)^{8/3}$ with E_{52} the energy in 10^{52} erg and n_1 the density of the surrounding medium. Furthermore, when the jet becomes less relativistic, it will spread sideways and declerate even faster. After the break the following relations yield: $\nu_m < \nu < \nu_c$: $\alpha_2 = p, \beta_2 = (p-1)/2$ and $\alpha_2 = 2\beta_2 + 1$ and for $\nu > \nu_c$ $\alpha_2 = p, \beta_2 = p/2$

and $\alpha_2 = 2\beta_2$. This all yields for a constant density medium and slow cooling as it is valid at t>1h. If broadband data of the afterglow are available, these frequencies can be and have been determined confirming the valditiy of this relativistic blastwave model.

As mentioned above, the flux behaves like a powerlaw inbetween the characteristic frequencies and the temporal evolution of the afterglow is emprically described by the so-called Beuermann equation (Beuermann et al., 1999)

$$F(t) = A/((t/t_b)^{n\alpha_1} + (t/t_b)^{n\alpha_2})^{1/n} \tag{1.1}$$

with A the parametrization constant, t_b the break time, α the slopes before and after the break and n the smoothness parameter as the jetbreak is generally not a sharp point in time. From the flux, one usually has to subtract a possible contribution from the host galaxy and the supernova components which both get more important at later times and lower fluxes.

The reality, however, has shown that whenever an afterglow lightcurve is densely sampled, it is far from being a smooth powerlaw but instead shows a number of smaller and larger variations. Before the launch of *Swift*, this has only been possible in a few rare, bright cases such as GRB 021004 (e.g. de Ugarte Postigo et al., 2005) and GRB 030329 (e.g. Lipkin et al., 2004) which showed several rebrightenings and small scale variations. The era of *Swift* afterglows and the earlier and more densely sampled lightcurves have shown frequent examples of nonsmooth behaviour with powerful late-time flares (e.g. GRB 060206, Woźniak et al., 2006; Monfardini et al., 2006; Stanek et al., 2007) or steps attributed to continued activity of the inner engine (e.g. GRB 071010A Covino et al., 2008). Also the X-ray lightcurves do not show the expected simple powerlaw behaviour with shallow decays and powerful X-ray flares attributed to the inner engine (for an extensive review on Swift afterglows and interpretations see Zhang et al., 2007).

The very early behaviour of the afterglow furthermore suggests that some of the flux observed is connected to the prompt emission and created by reverse shocks inside the jet when the material encountering internal shocks runs backwards into the jet. This is observed by early optical flashes, e.g. in GRB 990123 (Akerlof et al., 1999) or most recent in GRB 080319B (Racusin et al., 2008). If the peak of this flash can be observed, it offers also a possibility to determines the initial Lorentz factor as $\gamma_0 = 240 E_{52}^{1/8} n_1^{-1/8} \left(\frac{T}{10s}\right)^{-3/8}$. The higher the Lorentz factor, the earlier this happens. For some bursts with very early afterglow observations enable by fast responding robotic telescopes, e.g. GRB 060418 and GRB 060607A observed with the REM telescope Molinari et al. (2007), this could be determined to values of γ_0=150 to 300.

The large sample of afterglows collected since their discovery 10 years ago also shows that apparently, short GRB afterglows are intrinsically less luminous than those of long GRBs (Kann et al., 2007, 2008; Nysewander et al., 2008), see also Fig. 1.7. This has been seen as evidence for a lower density of the surrounding medium of short GRBs in contrast to long GRBs. However, Nysewander et al. (2008) conclude that as the total energy release of a short GRB is smaller, so has to be the afterglow which would imply a similar circumstellar density for long and short bursts. A number of bursts has also today, despite deep early searches, no detected afterglow and are called "dark bursts". Jakobsson et al. (2004a) derived a formal definition for dark bursts being subluminous compared to the standard fireball model which gives a spectral slope from X-ray to optical $\beta_{\rm OX} < 0.5$. It is still not clear why some burst are "dark", suggestions are dust extinction, intrinsic faintness due to a low density medium or nondetection due to a very high redshift.

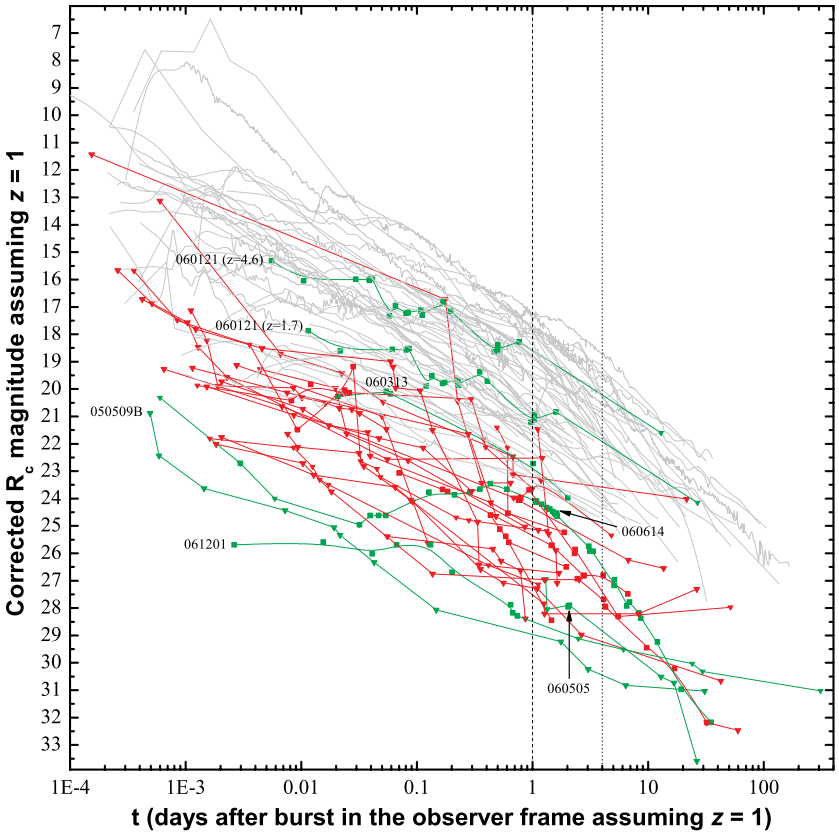

Figure 1.7: *Chart with the afterglows of long and short GRB afterglows in the Swift era shifted to z=1. Short burst afterglows (red) are clearly less luminous than those of long GRBs (grey). A few particular short bursts have been highlighted in green (from Kann et al., 2008)*

1.2.2 PROGENITORS OF GRBS

The clustering of GRBs into two more or less distinct populations according to their duration with the dividing line at about T_{90}=2 s and spectral hardness lead to the suggestion that GRBs might have different progenitors. The timescales involved indicate that not one model could explain such a large range of durations. The first theories on GRBs favoured magnetic energy outbreaks from neutron stars or compact object mergers. But even before the connection between SNe and long-duration GRBs was made, it was suggested that the collapse of a massive star could cause a SN. Today there is little doubt about the collapsar model for long GRBs, however, a conclusive scenario for short GRBs is still missing.

Long GRBs

The favoured model for long GRBs today is the "collapsar model" (Woosley, 1993) as first described in detail by (MacFadyen & Woosley, 1999). If a star has a main sequence mass of above 25–30 $M_\odot$, the iron core formed at the end of the silicon burning creating a proto-neutron star at the first collapse of the core ultimately collapses further to a black hole (BH). The infalling matter than does not get stopped at the surface of the proto-neutron star and creates an outward shock but instead freely falls into the BH and the explosion "fails".

If the star has a considerable angular momentum, however, most of the matter will not fall

directly into the black hole but form an accretion disk which feeds the BH. Along the axes, there are several mechanisms which can create highly relativistic outflows, e.g. neutrino annihilation or extraction of the rotation energy of the BH through magnetic fields created by the accreting ionized matter. The accretion around the equatorial plain creates a low density area around the polar axes where the energy deposition leads to a reverse of the infall and creates a powerful outflow confined by pressure, density and probably magnetic fields into a jet. If the outer layers of the star are not too thick, the jet will then reach the surface within a few seconds. The actual GRB is created once the jet has broken through the star by internal shocks in the jet as described above.

The jet also deposits energy in the star on its way out and probably strong winds from viscous interactions in the disk lead to an explosion of the remainings of the star that have not yet accreted. The result is a SN like explosion as observed in nearby long-duration GRBs. The key criterion of producing a GRB therefore seems the right amount of angular momentum, if it is too low, a BH forms without any outflow or explosion, if it is too high, the accretion disk forms far away from the BH and there might be at best a weak equatorial explosion.

Another important issue is the amount of mass left in the envelope of the star. Simulations show that at least the hydrogen envelope had to be removed in order for the jet to reach the surface. The mass loss of a star is determined by its metallicity (e.g. Heger et al., 2003) as radiation pressure from Fe UV emission lines (e.g. Vink et al., 2001) leads to powerful winds driving mass away from the star. This process also leads to a larger radius of the entire star and usually to loss of angular momentum. Producing a GRB in the end therefore might either require very high masses so that enough mass is left for the collapse after the wind has removed the hydrogen envelope (lower metallicites require higher masses) (Heger et al., 2003), effective mixing of the hydrogen layers (max. $Z \sim 1/10$ solar) (Yoon et al., 2006) or removal of the envelope by a close companion star (e.g. Fryer et al., 2007).

Short GRBs

The timescales for short GRBs with $T_{90} < 2$s are too short to be explained by the collapsar model. Instead, the widely accepted model for short bursts is the coalescence of two compact objects, two neutron stars or a NS and a BH, or in some models (King et al., 2007) a white dwarf (WD) and another compact object. Binary neutron stars have been observed in the MW and they should eventually merge as they loose angular momentum through gravitational waves. When they merge, they might form a BH and a torus which carries the angular momentum. Alternative scenarios are e.g. the spiral in of a NS onto a BH which then gets disrupted. Strong magnetic fields transport energy from the torus to the poles where they can leave the merger in two opposite jets much like in the collapsar model described above. The time scales for such a merger is on the order of < 1s which fits well with the observed durations (for a review on short GRB progenitors see Lee & Ramirez-Ruiz, 2007).

A consequence of this model is the lack of a SN signature in the late lightcurve. Observations have so far confirmed this scenario even though short bursts do lack the dense sampling of long burst lightcurves. An example for a resonably deep limit on a SN component is GRB 070724A shown in Fig. 1.8 where the late time limit from the Keck telescopes excludes even the faintest SNe by several magnitudes (Kocevski et al. in prep.). So far, there is no direct observational evidence that short bursts do indeed trace the merger of two compact objects. The possibly only way to settle this issue would be the observation of gravitational waves from such an even but even future gravitational wave detectors might not be sensitive enough to detect those

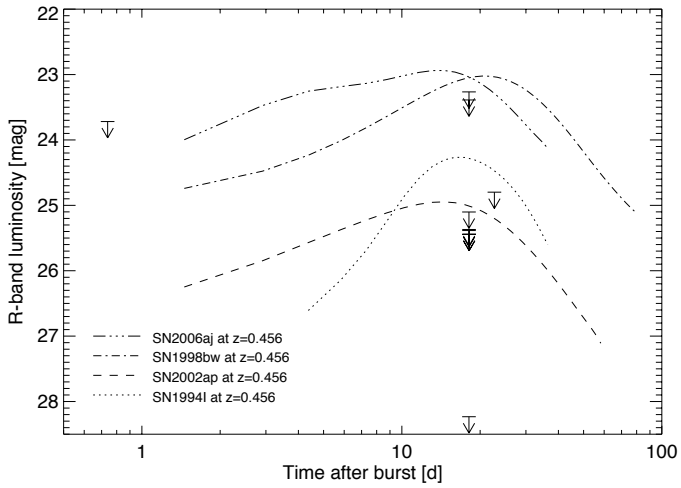

Figure 1.8: *Limits on core-collapse SNe in the late time lightcurve of the short GRB 070724A. The SN lightcurves have been shifted in magnitude and time to the redshift of the burst (z=0.4) and a rough k-correction has been applied.*

mergers.

It has been suggested that the merger of two compact objects will not consume all the material of both stars but that some nonrelativistic ejecta are expected, either from the tidal tail of the disruption or a wind driven by neutrino emission or ejection of the outer part of the torus in order to conserve the angular momentum (Li & Paczyński, 1998; Kulkarni, 2005). The macronova model proposed by (Kulkarni, 2005) calculates that the decay of free neutrons could extend the hot phase of the fireball and therefore lead to a plateau or even rebrightening of the afterglow at around a day. Until now, such a macronova component could be excluded (Kann et al., 2007; Ofek et al., 2007, Kocevski et al. in prep.).

The classification issue

These two prognitor models also seem to be reflected in the observations. Long duration GRBs had associated SNe (see Chapter 6.1.1) and short bursts had none. In 2006, however, two long-duration GRBs were discovered that, despite very deep searches, had no signature of a SN observed. This sample might be larger as not all nearby GRBs have been followed up closely enough. Theorists have suggested a range of collapsar models that would produce only a GRB with no or very weak SN explosion (e.g. Fryer et al., 2006). Others have suggested that those two GRBs were indeed short bursts with no expected SN component and voted for a reclassification of GRBs (Zhang, 2006). From the high energy properties, it is sometimes difficult to determine if a burst should be classified as long or short. The dividing line is not sharp and some therefore suggested that there might be a class of "intermediate bursts". Furthermore, the classification with duration and hardness from the BATSE instrument might not be applicable to e.g. *Swift* which has different high energy channels and a higher sensitivity, e.g. the soft tail of GRB 060614 might have been missed with BATSE if it would have been only about 8 times less energetic.

γ-ray outbursts detected over the years might also have some different origins. "GRB" 070610 turned out to be a galactic transient (Kasliwal et al., 2008, Castro-Tirado et al. Nature, accepted, Stefanescu et al. Nature, accepted). The IPN error box of GRB 070201 lied partially on M 31 and it has been suggested that this GRB might infact have been a magnetar outburst as

e.g. the giant flare from SGR 1806 - 20 detected by INTEGRAL in 2004. SN 2008D, discussed in Chapter 6.1.3 had an X-ray flare with similar properties as a GRB but at much lower energies. The high energy properties of a GRB or GRB-like event might therefore not always be enough to determine if the event was from a collapsar or a merger (and hence a GRB in the usual sense) or something very different.

1.2.3 COSMOLOGY WITH GRBS?

GRBs can be used for cosmology in two different ways, either directly for distance determination, if they could be somehow made to standard candles, or to study the high redshift universe. Despite their large variation in durations and luminosity both in the promt and afterglow emission, there were attempts from early on to investigate if all GRBs can somehow be standardized and used as distance indicators as it is done with SNe Ia. Frail et al. (2001) found out that while the isotropic energy release E_{iso} has a large range of values, the energy corrected for the beaming $E_\gamma = E_{\rm iso}(1 - cos\theta)$ clusters around a value of about 5×10^{51} erg.

In the last years, it was suggested that there is a correlation between the peak energy E_{pk} and the apparent isotropic energy E_{iso} with $E_{pk} \propto \sqrt{E_{iso}}$, called the Amati relation (Amati et al., 2002). The Ghirlanda relation (Ghirlanda et al., 2004) claims a correlation between the beaming corrected energy E_γ and E_{pk} with $E_{pk} \propto E_\gamma^{0.7}$ which is inconsistent with the Frail relation. For that, both the redshift and the jet angle determined from the jet break must be known. Both relations have a number of outliers that are not easily explained. The problem with deriving cosmological parameters for those correlations that in order to fit the slope, a certain cosmology has already to be assumed (as E_γ depends on d_L). Furthermore, Kocevski & Butler (2008) find for *Swift* that assuming a fixed E_γ the inferred X-ray jet break times are inconsistent with observations. A number of other possible correlations have been suggested but none of them have proven to hold for the complete sample. So far it seems that attempts to use GRBs directly for cosmology have still not been fruitfull.

However, GRBs can be used indirectly to study the high redshift universe and the evolution of the star formation over time. GRBs have been detected up to redshift 6.3 (Kawai et al., 2006) and are assumed to be found at even higher redshifts (Bromm & Loeb, 2002). Therefore (1) they might then be the signatures of the first stars which probably had masses of 100-1000 $M_\odot$ and can provide some important information about the properties of the first stars. (2) They are powerful lightsources to probe the ISM of distant galaxies (see Chapters 2–5), more luminous than quasars and probably detectable to even higher redshifts. And (3), as long GRBs are connected to the most massive stars, they likely trace the starforming galaxies at different redshifts.

1.3 THE GALAXY

Along with the different scenarios for the progenitors for long and short GRBs, it was always suggested that this might be reflectet in the type of galaxies that host either long or short bursts. Long bursts coming from the collapse of a massive star should preferentially be located in star-forming galaxies that are typical for the population of star-forming galaxies at all redshifts. It is suggested that the places of heavy star-formation change over time from the progenitor of massive galaxies in the early universe to low-mass small irregulars in the local universe. This scenario is called "downsizing" and has been confirmed with observations of large galaxy populations (e.g. Juneau et al., 2005, with data from the Gemini Deep Survey). The SR in the

universe was significantly higher at higher redshifts and likely peaked around z∼1 (Madau et al., 1996).

Short GRBs, however, were suggested to either be located in early type galaxies where star formation ceased a long time ago and where enough time has passed for binaries of compact objects to spiral in. They should then also have lower redshifts on average in order to accomodate the long time scales needed for merging. But short GRBs would also be expected in later galaxy types, e.g. spirals, as they also have an older component present and because some binary merger models suggest a short coalescence time channel of only a few Myrs for very close binaries (Belczynski et al., 2006).

Host identifications were successfull for a significant fraction of both long and short GRBs. About 10–15% of all long bursts with arcsec localizations have host galaxies detected but the fraction of those that were explicitely searched is about 70–90% [10]. Almost all short GRBs with at least X-ray afterglows, however, have detected or at least candidate hosts.

1.3.1 LONG GRB HOSTS

From the earliest detections of long GRB hosts, it became clear that they are indeed star forming galaxies with pronounced emission lines such as the Balmer lines, [O III], [O II], [N II] and in some cases even [Ne III]. Those emission lines are typical for local star-forming galaxies and HII regions and are produced by redistribution of the UV radiation from young stars.

Different studies on long GRB hosts targeted their optical-IR colors, spectral energy distributions, masses, star-formation rates and ages in order to compare them to star forming galaxies at different redshifts. IR data obtained with ground based (Le Floc'h et al., 2002) and *Spitzer* data (Le Floc'h et al., 2006) indicated that long GRB hosts have very blue colours (R–K = 2–3), even bluer than local star burst galaxies, and rather low masses as derived from the K-band luminosity (Le Floc'h et al., 2006; Castro Cerón et al., 2008; Savaglio et al., 2008). They are, however, significantly different from dusty star burst galaxies detected at high redshifts that would have redder colours and higher masses and which harbour about 70% of the star formation activity at z>1. One explanation to that problem is that dark bursts might originate in those more "typical" SF galaxies but go undetected.

The UV star-formation rates of long GRB hosts are also higher than comparable field galaxies (Christensen et al., 2004) but similar to the population of starforming galaxies. By normalizing the SFR to the mass (Castro Cerón et al., 2006, 2008) or the B-band luminosity (Christensen et al., 2004), one can obtain specific SFRs reflecting the efficiency with which a galaxy produces new stars. SSFRs seem to be also higher than for field galaxies but lower than for known massive star-forming galaxies such as Lyman Break Galaxies or Lyman α emitters. The UV, however, only traces the unobscured SFR and there are indications that at least a part of the GRB host sample has some extinction. Radio and sub-mm observations of GRB hosts suggested very high SFRs (Berger et al., 2003; Tanvir et al., 2004) which might be a further indication for extincted SF, hidden in molecular clouds, in those galaxies (Michałowski et al., 2008).

In most cases where the SED could be well constrained, GRB hosts fit best with models of starburst galaxies. Those galaxies have experienced an instataneous burst of star formation which uses up all the gas in available in the galaxy. Furthermore, low extinction values, very young ages and low metallicities are inferred from those studies (Christensen et al., 2004; Michałowski et al., 2008; Savaglio et al., 2008). A thorough study of 40 long GRB hosts of which

[10] the exact number is difficult to determine, especially for post-*Swift* bursts due to different ongoing host searches with different sample selections whose results are still unpublished

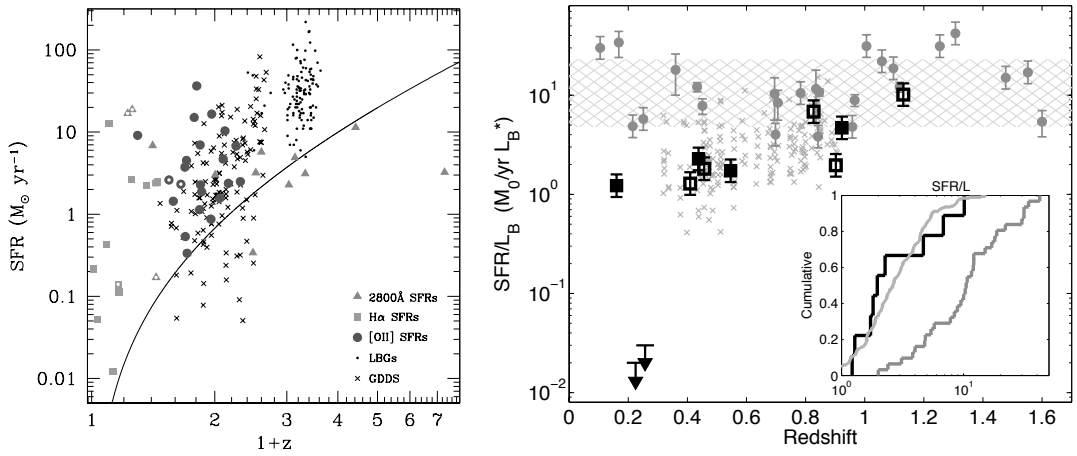

Figure 1.9: *Left panel: SFRs for long GRB hosts using different emission lines and comparison to a sample of LBGs and GDDS galaxies. Right panel: specific SFRs for short GRB hosts (black squares) compared to those of long GRB hosts (grey squares, hatched area indicates the median and 1σ error of the long host distribution) and the GOODS-N survey (crosses). (From Savaglio et al., 2008; Berger, 2008).*

33 had emission line spectra published came to similar conclusions (Savaglio et al., 2008) about high SFR, low metallicity, young age and moderate extinction values. Some GRB hosts have also been found to be Lyman α emitters as expected for low metallicity and high, unobscured star-formation. While earlier studies suggested that most GRB hosts show Lyman α emission (Jakobsson et al., 2005), new results with larger samples do not seem to confirm this result (Milvang-Jensen et al. in prep.).

It is still not clear whether long duration GRBs and subsequently their host galaxies are unbiased representatives of star formation throughout the universe. Most studies conclude that the properties of long GRB hosts put them in the average sample of star forming (but not necessarily "typical") galaxies at different redshifts. Star forming galaxies are also selected by different techniques, each of them with different limitations related to their properties (e.g. Lyα emitters) or their luminosities. This might not be the case for GRB hosts. The lower mass generally found for GRB hosts compared to other samples might be just due to those observational biases which selects more massive hosts in luminosity limited samples whereas the typical SF galaxy might have on average a lower mass.

1.3.2 SHORT GRB HOSTS

The number of short hosts with detected optical or X-ray afterglows is still rather small with 23 of which 10 had detected afterglows and 18 host galaxies or candidate hosts (Berger, 2008). The first host galaxies detected in 2005 seemed to fit in the picture of early type, massive hosts with low SFRs. GRB 050509B and GRB 050724 were associated with low redshift elliptical galaxies (Bloom et al., 2006; Hjorth et al., 2005a; Berger et al., 2005) and for GRB 050813, several early-type candidates were found (Prochaska et al., 2006a). It was also suggested that short GRB hosts could preferentially be situated in galaxy clusters. Only three short GRBs have been associated with clusters, namely GRB 050509B (Bloom et al., 2006), GRB 050813 (Gladders et al., 2005) and GRB 050911 (Berger et al., 2007) whereas 6 more short host environments have been specifically investigated for cluster associations (Prochaska et al., 2006a; Berger et al., 2007, Kocevski et al. in prep.). No long GRB host so far has been found in a cluster environment (Bornancini et al.,

2004) which some see as further indications for the merger nature of short GRBs.

With more host detections, the picture of short hosts being preferentially early type galaxies changed. Berger (2008) conclude that only 10% are located in elliptical galaxies whereas 45 % are found in galaxies with considerable star-formation of 1–6 $M_{\odot}$/yr. However, they seem to be on average about one magnitude brighter than long GRB hosts and likely more massive. They also show higher metallicities of around of even above solar, which is expected according to the known luminosity-metallicity relation and the fact that short hosts seem to be luminous galaxies. Short GRBs furthermore have larger offsets from their hosts than long GRBs (Bloom et al., 2002). This is expected as assymmetric SN explosions are known to give kicks to their NS remnants and velocities have been measured up to $\sim$ 1000 km/s for pulsars in the Milky Way.

These results puts some tight limits on the progenitor models for short GRBs, even though the wide distribution of host types might ressemble the one inferred for SN Ia (Prochaska et al., 2006a). Either there is indeed a significant fraction of mergers with very short coalescence times (Berger (2008) suggests it could be as high as 1/3) or short GRBs can also be produced by other progenitors.

1.4 IT'S ALL ABOUT BEING FAST OR WHEN THE MOBILE RINGS TWICE

A significant amount of time for someone doing follow-up observations of GRBs goes into triggering various telescopes using a special form of proposal, the so-called "Target-of-opportunity" (ToO), or for very rapid observations, automatic overrides of current observations (and observers) called "Rapid response mode" (RRM). Automatic triggering systems have also been installed at a large number of small robotic telescopes around the world within the last years, especially driven by the possibility of very rapid and accurate position determination by the *Swift* satellite.

1.4.1 THE GCN NETWORK

The early searches for afterglows in the era of CGRO and BeppoSAX showed that not only pinpointing the exact location of a GRB is important for follow-up, but also the fast reaction time as afterglows often fade beyond the reach of most telescopes within a day. In 1994, an automatic system called BACODINE (BATSE CoOrdinate DIstribution NEtwork) was installed to distribute the coordinates of a GRB in real-time around the world to interested follow-up observers (Barthelmy et al., 1995). After the end of the CGRO mission, it was subsituted with the more general distribution system called GCN (Gamma ray burst Coordinate Network). It provides two services, the distribution of essential information on the trigger as well as short email notices about observations written by the observers. The GCN notices have recently gotten another, longer form called "GCN report", that summarize the *Swift* observations in a sort of very short paper with all the available data, lightcurves etc. from the satellite.

Currently, *Swift*, INTEGRAL, HETE-II, AGILE and in the future GLAST provide position information to the GCN. *Swift* distributes BAT, XRT and UVOT positions as well as lightcurves, spectra, images and source lists. Whenever a GRB is detected by the satellite, the position is sent to the GCN system at the Goddard Space Flight Center where it is sent out via pager, email or socket connection. [11]. *Swift* provides both rate and image triggers The delay between the onset of the burst and the position information is about 10–40s for BAT and $\sim$ 1 min for XRT.

[11] The recipients of the position information and their setups are stored in http://gcn.gsfc.nasa.gov/sites_cfg.html.

Most automatic telescopes use the socket connection and a local system filters the important information and decides whether to observe or not according to predefined observating constraints. Processing the information at the GCN system and distribution to the GCN recievers takes only a few seconds. Small telescopes have been observing the burst already a few tens of seconds after the onset of the burst, sometimes conincident with the prompt emission [12]. Some wide field monitoring telescopes such as TAROT furthermore use additional information provided by *Swift* about the slewing directions which provides even faster reaction time or they might then even have imaged the field already before a GRB was detected. So far the search for precursers of GRBs has not been successfull yet.

Nonautomatic sites get their position information via email where it is processed and eventually distributed e.g. via sms to a mobile phone. Our group in Copenhagen processes the information into an email and creates a page with all necessary information in order to decide whether it is worth and possible to follow up this burst: coordinates, Galactic extinction, observability from the main observing sites and a finding chart which gets updated with an error circle one there is an XRT position. This site is available under www.astro.ku.dk/∼brian_j/GRBYYMMDD_[triggernumber]. Furthermore, it provides a short version of that page that is sent out via sms to the follow-up team. At the moment, about 6 people are actively involved in the follow-up work who take weekly shifts during which this person is the first one responsible for coordinating the observations. [13]

1.4.2 ToO OBSERVATIONS

Our group has currently two main ToO proposals for the Nordic Optical Telescope (NOT) on La Palma and at the ESO observatories Paranal and La Silla. According to predefined restrictions in the proposal and coordination with competing groups, we can either obtains imaging or spectroscopy in the optical and imaging in the infrared. For the NOT, the triggering process is rather informal and there are no specific constraints except those imposed by the position, the weather condition or the instrument mounted. The information is sent to the NOT staff and the observer using a template email where also an observing script is attached and it is then to the observer to decide whether and when to perform the observations. The preferred instrument is ALFOSC (Andalucia Faint Object Spectrograph and Camera), but if another instrument is mounted, a stand-by camera StanCam can be used for imaging. In rare cases, NOTCAM is used for IR imaging. With NOT+ALFOSC, the limiting magnitude is about R = 25 mag in 1h, StanCam is slightly less sensitive. For triggering the ESO-ToO proposal, there is a designated form on the internet which the sends the information to the astronomer on duty at the telescope. At the VLT, there is furthermore an automatic RRM override system installed which can in principle be activated by mobile phone and is triggered automatically if the burst is immediately observable and some constraints are met.

Once the observations are made and the results sufficiently interesting, a GCN notice is written and sent out via the GCN network which has currently $\sim$ 1000 subscribers. In order to avoid spam, the header has to include some string that relates the observation to a GRB like "GRB, XRF, SN, transient, [name of a large observatory] etc". In contrast to the IAU circulars, GCN notices are free and everyone who can justify to distribute relevant observing information

[12] The personal nonautomatic reaction time of the author to a GRB is 6 min, achieved with the Danish 1.54m on La Silla for GRB 060313 thanks to Chloé Féron and a gravitational lense observed before the GRB that happend to be only a few degrees from the burst

[13] There are usually 2 sms distributed, one for the BAT and one for the XRT position, as we usually only trigger if there is an XRT position the mobile has to ring twice before one starts thinking about leaving the bed at night.

to the list can subscribe and get permission to submit GCN notices. Below is an example of such a notice which was the authors first afterglow discovery:

==========

TITLE: GCN GRB OBSERVATION REPORT
NUMBER: 5003
SUBJECT: GRB060424: optical afterglow detection
DATE: 06/04/25 08:25:50 GMT
FROM: Christina Thoene at Niels Bohr Institute,DARK Cosmo Ctr <cthoene@astro.ku.dk>

Christina C. Thoene, Kim Nilsson, Brian L. Jensen, Johan Fynbo (Dark Cosmology Centre) report:

We observed the BAT error circle of GRB060424 (GCN 5000) in I with the NOT and ALFOSC on La Palma, starting at UT 05:03:40 at very high airmass. Inside the BAT revised error circle (GCN 5001) we detect a new source at the position (J2000)
RA = 00:29:25.8
Dec =+36:47:58.7
The preliminary I magnitude obtained from 5x300s stacked images with a mean time of about 1h after the burst is I = 19.1 (compared to a nearby USNO star). The source is not visible in observations obtained the following night and therefore likely to be the afterglow of GRB060424

A finding chart is available at:
http://www.astro.ku.dk/∼brian_j/grb/grb060424.178/

==========

1.4.3 EXAMPLES OF TOO OBSERVATIONS AND RESULTS

During the last 3 years, the author of this thesis discovered 4 optical counterparts, 5 hosts and determined 9 redshifts together with a large number of afterglow confirmations or lightcurve follow-up. These and other observations lead to 74 GCN notices with 32 as main author (as of September 11, 2008). In contrast to the careful data analysis needed for the publication in a paper, ToO work is all about quick and dirty reduction and analysis. Photometric data usually need bias frames and flat fields to correct for sensitivity differences on the chip and imperfections of or on the CCD. Furthermore, standard star observations would be required in order to derive accurate zero points. As calibration files are not always transferred together with the science frames or are first obtained in the morning in case of skyflats, one has to either use old calibration files or work with the raw data. Photometry is then obtained by doing aperture photometry of the afterglow and a number of comparison stars of which the magnitudes are listed in one of the star catalogues such as USNO (Monet et al., 2003). If zeropoints are available and the night was photometric, one can also determine the magnitude directely with $m = m_0 - 2.5log(\mathrm{cts} \times \mathrm{gain/s}) - \mathrm{ext.coeff} \times \mathrm{airmass}$ [mag] [14]. The counts are either determined through aperture photometry or psf photometry. Aperture photometry can be done with a range of programs, e.g. the magn/circ command in MIDAS [15] or with GAIA/skycat (for a thorough description of how to do aperture photometry with GAIA see Castro Cerón (2008)). Psf photometry can be done with the `daophot` package in either MIDAS or IRAF or with SExtractor

[14] If non-standard filters are used, color corrections have to be done which are defined for each instrument
[15] http://www.eso.org/sci/data-processing/software/esomidas/

(Bertin & Arnouts, 1996).

In the following, there will be a few examples of afterglow discoveries or light-curve follow-up. Fig. 1.10 shows a two I band images of the field of GRB 060424 at the night after the burst and a comparison image one night later. Both were obtained with ALFOSC at the Nordic Optical Telescope. The detection is the one reported in the GCN above. The high airmass at the time of the observations and the subsequent heavy fringing made the afterglow discovery quite challenging. Fig. 1.11 shows the lightcurve of GRB 070508 from preliminary photometry. The observations were obtained with DFOSC at the Danish 1.54m at La Silla by the author during an observing run. Observations were obtained at two epochs and showed a rather steep decay (GCN 6389). The nondetection in V band first suggested a high redshift due to the Lyman dropout, however, UVOT detected the afterglow in V band 2 min after the burst which rather argues for reddening due to extinction. Also Jakobsson et al. (GCN 6398) detected a single tentative emission line, which would imply z=0.82. Fig. 1.12 finally shows observations of the field of GRB 080613 with NOTCAM in the K band and a total exposure time of 1350s (GCN 7878). The frames were reduced with an automatic reduction script (credit: A. A. Djupvik) and then stacked. There is no source visible at the position of the X-ray afterglow and also other groups could only report nondetections both in the optical and the infrared.

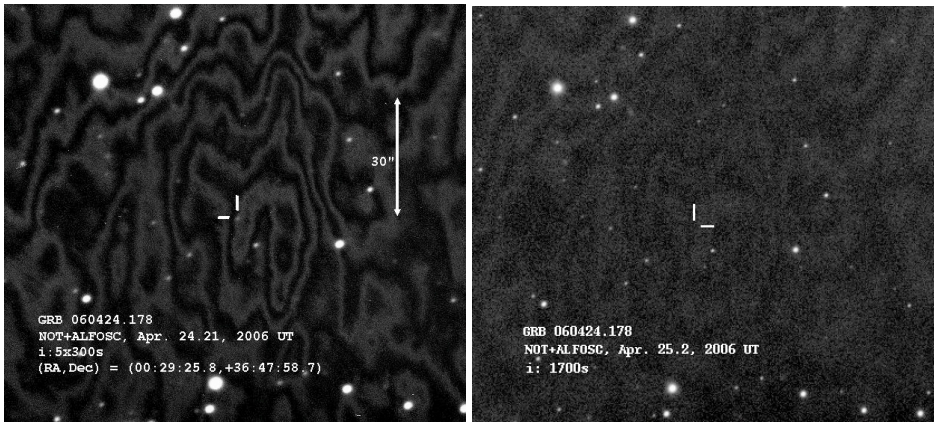

Figure 1.10: *Field of GRB 060424 45 min after the burst with the detection and a comparison image the following night which clearly shows that the afterglow had faded (credit: B. L. Jensen)*

For spectroscopy, the reduction is in principle a bit more complicated. After the preprocessing (bias, flatfielding with sky and spectroscopic flat, eventually cosmic removal with lacos_spec (van Dokkum, 2001)), the spectrum has to be extracted, wavelength and possibly flux calibrated. This is usually done with the standard IRAF tasks `apall`, `identify`, `refspec` and `dispcor`. It is desirable to have arcspectra from the same night, but usually those are not available and there has been a database created with old calibration files for different instruments and different settings. The accuracy should still be good to a few Å which is enough to determine the redshift with an accuracy of ± 0.01, especially with low resolution spectra. In addition, one can look for prominent skylines, e.g. at 5300 and 5890 Å, if they have the right wavelengths. Reporting a redshift is usually a very time pressing business and e.g. the preprocessing can be left out as we only want to detect features and do not need any flux calibration. Cosmic removal can sometimes be useful if the spectrum had a long exposure time and/or a cosmic happened to fall exactly on top of the spectrum as then the extraction becomes difficult as cosmics dominate over the flux of the objects trace.

One of the most recent redshift determination of the author was GRB 080411 which was

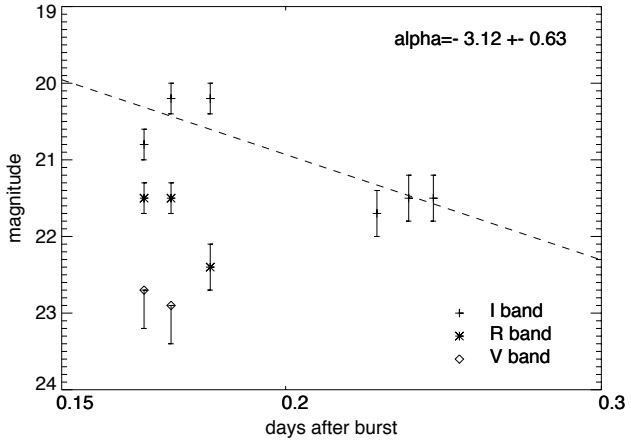

Figure 1.11: *Preliminary lightcurve of the afterglow of GRB 070508 in R and I bands as well as upper limits in the V band. The dashed line gives a powerlaw fit to the I band lightcurve with a value of $\alpha = 3.12 \pm 0.63$.*

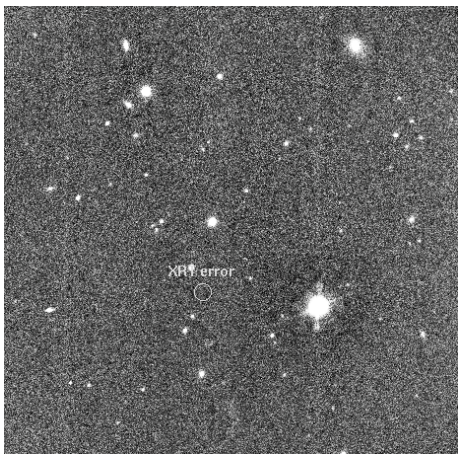

Figure 1.12: *Field of GRB 080613 observed with NOTCAM in K-band. No IR afterglow is visible at the XRT position.*

observed with FORS1 at the VLT 2.6 h after the burst. The spectrum shown in Fig. 1.13 had a number of strong features which even in the low resolution grism 300V ($\Delta\lambda \sim 11$Å) had several components. From the Fe II triplet, the Mg II doublet and Mg I we determined a rather low redshift of z=1.03. The redshift of this burst which happened on a Friday evening, was followed by two other redshift determination by our group the same weekend, those of GRB 080413A (GCN 7601) and GRB 080413B (GCN 7602). Another example is the redshift of GRB 070810 which has been obtained with the LRIS instrument at the Keck I telescope 3.5 h after the burst. The author of this thesis happened to be at the observatory already as the following night an observing run of the group by J. Bloom was scheduled at which the author participated. The blue part of the spectrum showed a clear damped Lyman α absorption from neutral hydrogen as well as a number of other absorption lines which lead to a redshift of z = 2.17 (GCN 6741). The spectrum is shown in Fig. 1.13. Due to successfull ESO proposals and a large effort to get redshifts, our group has determined the majority of *Swift* redshifts (see Fig. 1.14 and almost every spectroscopic observation also lead to a redshift determination (for an exception see GCN 5737). The second panel in Fig. 1.14 shows how crucial a fast reaction time is in order to obtain

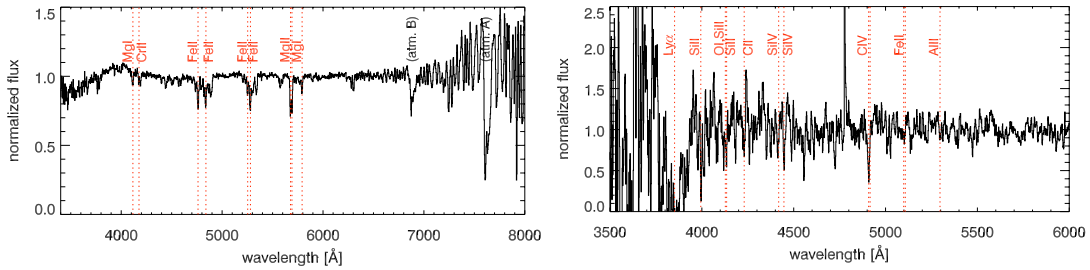

Figure 1.13: *Left plot: Normalized spectrum of GRB 080411 from FORS 1/VLT with the detected features indicated. Right plot: Blue part of the spectrum of GRB 070810 from LRIS/Keck I with the DLA and several absorption lines indicated.*

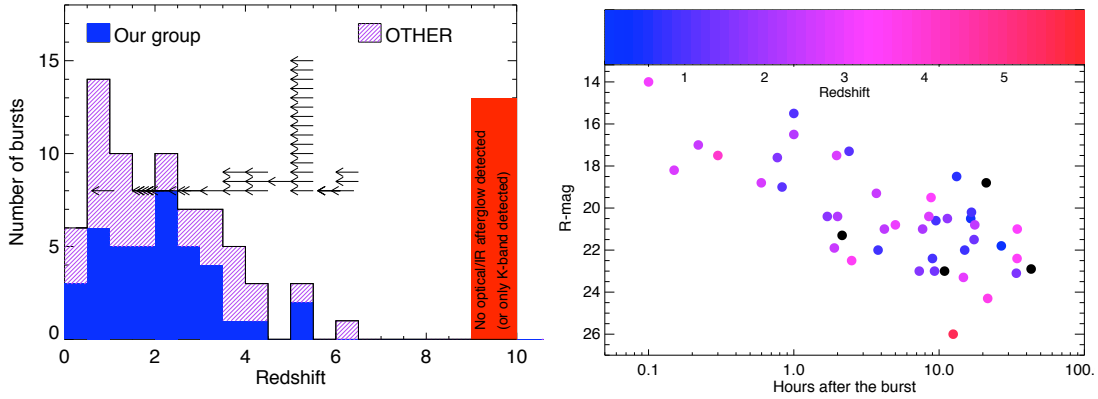

Figure 1.14: *Left panel: Redshift detections of Swift GRBs by the Copenhagen GRB group and other groups sorted according to redshifts. The red bar is the number of nondetection, the arrows indicate lower limits for the redshift of these nondetections. Right panel: R-band magnitude at the time of the spectrum that lead to the determination of the redshift. The color of the dots indicates the redshift (from Fynbo et al. in prep.).*

a spectrum as already a few hours after the burst, the afterglow can have faded beyond reach of e.g. the FORS spectrographs at the 8m VLT telescope (1 h limiting magnitude for spectroscopy around R=23).

All GCNs with participation of the author of this thesis are listed in the Appendix "Publications". Even though GRB follow-up is usually hard and stressfull work, especially when it happens at night, sometimes it can also be a lot of fun. Funny acknowledgements in the GCNs are a speciality of the author (see e.g. GCN 6410, GCN 6756 and GCN 8106), private communication allows to cite a future GCN (GCN 6142) and partying and doing serious redshift determinations does not exclude itself (e.g. GCN 7587, the burst went off during a party at DARK and the trigger sent to ESO was called "GRB080411_ party").

Part I

Absorption Line Spectroscopy of GRB Afterglows

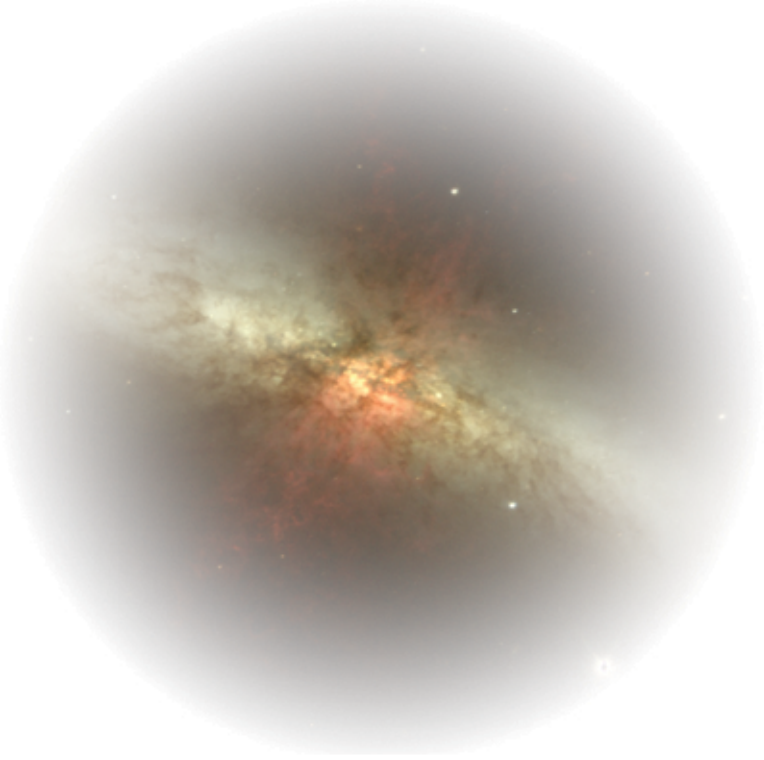

2

WHAT DO WE LEARN FROM DISTANT GRB HOSTS?

2.1 THE HIGH REDSHIFT UNIVERSE

Since the discovery of their cosmological distances and their powerful afterglows GRBs have become another important method to study the high redshift universe as well as faint galaxies. GRB afterglow spectra have the advantage that they are intrinsically smooth powerlaws. Material along the line of sight then imprints a large range of absorption features from resonant and fine structure transitions on the smooth continuum. Redshifts helps us in a fortunate way for these studies as those transitions are usually in restframe UV and hence not observable from ground. Above z$\sim$ 2 the strong absorption from neutral hydrogen (HI) inside the host galaxy is shifted into the optical and can be used to derive metallicities.

Since the launch of *Swift*, GRBs beyond redshift 4–5 have been detected with four so far at $z > 5$ (Jakobsson et al., 2006b; Cenko et al., 2006; Ruiz-Velasco et al., 2007; Haislip et al., 2006; Kawai et al., 2006). The observed flux at a given time after the burst is not expected to fade significantly with increasing redshift as time dilation leads to earlier observations of the afterglow in the GRB restframe and it is expected that GRBs should be detectable out to $z \gtrsim 10$ (Ciardi & Loeb, 2000) making them the most easily observable distant objects in the very early Universe. Before we give an introduction to the current status of GRB afterglow spectroscopy, espcially with high resolution spectra, we mention a range of other methods to study high redshift galaxies.

2.1.1 INDIRECT OBSERVATIONS - QUASAR ABSORPTION LINE SYSTEMS

Before direct imaging of high-redshift galaxies were available, the only way to study high redshift galaxies were via intervening absorption systems in spectra of high redshift quasars (e.g Pettini et al., 1997; Rauch, 1998; Wolfe et al., 2005). The sample of these QSO absorbers comprises several thousand systems now (Steidel & Sargent, 1992; Prochaska et al., 2005, e.g.) and for some of these systems, there are high resolution spectra available (e.g. Boksenberg et al., 2003). The host galaxies of QSO absorbers have only been detected in a few cases, e.g. Warren et al. (2001) for detections with NICMOS/*HST* or Fynbo et al. (2003b) by searching for Lyman α emission. This is not only a consequence of the faintness of those galaxies, but also due to their small angular distance from the QSO itself (e.g. at z=3, an impact parameter of 10 kpc corresponds to only 1.″0).

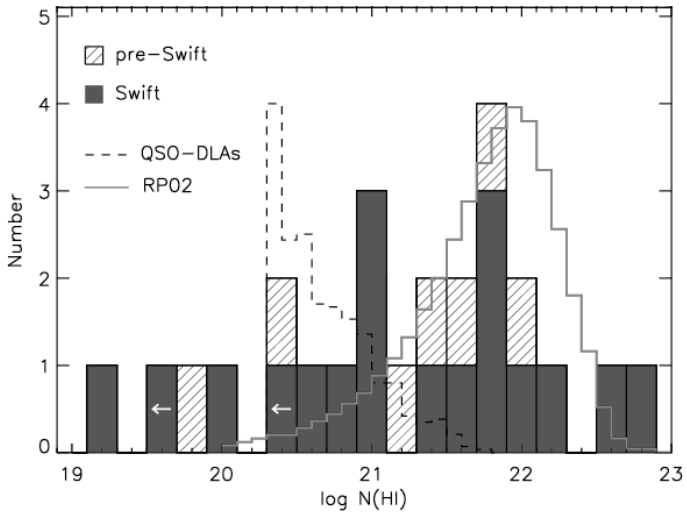

Figure 2.1: *HI distribution in GRB and QSO sightlines, RP02 denotes the expected HI distribution for bursts in moleculars clouds similar to those in the Galaxy (from Jakobsson et al., 2005).*

The use of QSOs as a lightsource to study those high redshift galaxies has its advantages and disadvantages. Compared to GRBs, they are not fading rapidly and hence observations can be done and repeated at any time. However, immediately after the burst, a GRB has a much higher luminosity than the most luminous quasar giving a huge increase in the S/N, therefore, early observations of GRBs are so crucial. Furthermore, the underlying spectra of QSOs are not simple powerlaws as it is the case for GRBs. This makes it difficult to derive the amount of dust and the extinction law in those galaxies from the spectral shape of the continuum. And last, they do not necessarily probe dense star-forming regions inside a galaxy as GRBs do. It is likely that if a QSO sightline passes through the main part of a galaxy, it would become undetectable, but note Prochaska et al. (2007) who suggest that GRB-DLAs column densities should also be observable in QSO sightlines and the nondetection is only an effect of the very low cross section of those systems.

According to their N_{HI}, QSO absorbers are divided into different populations, Damped Lyman Alpha Systems (DLAs) with $\log N_{HI} > 20.3$ cm^{-2}, Lyman Limit systems (LLSs) with $17 < \log N_{HI} < 20.3$ and Lyman α forest absorbers with $\log N < 17$. QSO-DLAs hardly extend out to $\log N = 21.8$, whereas GRBs have been observed with $\log N > 22.5$ (Jakobsson et al., 2005; Prochaska et al., 2007) (see Fig. 2.1). This suggests that QSO-DLAs tend to probe the halo gas or the outer parts of the ISM of the intervening galaxies whereas the GRB probes more centrally located ISM (see Fig. 2.2). Interestingly, however, GRB sightlines seems to span a larger range of neutral column densities than expected from the distribution of column densities from molecular clouds (see Fig. 2.1).

DLAs and LLS do usually also show strong absorption lines of Mg II, Fe II and/or higher ionization lines such as C IV. Their column densities correlate roughly with the neutral hydrogen column (for a review on DLAs see Wolfe et al., 2005). It is suggested that Mg II absorbers are connected to galaxy halos (Churchill et al., 2005), but Mg II and C IV are likely probing different regions in QSO sightlines. Interestingly, the number of Mg II absorbers along GRB sightlines is larger than for QSO absorbers (Prochter et al., 2006) while this is not the case for C IV (Sudilovsky et al., 2007; Tejos et al., 2007). Recently, also highly excited lines like O VI have been discovered in QSO absorbers (e.g., Churchill et al., 2000; Tripp & Bowen, 2005). When

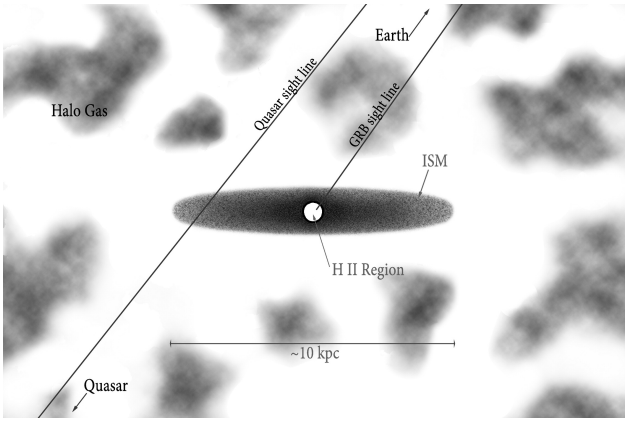

Figure 2.2: *Suggested sightlines of QSO and GRB absorbers (from Prochaska et al., 2008a, Fig. 1)*

studied with high resolution spectroscopy, the absorption lines usually split into a number of narrow velocity components which have total velocity spread of a few 100 km/s, some extending out to $\sim$ 1000 km/s. Theories suggest that DLAs might be the early universe progenitors of todays spiral galaxies.

2.1.2 DIRECT IMAGING

Lyman break galaxies (LBGs) are galaxies that are discovered through the drop of the flux at the Lyman break (912 Å) which gets redshifted into the optical regime above z$\sim$2.5 (Steidel et al., 1996, 2003) and can be detected using several broadband filters blue- and redwards of the expected Lyman dropout. Subsequent spectroscopic analysis of those galaxies reveals a high star formation rate of up to 70 $M_\odot$/yr and higher metallicites than DLAs (Pettini et al., 2001; Erb et al., 2006). Spectra with both emission and absorption lines detected usually show redshifted Lymanα emission with v up to 1000 km/s and blueshifted absorption lines suggestive of a large-scale outflow from star forming regions (see Chapter 2.5.2). There are indications that these high SFRs are sustained over a long timescale, therefore, these galaxies accumulate quickly a large mass and might be the progenitors of today's elliptical galaxies or the bulges of spirals.

Another method to detect high redshift galaxies is to look for Lyman α emission. This is mostly done through narrow band imaging targeting Lyman α emitters at a fixed redshift. Several hundred of them have been identified out ot $z = 6.7$ and future surveys might detect them out to $z = 8.8$ (Nilsson et al., 2007). They probe the star forming galaxy population as Lymanα emission is directly related to the age of the stellar population if there is no issue of dust extinction or geometric effects from different viewing angles (Laursen & Sommer-Larsen, 2007). Spectroscopic follow-up, even though often very challenging and time consuming, confirm the high SFR and the young ages expected.

A few other samples have been identified with other techniques such as SCUBA galaxies selected by their strong sub-mm emission indicating a very high SFR (e.g. Smail et al., 2002). Dustobscured galaxies (DOGs) deteced in the mid-IR by *Spitzer* at z$\sim$ 2 might be a population of dusty starburst galaxies in an evolutionary stage between SCUBA galaxies and LGBs or distant red objects (DRGs) (Dey et al., 2008). And a last method to look for very high redshift galaxies is to do spectroscopy of lensed galaxies that lie at the critical lines following caustics of lensing clusters for a certain redshift (e.g. Stark et al., 2007).

2.2 ABSORPTION LINE PROFILES AND COLUMN DENSITY DETERMINATIONS

Before we dig deeper into the processes happening in the interstellar medium and what can be derived from them, there will be a brief description of the basic properties of absorption lines. This section derives the absorption line profile and its dependence on the optical depth, how to obtain equivalent width and column densities by using different methods and issues arising from line blending and limited instrumental resolution.

2.2.1 DOPPLER, LORENTZ- AND VOIGT PROFILES

Absorption lines in the interstellar medium are broadened by two main mechanisms. The first is the so-called Doppler broadening from the movement of the atoms with different velocities with typical velocities of a few to a few tens of km/s. As the velocities follow a Maxwell distribution, the resulting line profile is a Gaussian. The other mechanism is the natural broadening from the lifetime of the transitions quantified by the damping parameter γ and the resulting line profile a so-called "Lorentz profile" with shallower wings than a Gaussian. The combined profile from these two effects is then a convolution of the two functions and called a "Voigt" profile. The line profile f(λ) is obtained by the following equation:

$$f(\lambda) = e^{-\tau(\lambda)} = e^{-\tau_0 H(a,u)} \tag{2.1}$$

where H(a,u) is the Voigt function

$$H(a,u) = \frac{a}{\pi}\int_{-\infty}^{\infty}\frac{e^{-y^2}dy}{a^2+(u-y)^2} \tag{2.2}$$

$$a = \frac{\gamma\lambda}{4\pi b} \tag{2.3}$$

$$u = -\frac{c}{b}\left(1-\frac{\lambda}{\lambda_0}\right) \tag{2.4}$$

with b the Doppler parameter in km/s, and c the speed of light. $\tau(\lambda)$ is called the optical depth which is related to the line intensity according to $I(\lambda) = I_0 e^{-\tau(\lambda)}$. Fig. 2.3 illustrates what happenes with the lineshape for different optical depth. For this plot, the voigt function in IDL was used taking different values for τ_0, the central optical depth. The equivalent width (EW) is defined as

$$W = \int 1 - e^{\tau(\lambda)}\delta\lambda = \int\left(1-\frac{I_\lambda}{I_0}\right)\delta\lambda \tag{2.5}$$

which is the width of a rectangular with height 1 and the same surface as the flux of the line.

The optical depth of the absorbing material depends either on its thickness or of the atoms per volume. As one cannot distiguish these two possibilities when measuring the strength of absorption lines, the column density N=$\int ndl$ is introduced with n the density of the atoms and l the path length of the absorbing material. For $\tau << 1$, the column density grows linearily with the EW whereas later on, it can only grow in the wings and therefore the W $\propto \sqrt{ln(N)}$. For very strong lines, the relation is W $\propto \sqrt{N}$.

If one now has a series of lines with different strength more or less blended together (as is the case f.ex. if the line-of-sight intersects several clouds with similar composition), the situation becomes more complicated. If the resolution is high enough, one can fit the different components and get the true column density. If the instrumental resolution however is larger than the

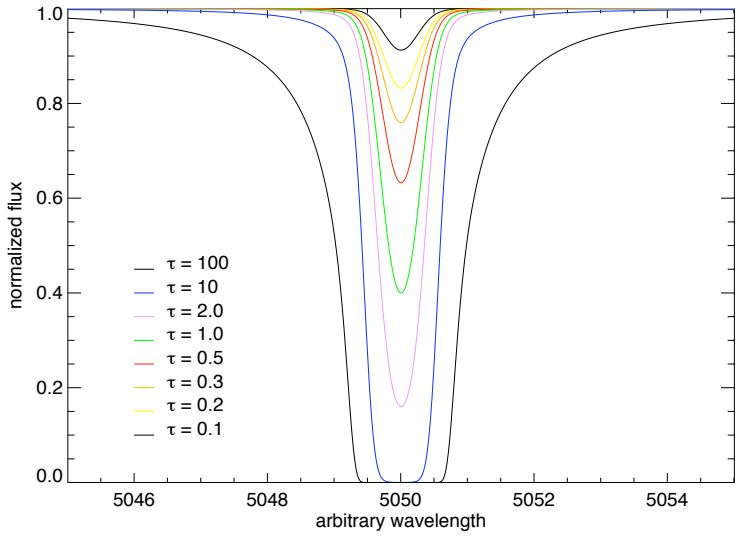

Figure 2.3: *Plot with Voigtprofile for different values of the central optical depth.*

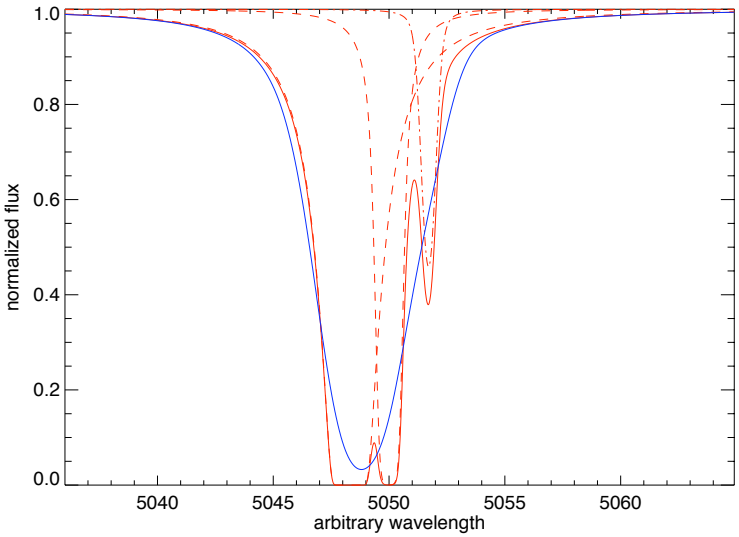

Figure 2.4: *Simulated absorption lines where the line of sight intersects three clouds with three different optical depths. The red dashed lines are the profiles of the individual cloud, the red thick line the combined profile as if would be observed with infinite resolution and blue the profile observed with an instrument with lower resolution.*

distances of the different lines, the lines get blended as they are convolved with the resolution of the instrument. Fig. 2.4 shows a simulated line consisting of 3 different components with different optical depths (red dashed lines), the true combined profile that would be observed if the instrumental resolution was 0.01 Å (red thick line) and in case the resolution was $\sim$ 5 Å (blue line). The reduced resolution affects both the position of the line center and the measured EW. In the case present in Fig. 2.4, the true EW from integrating the total resolved profile is 5.06 Å, whereas the low-resolution EW is only 4.88 Å.

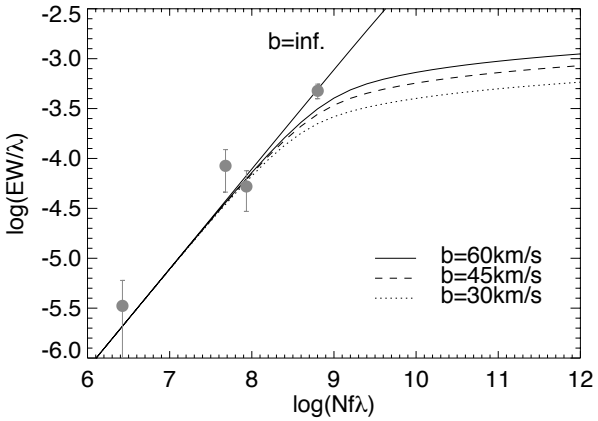

Figure 2.5: *CoG fit with simulated Si II absorption lines. The best fit b parameter is shown the bold line, as comparison, b=45 and 30 km/s are plotted.*

2.2.2 THE CURVE OF GROWTH METHOD

The Curve of Growth was originally developped for determining column densities for a certain ion if several transitions of the same ion in the same ionization state are available. However in most objects there are not enough transitions of the same species available. Therefore, the method has been used taking different ions and fitting them with the same b parameter, the "effective b-parameter", which is then called "multi-ion-single-component curve of growth" or MISC-CoG. This neglects the possibility that the different ions might originate in different parts of the ISM with different properties.

As mentioned above, N depends on EW according to the saturation of the line. For unsaturated lines ($\tau < 0.1$), the relation is

$$N = \frac{W}{\lambda} \frac{1.1 \times 10^{20} \mathrm{cm}^{-2}}{f\lambda[\text{Å}]} \tag{2.6}$$

and on the flat part

$$\frac{EW}{\lambda} = 2b/cF(\tau) \tag{2.7}$$

$$F(\tau) = \int_0^\infty (1 - exp(-\tau_0 e^{-x^2})\delta x \tag{2.8}$$

$$\tau_0 = 1.497 \times 10^{-15} \frac{f\lambda_0 N}{b} \tag{2.9}$$

We did a CoG fit with arbitrary EWs for different transitions of Si II shown in Fig. 2.5, the best fit b parameter is 60 km/s due to the one saturated line which lies on the flat part and the derived column density is then log N(Si) = 13.2 cm^{-2}. Taking our simulated line profiles from above and assuming they are Si II transitions, high resolution spectra would give the EWs for each of the three components separately. The column densities according to the simulated CoG fit would be log N = 14.3, 15.4 and 16.3 cm^{-2} and the total column densitiy would then simply be the sum of the three column densities log N = 16.4 cm^{-2} . If we take instead our smeared profile, we do not know how many transitions with which EWs the line actually consists of and we would take the total EW which would place them on the flat part of the CoG and give a column density of log N = 18.1 cm^{-2} but this value is very sensitive to the b parameter taken.

It is also clear that if one includes saturated transitions in the fit, the CoG best fit leads to a higher b value. This again means that the column densities derived from the fit are lower. Saturated transitions in low resolution spectra would usually split up into several components that are each of them unsaturated, which would then lead to lower b parameters. If we exclude the saturated transition in our simulated CoG fit, the best fit b parameter is only 25 km/s and therefore the transitions which before lied on the linear part infact are somewhat saturated and we also get a higher column density of log N(Si) = 13.6 cm^{-2}. Prochaska (2006) have investigated this issue for GRB spectra in detail.

2.2.3 APPARENT OPTICAL DEPTH

For high resolution spectra and not heavily saturated lines, it is possible to use another method to find the column densitiy which is called "apparent optical depth" (AOD) as first introduced by (Savage & Sembach, 1991). The column density is obtained by the following equation:

$$\log N_{\rm a}(v) = \int N_{\rm a}(v)\delta v = \int \log\tau_{\rm a}(v)\delta v - \log(f\lambda) + 14.576 \tag{2.10}$$

We write the equation here in the logarithmic form as column densities are usually given as log N. The optical depth is simply the ratio of the intensities (see eq. 1.5). If the instrumental resolution is high enough, we can ignore the instrumental broadening and $\tau_{\rm a}(v) = \tau(v)$.

Savage & Sembach (1991) then show that if we now take two transitions of the same ion and determine their column densities, they should give the same value when applying the AOD method if there is no hidden saturation in any of the profiles. If this is the case, then the column densitiy would be smaller for ions with smaller fλ values. Thus, in order to apply this method, we need both a sufficiently high resolution and weak transitions or correspondingly small column densities for strong ions.

2.2.4 VOIGT PROFILE FITTING

If the spectra provide high enough resolution to resolve the actual shape of the line profile with the dampling wings, one can adopt a direct fit of the Voigt profile.

$$EW = \int (1 - e^{-\tau(\lambda)})\delta\lambda = (1 - e^{-\tau_0 H(a,u)})\delta\lambda \tag{2.11}$$

Today, a range of programs is available that reads in atomic data from a database (most programs use the atomic data provided by Morton (2003) and fits the different lines. One example is the FITLYMAN programm in MIDAS (Fontana & Ballester, 1995) which fits multiplets by simply giving the redshift and the name of the lines and also different velocity components. As an example, Fig. 2.6 shows a fit of the DLA of GRB 07011 which has a column density of 21.3 cm^{-2}. Further fitting examples will be shown in Chapter 4 and 5.

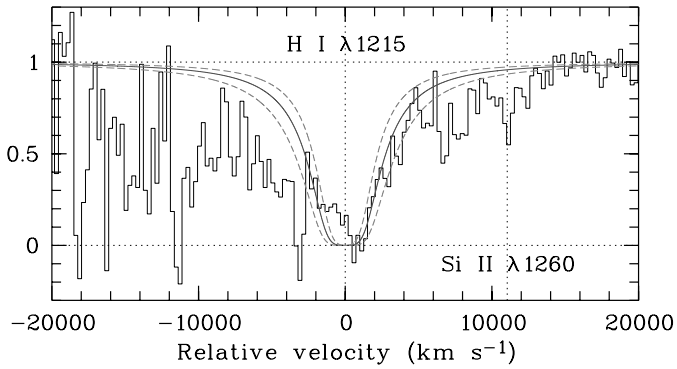

Figure 2.6: *FITLYMAN fit of the Lyman α absorption in the spectrum of GRB 070611 (credit: C. Ledoux)*

2.3 THE METALLICITY PROBLEM

2.3.1 QSO AND GRB METALLICITIES

The determination of the metal column densities allows us to derive the abundances of the individual elements in case also HI is detected. We can then compare the measured abundance with the one in the solar neighbourhood (Asplund et al., 2004) which then gives us the metallicity of the material we are probing:

$$[\mathrm{M/H}] = \log(\mathrm{N(M)/N(HI)}) - \log(\mathrm{N(M)}_{\odot}/\mathrm{N(HI)}_{\odot}) \tag{2.12}$$

[M/H] = 0 is solar metallicity ($Z_{\odot}$), [M/H] = –1 corresponds to 1/10 $Z_{\odot}$. This is, however, not necessarily the metallicity of the GRB or QSO absorber host galaxy, but only the metallicity along the line of sight, which can be very different from the average metallicity of that galaxy. The best element to determine the metallicity is Zn II as it is almost not affected by dust depletion (see next Chapter). If Zn II is not available, one uses Fe II, Si II, or S II, but Si II is often saturated in GRB spectra and the metallicity only a lower limit.

QSO-DLAs as well as GRB hosts show an evolution of metallicity with redshift in such a way that the metallicity increases with decreasing redshift (Fynbo et al., 2006a; Savaglio, 2006; Prochaska et al., 2007). However, GRBs have on average higher metallicities than QSO absorbers and also higher than the cosmic mean metallicity (see also Prochaska et al., 2007, Fig. 3). Most of them lie above $1/10\ Z_{\odot}$ which is the value expected for GRB progenitors from some theortical models (Woosley & Heger, 2006). As mentioned in Chapter 2.2.2, when low-resolution data are taken for the determination of the column densitiy by the CoG method, column densities tend to be underestimated and thus the metallicity. Therefore, the slope of the metallicity evolution of GRBs with redshift becomes very shallow. Savaglio et al. (2008) even claim that there is no metallicity evolution with redshift at all. Furthermore, GRB-DLAs also have higher metal column densities than QSO-DLAs (e.g. Savaglio et al., 2003).

The difference to QSO absorbers can be explained if GRB sightlines probe denser parts of the galaxy, or if GRBs reside in galaxies with higher masses and therefore higher metallicities. It is interesting to note that LBGs around z$\sim$3 have higher metallicities than QSO-DLAs, about the same range that is occupied by GRB-DLAs (Pettini et al., 2001), however, those metallicities have usually ybeen derived from emission lines (but see Pettini et al., 2002). LBGs might be the predecessor of todays massive ellipticals and the heavy star formation observed for LBGs seems

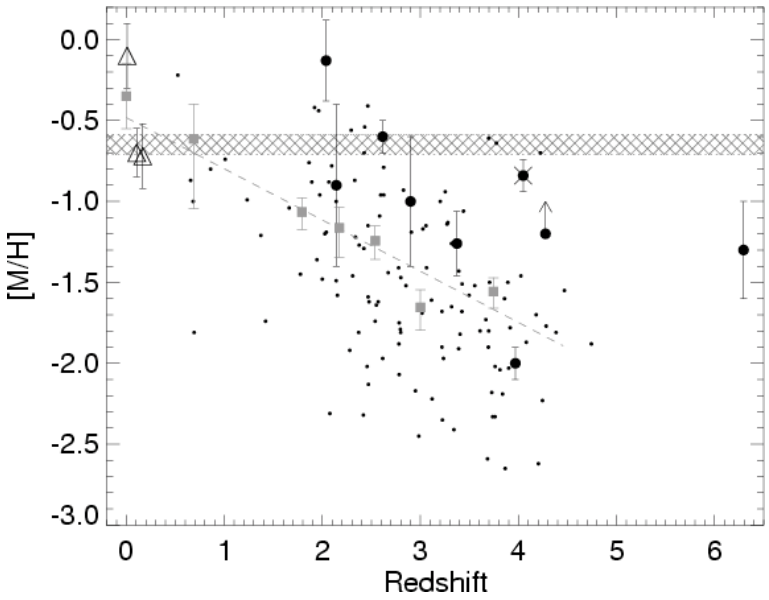

Figure 2.7: *Metallicities for GRBs (thick points) and QSO absorbers (small dots) at different redshifts The grey squares are the average column density weighted metallicity evolution as derived by Zwaan et al. (2005). The very nearby GRBs (open triangles) have emission line determined metallicities while the rest are metallicities from resonant absorption lines. The hatched line indicates the theoretical threshold for a start to produce a GRB (from Fynbo et al., 2006a).*

to have enriched them already quite early on. On the other hand, sub-DLAs ($19 < \log N_{HI} < 20.3$) also show higher metallicities (Péroux et al., 2007), especially at $z < 2$. They argue that sub-DLAs might be less affected by dust extinction (in case this scales with the Zn column density) and therefore higher metallicity systems can be detected. Or it might be that sub-DLAs arrise in more massive galaxies than DLAs. However, this is in conflict with the suggestion that the HI column densitiy correlates with the path length through the galaxy and one would assume then that sub-DLAs probe the very outermost regions which likely are not strongly enriched whereas a DLA would probe regions closer to the center of the galaxy.

By taking a sample of QSO-DLAs observed with high resolution spectrographs to resolve the absorption lines, there seems to be a correlation between the velocity width of low ionization lines and the metallicity (Ledoux et al., 2006) for z>1.8 galaxies. Cold dark matter simulations show further that the velocity width of DLAs are correlated with the mass of the dark matter halo and this again with the luminosity. Luminosity-metallicity relations and velocity metallicity relations were also found for very low redshift galaxies (Tremonti et al., 2004) and Mg absorbers at redshift z = 1 – 2 (Nestor et al., 2005). Apparently, this relation is valid from the early to the present universe even though the slope of the correlation at different redshifts seem to vary.

Fynbo et al. (2008b) investigated the theoretical correlation between the mass, the HI cross-section and the metallicity and find that higher they are consistent with the mass-metallicity relation. This would imply that GRB hosts do simply have higher metallicities because they have higher masses. The few detections of GRB hosts at high redshift might be consistent with that assumption, but it could also be that most of the population are faint galaxies that go undetected. Whether the high metallicitiy of GRB hosts at high redshift is simply a scaling issue or due to internal properties of the hosts is still not fully explained.

2.3.2 RELATIVE ABUNDANCES AND DUST DEPLETION

The relative abundances of elements produced in different nucleosynthesis processes in stars and during the collapse of massive stars tells us something about the star formation history and age of the galaxy. The so-called α elements Ne, Mg, Si, S, Ar, Ca and Ti are produced by α -capture (He) during silicon fusion taking place in massive stars before the SN explosion. Iron-peak elements like V, Cr, Mn, Fe, Co and Ni get produced in SN Ia which come from less massive stars. GRB-DLAs show generally a higher α/Fe ratio than QSO-DLAs (Prochaska et al., 2007) which can either have a nucleosynthesic origin or also be due to dust depletion differences for α elements and Fe (differential dust depletion). The first possibility seems likely as GRBs are expected to occur in actively star forming galaxies and the timescales to enrich the ISM significantly with Fe produced in SN Ia might be too short for galaxies at high redshifts.

It is known from the local universe that some elements get depleted onto dust grains which are present in all star forming regions to some extend. This means that they get attached to the grains and therefore are not longer in the gas phase of the ISM so they cannot be detected. The measured column densities of these elements do therefore underestimate the total column density and hence their actual abundance. How large a fraction of each element is affected by this dust depletion depends on the properties of the element such as the ionization potential or the condensation temperature (Savage & Sembach, 1996) as well as the temperature of the ISM.

Zink gets very little depleted and is therefore in principle the most suited element to determine the metallicity. However, already for z$\sim$3, Zn II is quite far in the red and often affected by atmospheric absorption lines. S II is also little affected by dust depletion, but it is a rather weak line and not always detected. The other elements taken for the metallicity determination are affected by dust depletion and the column densities have to be corrected. Savaglio (2006) compared the [Fe/Zn] and [Si/Zn] abundances to the Zn column density for GRBs, QSOs and nearby stars and found empircal fits how to correct Fe dust depletion:

$$\log\mathrm{N_{ZnII}} = (1.47 \pm 0.11)\log\mathrm{N_{FeII}} + (-9.4 \pm 1.7) \tag{2.13}$$

If one has several elements detected, it is possible to derive a relative abundance pattern which depends on the temperature and density of the ISM. An example for five GRB hosts and the expected pattern of different ISM states in the MW is shown in Fig. 2.8.

From the relative abundances, one can also determine the absolute extinction in the line of sight assuming a certain extinction law. Measurements of the extinction in the line-of-sight towards stars in the MW, the LMC and SMC have established three different extinction laws. The MW extinction law shows a characteristic "bump" at 2175 Å likely caused by carbon or oxygen rich dust particles which is also present in the LMC but less pronounced. The continuum of GRB afterglows is usually smooth and therefore the SMC law is usually applied. Prochaska et al. (2007) derive the extinction in the V-band, $\mathrm{A_V}$ by assuming a relative gas-to-dust ratio compared to the SMC $\kappa/\kappa_{\mathrm{SMC}}$ and therefore

$$A_{\mathrm{V}} = 2.74\mathrm{E(B-V)}\kappa/\kappa_{\mathrm{SMC}} \tag{2.14}$$

$$\log\mathrm{E(V-B)} = \log\mathrm{N_{HI}} - 22.95 \tag{2.15}$$

$$\kappa/\kappa_{\mathrm{SMC}} = 10^{[\mathrm{M/H}]+0.7}\left(\frac{1-10^{\Delta_i-[\mathrm{M/Fe}]}}{0.9}\right) \tag{2.16}$$

where M is some metal (usually sulphur) and Δ_i is the contribution to [M/Fe] originating from the nucleosynthesis history and not the dust depletion where $\Delta_i = 0$ for the SMC and $\Delta_i = 0.3$dex for GRB-DLAs.

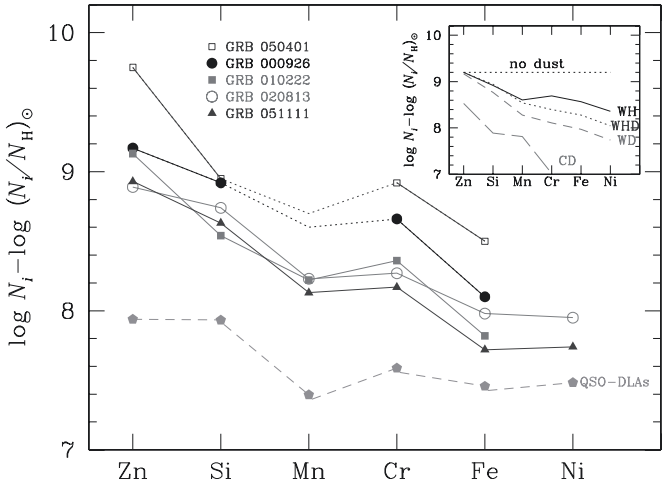

Figure 2.8: *Relative depletion pattern of 5 GRB sightlines, QSO-DLAs and the expected pattern for the MW warm halo (WH), warm disk (WD), warm halo+disc (WDH) and cold disc (CD) (from Savaglio, 2006).*

Taking these calculations, GRB hosts seem in general to show a low extinction along the line-of-sight (Prochaska et al., 2007). However, the relative abundance pattern indicate that some of the ions must be depleted onto dust grains and the depletion pattern resembles the one found in the warm disc and halo of the MW (Savaglio, 2006). How this can be explained together with the low extinction as also derived from the spectral energy distribution (SED) of the afterglow (Kann et al., 2006; Starling et al., 2007; Kann et al., 2007), is still an open question. One possible solution to this problem is destruction of the dust present in the line-of-sight by the GRB and afterglow radiation (e.g., Waxman & Draine, 2000). Lately, there has also been a MW like dustbump discovered in a GRB afterglow spectrum (Krühler et al., 2008, Éliasdóttir et al. in prep.).

2.4 DISTANCES

One of the main problems by studying absorbers in the line of sight towards GRBs is their exact location with respect to the GRB itself. This again is important to know which part of the GRB host galaxy we are actually probing and whether we can use the GRB absorbers to study the near environment of the GRB or the galaxy itself or even the intergalactic medium. If we are lucky that the burst has the right (low redshift) to observe both emission lines from the galaxy (see also Chapter 6) and absorption lines from the line-of-sight plus the spectrum has high enough resolution to obtain kinematical information, this issue is easy to settle. The only two fortunate cases so far were GRB 030329, presented in Chapter 4 at z=0.1686 and GRB 060218 (Wiersema et al., 2007) which showed a double component in both emission and absorption at the same velocities suggesting a common spatial origion. A few other hosts had both emission and absorption lines detected but only at low resolution: GRB 990712 (Vreeswijk et al., 2001), GRB 970508 (Reichart, 1998), GRB 020813 (Barth et al., 2003) and GRB 020405 (Masetti et al., 2003).

In the last few years, a number of discoveries and new methods have become available and new ideas have been developed in order to get rough assumptions on the distance from the burst only from absorption line spectra. The picture which is now emerging is that most of

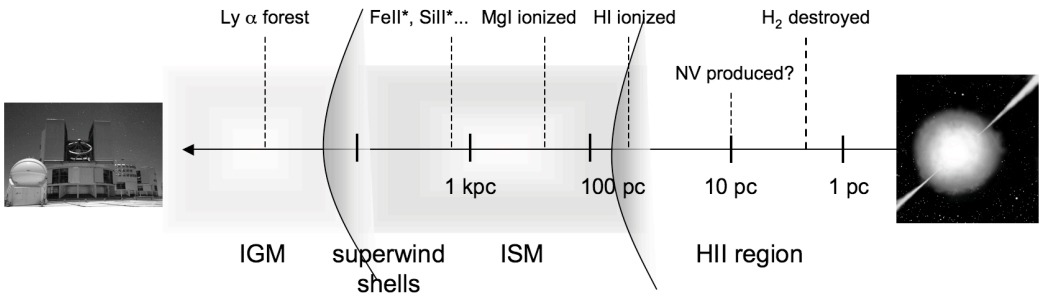

Figure 2.9: *Scematic illustration of the different locations where the absorption components are created in the GRB host (adopted from J. Prochaska, private communication).*

the material we see in absorption is very likely not from the circumstellar medium of the GRB but from material in the ISM of the galaxy, at least 1 kpc away from the GRB, or even due to galactic outflows. However, it is still under debate if this can necessarily be applied to high ionization transitions such as C IV. Fig. 2.9 illustrates where the absorption components are likely to happen.

2.4.1 FINESTRUCTURE LINES

The first conclusive evidence that the GRB indeed has an effect on its surroundings was the discovery of finestructure lines (Vreeswijk et al., 2003). Those were only detected in environments with extreme radiation fields such as in η Carinae (Gull et al., 2005) or Broad absorption lines quasars (BALs) (Hall et al., 2002). In QSO absorbers CI* and CII* have been found (see Silva et al., 1998, and references therein) and SiII* had been found in one LBG (Pettini et al., 2002). Fine structure transitions arrise from the split of the atomic transitions into different J (the total angular momentum) due to spin-orbit coupling. The transitions between the different fine structure levels of one main level lie in the IR for common elements of the ISM like C, Si, Fe and O. The energy difference between the ground state and the finestructure transition is then very close to those of the normal excited states and have therefore similar wavelengths as their corresponding resonant transitions. But how are these levels then populated?

Silva et al. (1998) modelled the population of the fine structure levels assuming steady state conditions, which means the processes populating and depopulating the level equal out. Three mechanisms seem plausible to populate the finestructure levels: Direct excitiation by the cosmic microwave background (CMB), collisional excitation and direct excitation by IR or indirect excitation by UV photons and subsequent fluorescence. They calculate the expected ratios for C, Si and Fe and for different population mechanisms. Their code "popratio" can be downloaded at http:/www.cpc.cs.qub.ac.uk/cpc .

From the ratio between finestructure and groundstate transitions one can now determine rough distances if the flux at the actual GRB site is know. The ratio depends on the strength of the radiation field which is usually written relative to the average MW far-UV radiation field G_0=1.6$\times 10^{-3}$ erg/cm^2/s (Habings constant). Different atoms and different excitation levels than have different dependences on the relative radiation field as shown in Fig. 2.10 for the first excited states of Si II, Fe II and O I. The radiation field can be estimated to decrease with $G/G_0 \propto 1/r^2$ and if one calculates the radiation field G/G_0 at the GRB from afterglow observations (see next Section), this gives a rough estimate on the distance for the other components.

The story becomes even more constraining if variations in the finestructure transitions can be

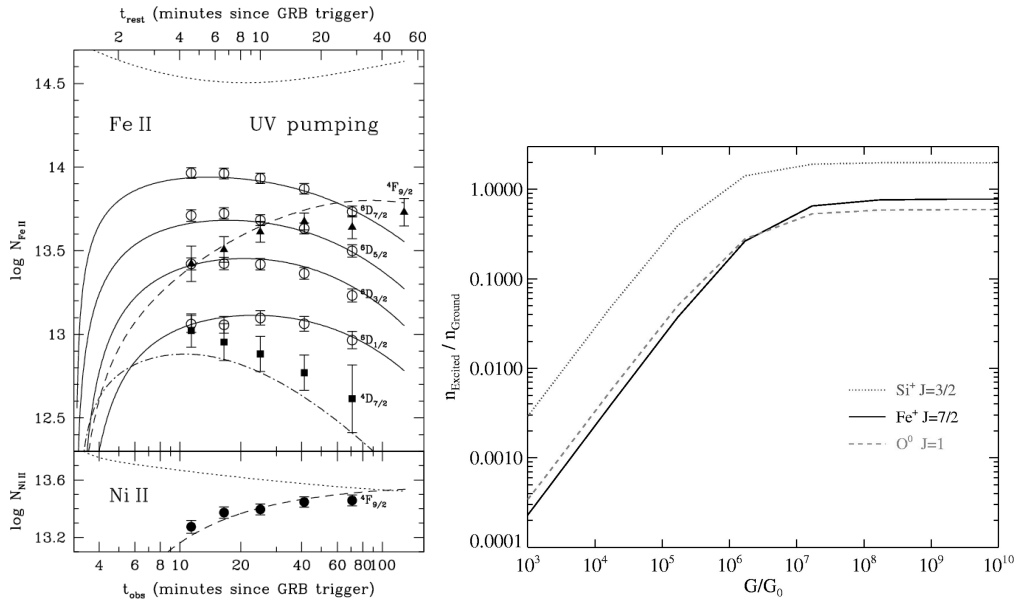

Figure 2.10: *Fits to the varying finestructure lines in GRB 060418 assuming IR and UV pumping .*

observed. Vreeswijk et al. (2007) obtained for the first time a series of very early high resolution spectra which showed clear variations of the finestructure transitions from Fe II and Ni II. Their modelling provides strong evidence for the UV pumping scenario and excludes both pumping from IR photons as well as collisional excitiation with high confidence (see Fig. 2.10). They can then also derive a rather accurate distance from the burst from the radiation field needed for the levels to get excited and decay as observed.

2.4.2 NEUTRAL SPECIES

The strong emission from the GRB and its afterglow is expected to ionize the ISM around it. However, neutral species, especially Mg I, have been detected in most of the GRB afterglow spectra. If we know the number of ionizing photons from the afterglow, we can derive a minimum distance to the GRB:

$$r_{\rm min} = 100 \left(\frac{\phi \sigma_{\rm ph}}{1.1 \times 10^{43}} \right) [\rm pc] \tag{2.17}$$

$\sigma_{\rm ph}$ is the cross section for Mg I which peaks at the ionization potential at 7.64 eV corresponding to $\sigma_{\rm ph}$=1.7×10^{-18} cm^2. ϕ is the total photon number that have the energy of the adopted cross section value, e.g. 7.6 eV, emitted over the time until the observations. The luminosity of the afterglow at a certain time t can be obtained from the flux observed at Earth at a certain frequency ν with $L_\nu(t) = F_\nu^{\rm obs} \frac{4\pi d_{\rm L}^2}{1+z} \nu[\rm Hz](t[s])^{-\alpha}$. In order to get the total luminosity, one needs to integrate $L_\nu(t)$ over the time until the observations (neglecting any non-powerlaw behaviour of the afterglow) and then determine the number of photons of the needed energy to obtain the luminosity [1]. The distances derived are usually $>$ 50 pc or more implying that the absorbing material is not in the vicinity of the burst, otherwise it would have been ionized.

[1] 1eV=1.602×10^{-12}erg, 1Jy = 10^{-23} erg/cm^2/s/Hz

It has also been suggested by (Perna & Loeb, 1998) that as the ionization front from the GRB expands, more and more ISM gets ionized and the EW of neutral species should decrease. If one can exclude a variability of the EW, an even stronger limit can be derived by

$$r_{\min} = \sqrt{\frac{\phi \sigma_p h}{4\pi ln(N_i/N_f)}} \,[\mathrm{pc}] \tag{2.18}$$

with N_i/N_f the upper limit on the variability of the column density (or the EW). Those limits usually lie in the order or 0.5–1 kpc for an upper limit on the variability of 25%.

It is also interesting to note that there is no firm detection of molecular hydrogen in GRB afterglow spectra so far (Tumlinson et al., 2007), but see also Fynbo et al. (2006a). GRBs are assumed to be situated in molecular clouds as all SF in the local universe is because cooling through molecular hydrogen provides the necessary high densities for stars to form. This is also suggested by the large observed HI column density for GRBs. However, the radiation of the progenitor itself is enough to ionize the HII region and hence dissociate also H_2. An average UV radiation field in the galaxy from young stars would also be sufficient to dissociate H_2 in the line-of-sight (Whalen et al., 2008).

2.4.3 Indication for material from the circumburst medium? - NV in GRB sightlines

Highly ionized species might instead probe a different region in the line-of-sight. N V, which has a high ionization potential of 77 eV, has been detected in both the spectra of LBGs and GRB afterglows and also in sightlines across the halos of the MW and starburst galaxies. NV absorption in LBGs and GRBs usually trace the velocities of the lower ionization species and for GRBs also those of the finestructure transitions. The main optical depth lies usually within 20 km/s of those for the lower ionization species. In GRBs, they are also relatively narrow (b $<$ 50 km/s) and have a large column densitiy of log N $> 10^{14}$ cm^{-2} (Prochaska et al., 2008b). In LBGs as well as in the local universe, the column densities observed are much smaller, only gas local to quasars show strong N V absorption.

Their origin in the local universe is believed to be either collisionally ionized gas with very high temperatures or gas cooling after a shock. In LBGs it is usually associated with a galactic scale outflow. Prochaska et al. (2008b) also excludes collisional ionization by wind from the progenitor star as the shock has to reach beyond the distance where the GRB fully ionizes the gas. He therefore concludes that direct photoionization by the GRB and afterglow emission like suggested for the quasar N V absorption might be the best explanation. From similar considerations as above, the estimates distances are in the order of a few tens of pc.

2.5 The dynamical universe

2.5.1 Winds from the progenitor star?

Some of the first high resolution spectra obtained showed a very large velocity spread in some of the absorption lines, e.g. GRB 021004, GRB 020813, GRB 050505 and GRB 051111. GRB progenitors are likely Wolf Rayet (WR) stars the experience winds and mass loss over the stage of their evolution. Already the radiation from the main sequence star creates a shell as it sweeps up the interstellar medium later hit by the denser red giant wind. The powerful WR wind then again disturbes the structures created before. A first suggestion was therefore that those

components might originate either from material swept up by the prognenitor wind or by mass losses from the star. Indeed, absorption from mass losses has been observed, e.g. spectra of η Carinae, a massive luminous blue variable star that experienced a large outburst and mass loss about 150 years ago. Those spectra have e.g. blueshifted Mg II absorption profiles with widths of $\sim$ 200 km/s. Also P-Cygni profiles [2] with absorption from winds up to several 3000 km/s have been observed (for a review on WR stars see Crowther, 2007).

Inspired by the observed profiles in GRB afterglow specra, van Marle et al. (2005) modelled the outflow and clumping from the progenitor and calculated the expected absorption profiles. They conclude that narrow profiles come from the wind-blown ISM while broad profiles originate in shocks. The total profile should then have a strong absorption in the middle accompagnied by two narrow profiles. The expected velocities range to about 700 km/s but higher velocities are acceptable. Such a scenario has been favoured by most authors for the high velocity components. For the absorption lines in GRB 021004 and GRB 050730, however, Chen et al. (2007) note that the detection of low ionization species in the spectrum which are not expected from the calculations in the previous section and therefore, they disfavour an origin in the vicinity of the burst. However, Starling et al. (2005b) suggest a double jet model for GRB 021004 where the low ionization species could survive in a wider and weaker jet.

It had been argued that the frequent occurance in GRB spectra would disfavour the possibility that those structures could arrise from an intervening system. However, those high velocity components do not seem so frequent after all as they should also be detectable in low resolution spectra. Chen et al. (2007) concluded that only 1 out of 5 systems show high velocity components in C IV and conclude that their incidence in GRB sightlines is consistent with the one found for QSO-DLAs. Fox et al. A&A submitted, however, see these components in 5 out of 7 high resolution spectra. Chen et al. (2007) furthermore detect a faint galaxy near the position of the host in *HST* images which they conclude might be the host of the intervening system causing the "high velocity" component. Even though the possibility of an origin in the circumburst medium cannot be completely ruled out, it is nowadays mostly disfavoured.

2.5.2 Rotating disks and Superwinds

Most afterglow spectra only show a relatively small velocity spread of a few hundred km/s, however, larger than is it usually observed for QSO absorbers. One explanation for these systems is that simply the interstellar medium in the host galaxy in the line of sight causes those absorption systems. If one assumes a sort of rotating disk with the GRB shining through parts of most of it, one expects absorption lines as scematically shown in Fig. 2.11.

Not always, however, can all the components be explained with a rotating disk or infalling material. The velocity components trace the rotational velocity of the disk, if the velocity spread of these components is higher than either expected for those galaxies or directly determined from the broadening of interstellar emission lines (only possible for lower redshifts), there must be another explanation for these structures. One that has been favoured recently are clumps from starburst winds in the line of sight. These winds were discovered already in high redshift starburst galaxies and should be expected also to happen in the highly starforming GRB host galaxies.

The first starburst wind was discovered over 40 years ago in M 82 (Lynds & Sandage, 1963) which has now become a sort of "prototype" starburst galaxy in the nearby universe. As we see

[2] combined absorption-emission line profile where the absorption component is blueshifted compared to the emission lines, the name comes from the luminous blue variable star P Cygni in the MW

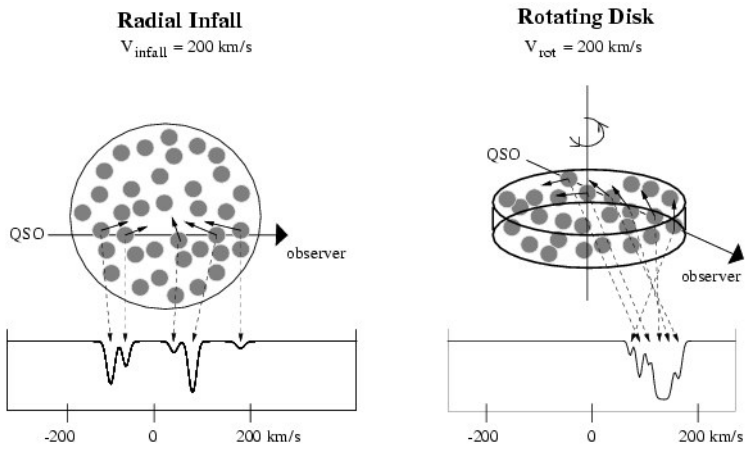

Figure 2.11: *Line profiles as they would be observed against a background QSO if the velocity components would trace radial infall of gas onto a protogalaxy or if they would come from an intersecting rotating disk from an already formed galaxy. The latter can also be adopted to GRBs which reside inside or slightly behind the disk and only show parts of those components.*

M 82 edge on, the outflowing material perpendicular to the disk can easily be observed (see the title figure of Part I). Today, a number of starburst galaxies in the nearby universe are known to show such global winds, including our own Milky Way (). Those winds arae now considered as one of the main sources for the metal enrichment of the IGM. The main drivers for those winds were suggested to be either powering from a central AGN or winds from O stars or supernova explosions. AGN activity and stellar winds only seem to play a minor role, most of the galactic winds are coming from the cumulated SN explosions happening during starburst activity.

The central energy source then creates a cavity that is driven outwards and cools adiabatically. It creates a shock front when it hits the ISM and finally slows down as it accumulates more matter which then results in an onion like structure. If it has enough energy to overcome the gravitational potential, it reaccelerates and fragments due to Rayleigh-Taylor instabilities. Most of that material is expected to be situated along the minor axis of the galaxy as it dissolves at larger angles when the ram pressure becomes equal to the thermal pressure of the ISM.

Surprisingly, both low (Na I, Si II etc.) and high ionization lines (O VI) have been observed in these galactic winds. Winds observed in emission in nearby galaxies (e.g. through Hα narrowband imaging) show a complex morphology with clumps, large filaments and bubbles. Also X-ray and radio emission has been detected with often similar patters as observed in the optical. For a comprehensive review on galactic winds see (Veilleux et al., 2005). LBGs frequently show blueshifted absorption lines which have been interpreted as signs of galactic outflows (Pettini et al., 2002; Shapley et al., 2003) and correlated with the amount of extinction measured. For QSO absorbers, the situation is less clear. Ellison et al. (2003) argue for an expanding superbubble due to the absence of absorption at the expected center of the galaxy. Symmetric structures with little absorption in the middle can be indicative for an outflow origin and has also been observed in QSO spectra. Others argue that infall of gas or rotation can account for the absorption systems detected (e.g. Steidel et al., 2002).

In the following three Chapters, we will present three GRB afterglows studied with absorption line spectrosocpy. The first case, GRB 060526, only had a dataset of low resolution spectra and we have to use the curve-of-growth method to derive column densities and metallicites.

Furthermore, in this Chapter, we present an extensive photometric dataset of the optical and IR afterglow and model the non-smooth lightcurve with broken powerlaws and energy injection models. The next Chapter deals with UVES high-resolution spectra of GRB 030329 where we detect Mg absorption lines as well as emission lines from the host. The absorption lines can be resolved into several components and are blueshifted compared to the emission lines which leads us to the conclusion that this might be a good candidate for a galactic wind outflow. For the third spetrum, GRB 060206, we have a large range of absorption features due to the high redshift (z=4.048) with a larger velocity spread than for 030329. Finestructure lines detected indicate distances of 1–8 kpc from the burst, but here, some of the structures might actually trace the rotation of the galaxy.

Published as: C. C. Thöne, D. A. Kann, G. Jóhannesson, J. H. Selj, A. Jaunsen, J. P. U. Fynbo, K. S. Baliyan, C. Bartolini, I. F. Bikmaev, J. S. Bloom, R. A. Burenin, B. E. Cobb, P. A. Curran, S. Covino, H. Dahle, J. French, S. Ganesh, G. Greco, A. Guarnieri, L. Hanlon, J. Hjorth, M. Ibrahimov, G. L. Israel, P. Jakobsson, B. L. Jensen, U. G. Jørgensen, I. M. Khamitov, D. Malesani, N. Masetti, J. Näränen, E. Pakstiene, M. N. Pavlinsky, D. A. Perley, A. Piccioni, G. Pizzichini, A. Pozanenko, D. Nanni, V. Rumyantsev, D. Sharapov, D. Starr, R. A. Sunyaev, F. Terra, P. M. Vreeswijk & A. C. Wilson *"Photometry and Spectroscopy of GRB 060526: A detailed study of the afterglow and host of a high-redshift Gamma-ray burst"* submitted to Astronomy and Astrophysics, preprint: astro-ph/0806.1182

3

PHOTOMETRY AND SPECTROSCOPY OF GRB 060526: A DETAILED STUDY OF THE AFTERGLOW AND HOST OF A HIGH-REDSHIFT GAMMA-RAY BURST

ABSTRACT – *With this Chapter we want to investigate the highly variable afterglow light curve and environment of Gamma-Ray Burst (GRB) 060526 at z=3.221. We present one of the largest photometric datasets ever obtained for a GRB afterglow, consisting of multi-color photometric data from the optical to the NIR. The data set contains 218 data points in total to which we add additional data from the literature. Furthermore, we present low-resolution high signal-to-noise spectra of the afterglow. The afterglow light curve is modeled with both an analytical model using broken power-law fits and with a broadband numerical energy injection model. The absorption lines detected in the spectra are used to derive column densities using a multi-ion single-component curve-of-growth analysis from which we derive the metallicity of the host of GRB 060526. The overall light curve follows a broken power-law with a break at* $t = 2.401 \pm 0.061$ *days. It shows deviations from the smooth power-law that can be explained by additional energy injections from the central engine. The broadband SED of the afterglow shows little extinction along the line of sight. The metallicity derived from* S II *and* Fe II *is relatively high for a galaxy at that redshift but comparable to the metallicity of other GRB hosts at similar redshifts. There is a candidate host galaxy at a relatively large offset of 7.7 kpc from the afterglow position with* R *=26.5 mag which would imply a rather luminous host.*

3.1 INTRODUCTION

This chapter presents a set of low-resolution spectra of the high redshift burst GRB 060526 obtained with the FORS1 spectrograph at the VLT. This is preceeded by the results of a large observing campaign involving photometric data from 13 telescopes around the world from B to K band (Chapter 3.2. The multicolor lightcurves are not smooth as expected from the simple fireball model, but show instead a number of bumps and wiggles and changes in the temporal slope. Those lightcuves are then fitted with broken powerlaws (Chapter 3.2.4) and with a numerical model that explains the deviation from the smooth powerlaw with energy injections from the inner engine (Chapter 3.2.5). The extinction is derived from the spectral energy distribution (Chapter 3.2.6). Deep late-time imaging of the field reveals a possible host

galaxy, which seems to be confirmed by the detection of a spectral continuum redwards of Lyman-α at the burst redshift. The spectral dataset is then used in Chapter 3.3 to derive column densities from the CoG method, metallicities and other properties.

GRB 060526 was detected by the *Swift* satellite on May 26.686458 (16:28:30 UT). The satellite slewed immediately to the burst, detecting both the X-ray and the optical afterglow (Campana et al., 2006). The BAT instrument on *Swift* measured two emission epochs. The first one lasted 13.8 s and consisted of two FRED peaks, followed by a second symmetric peak between 230 to 270 s (Campana et al., 2016). The second peak was coincident with a giant X-ray flare followed by a softer flare at 310 s (Campana et al., 2007) also detected in the V-band by the UVOT telescope onboard *Swift* (Brown et al., 2006). The gamma-ray fluence was $4.9\pm0.6 \times 10^{-7}$ erg/cm^2 during the first emission episode and $5.9\pm0.6 \times 10^{-7}$ erg/cm^2 during the second, the peak flux of the second episode was however only half of the peak flux of the first one. The spectral index of the two epochs changed from 1.66 ± 0.20 to 2.07 ± 0.18, thus showing the typical hard-to-soft evolution (Markwardt et al., 2006). The most rapid ground-based observations came from *Watcher*, which detected the afterglow at $R \approx 15$ mag (French & Jelinek, 2006) 36.2 seconds after the trigger. *ROTSE* observations showed a plateau for several thousand seconds after the GRB (Rykoff et al., 2006). A redshift of $z = 3.21$ was determined by Berger & Gladders (2006) with the Magellan/Clay telescope. The brightness of the optical afterglow allowed for a dense monitoring which revealed a complex light curve structure including several flares (Halpern et al., 2006a,b) and a steepening attributed to a jet break (Thöne et al., 2006).

Throughout this Chapter, we follow the convention $F_\nu(t) \propto t^{-\alpha}\nu^{-\beta}$. Uncertainties are given at 68% confidence level for one parameter of interest unless stated otherwise.

3.2 OBSERVATIONS

3.2.1 PHOTOMETRY

In order to get a good coverage of the light curve, we obtained data using several different telescopes around the world. Our complete data set comprises 18, 2, 27, 115, 21, 13, 10 and 10 data points in B, g', V, R, I, J, H and K_S respectively, a total of 218 points, one of the largest photometric samples of an optical/NIR afterglow in the *Swift* era.

Early optical data were obtained with the 1.5m telescope on Mt. Maidanak / Uzbekistan, the 2.6m Shajn telescope at CrAO (Crimean Astrophysical Observatory/Ukraine), the TNG (Telescopio Nazionale Galileo) on La Palma equipped with DOLoRES, the 1.2m MIRO telescope on Mt. Abu/India, with BFOSC (Bologna Faint Object Spectrograph & Camera) at the G. D. Cassini 152 cm telescope of the Bologna University under poor conditions and with the RTT150 (1.5m Russian-Turkish telescope, Bakirlitepe, Turkey), data of the latter are also presented in Khamitov et al. (2007).

The light curve was followed up sparsely every night over nearly a week with the DFOSC (Danish Faint Object Spectrograph and Camera) on the Danish 1.54m telescope on La Silla/Chile under partially photometric conditions and with MOSCA and ALFOSC (Andalucia Faint Object Spectrograph and Camera) at the Nordic Optical Telescope on La Palma. Furthermore, two epochs were obtained with the Tautenburg 1.34m Schmidt telescope and two sets of images were taken several days after the GRB with Keck/LRIS simultaneously in the Kron-Cousins R and the Sloan g' bands, the second observation was performed at high airmass under bad seeing conditions. Late images were obtained with FORS 2 at the VLT on Paranal/Chile on Feb. 23, 2007 and Mar. 30, 2008 under the ESO-LP 177.A-059 in the R band with exposure times of

time May 27 [UT]	exptime [s]	grism	spectral range [Å]	resolution [Å]
01:16:56	600	300V	3650 – 8900	11.1
01:29:46	900	600I	7000 – 9200	4.4
01:47:28	900	1200B	3860 – 4400	2.4
02:05:27	900	600V	4080 – 7200	4.5
02:24:00	1200	300V	3650 – 8900	11.1
02:57:05	1800	1200B	3860 – 4400	2.4
03:30:34	1800	600V	4080 – 7200	4.5
04:04:08	1800	600I	7000 – 9200	4.4

Table 3.1: *Observation log of the spectra of GRB 060526 from FORS1/VLT*

2500 and 7500s, respectively, to look for the host galaxy.

Near infrared data were collected with ANDICAM and the 1.3 m SMARTS telescope (Small and Moderate Aperture Research Telescope System) at CTIO under non-photometric conditions as well as with the robotic 1.3m PAIRITEL telescope on Mt. Hopkins.

For the photometric calibration, we determined the absolute magnitude of six comparison stars in the field using photometric zero points from DFOSC in V, R and I band (see Table 3.2). These stars were then used to perform relative PSF photometry to get the absolute magnitude of the afterglow, only for some of the late NOT images and the faint MIRO detections relative aperture photometry was done using a circle of 20 pixel diameter (10 for the sky). For the B-band we took zero points for only three comparison stars from the SDSS (see Table 3.2), converting them with the equations of Jester et al. (2005). g' zero points were taken from the SDSS. For the RTT 150 data, we used one USNO-B1 star as reference that was calibrated using Landolt standard stars. The results are in full agreement with the rest of the data set. The J, H and K band data from SMARTS/ANDICAM and PAIRITEL were calibrated using three and ten nearby stars, respectively, from the 2MASS catalogue.

All data and upper limits are given in Table 3.6, the data are not corrected for Galactic extinction. For the final light curve fitting, we add $Br'R_Ci'$ band data from Dai et al. (2007) and Watcher R and CR data from French et al. in prep. We shift the R band data of Dai et al. (2007) and French et al. in prep. by 0.1 magnitudes to bring it to our zero point. The multi-color light curves are shown in Fig. 3.1.

3.2.2 SPECTROSCOPY

Spectra were obtained with FORS1/VLT on May 27 from 9 to 12 hours after the burst. Four different grisms cover the wavelength range from 3650 to 9200 Å. For all four grisms a $1''.0$ slit was used which provides resolving powers between 2.4 and 11.1 Å. Reduction, cosmic ray removal, extraction and wavelength calibration were performed using standard tasks in IRAF[1]. The final spectra were then normalised as no absolute flux calibration was needed. In order to improve the S/N, we combined the datasets taken with the same grism weighted with their variance. A summary of the spectroscopic observations is given in Table 3.1.

3.2.3 THE MULTI-COLOR LIGHT CURVE

The early light curve up to two hours after the burst features an optical flare contemporaneous to the XRT/BAT flare at ≈ 250 s and a following plateau phase (Brown et al., 2006; French &

[1]http://iraf.noao.edu

#	coord.	B [mag]	V [mag]	R [mag]	I [mag]
1	15:31:19.6 +00:16:59.5	19.90	19.36	19.02	18.64
2	15:31:22.7 +00:17:21.2	20.30	19.51	19.09	18.71
3	15:31:20.9 +00:16:39.1	19.97	19.11	18.55	18.12
4	15:31:14.4 +00:17:49.9	—	19.78	19.43	18.81
5	15:31:16.5 +00:17:55.5	—	20.34	19.96	20.59
6	15:31:18.3 +00:18:17.7	—	20.49	19.45	18.23

Table 3.2: *Magnitudes of the comparison stars used for photometry*

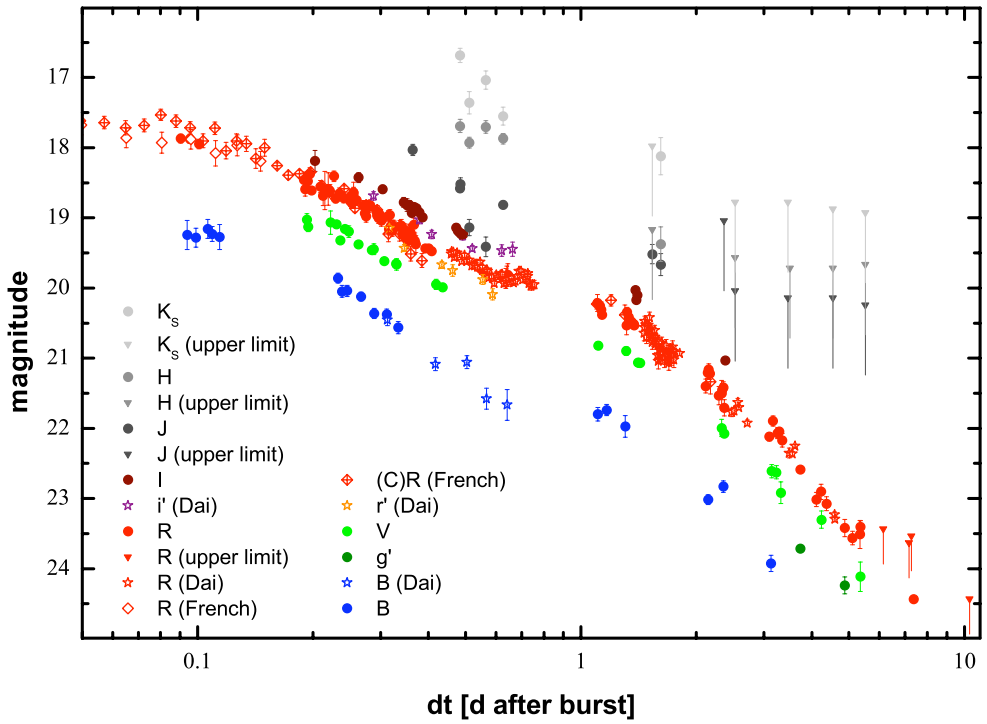

Figure 3.1: *Light curves of the optical afterglow of GRB 060526. Filled circles (detections, $Bg'VRIJHK_S$) and filled triangles (upper limits, $RJHK_S$) are presented in this work, open stars ($Br'Ri'$) are taken from Dai et al. (2007) and open diamonds are Watcher data from French et al. in prep. The strong variability and the large $V-R$, $B-R$ colours due to the high redshift are evident.*

Jelinek, 2006; Rykoff et al., 2006). These features will be discussed in French et al. in prep.

To analyse the evolution of the light curve, we use the R band which has the densest sampling, a total of 241 data points in all, from 2.2 hours to more than 7 days after the GRB (earlier data will be discussed in French et al. in prep. and are not included in these fits). For all fits, we fix the host magnitude to $m_h = 27$ (see 3.2.7). A fit with a single power law to this data is very strongly rejected, with $\chi^2/\text{d.o.f.} = 24.3$ (see Table 3.3 for all fitting results). A smoothly broken power law gives a much better fit ($\Delta\chi^2 = 4943$ for three additional degrees of freedom), but even so, the fit is formally rejected, with $\chi^2/\text{d.o.f.} = 3.89$. This is due to the strong variability in the light curve which was first found by Halpern et al. (2006a) and is also discussed in Dai et al. (2007). This fit, along with the residuals showing the strong variability, is shown in Fig. 3.2. The parameters we find for this fit are concurrent with those of Dai et al. (2007) (who find $\alpha_1 \approx 1.0$, $\alpha_2 \approx 2.9$ and $t_b \approx 2.55$ days). Due to the high data density, we are able to let the

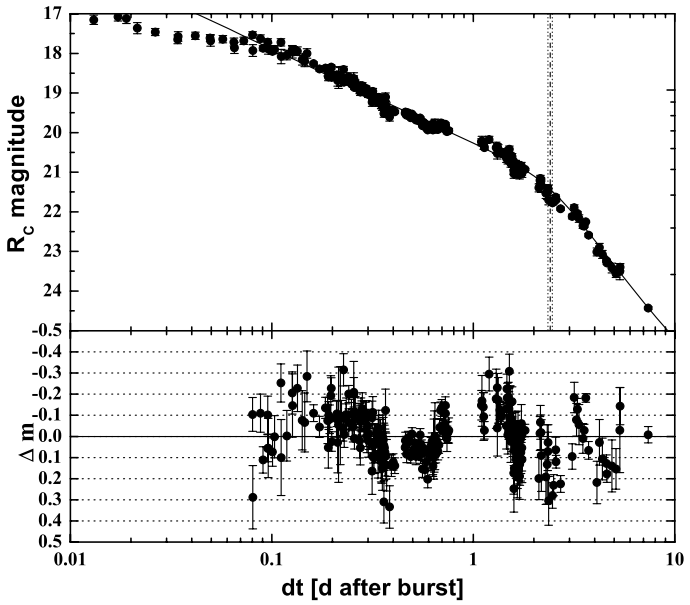

Figure 3.2: *The R-band light curve of GRB 060526 fit with a smoothly broken power law. The residuals of the fit show strong variations of up to 0.3 magnitudes. The dashed vertical line marks the break time, the dotted lines the 1σ region of uncertainty. Note that this is the time when the two asymptotic power-laws would meet for a maximally sharp break ($n = \infty$), in reality, the break is soft ($n \approx 3$) and is thus seen as a smooth rollover.*

break smoothness parameter n vary, and our result is in agreement with the tentative $\alpha_1 - n$ correlation found by Zeh et al. (2006). Still, the significant improvement shows that the light curve is basically a smoothly broken power law, and the very steep late decay indicates that this break is a jet break, as first noted by Thöne et al. (2006) and also found by Dai et al. (2007). The rest frame jet break time of 0.57 days is typical for the optical afterglows of the pre-*Swift* GRB sample (Zeh et al., 2006).

Jet breaks, a common feature in well-monitored pre-*Swift* optical afterglows (e.g., Zeh et al., 2006), have not been found in many *Swift* afterglows, especially in the X-rays (e.g., Mangano et al., 2007; Grupe et al., 2007; Sato et al., 2007), and if there are breaks, then the comparison between the optical and X-ray light curves show them to often be chromatic (Panaitescu et al., 2006; Oates et al., 2007). Analysing both the optical and X-ray data of GRB 060526, Dai et al. (2007) suggest that the (jet) break is achromatic. If we take the X-ray data from Dai et al. (2007) and fit it with the parameters of our smoothly broken power law fit using X-ray data from 0.06 days onward, we concur that the fit is acceptable, with $\chi^2 = 46.2$ for 39 degrees of freedom. A fit to the X-ray data alone results in a much earlier break time and slopes that are less steep (again in agreement with Dai et al., 2007), but we caution that the late X-ray afterglow is only sparsely sampled and shows large scatter. Similar results are obtained with the X-ray data as to be presented by French et al. in prep. as well as the light curve from the *Swift* XRT repository (Evans et al., 2007).

3.2.4 Analysis of the light curve variability

One approach to analyse the variability of the light curve is to split it into different parts and fit these with smoothly broken or single power laws. This is possible due to the high data density. The results of this approach are given in Table 3.3 and shown in Fig. 3.3. The early data from

#	time span [days]	χ^2/d.o.f.	m_k [mag]	α_1	α_2	t_b [days]	n
$27-269$	$0.08-7.38$	24.3	20.45 ± 0.01	1.18 ± 0.01	—	—	—
$27-269$	$0.08-7.38$	3.89	21.19 ± 0.03	0.96 ± 0.01	2.76 ± 0.07	2.41 ± 0.06	3.01 ± 0.43
$27-120$	$0.08-0.41$	1.25	18.69 ± 0.12	0.82 ± 0.05	1.60 ± 0.12	0.26 ± 0.02	10
$121-144$	$0.46-0.59$	1.35	19.78 ± 0.04	1.11 ± 0.14	6.74 ± 3.59	0.59 ± 0.01	10
$145-171$	$0.60-0.76$	1.53	19.83 ± 0.03	-0.16 ± 0.24	7.12 ± 5.31	0.74 ± 0.01	10
$172-185$	$1.09-1.38$	1.18	20.17 ± 0.05	0.97 ± 0.18	—	—	—
$186-206$	$1.46-1.58$	1.42	19.74 ± 0.23	2.03 ± 0.50	—	—	—
$207-235$	$1.59-1.81$	0.88	20.61 ± 0.15	0.50 ± 0.25	—	—	—
$236-250$	$2.11-2.71$	1.85	19.18 ± 0.27	2.50 ± 0.26	—	—	—
$251-268$	$3.17-5.35$	5.83	17.93 ± 0.12	3.19 ± 0.09	—	—	—

Table 3.3: *Fits to the afterglow of GRB 060526. Columns are the numbering of the data points in the respective fit, the time span of these data points, the goodness of the fit, the degrees of freedom, the magnitude normalisation (see Zeh et al., 2006), the pre-break and post-break decay slopes, the break time and the smoothness of the break. The first two fits are discussed in 3.2.3, all other fits in 3.2.4.*

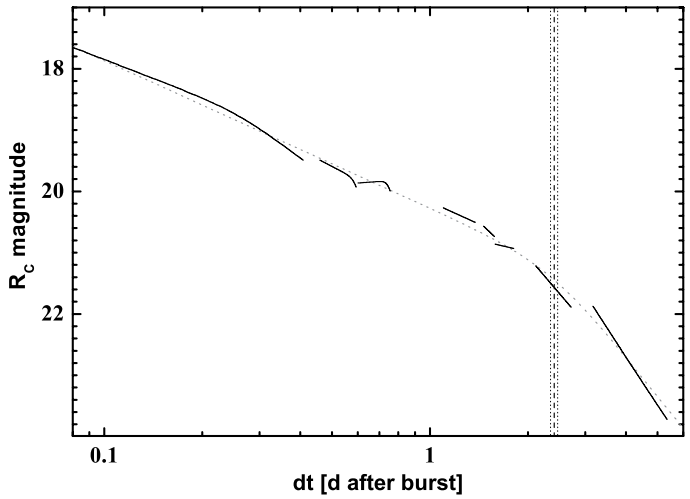

Figure 3.3: *Fits of the R-band light curve of GRB 060526. The gray dotted line shows the fit using a smoothly broken power law given in Fig. 3.2. The black lines show the fits (smoothly broken power laws or single power laws) to different parts of the light curve. The parameters can be found in Table 3.3. The flares at 0.5 to 0.7 days can be seen, as well as the "step" structure in the post-jet break decay.*

0.08 up to 0.4 days (# $27-120$ in Table 3.3) are decently fit (χ^2/d.o.f. $= 1.248$) by a smoothly broken power law (in all these cases, we fixed the break smoothness parameter, as it was not possible to leave it free to vary) which reveals a phase of rather steep decay early on. This situation is similar to GRB 030329, albeit less pronounced, where the steep decay of an early jet break goes over into multiple rebrightenings (Uemura et al., 2003; Zeh et al., 2006; Gorosabel et al., 2006). Such rebrightening features then follow (# $121-144$, # $145-171$ in Table 3.3), although once more less pronounced than in the case of GRB 030329. Both rebrightenings from 0.46 to 0.76 days feature a steep decay phase atypical for an external-shock driven afterglow, although we caution that the error bars are very large and it is not clear how close the derived slopes are to their hypothetical asymptotic values. The evolution of the residuals of GRB 021004 and GRB 030329 was very similar (Zeh et al., 2006), but we do not find a similar evolution in the residuals of GRB 060526 if we compare them to those of the two other GRBs.

Following a data gap, the afterglow of GRB 060526 can be modelled by a succession of single

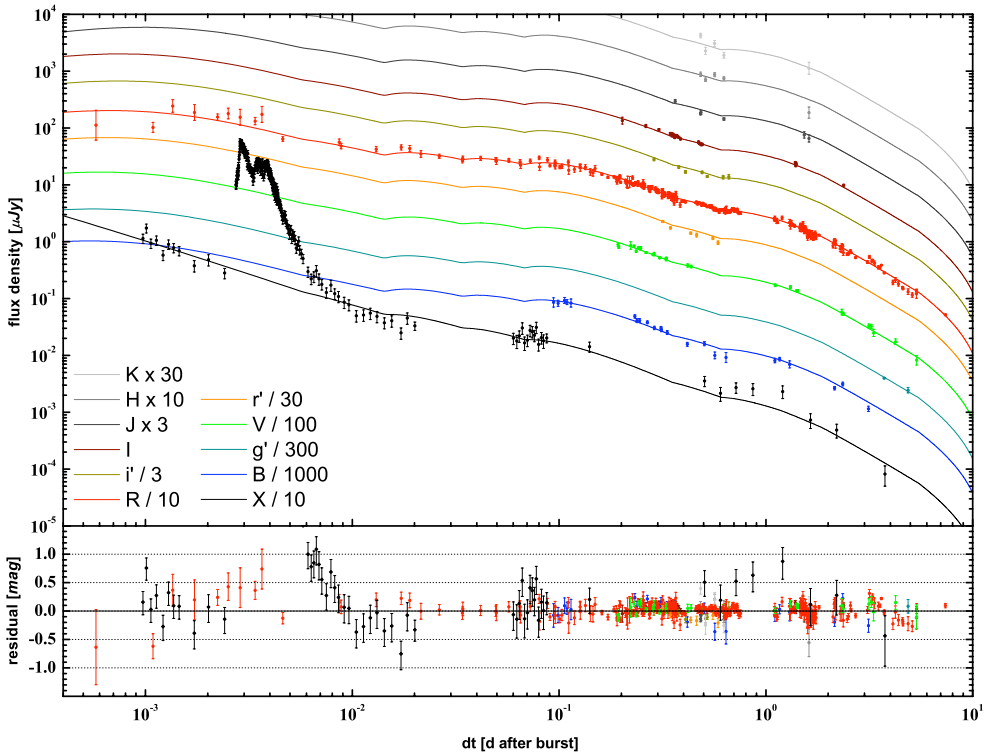

Figure 3.4: *Fit to the light curve in X-ray and optical/NIR $r'Ri'IJHK_S$ bands including a total of six energy injections. The strong X-ray flare is excluded from the modelling. The light curves have been offset by constant factors as given in the figure legend for better legibility. The $Bg'V$ bands are affected by additional Lyman forest absorption and were not included in the fit. For the $Bg'V$ bands, the fit curves the model predicts have been multiplied by 0.50, 0.55 and 0.82 respectively to match them with the data. The residuals are clearly improved in comparison to those plotted in Fig. 3.2, but short-timescale variations like the one at 0.7 days are still not fit satisfactorily.*

power laws which, with one exception, become successively steeper (the final five rows in Table 3.3). The sampling at later times is less dense, but there seem to be "steps", phases where the afterglow remains constant for a while (or even rebrightens) before going over into a steep decay again. Such features were also seen in the afterglows of GRB 000301C (Masetti et al., 2000), GRB 021004 and GRB 030329 (e.g. Lipkin et al., 2004; Zeh et al., 2006). The decay from 3.2 to 5.4 days is very steep, $\alpha = 3.2 \pm 0.1$ (concurrent with Dai et al., 2007, who find $\alpha = 3.4 \pm 0.2$ at late times), implying an abnormally large electron power law index $p = 3.2 - 3.4$, as the post-jet break decay is $\alpha_2 = p$ in the standard fireball model. We note that all fits have $\chi^2/\text{d.o.f.} \geq 1.25$ due to scatter in the data points. It is unclear whether this scattering is due to intrinsic microvariability or to the underestimation of photometric errors. The mixing of two data sets is probably not the reason, as the data from 0.46 to 0.76 days, for example, is almost exclusively from Dai et al. (2007).

3.2.5 Modelling the light curve numerically with energy injections

Motivated by the similarities to such highly variable light curves as that of the afterglow of GRB 021004, which was successfully modelled by multiple energy injections ("refreshed shocks")

(de Ugarte Postigo et al., 2005), we used the code of Jóhannesson et al. (2006) to model the afterglow light curve by applying several energy injection episodes as a possible scenario to explain the rebrightenings and shallow decay of the afterglow. Figure 3.2.5 shows the best fit (χ^2/d.o.f. $= 2.8$) found using a model with a total of six energy injections: at 0.006, 0.015, 0.04, 0.09, 0.4 and 0.6 days. The initial energy injected into the outflow is $E_0 = 5^{+3}_{-2} \cdot 10^{49}$ ergs[2]. The energy injections then add 0.8, 1.7, 2.6, 5, 8, and finally 13 times the initial energy release E_0 to the afterglow, for a total energy release in the afterglow of $1.5^{+1.1}_{-0.7} \cdot 10^{51}$ ergs.

The first four injections are responsible for the shallow afterglow decay between 0.008 and 0.25 days. The quality of the data does not allow to discriminate between this four-injection scenario and a continuous injection (French et al. in prep.). Also, since there are no direct indications of injections in the light curve, the time of each of the four injections is not well determined. A direct consequence of this is that the energy of each individual injection in this phase is not well determined, while the total energy released is fairly consistent. The time and energy of the last two injections are, however, better constrained by the data.

Further results of the modelling are a high density of the circumburst medium of $n_0 = 250^{+500}_{-150}$ cm^{-3} (a high value, comparable to the high-z GRB 050904, Frail et al., 2006), a rather low opening angle of $\theta_0 = 1^\circ.5^{+1.9}_{-0.8}$ and an electron index of $p = 2.1^{+0.3}_{-0.1}$. The peak frequency ν_m passes through the optical/NIR at very early times (French et al. in prep.), explaining the optical peak, and the cooling break ν_c is between the optical and X-rays up to 6 days after the burst, i.e., over the whole data span. Furthermore, we find $\varepsilon_e = 2 \cdot 10^{-2}$ and $\varepsilon_B = 8^{+40}_{-6} \cdot 10^{-5}$, with ε_e being the fraction of the energy in the electron population and ε_B the fraction of the energy in the magnetic field. Note that the definition of ε_e has been changed in the model from Jóhannesson et al. (2006) to the definition of Panaitescu & Kumar (2001) to allow for $p < 2$ in the model. In addition, we defined a maximum Lorentz factor for the electron energy distribution. This is limited by both synchrotron cooling (Dai & Lu, 1998) and, when $p < 2$, energy conservation (Panaitescu & Kumar, 2001). The steep decay at around 6 days is due to this restriction on the electron energy distribution, where the emission is cut off above the synchrotron frequency associated with this Lorentz factor. This interpretation is sensitive to the value assumed for the maximum Lorentz factor, which in turn is not well known. We have also assumed that the electron distribution is abruptly cut off at the maximum Lorentz factor, but a steepening at that point has also been suggested (e.g. Panaitescu & Kumar, 2001). Data at later times are needed to discriminate between the two and confirm this explanation for the steep decay.

This model reproduces the optical/NIR light curves well, with the rather high χ^2/d.o.f. $= 2.8$ resulting from the inability to fit the microvariability of the afterglow. We excluded both V and B bands from the fit due to Lyman forest blanketing. The X-ray light curve is also fitted reasonably well, but the model underpredicts the X-ray flux after the last energy injection and does not fall as steeply as the data. Here, the powerful X-ray flare has not been included in the fit, as it most likely originates in an internal shock caused by late time central engine activity (e.g., Burrows et al., 2005b).

3.2.6 THE SPECTRAL ENERGY DISTRIBUTION AND HOST EXTINCTION

Following the procedures outlined in Kann et al. (2006), we derive the optical spectral energy distribution (SED) of the GRB 060526 afterglow and fit it with several dust models (Milky Way (MW), Large (LMC) and Small Magellanic Clouds (SMC), Pei, 1992) to derive the line-of-sight

[2]The error limits presented here are 1 sigma estimates, but due to degeneracy in the model parameters, the actual range of parameter values can be much larger.

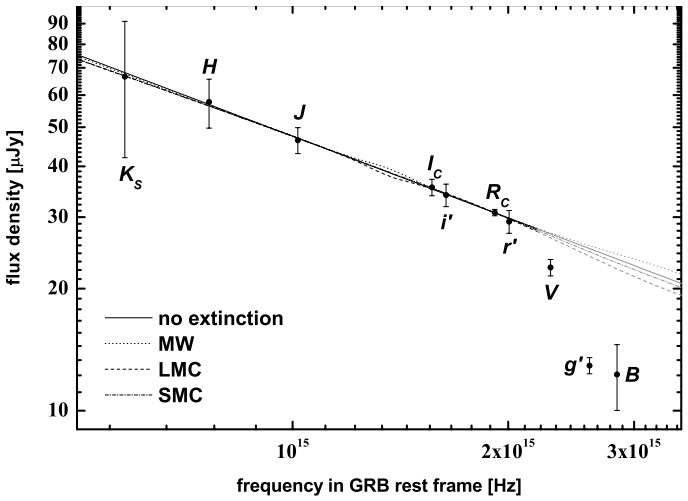

Figure 3.5: *Spectral energy distribution of the afterglow of GRB 060526 in $Bg'Vr'R_Ci'I_CJHK_S$, and fits with no extinction (straight black line), MW extinction (dotted line), LMC extinction (dashed line) and SMC extinction (thick dash-dotted line). Data beyond 2.2×10^{15} Hz ($Vg'B$) were not included in the fit due to Lyman forest blanketing, the grey curves represent extrapolations. The flux density scale is measured at the break time of 2.4 days.*

extinction in the host galaxy. Due to the strongly variable light curve, we choose the approach Kann et al. (2006) used for the SED of GRB 030329, and shift the other bands to the R band zero point to derive the colours. With this method, we can also look for colour changes. There may be marginal variations in $B - R$, but this colour remains constant within conservative errors.

The $Bg'Vr'R_Ci'I_CJHK_S$ SED clearly shows the decreasing flux in the B, g' and V bands due to the Lyman forest blanketing (see Fig. 3.5), and we thus do not include these filters in our fit. Due to the conservative errors, all fits, even with no extinction, are acceptable (see Table 3.4) and we are thus unable to strongly prefer one dust model over another. Furthermore, the extinction found is consistent with being zero in all cases, similar to the results for several other high redshift *Swift* GRBs (Kann et al., 2007). The MW and LMC extinction laws are disfavoured, as they result in unphysical negative extinction and a too flat spectral slope, respectively. The lack of z band data does not allow us to constrain the existence of a 2175 Å bump. Thus, we henceforth use the SMC dust fit, again in accordance with pre-*Swift* (Kann et al., 2006; Starling et al., 2007) and *Swift*-era (Schady et al., 2007; Kann et al., 2007) results. Assuming the cooling break ν_c to lie blueward of the optical bands (highly likely considering the X-ray spectral slope $\beta_X \approx 1$, Dai et al., 2007, French et al., in prep.; and the result of the numerical modelling), the standard fireball model gives for the electron power law index $p = 2\beta + 1 = 1.99 \pm 0.29$. This result is in agreement with the result from the broadband modelling (3.2.5) and with the canonical $p = 2.2$, and very similar to many other GRB afterglows (e.g. Kann et al., 2006). On the other hand, it does not agree with $p = 3.2 \pm 0.1$ from the late optical decay. Our results are in contrast to Dai et al. (2007), who derive a very steep slope $\beta_0 = 1.69^{+0.53}_{-0.49}$ from $Br'i'$ data only (correcting for Lyman absorption) and conclude that the optical and the X-ray data lie on the same slope.

3.2.7 HOST SEARCH

In the VLT images, we do not detect any source at the position of the afterglow down to a limit of $R = 27.1$ mag (which transforms into an absolute magnitude limit of M_R=–20.1), see Fig.

dust	χ^2/d.o.f.	β	A_V
none	0.054	0.663 ± 0.025	—
MW	0.062	0.691 ± 0.044	-0.038 ± 0.048
LMC	0.052	0.327 ± 0.323	0.163 ± 0.156
SMC	0.048	0.495 ± 0.144	0.049 ± 0.041

Table 3.4: *Fits to the spectral energy distribution of GRB 060526. Columns are the dust model, the goodness of the fit, the spectral slope and the derived extinction in the rest-frame V band.*

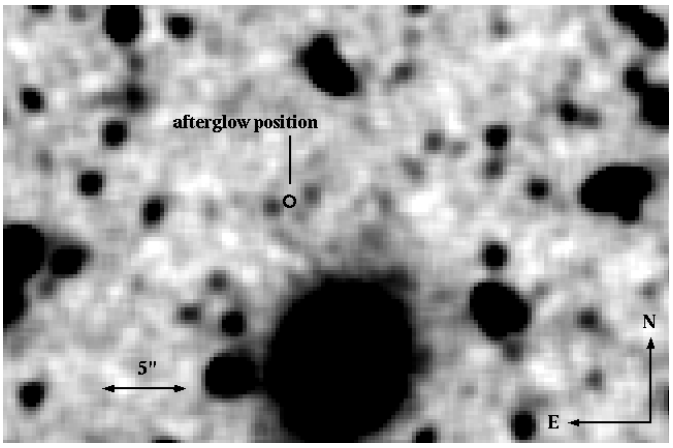

Figure 3.6: *R band image of the field of GRB 060526. The afterglow position is indicated and no source is detected at that position. The image has been smoothed to enhance weak sources.*

3.6 for an image of the field. However, there is are two sources present, the first one ∼1 arcsec South-East of the afterglow position with R =26.4±0.2, the second one ∼ 1.″5 North-West with R =26.3±0.2, which at a redshift of z =3.221 would transform into a physical distances of ∼ 7.7 and 11.5 kpc. A longslit spectrum covering the afterglow position and the source close to the GRB site does not show any trace at these positions, however, collapsing the entire spectrum blue– and redward of Lyman-α at the redshift of the burst respectively and plotting the two values along the slit gives a small enhancement near the source to the South-East (Milvang-Jensen et al. in prep). If this detection is significant, it gives a lower limit for the source of $z > 3.221$ and makes this source likely to be the host of GRB 060526. We note, however, that this would be one of the largest offsets found between a GRB and its host galaxy in a large sample of *Swift* long GRB host galaxies (Hjorth et al. in prep.).

Host galaxies of long-duration GRBs have been found to often be faint irregular galaxies (Fruchter et al., 2006; Christensen et al., 2004) which are difficult to detect at higher redshifts. So far, there are only five bursts with $z > 3$ where the detection of a host galaxy has been published, namely GRB 971214 (z =3.42) (Kulkarni et al., 1998), GRB000131 (z =4.5) (Fruchter et al., 2006), GRB 030323 (Vreeswijk et al., 2004), GRB 060206 (z =4.047) (Thöne et al., 2007b) and GRB 060605 (z =3.773) (Ferrero et al., 2008). The host galaxies of GRB 020124 (Berger et al., 2002) and GRB 050904 (Berger et al., 2007), on the other hand, were not detected to very deep limits.

The distribution of pre-*Swift* R band host galaxy magnitudes peaks at $M_{AB} = 25$ (Fruchter et al., 2006) but extends out to 29 with a typical redshift $z \approx 1.4$. Swift GRBs (and thus their hosts) however have a higher mean redshift of $z = 2.8$ (Jakobsson et al., 2006b), so the distribution will be shifted out to even fainter magnitudes. Ovaldsen et al. (2007) also find a higher magnitude for *Swift* hosts than for pre-*Swift* bursts by comparing the expected detection rate from pre-*Swift* hosts with detections and upper limits derived from imaging the fields of 24 *Swift*

and *HETE* bursts from 2005 – 2006. If the source close to the GRB position is indeed the host galaxy of GRB 060526, it would be among the more luminous hosts detected for long-duration GRBs.

3.3 SPECTROSCOPY RESULTS

3.3.1 LINE IDENTIFICATION

We detect a range of metal absorption lines as well as a Lyman limit system (LLS) originating in the host galaxy of GRB 060526. A redshift of z=3.221 was determined in Jakobsson et al. (2006a) from a number of these absorption lines using the spectra taken with the 600V grism presented in this article.

Most of the lines were fitted from the combined 600V spectrum which covers all metal absorption lines detected longwards of Ly-α, but provides a higher resolution than the 300V spectra. The 600I spectra only covers the AlII λ 1670 line at the same resolution as the 600V grism. The range of 1200B is entirely within the Lyman-α forest but does not have a high enough resolution to deblend metal transitions from absorption caused by the Ly-α forest lines. We do, however, detect Ly-β and Ly-γ absorption in the 1200B grism. In the blue end of the 300V spectrum, one can clearly see the 915 Å Lyman break at the redshift of the host galaxy. In Fig. 3.7, we show the combined spectrum of the 300V grism with the identified lines indicated.

In order to determine the equivalent width (EW) of strong absorption lines, we fitted the continuum around the lines in regions that were free of absorption and summed over the absorption contained within two times the full-width at half-maximum (FWHM) of the lines. For weak lines, we obtained better results due to the low S/N by fitting Gaussians. For this fit, we used a modified version of the gaussfit procedure provided in IDL [3] which is more reliable in determining the continuum and fitting the actual line even if it is slightly blended with a neighbouring line. The upper limits on the EWs for a range of ions noted in Table 3.5 was determined from the spectra taken with the 300V grism due to the better S/N of those spectra.

S II λ 1259, Si II λ 1260 and Fe II λ 1260 are blended and cannot be fitted separately, the same is the case for C II $\lambda\lambda$ 1334, 1335. We therefore cannot consider them for the derivation of the column density from the curve of growth fit as described below and only give the total EW Table 3.5. In contrast to what is noted in Jakobsson et al. (2006a), we cannot reliably detect any fine-structure lines and only give an upper limit for Si II*. Fine structure lines would be a clear indication that the absorption lines detected are indeed originating in the host galaxy of the GRB (e.g. Prochaska et al., 2006b; Vreeswijk et al., 2007). The redshift derived is therefore strictly taken only as a lower limit. Investigating the individual, uncombined spectra we could not detect any variability in the EW which is most likely due to the relatively low S/N of the individual spectra.

3.3.2 COLUMN DENSITIES FROM CURVE OF GROWTH ANALYSIS

Some of the strong absorption lines are saturated, which is a problem in low resolution spectra as the damping wings are not resolved and Voigt profile (VP) fitting cannot be adopted to derive a reliable column density. Furthermore, high resolution spectra of GRBs (Prochaska, 2006) have shown that the strong metal absorption lines unresolved in low resolution spectra usually consist of a number of narrow, unsaturated components that would allow an accurate

[3] available at http://www.pa.iasf.cnr.it/∼nicastro/IDL/Lib/gfit.pro

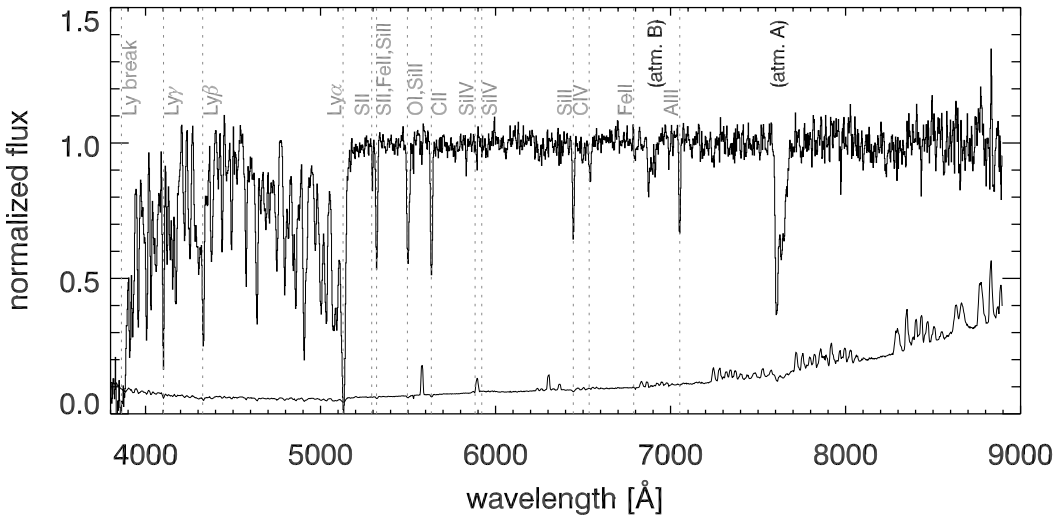

Figure 3.7: *The spectrum taken with grism 300V where the two exposures have been combined to improve the S/N. The identified lines are labelled as well as the main atmospheric absorption bands. The line at the bottom shows the error spectrum.*

λ_{obs} [Å]	λ_{rest} [Å]	Line ID	z	EW_{rest} [Å]	log N [cm^{-2}]
4102.26	972.54	Lyγ	3.218	2.39±0.10	—
4329.70	1025.72	Lyβ	3.221	2.92±0.06	—
5131	1215.67	Lyα	3.221	—	20.01±0.15
(5254)	1242.80	N V	(3.221)	<0.05	<13.66
(5276)	1250.58	S II	(3.221)	<0.04	<14.71
5291.01	1253.81	S II	3.220	0.05±0.02	14.58±0.25
5320.00	1259.52	S II	3.221	(1.32±0.07)	—
	1260.42	Si II	3.221	*blended*	>13.89
	1260.53	Fe II	3.221		—
(5335)	1264.74	Si II*	(3.221)	<0.09	<12.76
5497.30	1302.17	O I	3.222	1.07±0.06	>15.15
5506.82	1304.37	Si II	3.222	0.70±0.21	>14.72
(5559)	1317.22	Ni II	(3.221)	<0.09	<13.59
5634.24	1334.53	C II	3.222	(1.51±0.22)	—
	1335.71	C II	3.222	*blended*	—
5884.87	1393.76	Si IV	3.222	0.20±0.08	13.50±0.14
5923.05	1402.77	Si IV	3.222	0.12±0.05	13.50±0.14
6444.50	1526.71	Si II	3.221	0.86±0.04	>14.48
6539.58	1548.20	C IV	3.223	0.26±0.08	14.10±0.13
6546.39	1550.78	C IV	3.221	0.22±0.09	14.10±0.13
6790.24	1608.45	Fe II	3.221	0.17±0.03	14.28±0.24
6800.38	1611.20	Fe II	3.221	<0.01	—
7052.62	1670.79	Al II	3.221	1.02±0.05	>13.34
(7829)	1854.72	Al III	(3.221)	<0.09	<12.71
(8552)	2026.13	Zn II	(3.221)	<0.10	<12.73
(8679)	2056.25	Cr II	(3.221)	<0.12	<13.47

Table 3.5: *EWs of detected absorption lines and 2σ upper limits on some undetected lines, the EW for the blended systems include the contributions from all lines. The column densities were derived from CoG fitted for S II, Si II, Fe II and C IV. Upper and lower limits were determined by assuming the ions to lie on the linear part of the CoG. The Lyα column density is taken from Jakobsson et al. (2006a) and is based on the 600V grism.*

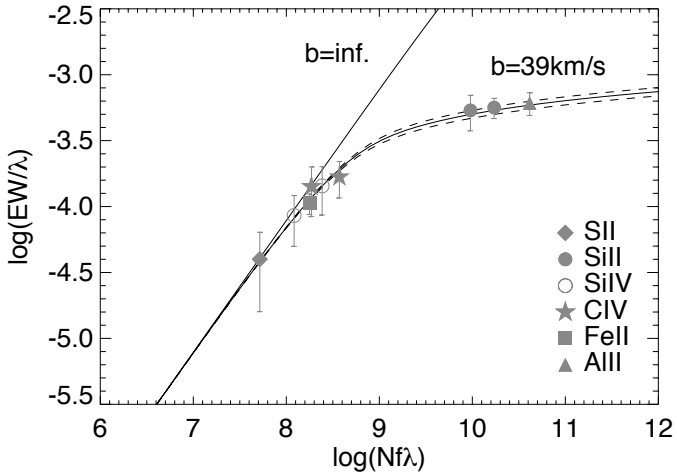

Figure 3.8: *Multi-ion single-component curve of growth fit for the absorption systems in GRB 060526 using 6 different ions. As comparison, $b = \infty$ is plotted, the dotted line marks the 1 σ deviation from the fit*

determination of the column density by fitting the different components separately.

If only low resolution spectra are available, one has to adopt a curve of growth (CoG) analysis (Spitzer, 1978) which directly relates the EW to the column density on the linear part of the CoG where the lines are not saturated (optical depth $\tau_0 < 1$), but depends on the Doppler b parameter of the medium on the flat part of the curve which applies for mildly saturated lines. For GRBs, one usually has to do a multiple-ion single-component CoG (MISC-CoG) analysis, adopting the same effective Doppler parameter for all ions. Here, we used all unblended ionic lines that were not heavily saturated, namely S II, Si II, Fe II, Al II as well as C IV and Si IV and calculate the χ^2 minimum going through the parameter space for the column densities of each ion and a range of b parameters. We then find the best fit for $b = 39 \pm 3$ km/s (see Fig. 3.8) and the column densities as noted in Table 3.5. Most of the ions lie near the linear part of the CoG and are therefore rather independent of b, Si II and Al II lie on the flat part of the CoG and the column densities are only noted as lower limits as derived from the linear part of the CoG. We excluded the saturated O I transition from the fit as well as Si II λ 1260 which is blended with S II and Fe II where, however, Si II is the dominant contribution.

There are several problems connected with the use of the CoG that have to be considered. Different ionisation levels should actually be treated in separate analyses as they might occur in different regions in the absorbing system. However, we assume that the absorption takes place in a relatively small region of the host galaxy and also fit the higher ionisation levels of Si IV and C IV in the same CoG. Furthermore, they lie on the linear part of the CoG and excluding them from the common fit would not change the derived b parameter. Another problem with doing multiple-ion CoG analysis using strong lines in low-resolution spectra has been noted by Prochaska (2006), who compared column densities derived from low resolution spectra and CoG with high resolution data and VP fitting from the same bursts. He found that when including saturated lines in the fit, column densities are generally underestimated. Indications for that are if an effective b parameter of $>> 20$ km/s is found as strong lines actually consist of a range of components with $b < 20$ km/s and that weak lines are underestimated when including saturated lines in the CoG. Savaglio (2006) however performed a similar analysis using CoG and the apparent optical depth (AOD) method as described in Pettini et al. (2002) which can be applied for medium resolution high S/N spectra and found a good agreement between

the two methods. We also find that the column densities of the saturated lines Al II and Si II are quite sensitive to the adopted b parameter. These lines consist very likely of a number of unresolved weaker components which would lie on the linear part of the CoG. For Al II and Si II we therefore give the column density derived from the linear part of the CoG as lower limit.

3.3.3 METALLICITY AND RELATIVE ABUNDANCES

Absorption lines that are likely not affected by dust extinction can be used to derive a metallicity of the medium in the line of sight to the GRB. The least dust-depleted element is Zn, which is, however, undetected in our spectra. We therefore use S II, Fe II and the strongest lower limit on Si II to derive relative metallicities compared to the hydrogen density with $[\mathrm{M/H}] = \log(\mathrm{N}_M/\mathrm{N}_H) - \log(\mathrm{N}_M/\mathrm{N}_H)_\odot$ using solar abundances from Asplund et al. (2004). Here we derive metallicities of $[\mathrm{S/H}] = -0.57 \pm 0.25$, $[\mathrm{Si/H}] > -0.80$ and $[\mathrm{Fe/H}] = -1.18 \pm 0.24$.

Fe is usually affected by dust depletion (Savage & Sembach, 1996) and corrections have to be adopted. Using the relation between the Zn and Fe abundance in Savaglio (2006), we find a metallicity of [Fe/H]=-1.09 ± 0.24 which marginally agrees within the errors with the value derived from sulphur. The only detected and unblended S II line at λ 1253, however, is only marginally detected and therefore the EW has large errors. The Fe II doublet taken for the CoG fit, in contrast, is also slightly blended, but the fit of the stronger component can be considered as reliable. Despite the dust depletion, the metallicity derived from Fe might be the most reliable one in this case and we therefore assume a metallicity of $[\mathrm{Fe/H}] = -1.09$ for the host of GRB 060526.

Independent of the ion used for the metallicity, it is rather high compared to other galaxies at redshift z $\approx$ 3, but among the typical metallicites derived for other GRB hosts (Fynbo et al., 2006a) at that redshift. For those measurements, different ions have been used depending on the quality and the wavelength coverage of the spectra. Our results show that caution is required when comparing the metallicities derived from different elements, as they might be differently affected by dust extinction and/or evolution. This is especially true when saturated lines in low resolution spectra are used to derive the column densities and hence the abundances as it is the case for, e.g., GRB 000926 (Savaglio et al., 2003) and GRB 011211 (Vreeswijk et al., 2006). For GRB 050401 (Watson et al., 2006) and GRB 050505 (Berger et al., 2006), the authors themselves note that due to saturation the metallicity is indeed a lower limit.

Our spectra do not allow us to determine a dust depletion pattern from the relative abundances of heavier elements, since at least four elements such as Zn, Si, Mn, Cr, Fe, Ni or S are necessary. However, the difference in the relative abundances between S, Si and Fe suggest the presence of some dust in the line-of-sight towards the GRB. On the other hand, this difference could also be due to an enhancement in α element production[4] which is likely to happen in the young star-forming host of a GRB. Generally, GRB hosts have higher α/Fe ratios than QSO-DLAs (Prochaska et al., 2007), which can either be interpreted as large dust depletion consistent with the higher metallicities of GRB sightlines or as α element enhancement. There are indications that most of the α/Fe ratio is due to dust depletion traced by a large [Zn/Fe] or [Ti/Fe] < 0. The latter is assumed to be a clear indicator of dust depletion ([Ti/Fe] < 0) vs. α enhancement ([Ti/Fe] > 0] (Dessauges-Zavadsky et al., 2002). Both elements are, however, not detected and the limit on Zn does not lead to a strong contraint on the [Zn/Fe] ratio to settle this issue in the case of GRB 060526.

[4] α elements are produced in massive, metal-poor stars through the α process and include elements with integer multiples of the He nucleus mass such as O, Si, S, Ca, Mg and Ti.

We do not detect N V in our spectra but provide an upper limit of log N $<$ 13.66. N V was detected in only four sightlines towards GRBs (Prochaska et al., 2008b) and likely traces the immediate environment of the GRB as it has a high ionization potential and requires a strong radiation field. Our upper limit is lower than the column densities for those GRB sightlines where N V could be detected which implies that the absorbing gas probed by our spectra are most likely not close to the GRB itself. Furthermore, we do not detect any fine structure lines and only derive an upper limit on Si II* of log N $<$ 12.76. Fine structure lines are assumed to be pumped by the UV radiation field of the GRB (Vreeswijk et al., 2007) which also indicates that the gas is likely very far from the GRB itself. Si II* requires a less strong radiation field and has been detected in Lyman Break Galaxies (Pettini et al., 2002) where the UV radiation from young stars provides the necessary radiation field. Our tentative host also has a large offset from the GRB and the gas in the sightline is therefore expected to be little affected by UV radiation from young stars in the host.

3.4 Discussion and conclusions

GRB 060526 had a relatively bright afterglow that allowed us to obtain a solid dataset, both photometrically and spectroscopically. We achieved a dense light curve coverage over several days which allowed a detailed study of the afterglow properties, and obtained a series of low resolution but high signal-to-noise spectra to study the host environment.

3.4.1 A highly variable light curve

The optical light curve can be fitted with a broken power-law with a break at $t_b = 2.401 \pm 0.061$ days and decay slopes of $\alpha_1 = 0.963 \pm 0.007$ and $\alpha_2 = 2.759 \pm 0.070$ before and after the break. The dense sampling of especially the R band light curve also reveals a number of variabilities on top of the broken power-law resembling what has been seen in a GRB 021004 (de Ugarte Postigo et al., 2005) and GRB 030329 (Lipkin et al., 2004).

These features could be explained either by extended activity of the central engine or through interactions of the shock with the interstellar medium. For the case that the variability arises from external shocks, several mechanisms have been considered. In GRB 021004, both density variations of the external medium into which the GRB jet plows and angular inhomogenities of the jet surface were considered (Nakar et al., 2003). However, Nakar & Granot (2007) show that density variations would cause much smaller fluctuations than those observed in GRB afterglows and can therefore be ruled out. Another possibility is the injection of additional energy into the shock by slower shells that catch up with the shocked region as it decelerates, this model was used successfully to describe GRB 021004 (de Ugarte Postigo et al., 2005) and also works better than two other models (double jet and density fluctuations) to describe the highly complex light curve of GRB 030329 (Huang et al., 2006). Thus, variability can give either information on the medium surrounding the GRB or on the activity of the central engine. A more intriguing possibility is that the flares may be emitted from another region closer to the central engine, resulting from late internal shocks. Powerful X-ray flares that are attributed to late central engine activity have been observed in about 50% of all *Swift* GRBs (e.g. Burrows et al., 2005b; Chincarini et al., 2007; Krimm et al., 2007), and strong optical/NIR flaring contemporaneous with the GRB prompt emission may also occur (Vestrand et al., 2005; Blake et al., 2005; Vestrand et al., 2006; Racusin et al., 2008), thus making optical flares from late central engine activity an interesting prospect (Kann, 2007; Malesani et al., 2007).

Indeed, Dai et al. (2007) have suggested that the optical variability of the afterglow of GRB 060526 is due to flares from late internal shocks. Khamitov et al. (2007) conclude that the short timescale of the variabilities requires the jet to be nonrelativistic already at ~ 1 day and could then be explained by external density fluctuations. Our analysis lends tentative support to the notion of flares from internal shocks, finding decay slopes for two flares that exceed what should be possible from external shocks. But we caution that the errors of these fits are large due to a low amount of data in the decaying parts. Furthermore, globally, a model using refreshed external shocks is able to account for the light curve variations, although microvariability remains. This creates the intriguing possibility of reverberation effects (see Vestrand et al., 2006, for a case of reverberation between gamma-rays and optical emission). Short flares in the X-ray or optical bands signal internal shocks from long-term central engine activity, and when these shells catch up with the forward shock front, they re-energise the external forward shock. The detection of such behaviour would probably require dense multi-band observations of a bright afterglow to search for SED changes at high time resolution combined with detailed modelling of the data. This way, one could discern between internal shocks (which are expected to have a different spectral index from the forward shock afterglow) and refreshed, external shocks (which are achromatic). Our data set of the afterglow of GRB 060526, while extensive and exemplary for the *Swift* era, does not allow us such a detailed decomposition.

3.4.2 A MODERATE METALLICITY ENVIRONMENT

From the analysis of our low resolution spectra with different resolutions, we detect a LLS and a number of metal absorption lines that all lie at a redshift of z=3.221. The low resolution only allows us to derive column densities from measuring the EWs of the absorption lines and adopt a MISC-CoG analysis where we exclude the most saturated as well as blended transitions. We find a best fit for the Doppler parameter of b=39$\pm$3.0 km^{-2} and most of the ions used for the fit lie on the linear part of the CoG which allows a reliable determination of the column densities. The relative abundances of different metals in the spectra indicate some dust extinction, but an intrinsic difference due to enhancement of the production of certain elements cannot be excluded. The very low amount of dust detected in the afterglow SED may indicate that the latter might be the favored possibility.

We derive a metallicity for the host of [Fe/H] = –1.09 which is slightly higher than metallicities determined from other GRB afterglow spectra. According to the definition of QSO absorbers, the host of GRB 060526 is classified as a LLS ($19 < \log N_{\rm HI} < 20.3$) which seem to have on average higher metallicities than Damped Lyman Alpha systems (DLAs) (Péroux et al., 2007) and a steeper evolution towards lower redshifts. Around redshift 3, however, the metallicities of both samples are within the same range. Also, GRB hosts show a trend towards increasing metallicity with lower redshifts (Fynbo et al., 2006a; Savaglio, 2006). Taking into account that most of the sample used only low-resolution spectra to derive the metallicity (which only gives lower limits for the column densities and the metallicity) this evolution might, however, not be as pronounced as for DLAs and LLS. This might imply that the enrichment of the ISM in the early universe had taken place at earlier times than assumed.

There is a possible detection of a host galaxy with $R = 26.4 \pm 0.2$ at a large offset of 7.7 kpc from the afterglow position, which would make it a rather luminous host, if the source is indeed connected to the GRB. GRBs are assumed to trace the star-formation history of the universe and star formation is assumed to shift towards smaller and fainter galaxies over time as massive galaxies prove to be rather unchanged throughout the history of the universe (e.g. Abraham

et al., 1999; Heavens et al., 2004). One would therefore expect that GRB hosts should also have higher luminosities towards higher redshifts. Fynbo et al. (2008b) concluded that the observed metallicity distribution of GRB hosts (as well as QSO absorbers) at $z \approx 3$ can be explained by the luminosity function of galaxies at that redshift and assuming a luminosity-metallicity relation as derived for other high redshift samples (Ledoux et al., 2006; Erb et al., 2006). GRBs are then assumed to reside in higher luminosity galaxies compared to QSO-DLAs which would match with the tentative host detection for GRB 060526.

Acknowledgements

We thank the support astronomer and staff at the Nordic Optical Telescope for obtaining the observations. Observations were obtained under the ESO proposals 077.D-0661 and 177.A-059. Based on observations made with the Nordic Optical Telescope, operated on the island of La Palma jointly by Denmark, Finland, Iceland, Norway, and Sweden, with the William Herschel Telescope and the Telescopio Nazionale Galileo in the Spanish Observatorio del Roque de los Muchachos of the Instituto de Astrofísica de Canarias and at the Astronomical Observatory of Bologna in Loiano (Italy). Collection of SMARTS data is supported by NSF-AST 0707627. MIRO is supported by the Department of Space, Govt. of India. The Peters Automated Infrared Imaging Telescope (PAIRITEL) is operated by the Smithsonian Astrophysical Observatory (SAO) and was made possible by a grant from the Harvard University Milton Fund, the camera loan from the University of Virginia, and the continued support of the SAO and UC Berkeley. The PAIRITEL project and JSB are further supported by NASA/Swift Guest Investigator Grant NNG06GH50G. We thank M. Skrutskie for his continued support of the PAIRITEL project. The W.M. Keck Observatory is operated as a scientific partnership among the California Institute of Technology, the University of California and the National Aeronautics and Space Administration and was made possible by the generous financial support of the W.M. Keck Foundation.

dt [**d**]	**exptime** [**s**]	**instrument**	**filter**	**mag**
0.09394	180	Maidanak	B	19.518 ± 0.207
0.09898	180	Maidanak	B	19.557 ± 0.135
0.10625	180	Maidanak	B	19.432 ± 0.136
0.10925	180	Maidanak	B	19.505 ± 0.107
0.11421	900	Maidanak	B	19.546 ± 0.179
0.23242	100	RTT150	B	20.133 ± 0.069
0.23813	100	RTT150	B	20.321 ± 0.083
0.24525	100	RTT150	B	20.316 ± 0.081
0.26704	300	RTT150	B	20.395 ± 0.064
0.28883	300	RTT150	B	20.636 ± 0.074
0.31108	300	RTT150	B	20.649 ± 0.073
0.33371	300	RTT150	B	20.839 ± 0.085
1.10542	900	RTT150	B	22.072 ± 0.097
1.16521	900	Maidanak	B	22.013 ± 0.079
1.30279	900	RTT150	B	22.246 ± 0.154
2.14626	2880	Maidanak	B	23.290 ± 0.072
2.35104	900	MOSCA	B	23.104 ± 0.082
3.13135	2700	Maidanak	B	24.198 ± 0.115
3.73439	660	LRIS	g'	23.952 ± 0.022
4.87114	660	LRIS	g'	24.480 ± 0.120
0.19284	60	DOLORES	V	19.235 ± 0.087
0.19443	60	DOLORES	V	19.338 ± 0.065
0.22210	120	MIRO	V	19.274 ± 0.167
0.23067	100	RTT150	V	19.302 ± 0.046
0.23583	100	RTT150	V	19.527 ± 0.047
0.24254	100	RTT150	V	19.364 ± 0.045
0.24818	1200	BFOSC	V	19.403 ± 0.081
0.26313	300	RTT150	V	19.584 ± 0.040
0.28487	300	RTT150	V	19.669 ± 0.040
0.28809	1200	BFOSC	V	19.655 ± 0.078
0.30667	300	RTT150	V	19.821 ± 0.040
0.32942	300	RTT150	V	19.861 ± 0.048
0.33005	1200	BFOSC	V	19.870 ± 0.083
0.41910	600	DFOSC	V	20.155 ± 0.073
0.43507	600	DFOSC	V	20.200 ± 0.057
1.10946	900	RTT150	V	21.027 ± 0.055
1.31288	900	RTT150	V	21.105 ± 0.060
1.40937	600	DFOSC	V	21.267 ± 0.037
1.41685	600	DFOSC	V	21.273 ± 0.040
1.42464	600	DFOSC	V	21.276 ± 0.038
2.32642	900	RTT150	V	22.203 ± 0.123
2.36561	600	DFOSC	V	22.279 ± 0.062
3.14483	3000	RTT150	V	22.818 ± 0.094
3.23404	3000	RTT150	V	22.834 ± 0.094
3.32054	3000	RTT150	V	23.123 ± 0.154
4.24058	7200	RTT150	V	23.508 ± 0.121
5.35387	8400	RTT150	V	24.322 ± 0.211
0.09030	180	Maidanak	R	18.039 ± 0.062
0.09539	180	Maidanak	R	18.042 ± 0.064
0.10079	180	Maidanak	R	18.117 ± 0.067
0.18919	60	DOLORES	R	18.627 ± 0.109
0.19079	60	DOLORES	R	18.763 ± 0.097
0.19165	180	MIRO	R	18.616 ± 0.066
0.19390	180	MIRO	R	18.646 ± 0.068
0.19615	180	MIRO	R	18.546 ± 0.094
0.19838	180	MIRO	R	18.775 ± 0.046
0.20914	600	BFOSC	R	18.723 ± 0.087
0.21225	180	MIRO	R	18.851 ± 0.143
0.21449	180	MIRO	R	18.778 ± 0.273
0.21897	180	MIRO	R	18.756 ± 0.232
0.22144	900	BFOSC	R	18.779 ± 0.083
0.22679	150	RTT150	R	18.576 ± 0.076
0.22892	150	RTT150	R	18.892 ± 0.061

Δt [d]	exptime [s]	instrument	filter	mag
0.23417	150	RTT150	R	18.831 ± 0.060
0.23428	900	BFOSC	R	18.821 ± 0.078
0.24058	150	RTT150	R	18.888 ± 0.066
0.24829	150	RTT150	R	18.881 ± 0.071
0.25054	150	RTT150	R	18.935 ± 0.071
0.25279	150	RTT150	R	18.960 ± 0.070
0.25504	150	RTT150	R	18.805 ± 0.070
0.25530	180	MIRO	R	18.815 ± 0.155
0.25729	150	RTT150	R	18.910 ± 0.071
0.25954	150	RTT150	R	18.917 ± 0.073
0.27050	150	RTT150	R	18.994 ± 0.075
0.27275	150	RTT150	R	19.105 ± 0.081
0.27468	900	BFOSC	R	19.017 ± 0.074
0.27500	150	RTT150	R	19.147 ± 0.081
0.27721	150	RTT150	R	18.993 ± 0.074
0.27946	150	RTT150	R	19.014 ± 0.073
0.28171	150	RTT150	R	18.986 ± 0.075
0.29208	150	RTT150	R	19.073 ± 0.080
0.29438	150	RTT150	R	19.131 ± 0.081
0.29662	150	RTT150	R	19.170 ± 0.079
0.29888	150	RTT150	R	19.129 ± 0.077
0.30113	150	RTT150	R	19.206 ± 0.079
0.30342	150	RTT150	R	19.183 ± 0.074
0.31462	150	RTT150	R	19.144 ± 0.078
0.31599	900	BFOSC	R	19.332 ± 0.080
0.31692	150	RTT150	R	19.128 ± 0.075
0.31917	150	RTT150	R	19.292 ± 0.082
0.32142	150	RTT150	R	19.349 ± 0.083
0.32371	150	RTT150	R	19.289 ± 0.087
0.32596	150	RTT150	R	19.303 ± 0.088
0.33725	150	RTT150	R	19.290 ± 0.083
0.33950	150	RTT150	R	19.275 ± 0.086
0.34179	150	RTT150	R	19.402 ± 0.089
0.34404	150	RTT150	R	19.336 ± 0.089
0.34629	150	RTT150	R	19.341 ± 0.089
0.34854	150	RTT150	R	19.454 ± 0.101
0.35083	150	RTT150	R	19.466 ± 0.103
0.35308	150	RTT150	R	19.505 ± 0.104
0.35533	150	RTT150	R	19.364 ± 0.105
0.35758	150	RTT150	R	19.383 ± 0.106
0.35983	150	RTT150	R	19.417 ± 0.106
0.36208	150	RTT150	R	19.434 ± 0.107
0.36433	150	RTT150	R	19.462 ± 0.111
0.36658	150	RTT150	R	19.270 ± 0.101
0.36883	150	RTT150	R	19.492 ± 0.109
0.37108	150	RTT150	R	19.542 ± 0.122
0.39230	600	DFOSC	R	19.603 ± 0.051
0.40064	600	DFOSC	R	19.607 ± 0.039
0.40800	600	DFOSC	R	19.644 ± 0.037
0.53319	600	DFOSC	R	19.820 ± 0.044
0.54030	600	DFOSC	R	19.868 ± 0.041
0.54841	600	DFOSC	R	19.899 ± 0.042
0.62960	600	DFOSC	R	20.058 ± 0.090
0.63685	300	DFOSC	R	20.030 ± 0.142
0.64096	300	DFOSC	R	20.001 ± 0.145
0.64468	300	DFOSC	R	19.982 ± 0.158
1.10432	540	Shajn 2.6m	R	20.382 ± 0.120
1.11983	900	RTT150	R	20.426 ± 0.069
1.12784	540	Shajn 2.6m	R	20.478 ± 0.113
1.13576	1080	Maidanak	R	20.551 ± 0.041
1.31530	900	BFOSC	R	20.700 ± 0.133
1.31725	900	RTT150	R	20.512 ± 0.068
1.33046	900	BFOSC	R	20.582 ± 0.108

dt [d]	exptime [s]	instrument	filter	mag
1.35328	600	DFOSC	R	20.648 ± 0.043
1.36091	600	DFOSC	R	20.668 ± 0.040
1.37108	600	DFOSC	R	20.686 ± 0.042
1.37829	600	DFOSC	R	20.699 ± 0.038
1.49769	600	DFOSC	R	20.864 ± 0.038
1.50549	600	DFOSC	R	20.836 ± 0.039
1.51330	600	DFOSC	R	20.871 ± 0.037
1.60597	600	DFOSC	R	20.954 ± 0.047
1.61369	600	DFOSC	R	21.031 ± 0.059
1.62117	600	DFOSC	R	20.986 ± 0.067
2.11423	1260	Maidanak	R	21.565 ± 0.100
2.14083	900	RTT150	R	21.373 ± 0.080
2.15346	900	RTT150	R	21.330 ± 0.080
2.16637	900	RTT150	R	21.389 ± 0.082
2.29040	2400	TLS 1.34m	R	21.700 ± 0.130
2.32674	900	MOSCA	R	21.671 ± 0.188
2.33858	900	RTT150	R	21.619 ± 0.091
2.35204	900	RTT150	R	21.587 ± 0.083
2.36504	900	RTT150	R	21.875 ± 0.115
3.10104	1800	Maidanak	R	22.286 ± 0.060
3.16792	3000	RTT150	R	22.062 ± 0.072
3.25538	3000	RTT150	R	22.239 ± 0.077
3.28438	1800	MOSCA	R	22.213 ± 0.052
3.34992	3000	RTT150	R	22.338 ± 0.095
3.73440	660	LRIS	R	22.758 ± 0.042
4.11354	2700	Maidanak	R	23.181 ± 0.100
4.23200	7200	RTT150	R	23.072 ± 0.108
4.37326	1800	MOSCA	R	23.244 ± 0.099
4.87336	900	LRIS	R	23.587 ± 0.123
5.10382	3420	Maidanak	R	23.733 ± 0.096
5.34483	9000	RTT150	R	23.680 ± 0.201
5.35173	3600	ALFOSC	R	23.571 ± 0.088
6.14534	3420	Maidanak	R	>23.6
7.17834	3600	Maidanak	R	>23.8
7.26820	12000	TLS 1.34m	R	>23.7
7.37882	3600	ALFOSC	R	24.602 ± 0.039
10.3198	3600	ALFOSC	R	>24.6
272.654	2500	FORS2	R	>27.1
672.332	7500	FORS2	R	*(combined)*
0.20221	180	MIRO	I	18.311 ± 0.149
0.26296	900	BFOSC	I	18.549 ± 0.070
0.30365	900	BFOSC	I	18.715 ± 0.055
0.34481	900	BFOSC	I	18.901 ± 0.070
0.35175	360	ANDICAM	I	18.940 ± 0.090
0.35683	360	ANDICAM	I	18.937 ± 0.062
0.36191	360	ANDICAM	I	19.052 ± 0.056
0.36692	360	ANDICAM	I	18.967 ± 0.043
0.37107	600	DFOSC	I	19.009 ± 0.048
0.37200	360	ANDICAM	I	18.987 ± 0.036
0.37888	600	DFOSC	I	19.050 ± 0.045
0.38632	600	DFOSC	I	19.118 ± 0.042
0.47240	360	ANDICAM	I	19.266 ± 0.059
0.47737	360	ANDICAM	I	19.310 ± 0.050
0.48238	360	ANDICAM	I	19.338 ± 0.052
0.48747	360	ANDICAM	I	19.361 ± 0.060
0.49254	360	ANDICAM	I	19.359 ± 0.048
1.38701	600	DFOSC	I	20.152 ± 0.039
1.39420	600	DFOSC	I	20.294 ± 0.042
1.40178	600	DFOSC	I	20.223 ± 0.049
2.37793	900	MOSCA	I	21.156 ± 0.041

$t - t_0$ [d]	exptime [s]	instrument	filter	mag
0.36436	360	ANDICAM	J	18.090 ± 0.080
0.48350	1177	PAIRITEL	J	18.638 ± 0.054
0.48494	360	ANDICAM	J	18.580 ± 0.090
0.51112	2260	PAIRITEL	J	19.196 ± 0.114
0.56496	683	PAIRITEL	J	19.472 ± 0.141
0.62604	2190	PAIRITEL	J	18.872 ± 0.054
1.53323	706	PAIRITEL	J	19.575 ± 0.138
1.61412	2237	PAIRITEL	J	19.725 ± 0.157
2.36277	360	ANDICAM	J	>19.1
2.52278	2237	PAIRITEL	J	>20.1
3.46425	2213	PAIRITEL	J	>20.2
4.50410	2266	PAIRITEL	J	>20.3
5.52048	2260	PAIRITEL	J	>20.3
0.48350	1177	PAIRITEL	H	17.726 ± 0.095
0.51112	2260	PAIRITEL	H	17.963 ± 0.077
0.56496	683	PAIRITEL	H	17.741 ± 0.089
0.62604	2190	PAIRITEL	H	17.908 ± 0.074
1.53323	706	PAIRITEL	H	>19.2
1.61412	2237	PAIRITEL	H	19.410 ± 0.244
2.52278	2237	PAIRITEL	H	>19.6
3.50562	2237	PAIRITEL	H	>19.8
4.54525	2260	PAIRITEL	H	>19.8
5.52048	2260	PAIRITEL	H	>19.7
0.48350	1177	PAIRITEL	K_S	16.710 ± 0.101
0.51112	2260	PAIRITEL	K_S	17.385 ± 0.159
0.56496	683	PAIRITEL	K_S	17.062 ± 0.132
0.62604	2190	PAIRITEL	K_S	17.576 ± 0.128
1.53323	706	PAIRITEL	K_S	$>18.0 \pm$ Ě
1.61412	2237	PAIRITEL	K_S	18.148 ± 0.265
2.52278	2237	PAIRITEL	K_S	$>18.8 \pm$ Ě
3.46425	2213	PAIRITEL	K_S	$>18.8 \pm$ Ě
4.54525	2260	PAIRITEL	K_S	$>18.9 \pm$ Ě
5.52048	2260	PAIRITEL	K_S	$>19.0 \pm$ Ě

Table 3.6: *Broad band observations of GRB 060526, times given are the midpoint of the observations. Data have not been corrected for Galactic extinction.*

Published as: Christina C. Thöne, Jochen Greiner, Sandra Savaglio & Emmanuël Jehin – *ISM studies of GRB 030329 with high resolution spectros- copy* Astrophysical Journal, vol. 671, pp. 628–636, December 2007.

4

ISM STUDIES OF GRB 030329 WITH HIGH RESOLUTION SPECTROSCOPY

ABSTRACT – *We present early UVES/VLT high resolution spectra of the afterglow of GRB 030329 at redshift* $z = 0.16867 \pm 0.00001$*. In contrast to other spectra from this burst, both emission and absorption lines were detected. None of them showed any temporal evolution. From the emission lines, we determine the properties of the host galaxy which has a star formation rate (SFR) of 0.198* $M_\odot$*/yr and a low metallicity of 0.17* $Z_\odot$*. Given the low total stellar host mass log* M_**=7.75* $\pm$ *0.15* $M_\odot$ *and an absolute luminosity* m_B*=–16.29, we derive specific SFRs (SSFR) of log SFR = –8.5/yr and SFR = 15.1* $M_\odot$*/yr/*L_**. This fits well into the picture of GRB hosts as being low mass, low metallicity, actively star forming galaxies. The Mg* II *and Mg* I *absorption lines from the host show multiple narrow (Doppler width b=5–12 km/s) components spanning a range of v*$\sim$*230 km/s, mainly blueshifted compared to the redshift from the emission lines. These components are likely probing outflowing material of the host galaxy, which could arise from former galactic superwinds, driven by supernovae from star forming regions. Similar features have been observed in QSO spectra. The outflowing material has high column densities of log* $N_{\rm Mg\,II}$*=13.9* $\pm$ *0.4 cm*$^{-2}$ *and log* $N_{\rm Mg\,I}$*=12.4* $\pm$ *0.4 cm*$^{-2}$ *and the nonvariability of the column densities implies a distance of at least 560 pc from the burst, further supporting an outflow scenario.*

4.1 INTRODUCTION

In this chapter, we present two epochs of high resolution UVES/VLT spectra from the famous and well-studied GRB 030329, which are the only high-resolution data on that burst published. The very low redshift of the burst and the large spectral coverage of the UVES setting chosen allowed to detect both absorption lines from Mg II and Mg I as well as a number of strong emission lines from the host. We first present the emission and absorption lines detected and a number of upper limits on nondetections in Section 4.3. The emission lines are then used to refine the redshift and to derive the extinction, star-formation rate and metallicity of the host galaxy in Section 4.4. The host absorption lines split into 5 components with velocity spread of Δv =280 km/s which we fit with Voigt profiles and determine the column densities in Section 4.5.1. The position of the absorption compared to the emission lines from the host are then used to interpret the kinematics of the ISM in the host galaxy and the nature of those components in Section 4.5.2.

The long GRB 030329 was detected by the HETE-2 satellite at 11:38:41 UT (Vanderspek et al., 2003) and lasted for $T_{90} = 22.9$ s at high energies. In terms of fluence, it was among the top 1% of all detected GRBs. A bright optical afterglow was detected 1.5 h after the burst with an

R-band magnitude of 12.5 (Price et al., 2003). The optical lightcurve showed a slow decay with a power law index of $\alpha = -1.2 \pm 0.1$ and several phases of rebrightenings 1.3, 2.4, 3.1 and 4.9 days (Matheson et al., 2003; Lipkin et al., 2004) after the onset of the burst. From the emission lines of the host in the UVES spectra presented here, a redshift of z=0.1685 was determined (Greiner et al., 2003b).

Due to its brightness and low redshift, a series of low resolution spectra could be taken over several weeks, which showed for the first time the connection between long-duration GRBs and supernovae (SNe) (Hjorth et al., 2003; Matheson et al., 2003; Stanek et al., 2003). Also, for the first time, it was possible to measure the time evolution of the afterglow polarization (Greiner et al., 2003a). Emission line analysis of the host galaxy was obtained from an extensive low resolution dataset taken with the FORS spectrograph (Hjorth et al., 2003; Sollerman et al., 2005b) and spectra from Matheson et al. (2003) who found a SFR of $0.5\,M_{\odot}/yr$ and a moderate metallicity of 12+log(O/H)=8.5, but they assumed the upper branch of the metallicity solution. None of them, however, was able to detect any absorption line as the wavelength range of their spectra missed the Mg II lines in the UV.

4.2 DATA SAMPLE

High-resolution spectra of the afterglow of GRB 030329 have been collected with the UV-Visual Echelle Spectrograph (UVES, Dekker et al., 2000), of the ESO Very Large Telescope (VLT), on the nights of March 30 (UT) and April 2, 2003 under good seeing conditions(0.″9-0.″7). Four 30 minutes exposures and two 1 hour exposures were secured on the first and fourth night after the burst, respectively, using two different beam splitters (dichroic #1 and #2). Two UVES standard settings were used, the so-called DIC1 (R346 nm, B580 nm), and the DIC2 (R437 nm, B860 nm). This combination allowed us to get on the first observing date two spectra covering the full optical range (303 – 1060 nm), except for small gaps near 575 and 855 nm, and one similar spectrum on the second observing night. We combined the two spectra of the first night into one epoch in order to improve the S/N, the spectra of the fourth night are then called epoch II. The use of a 0.″8 slit width provides a resolving power of $\lambda/\Delta\lambda \sim 55{,}000$ or 5.5 km/s (FWHM). The slit was oriented along the parallactic angle in order to minimize losses due to the atmospheric dispersion.

The raw data were reduced using the UVES pipeline (v1.4) implemented in the ESO-MIDAS software package (Ballester et al., 2000). This pipeline reduction includes flat-fielding, bias and sky subtraction and a relative wavelength calibration which has an accuracy of $\pm$ 0.5 km/s. The optimum extraction method has been used, which assumes a Gaussian profile for the cross-dispersion flux distribution and is optimized for low SNR spectra. The individual reduced spectra were also corrected for the airmass, the atmospheric absorption bands could, however, not be removed because of saturation. No correction for vacuum wavelengths or heliocentric velocities (– 16.23 and – 17.36 km/s for the two nights, respectively) was done for the final spectra, this was taken into account later for the redshift determination (see Sec. 4.4). The log of the observations are noted in Table 4.1.

We also did an absolute flux calibration using the master response curves determined by the ESO Garching Quality Control[1] (see also Hanuschik, 2003). Comparison with photometric data of the afterglow from the literature (Matheson et al., 2003) showed that the continuum of the flux calibrated spectrum was almost a factor 2 too low. This discrepancy can not be explained

[1] http://www.eso.org/observing/dfo/quality/UVES/qc/std_qc1.html#response

epoch	dataset	t-t_0 [d]	exptime [min]	R [mag]	seeing ["]	airmass	wavelength range [Å]
I.....	1.....	0.6556	30	15.27	0.73	1.45	3030-3880 + 4760-6840
		0.6785	30	15.31	1.03	1.49	3730-4990 + 6600-10600
	2.....	0.7016	30	15.38	0.97	1.59	3030-3880 + 4760-6840
		0.7244	30	15.46	0.75	1.74	3730-4990 + 6600-10600
II.....	3.....	3.5474	60	17.24	0.49	1.72	3830-4990 + 6600-10600
		3.5925	60	17.25	0.72	1.49	3030-3880 + 4760-6840

Table 4.1: *Log of the observations, times given are the start of the observations*

band	$\lambda_{\rm center}$ [Å]	mag (0.66d)	mag (0.71d)	mag (3.57d)
U	3590	15.23±0.02	15.31±0.01	17.25±0.10
B	4370	15.92±0.03	15.95±0.01	17.94±0.02
V	5445	15.49±0.01	15.69±0.01	17.47±0.01
R	7170	15.28±0.05	15.44±0.05	17.13±0.04
I	9000	14.81±0.01	14.94±0.01	16.72±0.02

Table 4.2: *Photometry used for the flux calibration of the three datasets. Magnitudes used are interpolations from data presented in Matheson et al. (2003); Lipkin et al. (2004) (A. Kann, private communication)*

with bad seeing, it seems, however, to be a common problem in UVES flux calibration. Comparison with FORS spectra taken at the same time suggest that the UVES flux calibration is about a factor of 1.6 too low (Wiersema et al., 2007). We therefore recalibrated the spectrum using photometric data from (Matheson et al., 2003; Lipkin et al., 2004), obtained at the same time as our spectroscopic observations (see Table 4.2) and fitted them with the extinction curve derived in Kann et al. (2006) for that burst which already includes the correction for the Galactic extinction of E(B-V)=0.025. As an example, the entire reduced spectrum of the second epoch is shown in Fig.

4.3 LINE ANALYSIS

4.3.1 EMISSION LINES

We detected a range of emission lines from the GRB host galaxy, listed in Table 4.3. The Balmer series down to Hδ, the forbidden lines [O II] $\lambda\lambda$ 3727, 3729 and [O III] λ5007 as well as [Ne III] λ3869 could be identified. Hα was also detected though it lies in the middle of the atmospheric A absorption band. Fortunately, it fell between two of the resolved atmospheric absorption lines in the atmospheric A band and is therefore very little affected by absorption (see Fig. 4.2). Hδ and Hγ could only be detected clearly in the data from the fourth night. Of the two [O III] lines at 4963 Å and 5007 Å, the 4963 Å line unfortunately falls in the gap of the detector in the red arm which consists of a mosaic of two chips. [N II] λ 6583 was not detected, but a reliable 2σ upper limit could be derived because of the high resolution, despite the fact that this region in the spectrum was also affected by atmospheric absorption bands. All upper limits for the flux were derived assuming resolved lines with a FWHM as given in brackets in Table 4.3. We then used the following formula to calculate the 2σ upper limits: $f_{\rm limit} = 2\sqrt{\rm disp * npix * \sigma^2}$ where disp is the resolution in Å, npix the number of pixels in the FWHM and σ the standard deviation of the continuum at the position of the nondetected lines.

The [O II] doublet was well resolved in the spectra of the fourth night (see Fig. 4.2) which

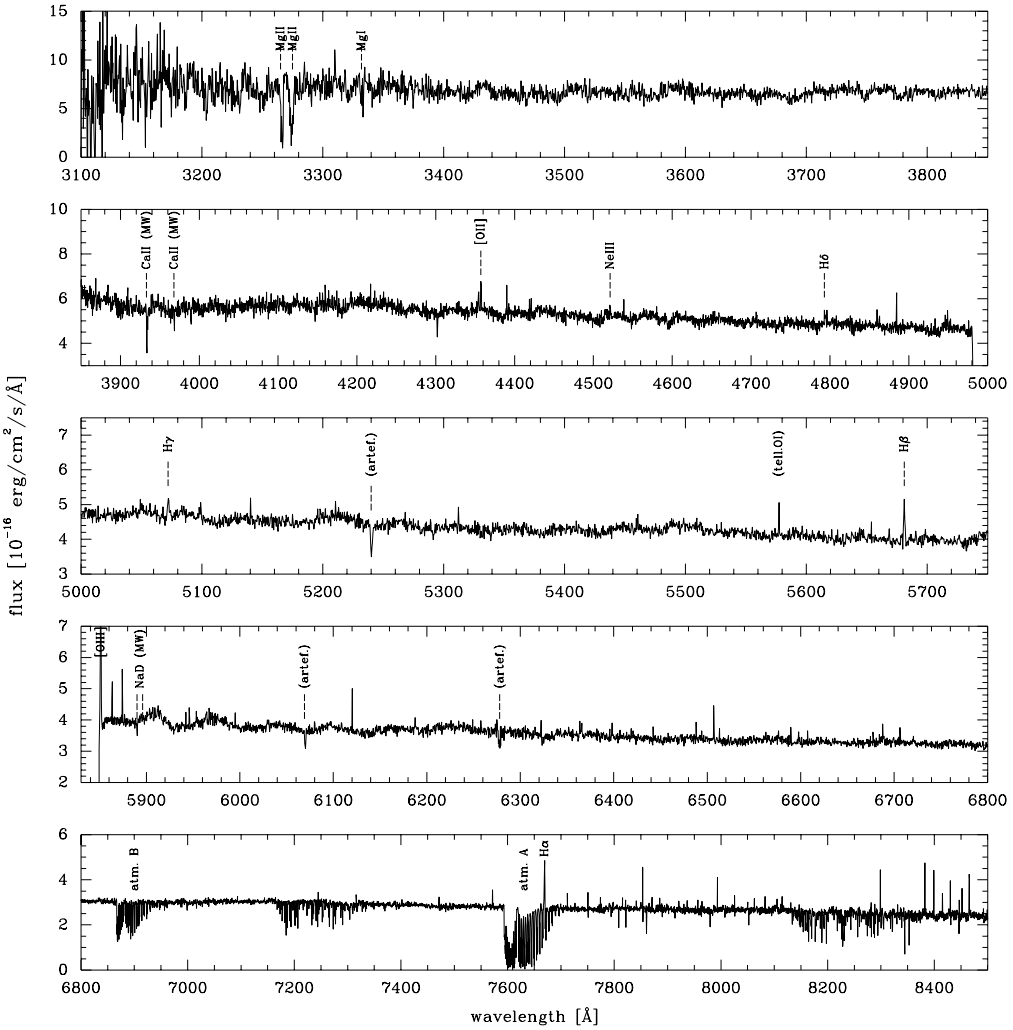

Figure 4.1: *Total UVES spectrum of the second epoch, the fourth night after the burst, where the afterglow continuum has faded away enough to result in a good S/N of the host emission lines. For better visualization of the spectral lines in this graph, the spectra have been smoothed and rebinned to 0.4 Å. Ca* II *and NaD lines are from absorption in the Milky Way (MW), all other absorption and emission lines are from the host galaxy at z=0.16867. The emission features not marked in panel 3 and 4 are due to imperfect atmospheric emission line removal as their FWHM is much smaller than from the lines of the host galaxy and they are only visible in the spectra of this epoch. The features at 5238, 6069 and 6975 Å are due to bad pixels or flatfield errors. Note that the scale of the y-axis changes for the different panels.*

was only possible in three other bursts, GRB 990506 and GRB 000418 (Bloom et al., 2003) as well as GRB 060218 (Wiersema et al., 2007). This is especially interesting because the [O II] $\lambda\lambda$ 3727, 3729 ratio allows the determination of the electron density n_e (Osterbrock, 1989). In our spectrum, the ratio of the two lines is 0.53 ± 0.10 for the fourth nights data when the S/N was high enough to resolve the 3727Å-line, because the afterglow continuum had faded away. This ratio is consistent with the lower value of 0.66 for $n_e \rightarrow 0$. Similar ratios were found for the hosts of GRB 990506, GRB 000418 and GRB 060218 (see references above) with values of 0.57 ± 0.14, 0.75 ± 0.11 and 0.62 ± 0.05, respectively.

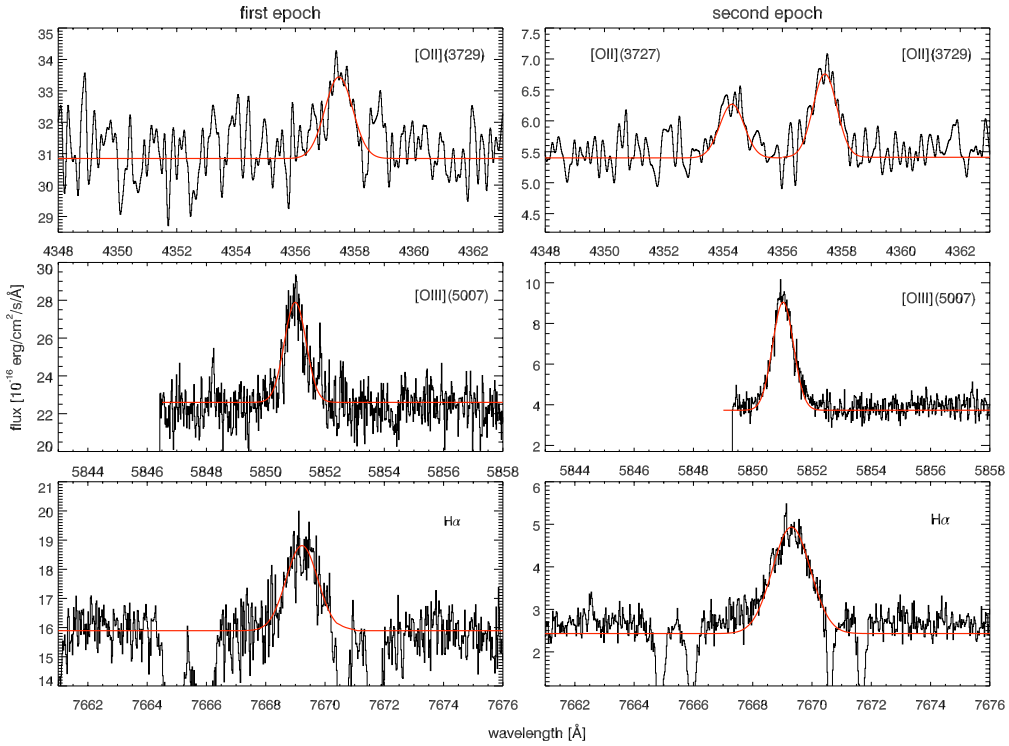

Figure 4.2: *Comparison of some selected emission lines at both epochs together with the fitted Gaussians. First pair: Resolved [O II] λλ 3727,3729, for better visualization, the spectrum has been smoothed with a box car width of 10 pixels. The noise of the continuum in the first epoch is too high to resolve the λ 3727 line. Second pair: [O III] λ 5007 near the gap of the spectrum. Third pair: Position of the Hα line inbetween two atmospheric absorption bands.*

To measure the emission line fluxes, we fitted the lines with a Gaussian and compared it with measuring the line flux directly which gave similar results. The flux of the emission lines is constant within the errors for both epochs, the errors are, however, larger for the first epoch due to the higher continuum. We also note that the light curve of the first night showed large variations and even small color changes (Matheson et al., 2003; Lipkin et al., 2004), which might affect the spectrum. For further calculations, we therefore, we take the emission line fluxes from the fourth night where all lines were detected and the upper limit for [N II] is smaller due to the lower continuum. After recalibrating the spectra with photometric data, our emission line fluxes are mostly consistent with the values found by Gorosabel et al. (2005) and Sollerman et al. (2005b) in FORS spectra of the host galaxy from June 2003 except for the weak detections of Hδ, Hγ and [Ne III] where we find higher values, the fluxes noted in these two papers are, however, consistent within our flux errors.

4.3.2 Absorption lines

Compared to other bursts from which spectra could be obtained, GRB 030329 has a very low redshift. Therefore, most of the metal absorption lines are still far in the UV, below the detection range of UVES. However, we detect the Mg II λλ 2797, 2803 doublet clearly resolved as well as Mg I λ 2852, which all reveal to have several well resolved velocity components. Voigt profiles were fitted to these absorption features using the FIT/LYMAN package (Fontana & Ballester,

Line	epoch	λ_{rest} [Å]	λ_{obs} [Å]	FWHM [Å] and [km/s]	Flux (obs., MW-corr.) [10^{-17}erg/cm^2/s/Å]	Flux (host-A_V corr.) [10^{-17}erg/cm^2/s/Å]
[O II]	I	3726.032	(4354)	(0.9)	<18.1	<30.6
	II		4354.29	0.91±0.10 64±7	9.89±2.1	16.8±4.2
[O II]	I	3728.815	4357.67	0.62±0.10 37±7	14.1±2.3	23.9±3.9
	II		4357.43	0.96±0.10 56±7	14.8±2.1	25.1±3.8
[Ne III]	I	3868.76	4520.80	0.74±0.10 42±6	8.94±3.6	15.0±6.4
	II		4521.27	0.91±0.10 51±6	5.97±1.44	10.0±2.7
Hδ	I	4101.74	(4793)	(0.9)	<18.8	<30.8
	II		4793.07	0.83±0.10 45±6	3.35±1.5	5.49±2.8
Hγ	I	4340.47	(5072)	(0.9)	<10.8	<17.3
	II		5072.21	0.81±0.10 41±6	6.64±2.0	10.6±3.3
Hβ	I	4861.33	5681.17	0.90±0.10 41±5	13.7±2.0	20.8±4.1
	II		5680.99	1.00±0.10 45±5	13.1±1.6	19.9±2.6
[O III]	I	5006.843	5850.90	0.77±0.10 33±5	45.7±1.9	68.4±6.2
	II		5851.03	0.76±0.10 33±5	44.7±1.5	66.9±6.1
Hα	I	6562.852	7669.24	1.33±0.10 45±4	32.6±4.1	43.3±5.3
	II		7669.29	1.40±0.10 47±4	32.5±3.0	43.2±4.3
[N II]	I	6583.45	(7695)	(1.20)	<6.20	<8.23
	II		(7695)	(1.20)	<1.82	<3.08

Table 4.3: *Values for the emission lines for the three different datasets with the numbers indicating the spectra taken in the first and the fourth night after the burst as described in Table 4.1. The measured wavelenghts are in air and not corrected for heliocentric velocity, FWHM is restframe corrected. Fluxes are given as the observed values, corrected for Galactic extinction, (column 6) and as the values corrected for the host extinction as described in Chapter 4.4.3 (column 7), errors include the errors from the Gaussian fits, the continuum and the error in the extinction correction in case of the corrected flux values.*

1995) in MIDAS and the column densities determined for each component (see Chapter 4.5.1).

Interstellar NaD $\lambda\lambda$5890, 5896 and Ca II $\lambda\lambda$ 3933, 3968 from our Galaxy were also detected. The stronger member of the NaD doublet could be resolved into three different clouds, whereas we find only one for the second NaD line as well as the Ca II doublet. The NaD line is affected by imperfect removal of atmospheric NaD emission which is worse in the spectra of the second epoch, the EWs should therefore be taken with care. The relative line strength of the doublets measured fits well to the expected ratio of about (1:1) for both elements. Na and Ca II do not necessarily occur in the same regions in the galaxy and their wavelength and properties can therefore be different (Welty et al., 1999), however, the lines are too weak in our spectra to derive any conclusion about possible differences in the three absorbing clouds.

We did not detect any NaD $\lambda\lambda$5890, 5896, Ca II $\lambda\lambda$ 3933, 3968 or Ti II λ 3242 absorption from the host galaxy. The ratio of Ca II to Mg I, which have similar ionization potentials, found in GRB 020813 (Savaglio & Fall, 2004) was around 1, in our spectra, the limit on this ratio is about 0.1. Ratios found in the MW can vary between 0.01 and 1 depending on the properties of the ISM (Welty et al., 1999). The properties of the absorption lines are listed in Table 4.4.

Line	epoch	λ_{rest} [Å]	$\lambda_{\rm obs}$ [Å]	FWHM [Å]	EW [Å]
Mg II	I	2796	3266.1	1.81±0.20	1.34±0.43
	II		3266.7	1.20±0.21	1.15±0.41
Mg II	I	2803	3274.6	1.66±0.20	1.01±0.42
	II		3274.8	2.60±0.19	1.76±0.51
Mg I	I	2852	3332.8	1.21±0.20	0.22±0.15
	II		3332.9	1.63±0.21	0.34±0.22
NaD	I	5890	5889.6	0.21±0.05	0.045±0.023
			5890.0	0.24±0.05	0.034±0.015
			5890.3	—	<0.015
	II		5889.6	0.20±0.05	0.044±0.018
			5890.0	0.10±0.05	0.047±0.018
			5890.3	0.14±0.05	0.029±0.015
	I	5896	5895.6	0.21±0.05	0.018±0.010
			5895.8	—	<0.009
			5896.1	—	<0.009
	II		5895.6	0.11±0.05	0.026±0.024
			5895.8	—	<0.020
			5896.1	—	<0.020
Ca II	I	3933	3933.5	0.24±0.04	0.24±0.05
			3934.6	0.29±0.04	0.10±0.05
	II		3933.5	0.51±0.15	0.25±0.16
			3934.5	0.65±0.15	0.11±0.07
	I	3968	3968.3	0.14±0.05	0.09±0.05
	II		3968.3	0.41±0.05	0.12±0.07

Table 4.4: *The upper part are absorption lines from the host galaxy, the lower part from the MW. All values are given in the restframe. The FWHM of the Mg lines are the widths measured in a spectrum rebinned to 1 Å. Note that the NaD interstellar lines from the second epoch are affected by imperfect sky line removal from telluric NaD emission. Only one component of the NaDλ 5896 has a clear detection, for the other components, we only give 1σ upper limits.*

4.4 Results

4.4.1 Redshift

The redshift of the host galaxy was determined from the [O III] λ 5007, Hα and Hβ emission lines of the first epoch (Greiner et al., 2003b) as $z = 0.1685$. We did a refined analysis using the emission lines [O II] $\lambda\lambda$ 3726, 3729, [O III] λ5007, Hα and Hβ, corrected for heliocentric velocities of -16.23 and -17.36 km/s for epoch I and II, respectively. From this, we derive a value of $z = 0.16867 \pm 0.00001$, consistent with the value found by Matheson et al. (2003) and Sollerman et al. (2005b). Note, however, that this is the mean redshift of the GRB host galaxy, not of the GRB itself.

4.4.2 Broadening of the emission lines

Low resolution spectra are usually not able to distinguish between instrumental resolution and intrinsic broadening of the host emission lines due to galaxy rotation and turbulence of the medium. From our high resolution spectra (FWHM = 5.5 km/s), we find that all emission lines in our spectra are clearly broadened compared to the resolution of the instrument. The FWHM

of the emission lines lies between 35 and 55 km/s, restframe corrected. This fits well to the fact that the host of GRB 030329 is a dwarf galaxy, which have typical rotational velocities up to 100 km/s. We might, however, not see the whole rotational velocity spread if the galaxy is not seen edge on.

4.4.3 GALACTIC AND HOST EXTINCTION

For the determination of the Galactic extinction, usually sky catalogs such as Schlegel et al. (1998) or Dickey & Lockman (1990) are used. The strength of interstellar lines like NaD, however, allows a different and more accurate determination of the extinction using e.g. the model of Munari & Zwitter (1997) who take the NaD λ 5890 line. In our spectra, Galactic NaD as well as Ca II show a triple absorption peak, indicating three clouds in our Galaxy in the line of sight. The NaD-line gives an extinction of $E_{B-V} = 0.012 \pm 0.006$, 0.007 ± 0.004 and 0.002 ± 0.001 for the three clouds, respectively, which results in a total extinction of $E_{B-V} = 0.021 \pm 0.014$ or $A_V = 0.065 \pm 0.043$ as $A_V = R_V E_{B-V}$ with R_V =3.1 for a MW extinction law (Cardelli et al., 1989). This is comparable to the extinction determined from the Schlegel sky catalog of $E_{B-V} = 0.025$.

The extinction in the host galaxy can in principle be derived from the Balmer line decrement, the constant flux ratio of the Balmer lines derived from line transition properties, with unextinguished values of Hα/Hβ = 2.76 and Hγ/Hβ = 0.474 for a temperature of 10,000 K and case B recombination (Osterbrock, 1989). From our spectrum we obtain Hα/Hβ = 2.49 $\pm$ 0.2 and Hγ/Hβ = 0.51 $\pm$ 0.15 which is consistent with no extinction for both epochs. In addition, the Balmer lines can be affected by absorption from an underlying stellar population depending on the age of the galaxy. However, in the UVES spectra, we could not identify any underlying stellar absorption, whereas Gorosabel et al. (2005) derive a relatively high correction, comparable to the value of the fluxes for Hγ and Hδ from their stellar population models. We consider it therefore to be more appropriate to use an extinction value derived from the broad band afterglow as it was done in Kann et al. (2006). They derive a value of $A_V = 0.39 \pm 0.15$, fitting an SMC extinction law, which differs, however, very little from the fit with a MW extinction law.

For the correction of the emission line fluxes of both epochs, we then use $A_V = 0.39 \pm 0.15$ for the host extinction applying a MW extinction law (see Table 4.3). The photometry used for calibrating the spectrum already includes the correction for the Galactic extinction of A_V = 0.078.

4.4.4 SFR

A direct indicator of the current SFR in a galaxy is the flux from nebular emission lines such as Hα that had been ionized by young, massive stars. Using the Hα flux from the 3rd epoch, which is corrected for extinction but not for a possible underlying stellar absorption, we derive a SFR of the host galaxy according to Kennicutt (1998) of SFR [$M_\odot$/yr] = $7.9 \cdot 10^{-42} 4\pi f_{H\alpha} d_L^2$ = 0.198$\pm$0.007 $M_\odot$/yr which is consistent with the value in Hjorth et al. (2003) of $SFR_{H\alpha}$ = 0.17 $M_\odot$/yr from the FORS spectra. Another indicator for the SFR are forbidden lines like [O II] with the drawback of being only indirectly coupled to the ionizing flux of young stars but very sensitive to the ionization state of the ISM. For [O II], the corresponding equation SFR [$M_\odot$/yr] = $1.4 \cdot 10^{-41} 4\pi f_{[OII]} d_L^2$ gives a value of 0.267 ± 0.009 $M_\odot$/yr taking the sum of the [O II]$\lambda\lambda$3726,3729 fluxes from the second epoch. As this indicator is less reliable, we therefore adopt here the SFR from Hα.

A SFR of 0.198 $M_\odot$/yr is not very high compared to other galaxies at this redshift, but one

has to consider the low mass of the host galaxy as already noted in Sollerman et al. (2005b). Savaglio et al. (2008) derive a low total stellar mass for the host of log $M_\star = 7.75 \pm 0.15$ $M_\odot$. This gives a specific SFR (SSFR) per unit mass of log SFR/M $= -8.5$/yr. Furthermore, the host galaxy of GRB 030329 is underluminous with an absolute magnitude of $m_B = -16.29$ (Gorosabel et al., 2005). This can be used to scale the SFR with the luminosity fraction compared to a standard galaxy with $m_{B(abs)} = -21$ to derive the SFR/L (Christensen et al., 2004). For our host, we get a value for the SFR/L of 15.1 $M_\odot/yr/L_*$ which is high compared to the average of other host galaxies of 9.7 $M_\odot/yr/L_*$ as found by Christensen et al. (2004).

4.4.5 METALLICITY OF THE HOST

There are a number of secondary, empirical metallicity calibrators derived from the abundances of nebular emission lines. The most frequently used, because easiest to measure, is the $R_{23} = \frac{f_{[\mathrm{OII}]\,\lambda3727} + f_{[\mathrm{OIII}]\lambda\lambda4959,5007}}{f_{\mathrm{H}\beta}}$ parameter (Kobulnicky et al., 1999). [O III] λ4959 was not detected due to the gap in the spectrum, there is, however, a fixed ratio between the two [O III] lines, $f_{[\mathrm{OIII}]\,\lambda5007}$=3·$f_{[\mathrm{OIII}]\,\lambda4959}$.

The R_{23} parameter gives two possible solutions, but this degeneracy can be broken using the [N II] λ6583 to Hα ratio (Lilly et al., 2003). As noted in Sollerman et al. (2005b), no [N II] was detected in the spectra of GRB 030329, except from the FORS spectrum of May 1st (Hjorth et al., 2003), which seems to be spurious. Due to the high resolution of the UVES spectrum however, we were able to put a strong 2σ upper limit of [N II] (see Table 4.4 and Chapter 4.4) and therefore to derive a ratio of [N II]/Hα from the strongest upper limit at the 3rd epoch of $< 0.06 \pm 0.01$, which favors a lower branch solution according to Lilly et al. (2003). We applied both the calibrations for the R_{23} parameter from Kewley & Dopita (2002), used for most GRB host metallicities and the most recent one from Kewley et al. (2007). These parametrizations give then values of 12+log(O/H) = $8.3^{+0.2}_{-0.3}$ and $7.9^{+0.2}_{-0.3}$, respectively, where the errors account for the error in the line fluxes from the second epoch which we use for the calculations. These values correspond to 0.44 and 0.17 $Z_\odot$, assuming 12+log(O/H)=8.66 for solar metallicity (Asplund et al., 2004). The low mass of the host galaxy supports a low value for the metallicity.

The R_{23} parameter, however, has turned out to be affected by systematic errors for high and low metallicities (Bresolin et al., 2004). Wiersema et al. (2007) showed that the metallicity of the GRB 060218 host, derived from the oxygen abundances, is 12+log(O/H) = 7.54, compared to 8.0 from the R_{23} parameter. For a direct calibration from the abundances, however, the electron temperature and density have to be known which rely on the detection of [O III] λ4363 and the detection or low error flux measurements of the [O II] $\lambda\lambda$3727, 3729 or [S II] $\lambda\lambda$6716,6731 doublets, which were not detected for the GRB 030329 host or only with large errors in the case of [O II].

4.5 ABSORPTION LINE KINEMATICS

4.5.1 FITTING OF THE ABSORPTION SYSTEMS

For the absorption lines in the host galaxy, we found five different velocity components for the Mg II doublet which we fitted together, whereas Mg I only shows four because of its lower line strength. The components span a velocity range of about 230 km/s (see Fig. 4.3) in both Mg II and Mg I. Mg I shows the same velocity differences as the Mg II components, except for the two components at v=-43 and -67 km/s for which we found only one component in Mg I, so it seems that both arise from the same structure. This does not necessarily have to be the case due

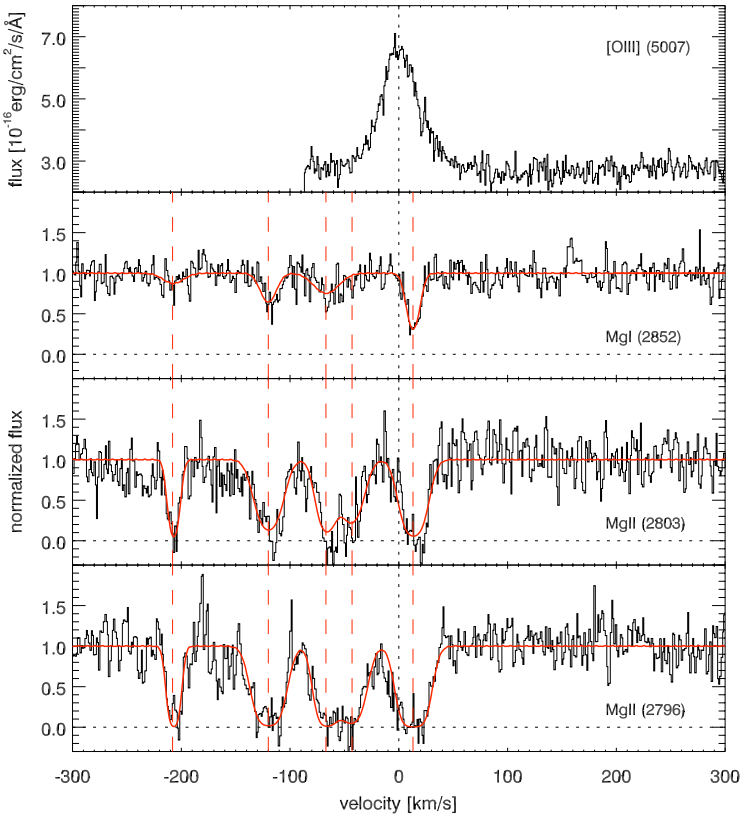

Figure 4.3: *Velocity distribution of the five components in the Mg* II*-doublet and four in Mg* I *and the corresponding fit to the different components with FIT/LYMAN where the Mg II lines where fitted as doublets. v = 0 km/s corresponds to the redshift determined by the emission lines from the host where the [O* III*] line is shown as an example in the top panel. We coadded all three datasets to get better statistics for the fit, as there were no changes in line strength between in the data from the individual epochs.*

Component	MgII[2796,2803]		MgI[2852]		log N_{MgI}/ N_{MgII}
	b [km/s]	log N [cm^{-2}]	b [km/s]	log N [cm^{-2}]	
v_1 = + 13 km/s	12.06±0.53	13.45±0.04	6.81±0.85	12.06±0.05	−1.39±0.19
v_2 = − 43 km/s	12.10±0.94	13.17±0.03	—	—	—
v_3 = − 67 km/s	9.77±0.78	13.24±0.05	15.15±5.83	11.75±0.10	−1.49±0.23
v_4 = − 120 km/s	13.09±0.70	13.33±0.04	9.22±1.98	11.74±0.07	−1.59±0.21
v_5 = − 208 km/s	4.82±0.54	13.20±0.15	12.45±4.10	11.35±0.15	−1.85±0.30

Table 4.5: *The Mg II doublet was fitted together, therefore column densities and b parameters are the same for the two lines of the doublet.*

to the different ionization stages. The b parameter of the five components is relatively narrow with 5−12 km/s.

No time variability of the absorption lines was seen between the different spectra and we therefore coadded all three datasets weighted according to their variance in order to improve the S/N. The constant value of the absorption lines rules out an origin in the vicinity of the burst (Perna & Loeb, 1998; Prochaska et al., 2006b), where one would expect a considerable weakening of the Mg absorption between the first and the fourth night. Furthermore, the Mg II

absorption in all components goes down to zero flux, supporting the suggestion that the absorption does not occur at a very short distance from the central source. Otherwise, scattered light could lead to a covering factor smaller than one (Savaglio & Fall, 2004).

From the absence of Mg I variability in between the two epochs, one can derive a minimum distance to the GRB according to Mirabal et al. (2002) (see also Prochaska et al., 2006b; Vreeswijk et al., 2006). For the fluence at the position of Mg I, we integrate the flux density in the U band between t_1=0.6 and t_2=3.5 d, F_1=1.826$\times10^{-26}$ erg s^{-1}cm^{-2}Hz^{-1} and F_2=2.0$\times10^{-27}$ erg s^{-1}cm^{-2}Hz^{-1} (data taken from Matheson et al., 2003), assuming a simple powerlaw evolution between the two epochs. This leads to a number of photons ϕ=1.27$\times10^{61}$ at the burst restframe and at the ionization energy of Mg I of 8.5 eV. We take a very conservative estimate of $< 25\%$ for the decline of the column densities N_I and N_{II} between the two epochs and assume the cross section $\sigma_{\rm ph}^{\rm Mg\,I}$ to be roughly 10^{-18} cm^2, which gives a minimum distance to the GRB of

$$r_{min} = \sqrt{\frac{\phi\sigma_{\rm ph}^{\rm Mg\,I}}{4\,\pi\,ln(N_{\rm I}/N_{\rm II})}} > 560\,{\rm pc}$$

This further supports the suggestion that the absorbing material is not in the vicinity of the burst as noted above.

The individual components at the different velocity shifts have similar column densities, though comparison of the ratios N(Mg II) to N(Mg I) show that the conditions in the different absorbing structures might vary slightly. The total Mg II column density is $\log N_{\rm MgII} = 13.99 \pm 0.42$ cm^{-2} which is in the regime of sub-DLAs (Rao & Turnshek, 2000). The gas in DLAs has a low ionization and a relatively large column density of $\log N_{\rm MgII} = 12.39 \pm 0.40$ cm^{-2} compared to N(Mg II) as shown in Table 4.5.

As the S/N of even the coadded spectrum is quite low, we also performed an appearent optical depth analysis according to Savage & Sembach (1991) in order to check the reliability of our VP fitting. The column densities derived from that are (13.9 cm^{-2}) for Mg II and (12.4 cm^{-2}) for Mg I which is fully consistent with the values derived from the VP fitting.

4.5.2 Interpretation of the Mg I & II velocity structure

Mg I and II have been detected in many GRB afterglow spectra (Castro et al., 2003; Fiore et al., 2005; Starling et al., 2005b; Penprase et al., 2006; Prochaska et al., 2007), where two types of velocity spreads were found. The first type shows saturated Mg lines with a velocity broadening up to 200 km/s, comparable to the instrumental resolution in low resolution spectra or resolved in high resolution spectra as a truly broad absorption feature as in Penprase et al. (2006). The broad features from low resolution spectra could sometimes be partially resolved as in Castro et al. (2003), who found a second component with a Δv of 180 km/s. Therefore, it is likely that the broad lines sometimes actually consist of several distinct components, which could have been resolved with higher resolution spectrographs. The other type shows many high velocity components with Δv up to 3000 km/s as in Fiore et al. (2005) and Starling et al. (2005b).

The high velocity components are usually explained as being connected to the GRB itself like tracing nebula shells from former mass losses of the progenitor star, excited by the GRB (Mirabal et al., 2002) or strong winds which blow material of the star away from the Wolf-Rayet progenitor. The latter scenario was suggested for the high velocity components in GRB 020813 (Fiore et al., 2005), GRB 021004 (Fiore et al., 2005; Starling et al., 2005b), GRB 030226 (Klose et al., 2004), GRB 050505 (Berger et al., 2006) and recently GRB 051111 (Penprase et al., 2006) who found absorption features up to 3000 km/s. For GRB 021004, however, Chen et al. (2005) argues against

the wind scenario due to the detection of low ionization lines in the highest velocity complexes. The velocities measured in GRB 030329, however, are much lower, such winds can therefore not be the explanation for the components seen in our spectra. If those high velocity features were common for GRBs, they should have also been detected in GRB 030329, in addition to the low velocity components, but there are no absorption features visible at comparable velocity distance from the main component. Neither were they detected in any other spectra than those of GRBs mentioned above though the distances are far enough to be resolved in low resolution spectra as in the case of GRB021004 (Mirabal et al., 2002). Either the ISM around the burst must be quite dense to produce these clumps, not all GRB progenitors have high mass losses and strong winds or the reason for these components is something completely different.

Since the Mg lines in GRB 030329 have much lower velocity, we have to seek for different explanations. One possibility are supergalactic winds from starburst regions as found in spectra of low-redshift starburst galaxies and clearly visible e.g. in Hα light from M82. These winds were discovered in X-ray data, as the heated ISM emits X-rays. Heckman et al. (2000) studied the structures of NaD lines from such starburst galaxies. They found blueshifted components relative to the host galaxy up to 600 km/s with Doppler width of more than 100 km/s which seems likely for a hot environment (T$\approx$70,000 K). This, however, rules out the possibility of an active starburst wind for our absorption line features as the velocities are too low for a wind origin and in addition, the lines are very narrow, so the absorbing atoms cannot be in a hot environment.

In the MW as well as in other galaxies, so-called "high velocity clouds" have been found, consisting mainly of HI, but O VI has also been discovered from the same region (Fox et al., 2005). This gave rise to the theory of the galactic fountain where starburst regions blow hot, ionized material out into the halo which then cools down and eventually falls back again onto the galaxy (Bregman, 1980). The Mg absorption lines in our spectra might therefore be caused by some intermediate stages of that process, when the starburst wind has cooled and slowed down. The fact that, except for the two lowest-velocity systems, the velocities are larger than the rotational velocity of the host galaxy as determined from the emission line width, indicates that they are most likely not just related to large structures in the host galaxy like spiral arms. With the escape velocity typically being less than 50% larger than the mean rotational velocity, half of our velocity systems are likely to be unbound to the gravitational potential of the host galaxy. Further support to an origin outside the galaxy comes from the minimum distance of the Mg I absorbing material to the GRB of 560 pc for the redmost component. The star burst wind suggestion is therefore an appealing scenario for those structures.

The same process might cause Mg II absorbers, which have often been found in the sightline of QSOs (Ellison et al., 2003) with large EW. Similar structures have also been discovered in Lyman break galaxies (LBG) (Adelberger et al., 2003) but only for C IV absorption lines. DLAs associated with Mg-absorbers show black bottom saturated Mg velocity components with narrow spreads of about 40 to 60 km/s. So-called "doubles" and "classics" have smaller EWs and highly complex features separated by a large Δv (Churchill et al., 2000) with their individual components having Doppler widths comparable to those found in GRB 030329. This might lead to the conclusion that Mg QSO absorbers and GRB absorbers have the same origin but that they are probing different regions of the galaxy. Bond et al. (2001) also suggested that QSO-Mg absorbers could arise in optically thick clouds in the galactic halos, created by material ejection from starburst regions, being the remnants of a former starburst wind.

In contrast to QSO absorbers, which can have lines both red- and blueshifted compared to the redshift of the intervening galaxies, in our case there exist only blueshifted lines except for

the first component. This might be a hint to the position of the burst in the galaxy. If these components are really due to some metal rich clouds in or around the host galaxy, the burst could lie slightly behind the center plane of the galaxy or the star burst cloud which causes the few redshifted components, whereas the rest of the lines come from material flowing away from the burst site.

4.6 CONCLUSION

In this paper, we have presented high resolution spectra of a typical long-duration GRB at z=0.16867, which had the rare case to contain both emission lines from the host galaxy as well as absorption lines from the surrounding medium of the burst. The host galaxy is a subluminous (m_B=−16.29), low mass ($\log M_\star = 7.75 \pm 0.15\,M_\odot$) starburst with a high SFR/L of 15.1 $M_\odot$ yr^{-1} L_*^{-1} or log SFR/M = -8.5 yr^{-1} compared to other galaxies at this redhsift. This confirmes the values of the SSFR found by Hjorth et al. (2003) and Sollerman et al. (2005b) from late FORS spectra of the host galaxy. Furthermore, the high resolution UVES spectra made it possible to derive a strong upper limit for [N II] and therefore to place the value of the metallicity in the lower branch with log(O/H)=7.9 or 0.17 $Z_\odot$.

In absorption, only Mg II and Mg I from the host could be detected. Due to the high resolution again, however, we were the first to resolve these usually broad absorption lines into eight and five narrow velocity components for Mg I and Mg II, respectively. These components span a relatively small range of velocities up to v∼230 km/s, which can usually not be resolved in low resolution spectra. The majority of these components are, however, outside of the galaxy whose emission lines have only a width of 55 km/s. Both Mg I and Mg II seem to originate in the same clouds which are predominantly neutral with N(Mg I)/N(Mg II) of around –1.5. Structures similar in width and velocity distance have been found in QSO Mg absorbers. They could be clouds in the halo of the host galaxy, possibly from material ejected from the inner regions of the galaxy by former starburst driven superwinds which have already slowed down.

The *Swift* satellite now provides faster information of the burst position and more early, high resolution spectra can be obtained. Very early spectra, compared with later times, now also reveal changes of the absorption lines due to ionization of the ISM by the burst (Vreeswijk et al., 2006, Vreeswijk et al. in prep.).

Acknowledgements

C.T. wants to thank Johan Fynbo, Alexander Kann and Daniele Malesani for reading and improving the manuscript, useful discussions about technical issues, pointing out errors and Alexander Kann in particular for providing the extinction law derived in his paper to fluxcalibrate the spectra. Thanks also to Klaas Wiersema for the preprint of his paper on GRB 060218 and informations about advanced line diagnostics. We would also like to thank the VLT staff for performing the ToO UVES observations. The observations obtained were based on ESO proposal 70.D-0087.

Published as: Christina C. Thöne, Klaas Wiersema, Cédric Ledoux, Rhaana L. C. Starling, Antonio de Ugarte Postigo, Andrew J. Levan, Johan P. U. Fynbo, Peter A. Curran, Javier Gorosabel, Alexander J. van der Horst, Alvaro LLorente, Evert Rol, Nial R. Tanvir, Paul M. Vreeswijk, Ralph A. M. J. Wijers & Lisa J. Kewley – *'The host of GRB 060206: kinematics of a distant galaxy"* Astronomy and Astrophysics, in press, preprint: astro-ph/0708.3448

5

THE HOST OF GRB 060206: KINEMATICS OF A DISTANT GALAXY

ABSTRACT – *We investigate the state and properties of the interstellar medium in the host of GRB 060206 at $z = 4.048$ with an early afterglow spectrum obtained with WHT/ISIS of GRB 060206, starting 1.6h after the burst. Additional information is provided by the afterglow lightcurve. The resolution and wavelength range of the spectra and the bright afterglow facilitate a detailed study and fitting of the resonant and fine-structure absorption line systems in order to derive column densities. We also use deep imaging to detect the host galaxy and probe the nature of an intervening system at $z = 1.48$ seen in absorption in the afterglow spectra. We detect four discrete velocity systems in the resonant metal absorption lines, best explained by shells within and/or around the host created by starburst winds. The fine-structure lines have no less than three components with strengths decreasing from the redmost components. We therefore suggest that the fine-structure lines are best explained to be produced by UV pumping from which follows that the redmost component is the one closest to the burst where also* NV *was detected. The host is detected in deep* HST *imaging with F814W$_{\rm AB}$ = 27.48 ± 0.19 mag and a 3 σ upper limit of $H = 20.6$ mag (Vega) is achieved. A candidate counterpart for the intervening absorption system is detected as well, which is quite exceptional for an absorber in the sightline towards a GRB afterglow. The intervening system shows no temporal evolution as claimed by Hao et al. (2007) which we prove from our WHT spectra taken before and Subaru spectra taken during the observations from Hao et al.*

5.1 INTRODUCTION

In this chapter, we present medium resolution spectra of a high redshift burst. A first paper on the dataset presented here (Fynbo et al., 2006a, hereafter Paper I) showed initial results of the WHT and NOT spectra of the afterglow of GRB 060206 focussing on the metallicity which they compared to a large sample of QSO absorber metallicities and the sample of known GRB afterglow metallicities. In the following chapter, we analyze the full set of absorption lines including resonant as well as finestructure transitions and derive the corresponding column densities for the different components in Chapter 5.4. The finestructure transitions trace the resonant transitions and we use the ratio between these transitions to derive a distance to the GRB of about 1 kpc which is in line which what has been found for other GRBs (Chapter 5.5.1). A host is detected in deep Gemini and *HST* imaging (Chapter 5.6). The claimed variability of an intervening system at z=1.48 is reinvestiaged with data from the Subaru archive and could be disproven (Chapter 5.7).

5.2 OBSERVATIONS

5.2.1 SPECTROSCOPY

We make extensive use in this paper of the dataset described in Paper I, to which we refer for details on the observations and data reduction. For clarity, we reiterate here the important steps. We obtained a medium resolution spectrum with the Intermediate-dispersion Spectroscopic and Imaging System (ISIS) on the 4.2m William Herschel Telescope (WHT) on 2006 February 6, starting 1.61 hours after the burst. We took two spectra with exposure times of 900 s each, separated only by the read-out time of the CCD. The spectrograph has a blue and a red arm, providing FWHM resolutions of 1.68 and 0.82 Å, respectively. A redshift of $z = 4.04795 \pm 0.00020$ was determined from several absorption lines within the host (Paper I). At this redshift, the WHT spectra cover the rest frame wavelength range of approximately 753 – 1030 and 1228 – 1387 Å for the blue and red arm, respectively. As the Lyα line falls into the gap between the two arms, we used the column density derived from the NOT spectra (Paper I) for deriving metallicities. The signal-to-noise ratios of the spectra are high, strongly aided by the sudden, strong rebrightening of the afterglow just prior to and during the spectroscopic observations reaching a maximum of R$\sim$ 16.4 mag Woźniak et al. (2006). Furthermore, we obtained 8 $\times$ 1800s low-resolution (R $\sim$ 300) spectra from the SUBARU archive Baba et al. (2002) from about 6 to 10 hrs after the burst. We reduced the spectra with standard tasks in IRAF.

The optical afterglow of this burst proved bright with R$\sim$ 18.1 mag after 1 day, and owing to its fortunate location on the sky (RA 13:31:43, DEC +35:03:03 (J2000)), it was observed at a large range of Northern observatories (e.g. Woźniak et al., 2006; Monfardini et al., 2006; Stanek et al., 2007). A detailed discussion of photometric afterglow observations and the lightcurve physics can be found in Curran et al. (2007). We use these observations together with Swift XRT data to analyze the broadband optical to X-ray extinction (see Chapter 5.3).

5.2.2 IMAGING

We observed the location of the afterglow on February 16, 2007, over a year after the burst, using the GMOS-N instrument on Gemini-North with the aim of detecting the host and intervening absorber galaxies in emission. Observations were performed in the GMOS r' band, which has a similar shape and throughput as the SDSS r' band. The dataset consists of 9 $\times$ 300 s exposures with a seeing of $\sim$1 arcsec and an airmass of $\sim$ 1.1. Reduction was done using the *Gemini* package in IRAF and the photometry was calibrated against archival SDSS observations of the GRB 060206 field (Cool et al., 2006). For the combined image we derive a 3σ upper limit of $r'_{\rm AB}$= 26.3 which was obtained by examining the standard deviation of 50 blank apertures placed at random positions on the image.

We also observed the GRB field in the near-infrared on June 3, 2007 using the Omega 2000 instrument on the 3.5m telescope at the Calar Alto Astronomical Observatory (CAHA). Observations consisting of 50 $\times$ 60 s were performed in the *H*-band with a limiting magnitude of H=20.6 mag (Vega).

GRB 060206 was finally observed with *HST* on 25 November 2006, using the ACS/WFC and F814W filter under the program 10817 (PI H.-W. Chen), which are now publicly available from the *HST* archive. 8 dithered exposures were obtained with a total exposure time of 9886 s. We processed these data through the standard multidrizzle pipeline, setting the linear drop size (`pixfrac`) to one, and the final output scale to 0.″033 per pixel. Performing relative astrometry between our early NOT observations (Fynbo et al., 2006a; Curran et al., 2007) allows us to place

the afterglow on this image with an accuracy of $\sim 0\farcs05$.

5.3 Extinction along the line-of-sight

To obtain limits on the absorption along the line of sight to GRB 060206, we fit the near-infrared to X-ray spectral energy distribution (SED) in count space Starling et al. (2007), and using the metallicity as determined through the sulphur lines of [S/H] = -0.86. The SED is created using RJHK$_S$ photometry and an X-ray spectrum from *Swift* XRT (Gehrels et al., 2004; Burrows et al., 2005a), centred at ∼2.8 hours after burst, detailed in Curran et al. (2007). We note that this is close in time to our WHT spectra, which were taken at mid-time 1.86 hrs after burst. We perform fits using an absorbed single power law, and then a broken power law to model a possible cooling break.

The SED is well fit with a single power law with $\beta = 0.93 \pm 0.01$ and χ^2/dof = 1.05. A broken power law does not provide a significant improvement in the fit according to the F-test. We find no evidence for intrinsic ($z = 4.048$) optical or X-ray extinction above the Galactic values. At this high redshift of $z = 4.048$ the metal edges that dominate the X-ray extinction are shifted out of the XRT energy range and are not sensitively probed. The near-infrared and optical data at this redshift, however, probe restframe UV and blue bands, and are therefore sensitive to extinction. We estimate a 3σ upper limit for the intrinsic optical/UV extinction of $E(B-V) < 0.01$. To derive this we fitted the SED in count space from X-ray to optical simultaneously (as described in Starling et al., 2007) with an LMC, SMC and MW extinction law and increased the value of E(B-V) until $\chi^2 = 1$, corresponding to a 1σ deviation. This shows that the intervening systems as well as the host velocity systems have low dust content, which can be used to distinguish between different origins of these systems.

5.4 Absorption line analysis

We reported equivalent widths and column densities for a selection of absorption lines in Paper I, with the aims of deriving a metallicity for the line-of-sight within the host, the exact velocity decomposition of the systems and the fine-structure line ratios as a function of velocity. In this paper we present a full analysis of all absorption lines in the host galaxy and the intervening systems. The results of the host galaxy systems are presented in Table 5.1 and Table 5.2 as well as Fig. 5.1 and 5.2, the fits for the intervening system can be found in Table 5.3 and Fig. 5.3.

For the host galaxy with a systemic redshift of $z = 4.048$, we detect four main velocity systems at $v_1 = 169$ km/s, $v_2 = 69$ km/s, $v_3 = -11$ km/s and $v_4 = -228$ km/s which we refer to as systems 1 to 4 respectively. In order to obtain a better fit, we had to introduce two additional subcomponents for all strong lines (see below) which are at velocities of $v_{1a} = 127$ km/s and $v_{3a} = -67$ km/s. In addition, we find an intervening system at $z = 1.47895$ which shows two components at $v_1 = 25$ km/s and $v_1 = -30$ km/s. Zero velocities are chosen arbitrarily as the midpoint of the entire system, as the exact redshift of the host and the intervening galaxies are unknown.

In order to fit the different components, we use the FITLYMAN package in MIDAS (Fontana & Ballester, 1995). The fitting is, however, complicated by the strong blending as well as saturation in a number of lines. We therefore use the weak, unsaturated S II λ1253 transition as a template for the position of the four main components v_1 to v_4. For the Si-lines as well as O I and C II and the corresponding fine-structure lines, we need two additional components 1a and 3a in the blue wings of the saturated components 1 and 3 in order to achieve a good fit. In order

to obtain a reasonable fit, we had to put component 2 at a slightly different redshift for Si II with a velocity difference of $\Delta v_{2-2*} = 18$ km/s, which is therefore denoted as component 2*.

Multiplet transitions were fitted such that for each component all individual transitions have the same column density. This is useful in those cases where one of the transitions is blended with another line in order to disentangle the contributions from the different elements to one absorption feature. Blended lines were fitted together such as C II* λ1335.6 and C II* λ1335.7 and Si II* $\lambda\lambda$1264 and 1265. In case of the blended lines Si II λ1260 and S II λ1259, S II was excluded for the common fit of the S II lines. For Si II and O I* λ 1304 that were fitted together, the contribution from O I* is negligible and only 2 components were fitted for the fine-structure line and the same for O I**. For the fine-structure lines C II* $\lambda\lambda$1335.6,1335.7, we fitted 3 components that are not blended with the ground state transition. The fitted values for the different components are then listed in Table 5.1 for the resonant transitions and Table 5.2 for the fine-structure lines.

As shown in Fig. 5.1, the resonant transitions of C, S, O and Si show four main velocity components, the strong transitions of C, O and Si have two additional subcomponents. These subcomponents might be present also in the weaker transitions but simply not detected in those transitions. N V $\lambda\lambda$1238, 1242 is detected in a single velocity component at $v_{1*} = 186$ km/s (see Fig. 5.2) which is at slightly higher velocity than comp. 1 of the other absorption lines. The fine-structure lines (Fig. 5.1) only show 2 or 3 components which is clearly visible from the only unblended fine structure line, Si II*λ1309.

For all host component lines, we assume only turbulent broadening and estimate the values to be $b_{\rm turb}$ = 15 km/s in the two narrow components 1 and 4, 25 km/s in components 2 and 3 and 20 km/s in the additional components 1a and 3a. The values are invoked by the best fits from unblended lines. The intervening system at $z = 1.478$ is unblended and the multiplet fits for the Mg II $\lambda\lambda$2796, 2803 and Fe II $\lambda\lambda$2586, 2600 doublets give consistent results.

5.5 VELOCITY COMPONENTS IN THE HOST GALAXY

The velocity components in the absorption lines span a range of about 400 km/s. The outer components at 169 km/s (#1) and -228 km/s (#4) are relatively narrow with b= 15 km/s (#2 & #3), whereas several absorption lines of the two components in between are heavily saturated with $b = 25$ km/s. In the highest redshift component, which is slightly offset in velocity, the high ionisation N V line is detected.

In Paper I we noted the tentative detection of H_2 at the redshift of the host galaxy. The position of the H_2 transitions are coincident with the redshift of the main absorption component at v = –11 km/s which would then be associated with dense molecular clouds inside the host. All other H_2 transitions are be blended with Lyman-α forest absorption lines and can therefore not be identified. The detection of H_2 is also consistent with the high metallicity derived for the host of GRB 060206 (Ledoux et al., 2003; Petitjean et al., 2006; Noterdaeme et al., 2008). However, the position of the H_2 absorption at the velocity of the main absorption component as seen from the metal line transitions might be the reason why we had identified it with H_2 transition which would not have been the case had the absorption occured at the velocity of one of the weaker components.

5.5.1 FINE STRUCTURE LEVELS

In Paper I we used the detected fine structure lines to determine the density and temperature for the highest redshift component, assuming that the lines were excited by collisional excitation.

ID	$\lambda_{\rm rest}$ [Å]	comp.	$\lambda_{\rm obs}$ [Å]	$\mathbf{v}_{\rm abs}$ [km/s]	log N [cm^{-2}]	$\mathbf{b}_{\rm turb}$ [km/s]	log $N_{\rm tot}$ [cm^{-2}]	[X/H]	blended with
S II	1250.584	1	6316.51	169	14.51±0.11	15	15.13±0.05	–0.86±0.09	
		2	6314.41	69	14.52±0.11	25			
		3	6312.71	–11	14.71±0.07	25			
		4	6308.13	–228	14.27±0.19	15			
S II	1253.811	1	6332.81	169	14.51±0.11	15	15.13±0.05		
		2	6330.70	69	14.52±0.11	25			
		3	6329.00	–11	14.71±0.07	25			
		4	6324.41	–228	14.27±0.19	15			
S II	1259.519	1	6361.64	169	14.51±0.11	15	15.13±0.05		Si II$_{1260}$
		2	6359.52	69	14.52±0.11	25			Si II$_{1260}$
		3	6357.81	–11	14.71±0.07	25			Si II$_{1260}$
		4	6353.20	–228	14.27±0.19	15			
Si II	1260.4221	1	6366.20	169	14.41±0.09	15	15.23±0.04	–1.08±0.07	
		1a	6365.28	127	12.64±0.13	20			
		2*	6363.70	51	14.66±0.05	25			
		3	6362.37	–11	14.79±0.07	25			
		3a	6361.19	–67	13.71±0.08	20			
		4	6357.76	–228	14.52±0.08	15			
Si II	1304.3702	1	6588.18	169	14.41±0.09	15	15.23±0.04		O I*
		1a	6387.22	127	12.64±0.13	20			O I*
		2*	6585.59	51	14.66±0.05	25			O I*
		3	6584.21	–11	14.79±0.07	25			
		3a	6583.00	–67	13.71±0.08	20			
		4	6579.44	–228	14.52±0.08	15			
O I	1302.1685	1	6577.06	169	16.02±0.53	15	16.33±0.29	–1.16±0.31	
		2	6574.86	69	15.72±0.24	25			
		3	6573.10	–11	15.52±0.47	25			
		3a	6571.88	–67	14.91±0.13	20			
		4	6568.33	–228	15.14±0.18	15			
C II	1334.5323	1	6740.52	169	16.40±0.39	15	>16.85	> –0.39	
		1a	6739.55	127	13.67±0.42	20			
		2	6738.28	69	15.10±0.40	25			
		3	6736.47	–11	>16.50	25			
		3a	6735.22	–67	14.69±0.18	20			
		4	6731.58	–228	16.09±0.24	15			
N V	1238.821	1	6257.46	186	13.73±0.06	25	13.73±0.06	—	
N V	1242.804	1	6277.58	186	13.73±0.06	25	13.73±0.06		

Table 5.1: *Velocity decomposition and Voigt-profile fitting of the different components in the host galaxy absorption systems. Metallicities are derived from the total column densities including the ground state and fine-structure transitions of the individual ionic species. As solar metallicities, we used the values from Asplund et al. (2004). The velocities of the Doppler parameters are given in rest frame. Zero velocity is the midpoint of the absorption complex, corresponding to* $z = 4.048$.

However, the VLT/UVES RRM campaign on GRB 060418 (Vreeswijk et al., 2007) has shown that at least some the Fe II and Ni II fine-structure lines in GRB afterglows are excited by indirect UV pumping from the bright GRB and its afterglow, rather than by collisional excitation. This was also put forward by Prochaska et al. (2006b) for the spectrum of GRB 051111.

Vreeswijk et al. (2007) measured strong variation with time of the columns of absorption lines and use this to obtain a direct distance determination of the absorbing material with respect to the GRB, by fitting the columns with indirect UV pumping models. Our spectra of

ID	$\lambda_{\rm rest}$ [Å]	comp.	$\lambda_{\rm obs}$ [Å]	$\mathbf{v}_{\rm abs}$ [km/s]	log N [cm^{-2}]	$b_{\rm turb}$ [km/s]	log $N_{\rm tot}$ [cm^{-2}]	blended with
Si II*	1264.7377	1	6388.00	169	14.17±0.04	15	14.38±0.03	
		1a	6387.08	127	12.89±0.14	20		Si II*$_{1265}$
		2	6385.87	69	13.72±0.07	25		Si II*$_{1265}$
		3	6384.16	–11	13.41±0.05	25		Si II*$_{1265}$
		3a	6382.97	–67	12.73±0.08	20		
Si II*	1265.0020	1	6389.33	169	14.17±0.04	15	14.38±0.03	
		1a	6388.41	127	12.89±0.14	20		Si II*$_{1264}$
		2	6387.21	69	13.72±0.07	25		Si II*$_{1264}$
		3	6384.16	–11	13.41±0.05	25		Si II*$_{1264}$
		3a	6384.21	–67	12.73±0.08	20		Si II*$_{1264}$
Si II*	1309.2757	1	6612.95	169	14.17±0.04	15	14.38±0.03	
		1a	6612.00	127	12.89±0.14	20		
		2	6610.75	69	13.72±0.07	25		
		3	6608.98	–11	13.41±0.05	25		
		3a	6607.75	–67	12.73±0.08	20		
O I*	1304.8576	1	6590.64	169	14.86±0.07	15	14.89±0.07	
		2	6588.44	69	13.47±0.06	25		Si II$_{1304}$
O I**	1306.0286	1	6596.55	169	14.15±0.09	15	14.37±0.07	
		2	6594.36	69	13.98±0.12	25		
C II*	1335.6630	1	6746.23	169	15.76±0.16	15	15.77±0.15	
		1a	6745.26	127	12.68±0.71	20		
		2	6743.98	69	13.92±0.06	25		
		3	6743.98	–11	14.02±0.06	25		
C II*	1335.7077	1	6746.46	169	15.76±0.16	15	15.77±0.15	
		1a	6745.49	127	12.68±0.71	20		
		2	6744.21	69	13.92±0.06	25		
		3	6742.40	–11	14.02±0.06	25		

Table 5.2: *Same as Table 5.1 for the fine-structure lines in the host galaxy system that only have 3 components.*

ID	$\lambda_{\rm rest}$ [Å]	comp.	$\lambda_{\rm obs.}$ [Å]	$\mathbf{v}_{\rm abs}$ [km/s]	log N [cm^{-2}]	$\mathbf{b}_{\rm rest}$ [km/s]	log $\mathbf{N}_{\rm tot}$ [cm^{-2}]
Fe II	2586.6500	1	6412.72	25	13.27±0.07	19.9±3.4	13.78±0.05
	2586.6500	2	6411.51	–30	13.62±0.07	14	
Fe II	2600.1729	1	6446.24	25	13.27±0.07	19.9±3.4	13.78±0.05
	2600.1729	2	6445.03	–30	13.62±0.07	14	
Mg II	2795.5280	1	6932.60	25	13.49±0.08	19.9±3.4	13.95±0.08
	2795.5280	2	6931.30	–30	13.77±0.11	14	
Mg II	2802.7050	1	6950.40	25	13.49±0.08	19.9±3.4	13.95±0.08
	2802.7050	2	6949.09	–30	13.77±0.11	14	

Table 5.3: *Absorption line fitting of the intervening system at $z = 1.48$*

GRB 060206 do not have the required temporal and spectral resolution for such an analysis. We can, however, determine approximate properties for the absorbers assuming that indirect UV pumping or collisional excitation is the way that the fine structure levels are populated. Furthermore, the combined WHT spectrum was taken when a significant optical rebrightening occurred in the afterglow light curve (see the light curve by Curran et al., 2007) and UV photons from this rebrightening may have played a significant role in the indirect UV excitation of the transitions. In Table 5.4 we note the ratios between the fine-structure and ground state

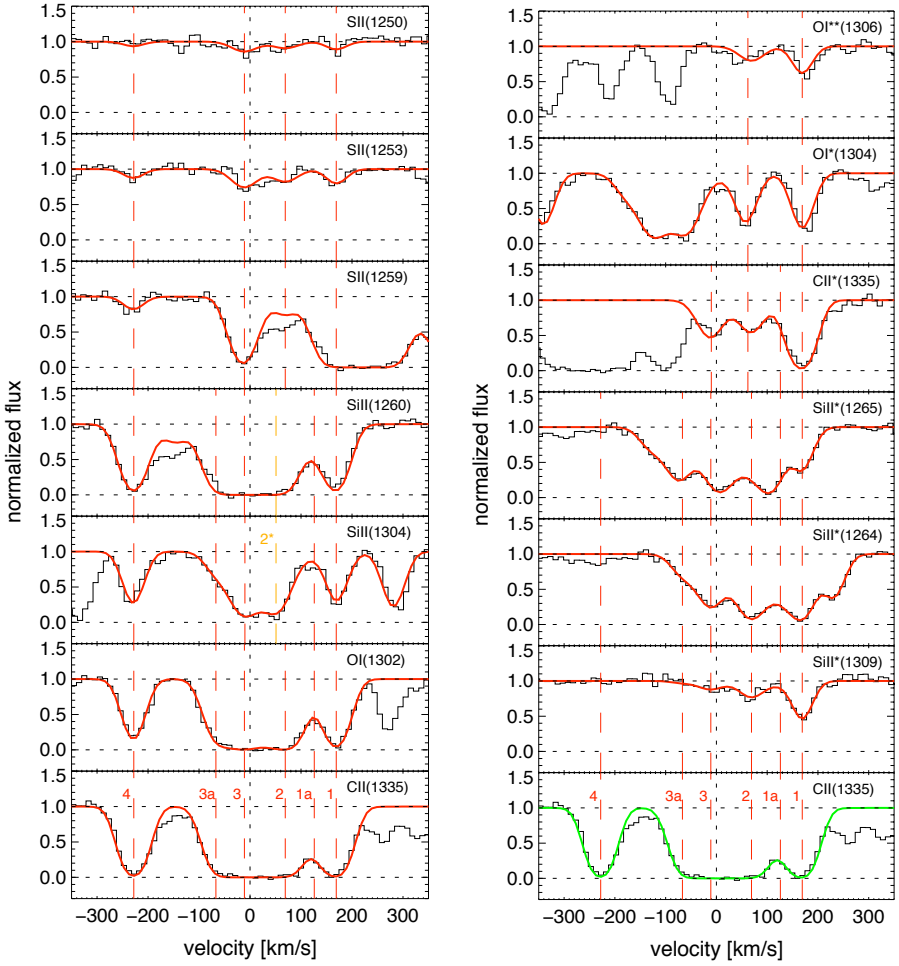

Figure 5.1: *Fits to the four velocity components (plus two subcomponents) of the resonant absorption transitions in the host galaxy. The dashed red lines indicate the different velocity components as denoted in the bottom panel, the dotted line is the adopted zero velocity corresponding to $z = 4.048$. Note that the second component of Si II marked in orange and denoted as 2* is at a slightly different position as for the other lines. The S II λ1259 is blended with Si II λ1260 and was excluded from the common S II multiplet fit, for the plot of the λ1259 line we therefore adopt the column derived from the fit of λλ1250 and 1253. The components and their derived properties are listed in Table 5.1.*

column densities for the four main components. Due to the uncertainties in the distribution of the column densities between comp. 1 and 1a and 3 and 3a, the densities of the main- and the subcomponent have been added.

We can now use these line ratios to estimate the UV radiation field needed to excite the levels, following (Prochaska et al., 2006b, Fig. 7), assuming that UV pumping is the dominant excitation mechanism for this component. The column density ratio [Si II*/Si II] indicates a radiation field intensity for the highest redshift component of $G/G_0 = 3 \times 10^5$ (with $G_0 = 1.6 \times 10^{-3}$ erg/cm^2/s). Using the ratio [O I*/O I] gives very similar values but with a larger uncertainty. A similar strength of the radiation field was found for the component with the second-highest redshift in the spectrum of GRB 050730 (D'Elia et al., 2007), and is somewhat

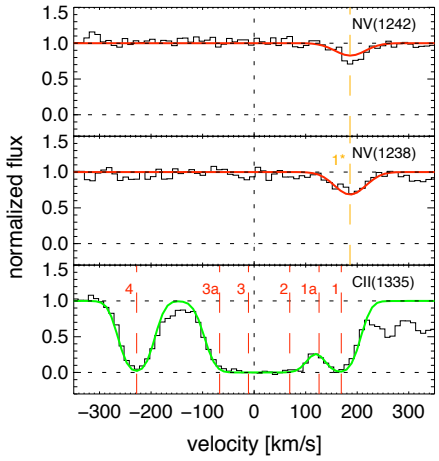

Figure 5.2: *Fit to the N* V *doublet at λλ1238,1242 and comparison to the components in C* II*. The only component detected, named 1*, is at a slightly higher redshift than comp. 1 in all other lines which might indicate a different origin in the host galaxy.*

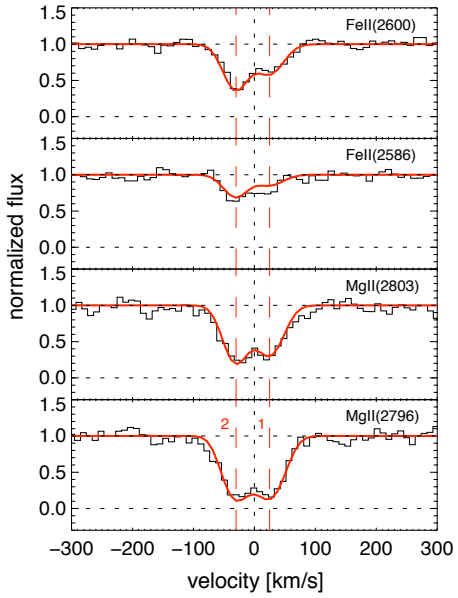

Figure 5.3: *Fit to the intervening system in the line of sight at redshift* $z = 1.48$*. The dotted lines indicate zero velocity which is the average of the velocity components. The two Mg* II *and Fe* II *transitions show two velocity components indicated by the dashed lines which have been fitted as doublets.*

lower than the value found for GRB 051111 (Prochaska et al., 2006b). The required photon field drops to values of 6×10^4, 2×10^4 and $\lesssim 10^4$ G/G_0 for the lower redshift absorbers 2, 3 and 4, the uncertainties for G, however, are quite large (see Prochaska et al., 2006b). If all the velocity components in the host are excited through indirect UV pumping by photons of the GRB and afterglow the highest redshift component would be closest to the burst, and the lowest lies furthest away. Fine-structure lines of Si II* were also detected in the spectra of LBGs (Pettini et al., 2002) which might be excited by the UV radiation field by young stars and might therefore

Comp.	v_{abs} [km s^{-1}]	Si II*/Si II	O I*/O I	O I**/O I*	C II*/C II	n_e [cm^{-3}]	G/G_0
1+ 1a	148	0.596±0.029	0.07±0.03	0.195±0.004	0.23±0.05	400 ± 50	$3 \pm 0.5 \times 10^5$
2	69	0.115±0.002	0.005±0.001	3.24±0.19	0.07±0.02	70 ± 5	$6 \pm 0.15 \times 10^4$
3 + 3a	−39	0.047±0.001	...	...	< 0.003	15 ± 2	$2 \pm 0.15 \times 10^4$
4	−228	< 0.005	...	...	...	< 2	$< 5 \times 10^3$

Table 5.4: *Properties of the four velocity systems observed in the WHT spectrum, see Section 5.5.1. The exact contribution of the subcomponents 1a and 3a is uncertain. For the ratios, we therefore add the column densities from the sub- to the corresponding main velocity component. For the calculation of n_e and G/G_0, the ratios derived from Si II*/Si II have been used as they have the smallest errors, according to (Prochaska et al., 2006b, Fig. 7 and Fig. 9).*

be present in any highly star-forming galaxy. The decreasing strength of the lines however are in favour of a well confined UV source like a GRB and its afterglow.

In case we assume collisional excitation being the mechanism responsible for the fine-structure lines, the required densities are 400, 70, 15 and $< 2\,\mathrm{cm}^{-3}$ for the systems 1 to 4 (see Table 5.4), using the method described in (Prochaska et al., 2006b, see Fig. 9). These values are comparable to the electron densities found in star forming regions and molecular clouds in our Galaxy and GRB host galaxy star forming regions (e.g. Thöne et al., 2006; Wiersema et al., 2007, and references therein).

We consider indirect UV pumping by the GRB and its afterglow radiation as the most likely scenario for causing the fine-structure lines although we cannot exclude that collisional excitation could play a role. The drop in the inferred radiation field from the higher to the lower redshift components and the lack of fine-structure absorption in component 4 indicates an increasing distance from the GRB from component 1 to 4. In the indirect UV pumping scenario we may interpret the decrease in fine structure line excitation with velocity along the line of sight as a distance effect.

No neutral species with ionization potentials lower than hydrogen are observed in the highest redshift absorber (O I has an ionization potential just over 1 Ryd and can therefore be screened by hydrogen), so we cannot set a constraining lower limit to the distance to the GRB for this system through ionization analysis. If we assume that indirect UV pumping by the afterglow of the GRB is exciting the levels in the highest redshift system, we can derive an order of magnitude estimate of the distance to the GRB (see Prochaska et al., 2006b) using the value of G found above. From the afterglow light curve (Curran et al., 2007) we calculate the flux received at Earth at the time of the spectrum, using the spectral index derived in Chapter 5.3 and the restframe frequency of 1.7×10^{15} Hz as in Prochaska et al. (2006b). We find a distance of the highest redshift system to the GRB of order one kpc, which is similar to the more accurate distance found for the absorbing gas through absorption line variability in GRB 060418 (Vreeswijk et al., 2007).

5.5.2 N V ABSORPTION LINES

N V has a large ionization potential (77.5 to 97.9 eV) and is therefore assumed to arise only in high temperature or shock environments. It has been frequently detected in GRB sightlines (Prochaska et al., 2008b) with large column densities of $\log(\mathrm{N}) > 14$ cm^{-2}. They seem to probe cold, narrow gas and often only have small offsets from low ionization and fine-structure lines as we also observe for the spectra presented in this paper. (Prochaska et al., 2008b) argue that the N V absorption likely arises from photoionization of the immediate (< 10 pc) environment of the GRB through the afterglow, but also shock ionization in starburst winds could in principle

play a role and N V has been observed in LBGs and starbursts (Pettini et al., 2002; Savaglio et al., 2002). Heated gas in the halo traced by other high ionization lines such as O VI, cannot produce the required high column densities while a connection to shocks from the progenitor wind would imply large offsets which are not observed.

N V has also been observed in many QSO spectra and in lines of sight towards stars in the LMC (e.g. Caulet & Newell, 1996) where these lines are however broader than those observed in QSO and high redshift starbursts. Galactic sightlines towards early type stars (e.g. Welsh & Lallement, 2005; Sembach et al., 2001), in WR star winds and galactic outflows. In the solar neighbourhood, it often occurs at the (conductive) interfaces between evaporating hot and cooler interstellar gas (Slavin, 1989; Welsh & Lallement, 2005), e.g. at the boundary of a hot bubble formed by O and B stars with the neutral ISM, where one would expect to find both high ionization and low ionization species at comparable velocities. The observed high b parameter is consistent with this picture (Savage & Sembach, 1996) but larger as observed for GRB N V absorption and the column density is usually $\log(N) < 14$ cm^{-2}.

5.5.3 THE NATURE OF THE ABSORPTION SYSTEMS

Features similar to what we observe in the spectra of GRB 060206 have been discovered in other GRB spectra such as GRB 020813 (Fiore et al., 2005), GRB 021004 (e.g. Fiore et al., 2005), GRB 030329 (Thöne et al., 2006), GRB 050730 (Starling et al., 2005b; Chen et al., 2005; Prochaska et al., 2007), GRB 050820 (Prochaska et al., 2007), GRB 050922C (Piranomonte et al., 2007), GRB 051111 (Penprase et al., 2006; Prochaska et al., 2007), GRB 060218 (Wiersema et al., 2007) and GRB 060418 (Vreeswijk et al., 2007; Prochaska et al., 2007). The velocity range of these systems span a wide range from 200 to 3000 km/s and might have different origins according to their widths, ionization states and abundance ratios.

Components with large velocity spreads were sometimes connected to earlier mass losses of the progenitor WR star. van Marle et al. (2005) numerically evaluate a scenario in which the progenitor star wind interacts with circumstellar material, including the mass loss of earlier stages in the progenitor evolution, forming shells of material propagating outwards at a range of velocities. The lower velocity components up to 400 km/s match very well with the models by Van Marle et al., but we do not detect the expected components at 2000-3000 km/s. In the spectra of GRB 021004, these high velocity components were only detected in C IV and Si IV which are outside the usable range of our WHT spectrum. Furthermore, all components of the GRB 060206 absorption systems show strong low ionization lines which disfavours an origin very close to the burst as the radiation field from the GRB ionizes the surrounding material. Chen et al. (2007) conclude from a sample of high-resolution afterglow spectra that high velocity components are absent in 80% of the spectra and the incidence of C IV absorbers along DLA sightlines nonnegligible which makes it more likely that those high velocity structures arise in intervening galaxies.

Excluding the connection to the immediate environment of the burst, the absorption features must originate in the host galaxy ISM. Systems with small velocity spreads ($v < 250$ km/s) have been found in high resolution spectroscopic studies on QSO absorbers using mainly Mg II and C IV systems (e.g. Nestor et al., 2005; Churchill et al., 2003; Boksenberg et al., 2003). These systems are often connected to strong Lyα absorption and consist of a saturated central profile and weaker subsystems at higher velocities. Churchill et al. (2003) and Ellison et al. (2003) suggested a rotating disc together with a halo to explain the different systems. However, as shown in Chapter 5.3, the extinction in the line-of-sight to the GRB is consistent with zero which

makes it unlikely that the GRB was situated behind most of the disc material. Also the hydrogen column densitiy of $\log N = 20.85 \pm 0.1$ (Paper I) is relatively low for a GRB-DLA (Jakobsson et al., 2006a) implying a position of the GRB inside or at the near end of the galaxy. Furthermore, fine-structure lines are usually detected only in the component that dominates the optical depth, associated with the gas inside the galaxy and their redshift has therefore been taken as a proxy for the redshift of the galaxy (Prochaska et al., 2007).

Another possible explanation for those components is absorption by material from a super-galactic wind Bond et al. (2001). The cumulative supernova explosions within a star forming region can expel gas out into the halo of the galaxy which fragments and produces clumps of material outside the galaxy. These galactic winds have been directly observed in some nearby galaxies (e.g. M82, NGC 3079 and NGC 4945). The inner parts of these superbubbles are relatively hot and show X-ray emission together with optical emission lines, followed by a warm transition phase traced by highly ionized metal absorption lines such as O VI and C IV. The outer shells are colder and show low ionized absorption systems (see e.g. Heckman et al., 2001). Low ionization absorption features in GRB spectra that can be explained by galactic winds have been found in GRB 030329 (Thöne et al., 2006) and GRB 051111 (Penprase et al., 2006). Bond et al. (2001) and Ellison et al. (2003) suggest that the symmetric structures in some Mg II absorption systems towards QSOs (Bouché et al., 2006) could also be an indication for a galactic-scale outflow scenario.

If we can transform the radiation field derived from the fine-structure lines into a distance scale for the different components, assuming that G $\sim 1/\mathrm{r}^2$ (see Prochaska et al., 2006b) and component 1 to be at ~ 1 kpc (see Chapter 5.5.1), component 2, 3 and 4 would then be at distances of 2.2, 5.5 and > 8 kpc from the burst. Comparing this with the velocity spread of 417 km/s, the absorbing systems can hardly be caused by the rotation field in an 0.3 L* galaxy with a typical size of a few tens of kpc and a rotational velocity of around 150–200 km/s. However, the distances are derived assuming steady-state conditions for the radiation field, which is clearly not the case for a GRB, and can only be considered as rough estimates. Therefore, some of the components could indeed be caused by the gas in the main part of the galaxy whereas others are due to an outflow.

Galactic winds are considered to be the main cause for the metal enrichment of the inter-galactic medium. Observing this in the spectra of a burst at $z = 4.048$, it shows that these mechanisms started quite early in the history of the Universe. To conclusively discriminate between the possibility of a galactic outflow and absorption within the galaxy, we would need the exact redshift of the galaxy from emission lines as it was possible for GRB 030329 (Thöne et al., 2007a). There, the host was a small starburst galaxy with the redshift determined from several emission lines, whereas the Mg I and II absorption systems detected spanning a range of 260 km/s were mostly blueshifted compared to the host emission lines. This indicates some sort of outflow from that galaxy which was interpreted as a sign of a galactic superwind.

5.5.4 Comparison with QSO-DLAs

To compare the kinematics with QSO-DLAs we follow the procedure of Ledoux et al. (2006) and calculate the line profile velocity width, Δv, as $c\left[\lambda(95\%) - \lambda(5\%)\right]/\lambda_0$, where $\lambda(5\%)$ and $\lambda(95\%)$ are the wavelengths corresponding to, respectively, the five and 95 percentiles of the apparent optical depth distribution, and λ_0 is the first moment (the average) of this distribution (see Fig. 1 of Ledoux et al., 2006). We choose the S II λ1253 transition as it is a low-ionization transition and the line is not saturated. The apparent optical depth for the line at the derived

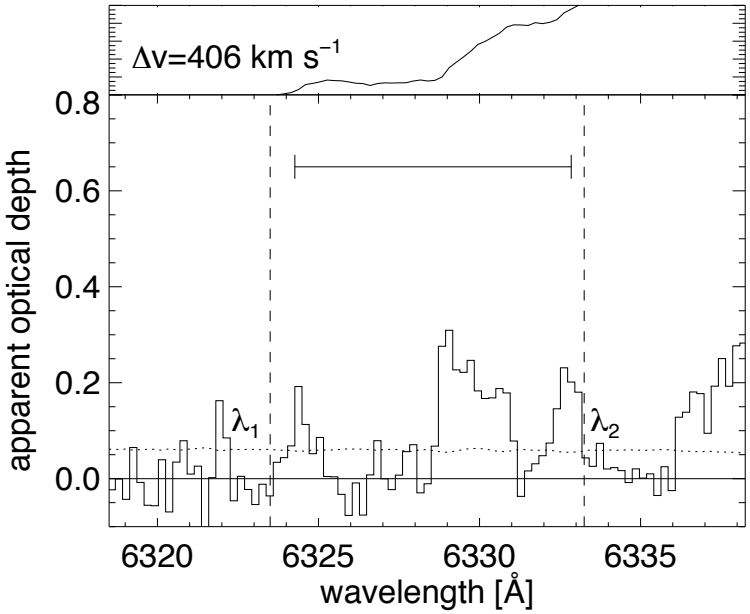

Figure 5.4: *Apparent optical depth distribution of the S II λ1253 system from which we infer a velocity width of 417 km s^{-1}. λ_1 and λ_2 indicate 5 and 95% of the apparent optical depth distribution. The top panel shows the cumulative EW along the line-of-sight*

velocity width is shown in Fig. 5.4. We infer a velocity width of 417 km/s, slightly larger than the distribution of DLAs with comparably high metallicities (Fig. 2 in Ledoux et al., 2006, see also Prochaska et al. 2007).

This indicates that the kinematics of GRB absorbers is similar to that of QSO-DLAs and hence that the immediate environment of the GRB, e.g. the wind from the progenitor star, is not strongly dominating the kinematics and metallicity of the system. This is consistent with the recent findings of Vreeswijk et al. (2007) and Watson et al. (2007) that the GRB absorbers probe gas that is more than several kpc away from the GRB site. It also supports our suggestion that the structures observed come from material in the galaxy or from a galactic outflow far away from the GRB.

5.6 THE HOST IN EMISSION

In the deep r' Gemini images of 2700 s, we find a candidate for the host galaxy with 25 ± 0.2 mag (AB). The host was not detected and the 3σ detection limit at the coordinates of the host is $H > 20.6$ mag (Vega). The right panel of Fig. 5.5 shows the Gemini r' band image. In this image, the host appears to have a rather low surface brightness with two slightly brighter knots where the afterglow position falls on top of one of them.

The HST image resolves the two knots of the possible host from the Gemini images into two objects. One of them is a faint galaxy underlying this position, with the burst offset roughly 0.″2 from its centroid (see Fig. 5.5). We assume that this is the host galaxy of GRB 060206. This galaxy lies close to two other galaxies, of which the one to the west was blended blended with the actual host galaxy at the resolution of our ground based Gemini image. One of these nearby galaxies may well represent the system seen as the foreground absorbers within our afterglow spectroscopy. The magnitude of the galaxy, measured in an aperture of radius 0.″2 is F814W$_{AB}$

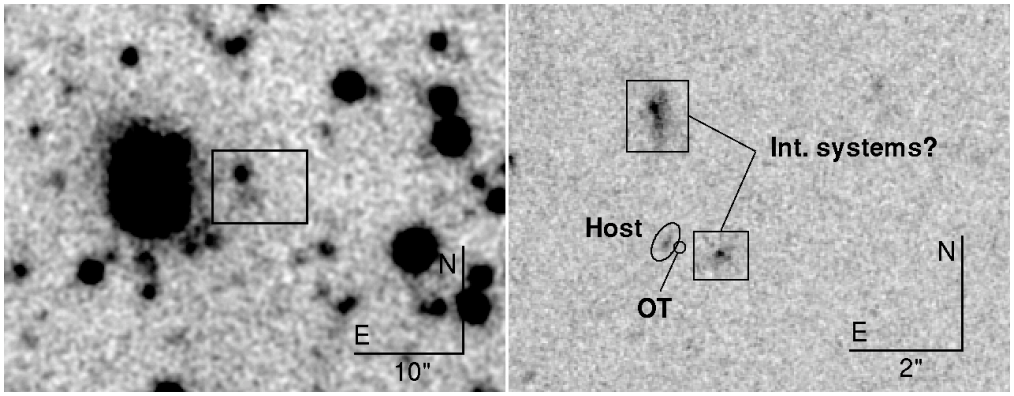

Figure 5.5: *Left panel: Gemini r′-band image of the host candidate for GRB 060206. The box marks the cut displayed in the panel to the right which shows an* HST *images of the host taken with the F814W filter. The OT (circle) lies about 0.″2 from a faint object (ellipse) which is most likely the host of GRB 060206. The two nearby objects (boxes) are likely candidates for the intervening system where the top one corresponds to the object seen inside the box in the Gemini image.*

= 27.48 $\pm$ 0.19 mag.

The detection of a GRB host galaxy at such high redshift is relatively rare: so far, only three hosts for long GRBs with afterglows at $z > 3$ have been found - GRB 971214 ($z = 3.42$) (Kulkarni et al., 1998), GRB000131 ($z = 4.5$) (Fruchter et al., 2006) and GRB 030323 (z=3.372) (Vreeswijk et al., 2004) despite the fact that 26 GRBs are known with $z > 3$ so far. At a redshift of $z = 4.048$, F814W$_{AB}$ = 27.48 corresponds to an absolute magnitude of -20.34 mag or roughly 0.3 L*, not taking into account the redshift evolution of the luminosity function. The nondetection of the host galaxy in deep H band imaging performed with the CAHA 3.5m telescope is consistent with a starforming host with the measured F814W$_{AB}$ magnitude.

5.7 AN INTERVENING SYSTEM AT $z = 1.48$

5.7.1 PROPERTIES OF THE INTERVENING ABSORBER

In addition to the systems intrinsic to the GRB redshift, we detect an intervening absorber at $z = 1.48$. It contains two velocity systems of the two doublets Mg II $\lambda\lambda$2796, 2803 and Fe II $\lambda\lambda$2586, 2600 with a separation of $\sim$50 km s^{-1}. In Paper I, we described a second absorbing system at $z = 2.259$. In the reanalysis performed in this paper, we conclude, however, that this system is not real.

In a sample of QSO absorbers, Churchill et al. (2003) find that the column densities of Mg II and Fe II correlate linearly. The column densities we find for both velocity systems fall within 1 sigma of the linear correlation of Churchill et al. (2003). The b values we find are very high for both components compared with the sample of Churchill et al. (2003), pointing either to very high temperatures or to more velocity components present that we cannot resolve at our intermediate resolution. The latter is supported by the correlation that Churchill et al. (2003) find between the restframe equivalent width of the Mg II λ2796 line and the number of velocity components in the absorber, which predicts a higher number of velocity components ($\sim$ 10) than the two we find in the WHT spectra.

Spectrum	Δ t [h]	Fe II$_{2658}$ EW [Å]	Fe II$_{2600}$ EW [Å]	Mg II$_{2796}$ EW [Å]	Mg II$_{2803}$ EW [Å]
WHT	1.73	0.64±0.07	1.11±0.06	2.01±0.09	1.83±0.10
WHT	2.01	0.50±0.06	1.12±0.09	2.34±0.19	2.03±0.24
Subaru ...	6.00	0.50±0.13	1.25±0.11	1.75±0.11	1.46±0.10
Subaru ...	6.54	0.47±0.10	1.20±0.12	1.84±0.11	1.99±0.11
Subaru ...	7.07	0.41±0.13	0.97±0.13	1.81±0.12	1.74±0.12
Subaru ...	7.60	0.43±0.11	1.22±0.14	1.83±0.11	1.67±0.10
Subaru ...	8.12	0.62±0.11	1.19±0.12	1.87±0.11	1.81±0.11
Subaru ...	8.68	0.37±0.12	0.74±0.12	2.06±0.11	1.79±0.12
Subaru ...	9.21	0.44±0.14	1.08±0.13	1.73±0.12	1.66±0.12
Subaru ...	9.73	0.33±0.13	0.95±0.13	2.00±0.11	2.01±0.11

Table 5.5: *Measurements of the intervening system lines which were reported to vary by Hao et al. (2007). The EWs have been measured in the WHT spectra, where we analyzed the two 900s exposures separately and in the Subaru spectra retrieved from the archive. EWs are in the observer frame.*

5.7.2 VARIABILITY OF THE INTERVENING SYSTEM?

Hao et al. (2007) claim significant variability in the equivalent widths (EWs) of the Mg II doublet and the Fe II λ2600 line, in the time interval between 4.13 hrs and 7.63 hrs after the burst, covered by 7 low resolution spectra. They fit the lines with Gaussian profiles, and report variation in both the equivalent widths and the relative velocities of the lines.

The two WHT spectra were taken earlier than those reported in Hao et al. (2007) with mid-points 1.73 and 2.01 hours after burst. The spectral resolution and signal to noise of the WHT spectra are significantly better than those used by Hao et al. (2007). Both the Fe II and Mg II lines can be split into two separate velocity components which would be unresolved in low resolution spectra, but we measure EWs of these two systems combined to compare directly with the Hao et al. (2007) values. We furthermore analyzed the low-resolution Subaru data, taken around the same time as the spectra reported in Hao et al. (2007). The measurements are listed in Table 5.5.

The EW measurements of the Fe II λ 2600 Å line from both the WHT and the Subaru data show no variations within the errors and are clearly in disagreement with the strong variability in Hao et al. (2007). The measurement of the Mg II lines is complicated by the fact that they are superimposed on the atmospheric B band and the continuum can therefore not be reliably determined. Hao et al. (2007) removed the absorption band before fitting the Mg II lines but note that they had a correction of about 25% of the variation in absorption band caused by the varying airmass during their observations. The apparent variability in the line shape and strength in their Mg II lines is therefore likely due to inadequate removal of the atmospheric band. We also note that the similar EW of the two components of the Mg II doublet which should have a ratio of 1:2 indicates that these lines are saturated. For a comparison between the WHT and the Subaru values and the ones derived by Hao et al. (2007), see Fig. 5.6.

5.7.3 IDENTIFYING THE ABSORBER IN EMISSION

Detecting intervening galaxies in emission is complicated in the case of QSOs, but the transience of GRBs makes them more suitable to detect intervening systems in emission once the afterglow has faded. While intervening systems can produce very clear absorption systems, the identification of specific absorbers with individual galaxies is difficult (e.g. Vreeswijk et al., 2003; Ellison et al., 2006). The Gemini and *H*ST images show several galaxies within a radius of 5 arcsec, with the two most promising candidates $\sim$ 1 and $\sim$2.5 arcsec from the host which

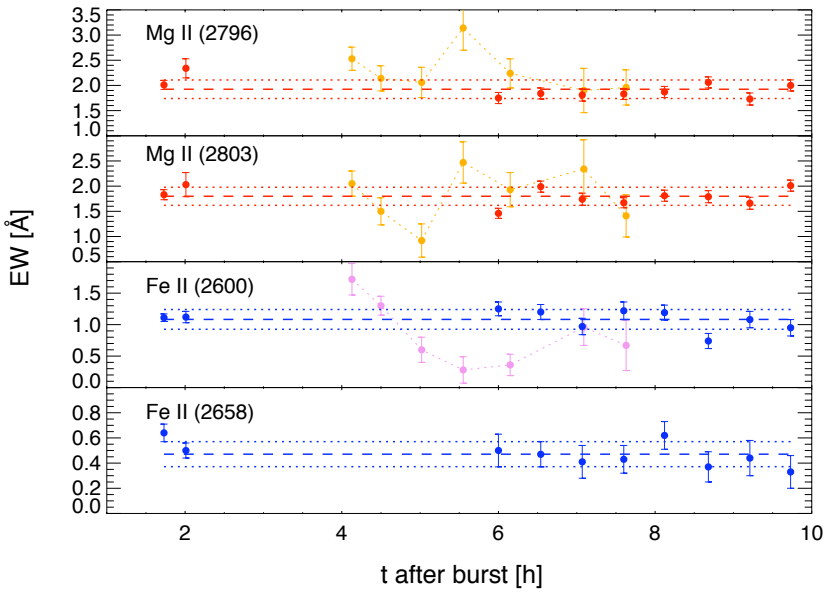

Figure 5.6: *Equivalent widths measured from the WHT and Subaru spectra (red and blue points) and values from Hao et al. (2007) (orange and violet). In addition, we plot the mean of the WHT and Subaru points (dashed lines) and the 1 σ errors (dotted lines) of the mean. Times given are the midtimes of the observations. The plots shows no trend in the evolution of the EW with time as claimed in Hao et al. (2007) and our values are consistent with the mean mostly within 1 σ.*

corresponds to distances of $\sim$ 8 and 21 kpc at $z = 1.479$. Photometry of those two galaxies yield magnitudes of F814W$_{AB}$ = 26.1 $\pm$ 0.1 for the one to the right, blended with the host in the Gemini images, and F814W$_{AB}$ = 24.7 $\pm$ 0.1 or $r'_{AB} = 23.9 \pm 0.1$ for the one north of the host.

At $z = 1.479$, the Gemini r' band and *H*ST F814W filter correspond to restframe 2540 Å and 3360 Å and probe restframe UV emission. We estimate the fluxes of the galaxies 1 and 2.5 arcsec north of the host at $\sim$2800 Å to be $\sim$0.4 and $\sim$1.2 μJy, which corresponds to UV star formation rates of $\sim$ 8 and 25 M$_\odot$yr^{-1}, not corrected for extinction, using the conversion from Kennicutt (1998). The non-detection of the host or absorber in the *H* band is consistent with the intervening absorber candidate being a blue star forming galaxy.

Correlations between parameters of the Mg II absorption lines and the galaxy that produces them has been studied extensively for QSO absorbers. Recently, Zibetti et al. (2007) used the large dataset of the SDSS to correlate the QSO Mg II absorber properties with the light of SDSS galaxies at a range of impact parameters (from 10 – 200 kpc) and found that stronger absorbers can be related to bluer galaxies. The restframe EW of 2.5 Å of Mg II λ2796 clearly places it in the category of the strong Mg II absorbers (though the definition of a strong absorber varies from author to author, but we assume $W_0(2796) \simeq 1$Å), which are generally associated with relatively bright galaxies, with luminosities from $\sim$0.1 to several L_*. For two other GRB hosts, GRB 021004 and GRB 020813, candidate host galaxies for intervening systems have recently been discovered which seem to lie within a few tens of kpc from the GRB afterglow (Henriksen et al. in prep.). Also GRB 030429 has a tentative detection of an emission line from the host of the intervening system in the afterglow spectrum (Jakobsson et al., 2004b) and the intervening absorber in the GRB 020405 spectra could be associated with a neighbouring galaxy with the detection of O II and O III at the same redshift (Masetti et al., 2003).

Ellison (2006) show that the velocity spread of the Mg II absorber in combination with the restframe equivalent width (the D parameter) supplies an efficient means to select possible DLAs. We find $D \sim 8$ for our absorber, making it likely that this absorber is a DLA which can be probed by Lyman α, which is however still in the UV at z=1.48 and could not be observed. The blue, luminous and rapidly star forming galaxy very nearby the GRB host fits in this picture.

We note that comparison with QSO absorber samples may be further complicated by the recently established over-abundance of Mg II absorbers on GRB lines of sight compared to QSO sightlines (Prochter et al., 2006), for which the cause is yet unclear. This difference is not present in line of sight detections of C IV, for reasons not fully understood (Sudilovsky et al., 2007; Tejos et al., 2007).

5.8 CONCLUSIONS

In this paper we have presented the full set of detected absorption lines in the medium resolution spectrum from WHT, as well as host galaxy observations with deep imaging in r' and H band, using Gemini North and the CAHA 3.5m telescope. The spectra show at least four main velocity components at the GRB redshift, spread over a range of ~ 400 km s^{-1}. For each component, we detect a series of absorption lines, including several species of fine-structure lines for 3 of the 4 components. Those fine-structure lines are not found in QSO absorbers, but seem abundant in GRB lines-of-sight (e.g. Vreeswijk et al., 2004; Starling et al., 2005a; Prochaska et al., 2006b; Fynbo et al., 2006a; Kawai et al., 2006; Penprase et al., 2006). We measure their column densities through Voigt profile fitting which is complicated by the blending of the lines of different velocity systems, for every velocity component, however, a diagnostic set of absorption lines can be measured.

The four velocity components show decreasing occupation of their excited fine structure levels as the redshift gets smaller. The column density ratios of [Si II*/Si II] indicate that lines in the component with the highest redshift are most likely excited through indirect UV pumping by a strong photon field equivalent to $\sim 3 \times 10^5\ G/G_0$, produced by the GRB and its afterglow. The powerful rebrightening of the afterglow (Woźniak et al., 2006; Monfardini et al., 2006; Stanek et al., 2007) may play an important role in this excitation. If indirect UV pumping through the afterglow is the source of excitation, the highest redshift absorber is in the order of one kpc away from the burst and the other components subsequently at $\sim$2, $\sim$5 and $>$8 kpc. The similarities of the highest redshift component with the values for GRB 050730 and GRB 051111 and the direct detection of absorption line variability of Fe II*, Ni II*, but not Si II*, in GRB 060418 make an origin of the lines through indirect UV pumping likely. From the fine structure level analysis which provides the relative positions of the velocity components with respect to the GRB, the velocity spread and the low ionization state of the medium, a starburst wind seems an appealing scenario to cause these absorption features. Their nature could be clarified through high resolution (space based) imaging and emission line spectroscopy of the host.

The possible host galaxy is detected at F814W$_{AB}$ = 27.48 $\pm$ 0.19 mag and an upper limit of H $\geq$ 20.6 (3 σ) is achieved which is in agreement with the spectral energy distribution of a blue star-forming galaxy at that redshift. In the image we find several galaxies close to the afterglow position, the closest ones at distances of 1 and 2.″5. In the spectrum we detect an intervening absorbers at $z = 1.48$ showing a two strong Mg II and Fe II absorption components which are likely caused by that bright galaxy. This galaxy is not detected in H band, consistent with it being a spiral or irregular galaxy, which is also suggested from the absorption line properties. Hao et al. (2007) claim significant variability in the equivalent width of the Mg II doublet and

the Fe II λ2600 line of this absorber. The WHT spectra taken earlier and Subaru spectra taken during the observations of Hao et al. (2007) do not confirm the variability in equivalent width of these lines or the trend in the variability as a function of time.

The high resolution spectroscopy of GRB 060206 has been taken with WHT, demonstrating that these detailed line analyses are clearly possible with 4m class telescopes when a bright afterglow presents itself and intermediate or high resolution spectroscopy is possible.

Acknowledgements

We thank the observers and ING staff for performing the reported observations. Based on observations made with the Nordic Optical Telescope, operated on the island of La Palma jointly by Denmark, Finland, Iceland, Norway, and Sweden and with the William Herschel Telescope, in the Spanish Observatorio del Roque de los Muchachos of the Instituto de Astrofísica de Canarias. Based on observations obtained at the Gemini Observatory, which is operated by the Association of Universities for Research in Astronomy, Inc., under a cooperative agreement with the NSF on behalf of the Gemini partnership: the National Science Foundation (United States), the Particle Physics and Astronomy ResearchCouncil (United Kingdom), the NationalResearchCouncil (Canada), CONICYT (Chile), the Australian Research Council (Australia), CNPq (Brazil), and CONICET (Argentina) and on observations carried out at the Centre Astronóminco Hispano Alemán (CAHA) at Calar Alto, operated jointly by the Max-Planch Institut für Astronomie and the Instituto de Astrofísica de Andalucía (IAA-CSIC). Based in part on data collected at Subaru Telescope and obtained from the SMOKA, which is operated by the Astronomy Data Center, National Astronomical Observatory of Japan.

Part II

Resolved Host Galaxies and the SN-GRB Mystery

Chapter 6.1.2 based on: J. P. U. Fynbo, D. Watson, C. C. Thöne et al. – *"No supernova in two long duration γ-ray bursts"*, Nature, vol. 444, pp. 1047– 1049, 2006
Chapter 6.1.3 based on: D. Malesani, J. P. U. Fynbo, J. Hjorth et al. – *"Early warnings of core-collapse SNe"* submitted to the Astrophysical Journal Letters, preprint: astro-ph/0805.1188
Chapter 6.3.2 based on: L. Christensen, P. M. Vreeswijk, J. Sollerman, C. C. Thöne, E. Le Floc'h & K. Wiersema – *"IFU observations of the GRB 980425/SN 1998bw host galaxy: Unusual emission line ratios in GRB regions"*, Astronomy and Astrophysics, in press

6

GRBs WITH SUPERNOVAE, SUPERNOVAE WITHOUT GRBs AND GRBs WITHOUT SUPERNOVA

6.1 THE SN-GRB CONNECTION

When stars above masses of ~ 8 $M_\odot$ have used up their fuel, the central iron core exceeds the Chandrasekhar mass (about 1.4 $M_\odot$) and the subsequent collapse to either a neutron star or a black hole leads to a SN explosion. Star with masses up to about 30 $M_\odot$ end their lives as Type II SNe which are classified according to hydrogen present in the spectra. Subclasses of II-L and II-P refer to the shape of the lightcurve with II-L decaying linearly and II-P showing a long plateau phase after maximum. These subclasses might be connected to the progenitor masses with II-P having more massive progenitors. Stars above 30 $M_\odot$ experience mass loss due to winds and/or instabilities driving the outer layers of the star out into the interstellar medium, called the Wolf-Rayet (WR) phase.

When those stars explode in a SN, they have either lost most of their hydrogen envelope (Type Ib SNe) or even their helium envelope (Type Ic SNe) and those elements are therefore lacking in the SN spectra. Some also suggest, these elements might be absent due to effective mixing of the outer layers and subsequent burning of H and He (Yoon & Langer, 2005). Due to their higher initial masses required, SNe Ib/c are much less frequent than SNe of Type II. As GRBs are expected to come from the most massive stars and the collapsar model requires the removal of the envelope, GRB SN were also expected to be Type Ic SNe which indeed is the case. The collapsar model eventually requires special conditions for a GRB such as high angular momentum and low metallicity and hence GRBs are even less frequent than SN Ib/c.

6.1.1 THE COMMON PICTURE BETWEEN 1998 AND 2006

The early papers on the collapsar model for GRBs assumed that most of the stars envelope would accrete and ultimately end up in the central black hole. Not enough material would be left for a SN explosion or at most, a connected SN explosion would be very faint. This "failed SN" model had to be revised when in 1998 a very bright broadline SN Ic (SN 1998bw) was detected at the same position as GRB 980425 (Galama et al., 1998). The first conclusive evidence for a SN coincident with a GRB was found for GRB 030329. The spectra of the afterglow showed a clear evolution from a powerlaw into a broadline SN Ic spectrum (Hjorth et al., 2003; Stanek

et al., 2003; Matheson et al., 2003). To date, 4 nearby GRBs have spectroscopically confirmed associated SNe, GRB 980425, GRB 030329, GRB 031203 (Cobb et al., 2004; Malesani et al., 2004; Thomsen et al., 2004; Gal-Yam et al., 2004) and GRB 060218 (Pian et al., 2006; Sollerman et al., 2006; Soderberg et al., 2006b; Modjaz et al., 2006; Mirabal et al., 2006) and one XRF, XRF 020903, also showed SN signatures in the late time spectra (Soderberg et al., 2004). All GRB-SNe found so far have been of type broadline Ic which is characterized by its broad emission lines indicating very large outflow velocities of $>$ 10,000 km/s.

In the lightcurve of a GRB afterglow, a SN manifests itself with an additional rebrightening (the SN "bump") when the afterglow has faded enough to reveal the underlying, less luminous but rising SN lightcurve mainly powered by the decay of Ni^{56}. The maximum of the SN is expected about 10–16 days after the onset of the burst. After the SN-GRB connection was established, lightcurves were searched for such additional late time bumps. All SNe with z $<$ 0.5 until 2006 have detected or at least claimed late time bumps. (Zeh et al., 2004) analyzed the complete pre-Swift sample and found that all nondetections of such a SN bump were consistent with the luminosities expected for SNe at the corresponding redshifts. For a review on the SN-GRB connection up to 2006 see Woosley & Bloom (2006).

6.1.2 2006 - THE DISCOVERY OF GRBS WITHOUT SN

This clear and convenient picture from the first decade of afterglow studies had to be revised in 2006. Two nearby bursts, GRB 060505 and GRB 060614, showed no late time SN component despite deep searches. The GRBs 060505 and 060614 were detected by BAT onboard *Swift* on 2006 May 5.275 and 2006 June 14.530 respectively. GRB 060505 was a faint burst with a duration of 4 s. GRB 060614 had a duration of 102 s and a pronounced hard to soft evolution. Both had X-ray afterglows identified by *Swift's* XRT. Subsequent follow-up of these bursts led to the discovery of their optical afterglows, locating them in galaxies at low redshift: GRB 060505 at z = 0.08913 and GRB 060614 at z = 0.125. The proximity of these bursts lead to the expectation that a bright SN would be discovered a few days after the bursts, as in all previous well-observed nearby bursts.

The afterglows of GRB 060505 and 060614 were monitored by several groups using a range of telescopes. This allowed to obtained stringent upper limits on any re-brightening at the position of the optical afterglows up to 12 and 5 weeks after the bursts, respectively. The lightcurves obtained based on our monitoring are shown in Fig. 6.1. For GRB 060505, the afterglow was detected at a single epoch and all subsequent observations resulted in deep upper limits. Ofek et al. (2007) obtained very deep limits $>$ 27 mag or an absolute magnitude of $>$-11 mag with the *HST* two weeks after the burst. For GRB 060614, we detected the afterglow until 4 nights after the burst. In later observations no transient source was detected to deep limits as confirmed by all groups.

A high extinction in the line-of-sight towards these two GRBs preventing the detection of the SN components could be excluded. The Galactic extinction was very low with E(B–V)=0.02 and the Balmer line decrement from optical spectroscopy of the host galaxies was consistent with zero. The host of GRB 060505 furthermore is seen nearly face on and the GRB occurred in a large SF region in one of the spiral arms. Also the SED of the GRB 060614 afterglow did not indicate any extinction. The properties of the host galaxies were also indicative of a young stellar population. The host of GRB 060505 had a SFR of 1 $M_\odot$/yr and a SSFR of 4 $M_\odot$/yr/(L/L*), the values for the host of GRB 060614 are 0.014 $M_\odot$/yr and 3 $M_\odot$/yr/(L/L*), similar to the other nearby SN-GRB hosts. Both are also sub-L* galaxies as expected for long GRB hosts.

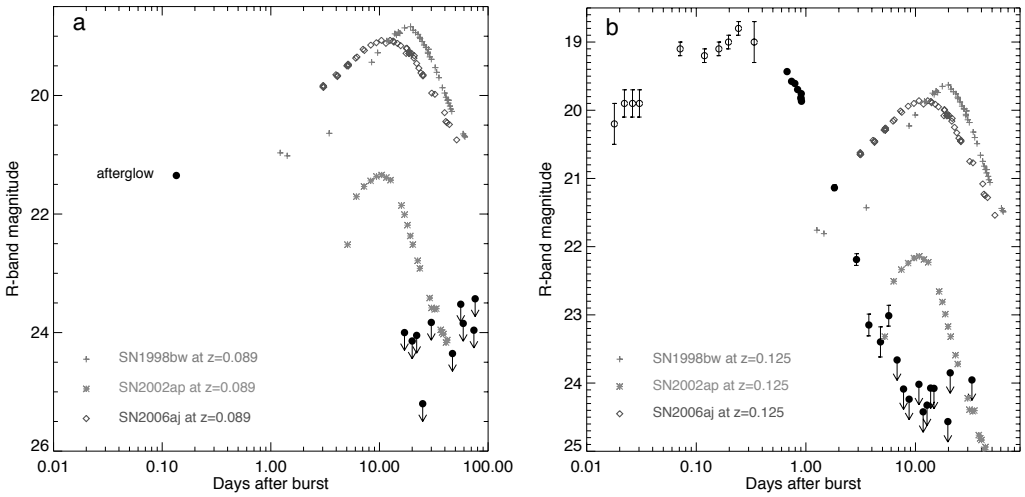

Figure 6.1: *Limits on a SN component in the lightcurves of GRB 060505 (left panel) and GRB 060614 (right panel). The empty dots in the lightcurve from GRB 060614 are data from other telescopes (from Fynbo et al. (2006b)).*

Fig. 6.1 shows that a SN connected to GRB 060505 or GRB 060614 would have been at least 80–100 times fainter than any other SN Ib/c observed with a limit of R > –13.5. GRB related SN Ic have peak magnitudes of around half a magnitude of SN 1998bw and non-GRB related SN Ic are at most 2 magnitudes fainter than SN 1998bw. Even the faintest SN Ic known, SN 1997ef, would have been easily detected, so would have been any SN associated to an XRF.

These two cases of a SN nondetection for very nearby bursts came as a surprise, but were not unexpected from early models of collapsars. If there is not the right amount of angular momentum, the explosion might fail or only be very weak and the matter falls back onto the BH. Of the six long GRBs or XRFs known to be at low redshift (z < 0.2), two now have no associated SN. Unfortunately, since 2006, no such close GRB was detected, neither with nor without SN, so the mystery remains unsolved so far.

6.1.3 2008 - THE DISCOVERY OF A SNE CONNECTED TO AN X-RAY FLARE

The next important discovery was the "once in a lifetime event" (A. Soderberg) of the serendipitous discovery of an X-ray flare (subsequently named "XT" for X-ray transient, as "XRF" is used for the low-energy, low-luminosity version of a GRB) that marked the onset of a supernova. This event was SN 2008D which occurred in the nearby galaxy NGC 2770 at a distance of only 27 Mpc. It was detected by the XRT instrument onboard *Swift* while it was observing continuous emission from SN 2007uy in the same galaxy. The flare lasted for about 400s and had a peak flux of 6.2 cts/s (Soderberg et al., 2008). Its high-energy properties and lightcurve resembled those of GRBs or XRF, but with a luminosity about 3 orders of magnitude lower. Soon after, an optical counterpart was detected (Deng & Zhu, 2008; Thöne et al., 2008b) and spectra revealed that this was a SN, subsequently named SN 2008D.

The SN was first classified as a Type Ib/c due to the absence of Si II and H lines (Malesani et al., 2008b). The early SN spectrum was relatively featureless except two W-shaped features that were suspected to be P-Cygni profiles of Fe II and Si II with velocities of 15 000 km/s. Its overall shape might be consistent with a black-body with T=20,000 K. Later on, broad He lines, although with lower velocities of about 10,000 km/s, were discovered which finally classified it

as a Type Ib SN (Malesani et al., 2008a).

This SN was one of the earliest ever observed with the onset marked by the X-ray flash. Determining the exact onset of a SN is difficult and has only been possible for GRB associated Ic SNe and SNe whose UV flash from the shock-break out was observed with the GALEX UV satellite (Schawinski et al., 2008; Gezari et al., 2008). The shock break out marks the time when the optical depth of the ejecta reaches the order of unity which is the case when the explosion reaches the stellar surface or further out in case of mass loss before the explosion. The early lightcurve of SN 2008D showed an initial decline before the typical rise of the SN likely marking the cooling after this initial flash. The nature of the X-ray flash itself is still debated. (Soderberg et al., 2008) suggested that it is also produced by the shock break out and theoretical models also anticipated such an event. Infact, Colgate (1968) who predicted GRBs before their discovery, associated such flashes with a SN shock-breakout. The fact that this has never been observed before for a SN is likely an observational bias due to the limited FOV of X-ray telescopes. The host galaxy itself, however, also turned out to be interesting to study as it had already hosted two other Type Ib SNe, the abovementioned SN 2007uy and SN 1999eh. This will be further investigated in Chapter 8.

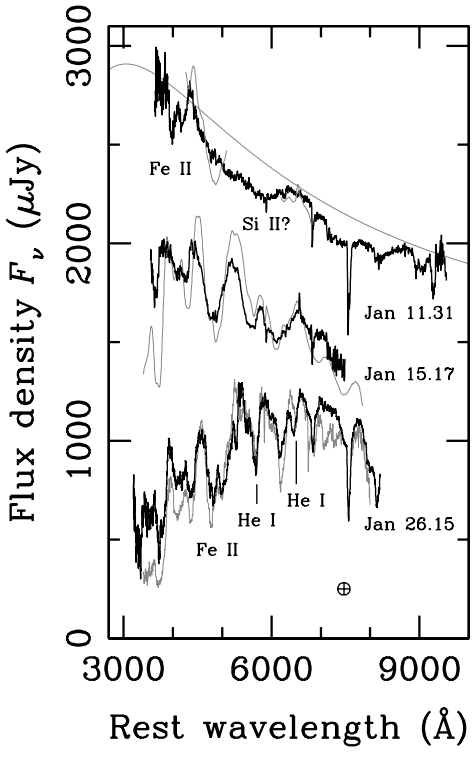

Figure 6.2: *Spectroscopic evolution of SN 2008D from a smooth black-body continuum to a typical SN Ib spectrum with broad absorption lines (credit: D. Malesani).*

6.2 EMISSION LINE DIAGNOSTICS - GRB HOSTS AT LOW REDSHIFTS

Low redshift GRBs do currently not allow to be studied by absorption line spectroscopy as there are no UV instruments available that would allow ToO observations which is not expected to change in the next years. [1] However, at low redshift, a range of emission lines produced in the SF regions of the host and at the GRB site allow us to determine properties of the galaxy. As long GRB hosts are highly star-forming, those lines are expected to be rather pronounced and easily detectable. The UV radiation from massive stars in those SF regions ionizes the gas around them and produces HII regions which ideally are the boundary layer of the molecular clouds that produced the stars. The redistribution of energy leads to the forbidden nebular transitions [O II] λ 3727, 3729, [O III] λ 5007, 4969, [N II] and [S II] as well as the Balmer recombination lines. In GRB host spectra, [Ne III] is also frequently detected which indicates the presence of a large number of massive stars. The so-called "Wolf-Rayet" bump around 4686 Å, which consists of a blend of [N III] λ4640, C III λ4650, C IV λ4658 and He IIλ4686, has been detected so far only in the host of GRB 060218 (Wiersema et al., 2007) and in an HII region next to the site of GRB 980425 (Hammer et al., 2006).

6.2.1 METALLICITIES AGAIN ...

Determining metallicities from emission lines is a bit more tricky than for absorption lines. The relation between the metallicity of the medium and the observable lines is more indirect and influenced by the ionization state of the medium, the temperature and density and the nebular cooling mechanisms as they scale with metallicity. The metallicity probed by emission lines is usually expressed through the oxygen abundance 12+log(O/H) where 12+log(O/H) = 8.66 corresponds to the solar value (Asplund et al., 2004).

Several calibrators have been developed that connect the abundance of different elements to the metallicity. The first and most widely used calibrator still is the so called R_{23} parameter (introduced by Pagel et al., 1979) defined as

$$R_{23} = \log_{10} \frac{[\mathrm{OIII}]\,\lambda 3727 + [\mathrm{OIII}]\,\lambda\lambda 4959, 5007}{H\beta} \tag{6.1}$$

This method however has a few caveats. First of all, it is a double valued function which means that for every value of R_{23} there are two different solutions, one giving a metallicity > 8.4 and one < 8.4 as the electron temperature at high abundances becomes too low to collisionally excite the oxygen forbidden lines. It furthermore depends on the ionization parameter $q = \frac{S_H}{n}$ with S_H the ionizing flux per unit area and n the hydrogen column density, which can be determined from the ionization state of O II (Kobulnicky & Kewley, 2004):

$$O_{23} = \log_{10} \frac{[\mathrm{OIII}]\,\lambda 5007, 4959}{[\mathrm{OII}]\,\lambda 3727} \tag{6.2}$$

$$q = \frac{32.81 - 1.153 O_{23}^2 + Z(-3.396 - 0.025 O_{23} + 0.1444 O_{23}^2)}{4.603 - 0.3119 O_{23} - 0.163 O_{23}^2 + Z(-0.48 + 0.0271 O_{23} + 0.02037 O_{23}^2)} \tag{6.3}$$

where a first guess for the metallicity Z is necessary, e.g. from other methods as described below. The oxygen abundance is then derived for the two branches as follows (Kewley & Dopita, 2002):

[1] The new UV "Cosmic Origins Spectrograph" (COS) which is going to be mounted on *HST* will not allow ToO observations due to calibration issues.

$$12 + \log\mathrm{O/H}_{\mathrm{lower}} = 9.4 + 4.65R_{23} - 3.17R_{23}^2 - q(0.272 + 0.547R_{23} - 0.513R_{23}^2) \quad (6.4)$$
$$12 + \log\mathrm{O/H}_{\mathrm{higher}} = 9.72 - 0.777R_{23} - 0.951R_{23}^2 - 0.072R_{23}^3 - 0.811R_{23}^4 \quad (6.5)$$
$$-q(0.0737 - 0.0713R_{23} - 0.141R_{23}^2 + 0.0373R_{23}^3 - 0.058R_{23}^4) \quad (6.6)$$

Several other slightly different parametrisations are on the market such as from McGaugh (1991) or Pilyugin (2001). In order to distantangle the low and high metallicity values Lilly et al. (2003) found out that the ratio of [N II]/Hα is dependent on the metallicity and at low metallicities, it can therefore be used to decide for the lower branch solution (and to get a guess on the metallicity). In the last few years, it was discovered that the R_{23} metallicities are usually too high and Kewley et al. (2007) therefore suggested the following recalibration:

$$R_{23}^{\mathrm{lower}}(\mathrm{new}) = (R_{23}^{\mathrm{lower}}(\mathrm{old}) - 0.613)/0.975 \quad (6.7)$$
$$R_{23}^{\mathrm{upper}}(\mathrm{new}) = (R_{23}^{\mathrm{upper}}(\mathrm{old}) - 0.613)/0.975 \quad (6.8)$$

Apart from the difficulties connected to the derivation of the R_{23} metallicity, this method has the practical disadvantage that the lines needed span over 3000 Å and for higher redshifts, not all of them might be detectable or have to be measured with different instruments. In order to solve this issue, the N2 and O3N2 parameters have been developed (e.g. Denicoló et al., 2002; Alloin et al., 1979).

$$\mathrm{N2} = \log_{10}\frac{\mathrm{H}\alpha}{[\mathrm{NII}]\,\lambda 6583} \quad (6.9)$$
$$\mathrm{O3N2} = \log_{10}\frac{[\mathrm{OIII}]\,\lambda 5007/H\beta}{[\mathrm{NII}]\,\lambda 6583/\mathrm{H}\alpha} \quad (6.10)$$

Pettini & Pagel (2004) investigated the dependence of the N2 and O3N2 parameter on metallicities derived by photoionisation modeling or the T_e method (see below) and found the following fits:

$$12 + \log\mathrm{O/H} = 9.37 + 2.03 \times \mathrm{N2} + 1.26 \times \mathrm{N2}^2 + 0.32 \times \mathrm{N2}^3 \quad (6.11)$$
$$12 + \log\mathrm{O/H} = 8.37 - 0.32 \times \mathrm{O3N2} \quad (6.12)$$

One large advantage of the N2 method is the independence from the extinction correction due to the small separation between Hα and [N II]. The N2 method is especially useful for low metallicities (below solar) because [N sc ii] saturates above solar metallicity and decreases again at even higher metallicities as the electron temperature drops. The one and two sigma accuracies of the N2 index are 0.38 and 0.18 dex. Also the O3N2 parameter is rather insensitive to the extinction correction, as the ratio of two respectively close emission lines are taken. Furthermore, it is useful beyond solar metallicity as [O III] does not get saturated. However, at higher metallicities, [O III] can eventually become too weak in low S/N data. The accuracies for O3N2 are 0.25 and 0.14 dex for one and two sigma.

It is also possible to directly determine the abundances of O/H from the electron temperatures and densities. For this, one needs a transition which is sensitive to the electron temperature, the most widely used is the [O III] λ 4363 line. From the ratio R=[O III] λ 4959, 5007 /

[O III] λ 4363, one can iteratively determine the electron temperature of O III: t=10^{-4}T$_e$ (O III) (Izotov et al., 2006b):

$$t = \frac{1.432}{\log_{10}\mathrm{R} - \log_{10}\mathrm{C_T}} \quad (6.13)$$

$$\mathrm{C_T} = (8.44 - 1.09t + 0.5t^2 - 0.08t^3)\frac{1 + 0.0004x}{1 + 0.044x} \quad (6.14)$$

where x is connected to the electron density by x=10^{-4}n$_e$t$^{-0.5}$, but the term is always very small if n$_e$ < 1000 cm^{-3} (which is usually the case for densities in the ISM). n$_e$ is usually obtained by taking the ratio [S II] λ 6717 / λ 6731 or [O II] λ 3727 / λ 3729 (Osterbrock, 1989). The electron temperature of [O II] can either be obtained by assuming that t(O II)=0.7t(O III)+0.3 (Stasińska, 1980) or taking the relations derived for different metallicity ranges from Izotov et al. (2006b). The abundances are then derived as follows (Izotov et al., 2006b):

$$12 + \log(\mathrm{OII/H}) = \log_{10}(\mathrm{OII}\lambda 3727/\mathrm{H}\beta) + 5.961 + 1.676/t - 0.4\log_{10}(t) - 0.034t + log_{10}(1 + 1.35\mathrm{n_e}) \quad (6.15)$$

$$12 + \log(\mathrm{OIII/H}) = \log_{10}(\mathrm{OII/H}\beta) + 6.200 + 1.251/t - 0.55\log_{10}(t) - 0.014t \quad (6.16)$$

with t being the electron temperatures of [O II] and [O III] respectively. Even though this method should in principle give the most reliable results, it can only applied in low metallicity regions because the [O III] λ 4363 line requires high electron temperatures to be produced.

6.2.2 STAR FORMATION RATE

The UV flux in the stellar continuum is only produced by very young stars which is therefore a good method to determine the star formation rate (SFR) of the region probed. The most widely used conversion is the one from Kennicutt (1998)

$$\mathrm{SFR}\,[\mathrm{M_\odot}/yr] = 1.4 \times 10^{-28} L\nu(\mathrm{UV})[\mathrm{erg/s/Hz}] \quad (6.17)$$

However, the UV flux is strongly affected by extinction and if one cannot reliably correct for the extinction, the SFR from UV is only a lower limit.

The strong recombination lines of hydrogen are also directly linked to the SFR as hydrogen gets ionized by the UV photons. If available, the Balmer lines, especially Hα are the preferred emission lines to determine the SFR. Also the nebular emission line doublet [O II] λ3727,3729 can be used, but the dependence on ionizing UV flux is more indirect and also depends on the ionization state of the gas. The SFR is then (Kennicutt, 1998)

$$\mathrm{SFR_{OIII}} = (1.4 \pm 0.4) \times 10^{-41} 4\pi \mathrm{F(OII)} d_\mathrm{L}^2 \quad (6.18)$$

$$\mathrm{SFR_{H\alpha}} = 7.9 \times 10^{-42} 4\pi \mathrm{F(H\alpha)} d_\mathrm{L}^2 \quad (6.19)$$

$$(6.20)$$

with F the fluxes of the lines in erg/cm^2/s and d$_L$ the luminosity distance in cm. Lyman α can in principle also be used by assuming an unextincted ratio between Ly α / Hα of $\sim$ 11.4 and taking the conversion for Hα above.

The absolute SFR of a galaxy, however, does not necessarily reflect the ability of the galaxy to form stars, especially if it has a very low mass, which is often the case for GRB hosts. To account for the large differences in galaxy masses, it had became common to introduce a so-called specific SFR (SSFR) which weights the SFR with either the restframe B-band luminosity (see e.g. Christensen et al., 2004) or the mass as determined from the K-band luminosity (see e.g. Castro Cerón et al., 2008; Savaglio et al., 2008). The luminosity weighted SFR is then calculated as

$$\begin{aligned} \mathrm{SSFR} &= \mathrm{SFR}[\mathrm{M}_\odot/\mathrm{yr}]\frac{L}{L^*} = \mathrm{SFR} \times 10^{0.4(m_{\mathrm{abs}}-m^*_{\mathrm{abs}})} && (6.21)\\ m_{\mathrm{abs}} &= m - 5(\log\ d_L[pc] - 1) && (6.22) \end{aligned}$$

with m and $\mathrm{m_{abs}}$ being the relative and absolute magnitudes of the galaxy in restframe B-band and d_L the luminosity distance. As magnitude for an L* galaxy, a value of –21 mag is usually chosen.

For the mass-weighted SFR, the stellar mass $\mathrm{M}_\star$ from the K-band luminosity is obtained by the following conversion (Castro Cerón et al., 2008):

$$M_\star[M_\odot] = 2.67 \times 10^{-48} \times \frac{4\pi d_L^2 f_\nu(\nu_{\mathrm{obs}})}{1+z} \times \frac{M_\star}{L_{K_{\mathrm{rest}}}}, \qquad (6.23)$$

with $\mathrm{f}_\nu(\nu_{\mathrm{obs}})$ being the flux density in μJy and d_L in cm. $\frac{M_\star}{L_{K_{\mathrm{rest}}}}$ depends to some extend on the stellar population and estimates range from 0.1 to 0.7 $\mathrm{M}_\odot/\mathrm{L}_\odot$, Castro Cerón et al. (2008) assumed a value of 0.4 $\mathrm{M}_\odot/\mathrm{L}_\odot$. The SSFR is then usually given as log ($\mathrm{SFR}/\mathrm{M}_\star$) [$\mathrm{Gyr}^{-1}$].

Kennicutt (1998) also mention a correlation between the SFR and the far-IR flux where the UV radiation gets reprocessed by dust, but a straightforward correlation might only be the case for young starburst regions and galaxies. The most reliable way to determine the unextincted SFR is by taking the radio flux. One has to be careful, however, as strong radio flux can also have a different origin, e.g. from an AGN. The radio flux in "normal" galaxies above $\lambda\sim$1.5 mm is produced by synchrotron radiation from relativistic electrons and thermal bremsstrahlung. The bremsstrahlung (free-free emission) and nonthermal radio luminosities are connected to the SFR (of stars with $\mathrm{M} > 5\ \mathrm{M}_\odot$) in the following way (Condon, 1992)

$$\begin{aligned} \mathrm{SFR_{th}}\,[M_\odot/yr] &= \nu^{0.1} L\nu_{\mathrm{th}} \times 1/5.5 \times 10^{20} && (6.24)\\ \mathrm{SFR_{nth}}\,[M_\odot/yr] &= \nu^{0.8} L\nu_{\mathrm{nth}} \times 1/5.3 \times 10^{21} && (6.25) \end{aligned}$$

and by measuring the total radio flux and determining the thermal to nonthermal radio flux by the above equations, one gets the SFR from radio. Furthermore, the radio flux also gives the expected supernova rate (SNR) by SNR/yr = 0.041 SFR [$\mathrm{M}_\odot$/yr].

6.2.3 EXTINCTION

Also for the extinction, there are several methods available, especially from spectroscopic data. The most widely used method for the determination of extinction from HII region is the so-called "Balmer decrement". The Balmer lines are the transitions from the $\mathrm{n}\geq 3$ level to n=2. From atomic transition probabilities and population of the individual levels by recombination, photoionisation, it is possible to calculate the theoretical ratio for the strengths of the individual Balmer lines which are $\mathrm{H}\alpha/\mathrm{H}\beta$=2.76 (and $\mathrm{H}\gamma/\mathrm{H}\beta$=0.474). The ratio is usually given for the

"case B recombination" (the stars emit no Lyman α and the gas is optically thick in Lyman α) and a temperature of 10^5 K which is typical for HII regions, however, the ratio is not very sensitive to the temperature. A higher value would then imply extinction due to the differential extinction which affects Hβ much more than Hα. The extinction is then:

$$E(B-V) = 2.21 \log_{10}\left(\frac{H\alpha/H\beta}{2.76}\right) \quad (6.26)$$

$$E(B-V) = -5.17 \log_{10}\left(\frac{H\gamma/H\beta}{0.474}\right) \quad (6.27)$$

The relation between the differential extinction and the extinction in a specific band, e.g. V-band is A_V=R_VE(B–V) with R_V=3.1 for the Milky Way. Different extinction laws can be applied which has already been discussed in Chapter 2.3.2. In order to correct the individual lines for the extinction, one needs the relative extinction according to the extinction law k_λ with A_λ=k_λE(B–V) and therefore

$$F(\lambda)_{\rm corr} = F(\lambda)\ 10^{0.4A(\lambda)} \quad (6.28)$$

If no emission lines are available to measure the extinction directly, another method that can be applied with optical spectra is the relation between the strength of Na D and K I and the extinction. Munari & Zwitter (1997) measured the strength of Na D towards stars in the LMC and compared it with other extinction measurements. They find a correlation

$$EW = \alpha \sum_{n=1}^{\infty} (-1)^{n-1} \frac{(\beta E_{B-V})^n}{n!\sqrt{n}} \quad (6.29)$$

with best fits for α(Na D1) = 0.354$\pm$0.01 Å and β(Na D1)=11.0$\pm$1.0, which however saturates for high EWs. A similar correlation exists between the strength of Diffuse Interstellar Bands (DIBs), but the correlation has an even higher scatter. DIBs are usually not detected in GRB spectra, but have been found in the high resolution spectrum of SN 2008D (see Chapter 8.4.2)

6.2.4 STELLAR POPULATION SYNTHESIS MODELING

The continuum of a spectrum or broadband photometric data also tell us something on the properties of the observed region or galaxy. The different contributions from young and old stars give the continuum a characteristic shape according to the galaxy type and the age of the population. From young to old stellar populations, the strength of the nebular emission lines decrease together with the blue continuum. The first prominent feature arising in the optical are the Ca H& K absorption and a subsequent jump in the continuum. Old populations only show absorption lines and a red continuum (for model spectra see e.g. Kennicutt, 1992b).

These general trends allow to determine the age, the SFR and a number of other properties can be derived from modeling the broad band continuum. The model input are different stellar evolution tracks convolved with an initial mass function (IMF) in order to calculate the output radiation and temperatures. The most widely used models, especially for young star forming galaxies, are those by Bruzual & Charlot (2003) and Leitherer et al. (1999) and template broad band models are available for certain types of galaxies. The correct treatment of the dust absorption and reemission in the IR is often an issue and a code has been developed by e.g. Silva et al. (1998). An issue with very young populations is also the nebular emission from the SF regions which has been included in the model of Zackrisson et al. (2001).

6.2.5 KINEMATICS

Spatially resolved spectra or high resolution observations allow us to probe the kinematical properties of the region or galaxy observed. By measuring the rotation curves of galaxies far out, Zwicky (1937) found that they are not dropping with $1/r^2$ as expected if the mass would be more or less confined in a small region in the central regions of the galaxy corresponding to the distribution of the luminous matter. Instead, they initially rise and then stay flat over the observable range. This has been the first evidence of a dark matter halo around the galaxies which actually contain most of the mass. The rotation curve is then the sum of the contributions from the disk, the bulge and the dark matter halo. Different models for shape of the dark-matter halo have been suggested. The most widely applied is the isothermal sphere (a constant density core which drops at large radii with $1/r^2$), others are the FNW (French Navarro White) or the Sersic profile. The velocity shift of the line center from the galaxy center then behaves like this:

$$v^2_{\rm disk} = 4\pi G\sigma_0 R_d y^2 (I(y,0)K(y,0) - I(y,1)K(y,1)) \quad (6.30)$$

$$v^2_{\rm bulge} = \frac{4\pi G\rho_{\rm b}}{r}\int x^2(1+r^2/R_{\rm b}^2)^{-3.5/2} \quad (6.31)$$

$$v^2_{\rm cdm} = 4\pi G\rho_0 R_{\rm c}^2(1-(R_{\rm c}/r)\arctan({\rm r/R_c})) \quad (6.32)$$

with G the gravitational constant, I,K the Bessel functions, $R_{\rm c,b}$ the radii of the dark-matter halo core and the bulge, R_d the scale length of the disk, y=r/(2$R_{\rm d}$), σ_0=$\Gamma\sigma_{\rm light}$ (mass to light ratio = σ exp(-r/$R_{\rm d}$) with σ the central luminosity density) and ρ_0 and $\rho_{\rm b}$ the densities of the halo core and bulge respectively, where ρ_b=0.572σ_0/$R_{\rm b}$. The total velocity is then $v_{\rm tot}$=$\sqrt{v^2_{\rm disc}+v^2_{\rm bulge}+v^2_{\rm dm}}$.

Rotation curves have been obtained for all nearby galaxies, either by measuring strong emission lines or using radio emission from HI which can be detected out to larger radii than the optical emission. Velocity maps are made with integral field spectrographs and often reveal deviations from a smooth rotation curve from interactions with other galaxies or internal dynamics. Recently, this has been extended out to high redshift galaxies with IR integral field spectroscopy (e.g. Förster Schreiber et al., 2006; Nesvadba et al., 2008).

6.3 RESOLVED STELLAR POPULATIONS

6.3.1 SNE AND THEIR PROGENITORS

There is little doubt today about the progenitors of core collapse SNe (CC-SNe), especially those of Type II. The first progenitor star identified from pre-SN imaging was the one of SN 1987A, a peculiar SN II-P in the LMC, Sanduleak 69-202, which was a blue supergiant (BSG) (Gilmozzi et al., 1987). Since then, about 10 SN II progenitors have been identified, e.g. SN 2004A (Hendry et al., 2006), SN 2002ov (Li et al., 2007) and SN 2006gl (Gal-Yam et al., 2007) (for a complete list up to July 2007 see Li et al., 2007). The typical progenitor of a Type II-P SN is not the BSG from SN 1987A but a yellow or red supergiant (YSG, RSG) with a mass between 7 and 20 $M_\odot$. For another $\sim$ 10 SN progenitors, mass limits have been established in the same range. SN II-P might be the population with the lowest progenitor masses, but other types such as II-L or II-n (narrow line) have not been identified yet. The group by S. Smartt has launched a large observing campaign with the *HST* in order to identify progenitors of future SNe.

SNe Ib/c have so far evaded an identification with a progenitor star despite deep searches also in the IR (Maund et al., 2005; Crockett et al., 2007, 2008) and the mass limits derived range

between very low masses for SN 2000ds (Maund & Smartt, 2005) and up to 40 $M_{\odot}$ for 2004gt (Maund et al., 2005). All of them were likely WR stars before they exploded. SN 2006jc, however, a Type Ib pec., was at the same position as a luminous transient two years prior to the explosion (Pastorello et al., 2007), interpreted as a LBV outbreak, which would be inconsistent with previous theories that LBVs do not yet undergone core-collapse but first have to develop into a WR star. SN Ia suffer from the same problem. The models predict them to be WDs with a massive close companion (or the merger of two WDs) that transfers mass onto the WD until it surpasses the Chandrasekhar mass and the pressure by the degenerate electron gas cannot hold up the gravitational collapse. However, none of the companion stars have been identified so far.

6.3.2 BIRTHPLACES OF GRBS

The large distances to GRBs makes it very difficult to nail down the progenitor of a GRB in case high resolution preexplosion images would be available. The lowest redshift of a GRB so far was z=0.0085 (GRB 980425). It is already a great achievement to determine properties of the actual stellar population the GRB was born in, but only a few very nearby ones allow a look to their birthsites. There are two approaches to get information on those, both have their caveats. Large molecular clouds usually have sizes of $\sim$ 100 pc which transforms into 0.5 and 0.05 arcsec at redshifts of z=0.01 and z=0.1. Very high spatial resolution is therefore crucial for these studies and only *HST* is so far capable to reach the needed resolution, but even *HST* cannot resolve stellar populations beyond z$\sim$0.1.

Photometry, however, has its limitations and spectroscopy would give a lot more information on the properties and state of the ISM. In order to study the birthsite and the surroundings, observations using Integral Field Units (IFU) with high spatial resolution would be the way to go, but long integration times are needed. One fortunate case will be described in the next section and others will follow due to accepted IFU observing proposals. Some, more limited information can also be derived from long-slit spectroscopy of the GRB sites which is also limited to a few nearby cases.

The sites of GRBs compared to SNe with the resolution of the *HST* has been studied in two papers by Fruchter et al. (2006) and Kelly et al. (2007). (Fruchter et al., 2006) compared the brightness of the pixel in which a GRB or a CC-SN occurred to the number of pixels in the host fainter or equally bright as the SN/GRB pixel (for a chart of all GRB hosts from this sample see Fig. 6.3). The result was that CC-SN trace the light distribution of their host galaxies meaning that the probability for a SN to occur at a certain place is proportional to the brightness of the pixel. GRBs however seem to prefer the brightest regions in their hosts. As both are the result of the death of a massive star, they conclude that it must be some intrinsic property rather than the host itself which makes a star producing a GRB, e.g. metallicity. Kelly et al. (2007) refined that analysis by analyzing all detected SN sites and taking the populations of GRBs, SNe Type II, Type Ib, Type Ic and broadline Type Ic separately. They found that SN Type II (as well as SN Type Ia) traced the light of their hosts, so do very likely SN Ib. SN Ic and GRBs however trace the brightest regions of their host as also found by Fruchter et al. (2006). The sample of broadline Ics is still to small to derive any conclusions. Both studies also agreed that the hosts of GRBs are on average smaller and less luminous than those of SNe.

GRB progenitors cannot be resolved even with the best telescopes. At very low redshifts, attempts have been made to study the stellar population at the site of the GRB which might not necessarily be the best representation of the properties of the GRB itself but still better than tak-

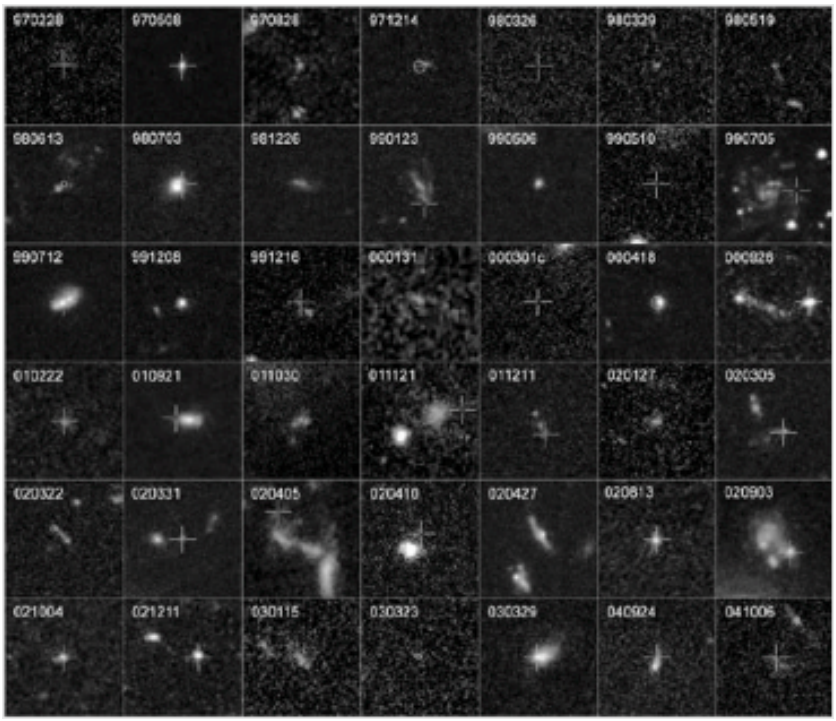

Figure 6.3: *Images of all hosts studied in the Fruchter et al. sample with the GRB position indicated (from Fruchter et al., 2006).*

ing the entire galaxy. Even though most GRB hosts seem to be small irregulars with probably more or less uniform properties throughout the galaxy, some counterexamples and measurements from nearby galaxies have shown that the global properties of a galaxy and those at specific SF regions can be quite different.

Östlin et al. (2008) fitted stellar population synthesis models (Zackrisson et al., 2001) to optical and IR photometry obtained by *HST* from the site of GRB 030329 after subtracting the underlying host galaxy. They find an age of $\leq$5 Myr for the stellar population at the GRB site which would correspond to the lifetime of a $\geq$ 47 $M_{\odot}$ star (Meynet et al., 1994). Fitting the entire galaxy, however, gives an age of $\sim$ 100 Myr which was also obtained by other studies (e.g. Gorosabel et al., 2005).

Another paper, Modjaz et al. (2008a), compared the metallicities at the sites of broadline SNe Ic with those of GRB-SN hosts as well as a population of star-forming SDSS galaxies from Tremonti et al. (2004). By applying different metallicity calibrators, the O3N2 parameter and two calibrations of the R_{23} parameter, they found that GRB-SNe have a rather low metallicity whereas broadline Ic SNe have average metallicites around solar and fit well into the metallicities of average star-forming SDSS galaxies (see Fig. 6.4). In this study, however, the metallicities for the GRB sample were derived from the global spectra of the hosts due to lack of spatial resolution and also for some Ic SN hosts, the metallicity was extrapolated from the value at the center assuming the usual metallicity gradient for spiral galaxies.

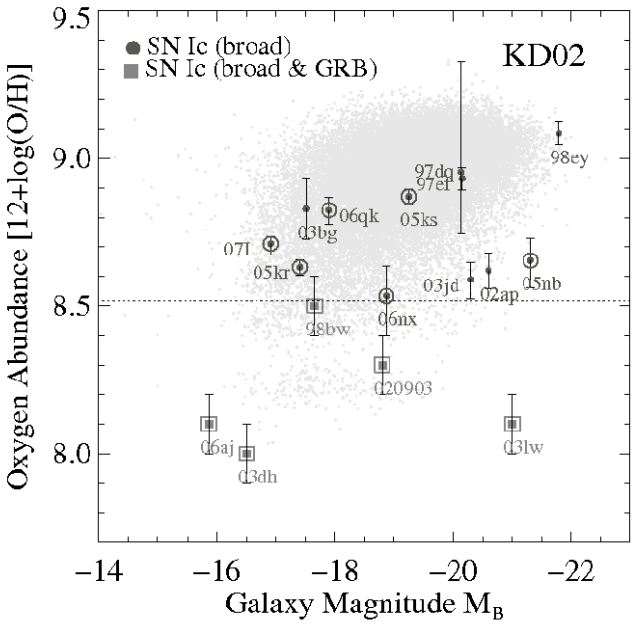

Figure 6.4: *Metallicities at the sites of GRB-SNe and broadline Ic SNe not associated with GRBs using the KD02 metallicity calibrator (from Modjaz et al., 2008a).*

6.3.3 THE TEST CASE: IFU OBSERVATIONS OF THE GRB 980425 HOST

The first GRB host ever studied in 2D spatial resolution using an IFU was the host of GRB 980425 associated to SN 1998bw (Galama et al., 1998). This was possible as the redshift of the host is only z=0.0085, until today still the lowest redshift for a GRB. The GRB/SN occured in the spiral arm of this SBc galaxy and *HST* images (Fynbo et al., 2000) revealed it to be coincident with a SF region not far from a very large SF region. This also lead to the suggestion that GRB 980425 could have been from a runaway star from this SF region (Hammer et al., 2006) but this suggestion is highly doubtful.

The host was observed with the VIMOS IFU unit at the VLT in April and May 2006 using lenses of 0.″67 diameter (corresponding to a physical size of 0.15 kpc) in an array of 4x400 spectra. Using this setup gives a field of view of 27″×27″ covering the central 1/3 of the galaxy. From the extracted and fluxcalibrated spectra in each of the spaxels [2], emission line and other property maps could be produced. Fig. 6.5 shows a map of the metallicity derived from the O3N2 parameter.

The most prominent region in the host is the large HII region next to the GRB/SN region which had also WR features detected. The Hα EW of both regions is relatively large with 1600 and 320 Å respectively corresponding to ages of 3.1 and 5 Myrs, both consistent with ages expected for GRB progenitors. Those ages were also confirmed by applying stellar population synthesis models (Leitherer et al., 1999) to the individual regions. The SFR of the WR region contributes about 1/3 of the SFR of the entire galaxy whereas the one at the GRB/SN site is not significantly higher than in other HII regions in the host. The WR region has also the lowest metallicity, but the SN region has the second lowest in the host. The extinction at the SN region is not low as for other GRB hosts and also seems to have more extinction than derived from the

[2]each "pixel" of an IFU contains one entire spectrum which leads to the expression spaxel for each of the datacubes

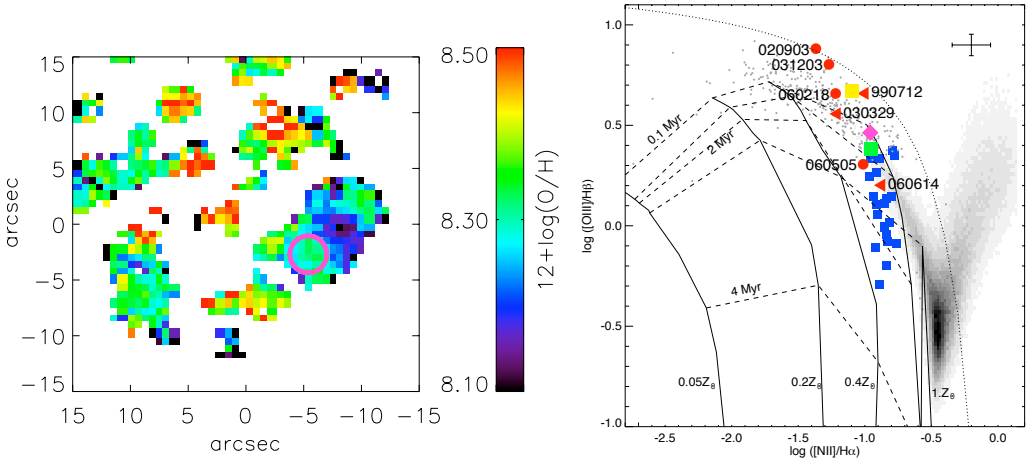

Figure 6.5: *Left panel: Metallicity map of the host of GRB 980425 using the O3N2 parameter, the circle indicates the GRB/SN site, the WR region mentioned in the text is the low metallicity region just next to the GRB site. Right panel: Metallicities at the SN and WR region compared to those of the other HII regions (blue squares), other GRB hosts (red dots), SDSS galaxies (grey scale) and low metallicity SDSS galaxies (small dots) (from Christensen et al. 2008).*

afterglow or fits to the SN SED.

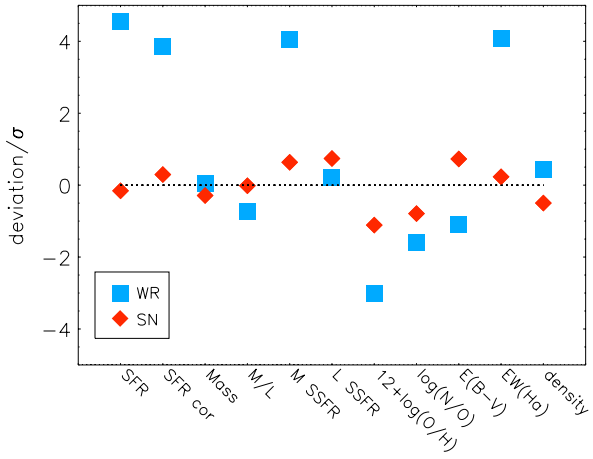

Figure 6.6: *Properties at the SN and WR region compared to the average host properties (from Christensen et al. 2008).*

Overall, the properties of the WR site are very different from the average properties of other HII regions in the galaxy whereas the SN region is not extremely special in most of its properties, except the metallicity (see Fig. 6.5 and Fig. 6.6). The results of this careful spatially resolved analysis tell us that the global results from high redshift GRB hosts have to be taken with caution as it is likely that they consist of different HII regions with eventually different properties. Older stellar populations will then lead to significantly higher ages derived from SED modeling or Hα EW as the old stars increase the continuum contribution. The same would be the case for the metallicity. In the case of the GRB 980425 host, the close distance of the GRB site from the highly

SF WR region would have lead to confusion of the GRB site with this HII region if the host had been further away.

Spatially resolved studies of GRB hosts have just been started but the available sample of very nearby GRB hosts is still very small. Chapter 7 will present the first attempt for a rough spatially resolved study of a GRB host, the one of GRB 060505 that had not SN detected, using longslit spectroscopy covering the major axis of the galaxy including the GRB site. This study will be extended after the end of this thesis using a VIMOS dataset similar to the one presented above, with the data being obtained in Summer 2008. Chapter 8 then presents a study with four longslit spectra of host of SN 2008D and its two other SN Ib sites. Also this galaxy will be studied with VIMOS data coming in winter 2008/2009.

Published as: Christina C. Thöne, Johan P. U. Fynbo, Göran Östlin, Bo Milvang-Jensen, Klaas Wiersema, Daniele Malesani, Desiree Della Monica Ferreira, Javier Gorosabel, D. Alexander Kann, Darach Watson, Michał J. Michłowski, Andrew S. Fruchter, Andrew J. Levan, Jens Hjorth & Jesper Sollerman – *"Spatially resolved properties of the GRB 060505 host - implications to the nature of the progenitor"* Astrophysical Journal, vol. 676, pp. 1151–1161, 2008 April 1.

7

SPATIALLY RESOLVED PROPERTIES OF THE GRB 060505 HOST- IMPLICATIONS TO THE NATURE OF THE PROGENITOR?

ABSTRACT – *GRB 060505 was the first well-observed nearby possible long-duration GRB that had no associated supernova. Here we present spatially resolved spectra of the host galaxy of GRB 060505, an Sbc spiral, at redshift $z = 0.0889$. The GRB occurred inside a star-forming region in the northern spiral arm at 6.5 kpc from the center. From the position of the emission lines, we determine a maximum rotational velocity for the galaxy of $v \sim 212$ km/s corresponding to a mass of $1.14\times10^{11} M_{\odot}$ within 11 kpc from the center. By fitting single-age spectral synthesis models to the stellar continuum, we derive a very young age for the GRB site, confirmed by photometric and Hα line measurements, of around $\sim$ 6 Myr which corresponds to the lifetime of a 32 $M_{\odot}$ star. The metallicity derived from several emission line measurements varies throughout the galaxy and is lowest at the GRB site. Using the 2dF galaxy redshift survey we can locate the host galaxy in its large scale ($\sim$Mpc) environment. The galaxy lies in the foreground of a filamentary overdensity extending south west from the galaxy cluster Abell 3837 at $z = 0.0896$. The properties of the GRB site are similar to those found for other long-duration GRB host galaxies with high specific star formation rate and low metallicity, which is an indication that GRB 060505 originated from a young massive star that died without making a supernova.*

7.1 INTRODUCTION

This GRB reinitiated the discussion on the connection between long GRBs and SNe as despite intense photometric and spectroscopic searches, no sign of a SN was detected for the nearby GRBs 060505 and 060614. GRB 060505 was especially debated due to its relatively short duration of only 4s and it was suggested that it indeed was a short GRB and no SN to be expected. In this Chapter, we present spatially resolved spectroscopic observations of the host galaxy of GRB 060505 in order to compare the galaxy and the burst site with the host galaxies of other long GRBs and to explicate the controversial nature of this SN-less long duration GRB. First, we describe the general properties of the galaxy concerning the classification, photometry of the entire galaxy, colors, mass determination as well as dynamical measurements. Thereafter, we examine the differences between several parts of the galaxy including the GRB site, the different stellar populations and their ages as well as differences in metallicity and extinction along the galaxy. The next Section presents new high-resolution spatially resolved observations of this

galaxy, which are not part of the original paper and will be incorporated into a future IFU paper on this host. We present and fit a refined rotation curve, radial changes of the line width as well as the evolution of the metallicity along the two slit positions covering (1) the same part as the low-resolution spectra and (2) a neighbouring SF region. The last section, finally, studies the large scale structure around the host galaxy.

The *Swift* satellite (Gehrels et al., 2004) detected GRB 060505 on May 5 2006, 06:36:01 UT, which had a fluence of $(6.2\pm1.1)\times10^{-7}$erg/cm^2 (Hullinger et al., 2006). With a duration of T_{90}=4 s and a statistically significant spectral lag measured from Suzaku data (McBreen et al., 2008) it very likely falls in the class of long-duration GRBs. The satellite did not, however, slew automatically as the GRB was too faint to be detected in-flight (Palmer et al., 2006) due to a high background caused by approaching the SAA. One of the two X-ray sources inside the BAT error circle detected by the XRT was finally established to be fading (Conciatore et al., 2006). An optical afterglow (Ofek et al., 2006) was found 1."5 from the center of the revised XRT error circle with a radius of 2."5, thereby localizing GRB 060505 to a region 4."3 north of the center of the 2dFGRS spiral galaxy TGS173Z112 at a redshift of $z = 0.089$. Later imaging and spectroscopy established the burst position to be coincident with a bright, compact star forming region in one of the spiral arms of the host galaxy (Thöne et al., 2006; Fynbo et al., 2006b), which was revealed to be a late-type, strong emission line galaxy at z=0.0889 from the 2dFGRS data (Colless et al., 2001). A redshift of z=0.0889 corresponds to a luminosity distance of 401 Mpc and 1" corresponds to 1.64 kpc according to standard cosmology.

7.2 OBSERVATIONS

Spectra were taken with FORS2 at the Very Large Telescope (VLT) on Cerro Paranal in Chile on May 23 2006, 18 days after the burst when there was no contribution from the afterglow. We used grism 300V, which covers the wavelength range $3500 - 9600$ Å, and a 1."0 wide slit resulting in a nominal resolution of 11 Å FWHM or 590 km s^{-1} at λ = 5600 Å. Seeing conditions were decent with a seeing of 0."75 FWHM, determined from the acquisition image. In order to minimize the effects of atmospheric dispersion, the FORS instrument uses a so called "Longitudinal Atmospheric Dispersion Corrector" (LADC) which reduces differential slit loss. We obtained two 1800 s and one 600 s exposures which were combined and reduced with standard packages in IRAF. The dispersion solution used for the wavelength calibration had an RMS of about 0.1 Å.

The coadded 2D spectrum was divided into four pieces of eight and one piece of nine pixels width along the spatial direction, where 1 pixel corresponds to 0."25 or 0.41 kpc at the redshift of the galaxy. These five parts represent distinct regions in the galaxy such as the spiral arms and the GRB site covered by the slit (see Figures 7.2 and Fig. 7.4). We used the continuum of the bulge which has the brightest trace to create a "template" trace and extract all five pieces using the same trace function, in order to account for the bending of the trace towards the blue. The individual parts were then flux calibrated with IRAF using observations of the spectrophotometric standard star LTT7379 from 2006 April 2 which was taken under photometric conditions. Cross-calibration with observations of the standard star LTT1788 on August 17 gave consistent results for the fluxes. We estimate the error of the flux calibration to be around 10% in the wavelength range between 4000 and 7500 Å which covers the range of the host galaxy emission lines. The flux calibration obtained in such a way can, however, only serve as a relative flux calibration and to determine the shape of the continuum.

Imaging was obtained with FORS1 at the VLT in the $BVRIz$ bands on 2006 September 14

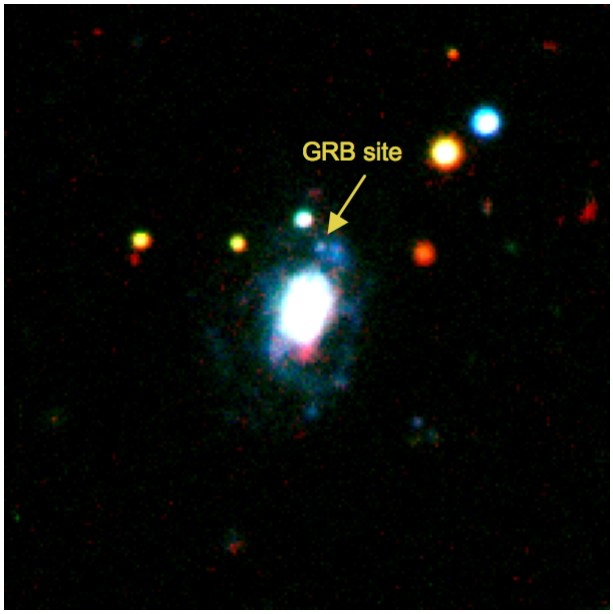

Figure 7.1: *Color picture of the host galaxy of GRB 060505 from BRK_S bands, field of view 40″ × 40″, North up, East left, the position of the OT is marked.*

and in U on 2006 October 1 under photometric conditions. Images in the K_S band were taken with ISAAC at the VLT on September 24. The images of FORS1/VLT in $UBVRI$ were calibrated using photometric zeropoints from the same night as the observations in the corresponding bands. For the z band, which has no zeropoints available, we calibrated a standard field observed on the same night with magnitudes from SDSS observations of the same field, which was then used to derive instrumental zeropoints in the z band. The K_S band image was calibrated using a comparison star in the same field from the 2MASS catalogue (Skrutskie et al., 2006).

7.3 Global properties of the Galaxy

7.3.1 Classification

The host galaxy of GRB 060505 is a late-type spiral galaxy with at least two major spiral arms, the GRB occurred in the northern arm of the galaxy (see Fig. 7.2). From the morphology and from the strength of the Hα, Hβ and the forbidden nebular emission lines (see Chapter 7.4), this galaxy can be classified as an Sbc spiral Kennicutt (1992a). We detect Ca H & K absorption lines and the 4000 Å break, Ca H is, however, only clearly detected in the bulge region. The three other spiral host galaxies of long GRBs are also late-type spiral galaxies with GRB 980425 occurring in an SBc spiral (Fynbo et al., 2000), 990705 in an Sc (Le Floc'h et al., 2002) and GRB 020819 presumably in an Scd spiral galaxy (Jakobsson et al., 2005).

We determined the magnitudes of the entire host galaxy using the images in $UBVRIz$ from FORS/VLT and in K_S from ISAAC. In order to get the total flux of the host galaxy, aperture diameters of 15″ were used for the U band, 12″ for $BVRIz$ and 8.″88 for the K band which were the smallest sizes to contain the total flux. The different aperture sizes were determined from a curve-of-growth analysis for each band. The flux of the three stars inside the apertures

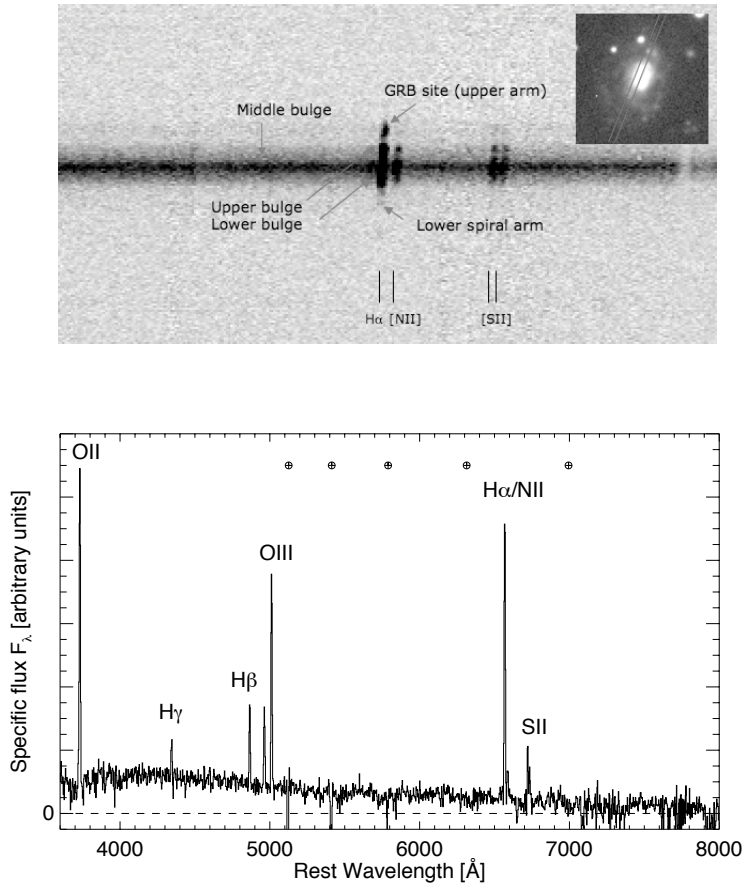

Figure 7.2: *Upper figure: 2D longslit spectrum of the host galaxy of GRB 060505 around the Hα emission line. Indicated are the 5 parts that were extracted from the spectrum. The inset shows the position of the slit across the host galaxy. Lower Figure: 1D spectrum at the GRB position, the crossed circles mark telluric lines.*

contributing about 10% to the total flux was subtracted. These magnitudes and the corresponding colors are listed in Table 7.1, the magnitudes are corrected for the foreground extinction of E(B−V)=0.021. From the R band magnitude we derive an absolute magnitude for the host of $M_R = -20.15 \pm 0.02$ mag (no K-correction applied) which corresponds to 0.4 L^* with $M_R{}^*= -21.21$ mag (Blanton et al., 2001) using h= 0.71. The colors of this galaxy are actually too blue for an Sbc spiral galaxy but rather resemble the values for an irregular galaxy (Fukugita et al., 1995). Also the equivalent widths (EWs) of the emission lines are generally stronger than expected for a normal Sbc spiral (Kennicutt, 1992b).

A closer look at the morphology reveals some asymmetry in the spiral structure and distortions in the western part of the galaxy which can also be seen in the HST images of the host galaxy presented in Ofek et al. (2007) (see also Fig. 7.5). This suggests a recent minor merger event which could have triggered the excess star formation in parts of the host which overall has an older stellar population (see Chapter 7.4.3). It might also explain the deviation of the colors and emission line strengths compared to usual Sbc spiral galaxies.

Filter	mag	color	mag
U	18.43 ± 0.05		
B	18.89 ± 0.02	U−B	-0.46 ± 0.05
V	18.27 ± 0.02	B−V	0.62 ± 0.03
R	17.90 ± 0.02	V−R	0.37 ± 0.03
I	17.51 ± 0.02	R−I	0.39 ± 0.03
z	17.29 ± 0.08	R−z	0.59 ± 0.08
K	15.85 ± 0.04	R−K	2.05 ± 0.04

Table 7.1: *Magnituds given are in the Vega system. The values are corrected for the foreground extinction of* $A_{\rm V}$*=0.06*

7.3.2 MEASUREMENT OF THE ROTATION CURVE

In order to measure the rotation curve of the host galaxy, the four brightest emission lines in the 2D spectrum were used, namely [O II], Hβ, [O III] λ 5008 and Hα (see Fig. 7.2). A 2D continuum subtracted postage stamp spectrum was produced for each emission line, with the continuum being modeled as a linear function fitted near each emission line. For each spatial point along the slit, the postage stamp spectrum, a Gaussian was fitted using the IRAF task `ngaussfit` from the STSDAS package. At first the FWHM was kept as a free parameter, resulting in a typical value of 9 Å. The FWHM was then fixed at 9 Å, and a Gaussian was fitted again to each row, now with only two free parameters, the center (i.e. observed wavelength) and amplitude. Uncertainties on the fitted parameters were calculated using `ngaussfit` based on an input noise spectrum which was calculated as photon noise and read-out noise from the 2D galaxy spectrum before sky subtraction.

The fitted observed wavelengths $\lambda_{\rm obs}$ were first corrected for a zero point error in the wavelength calibration and then used to calculate rest-frame line-of-sight velocities as $v_{\rm rest}^{\rm l.o.s.} = c(z - z_{\rm sys})/(1 + z_{\rm sys})$, with $z = \lambda_{\rm obs}/\lambda_{\rm rest} - 1$ where a systemic redshift of $z_{\rm sys} = 0.0889$ was used. The velocities were finally corrected for inclination (deprojected velocities) as $v_{\rm rest}^{\rm deproj.} = v_{\rm rest}^{\rm l.o.s.}/\sin i$, with i being the inclination. The row number in each postage stamp spectrum was transformed into a spatial coordinate with respect to the continuum center. The location of the continuum center as a function of observed wavelength (the "trace" of the continuum) was measured in a number of bins in an aperture of width 14 pixels = 3.″5 and fitted using a linear function. The used systemic redshift was chosen so that the median velocity of the 16 data points (4 per emission line) located within $\pm 0.''5$ of the continuum center was zero, therefore, the calculated velocities were defined to be zero at the continuum center.

To plot the rotation curve we only use points for which the fitted Gaussian amplitude was larger than three times its uncertainty. The rotation curves based on the 4 emission lines agreed reasonably well, although there were places where the difference was larger than what the calculated uncertainties could explain. The weighted mean rotation curve shown in Fig. 7.3 was calculated using inverse variance weighting.

7.3.3 GALAXY SIZE AND MASS

In order to determine the inclination of the galaxy, we measured the ellipticity of the disc with SExtractor Bertin & Arnouts (1996) using the photometric data in the V, R and I bands. We find e = 0.346 ± 0.006 which gives an inclination of 49 ± 1 degrees. The radius of the circle containing 80% of the light is about 4.″3 which corresponds to a line-of-sight radius of $\sim$11 kpc.

Furthermore, we determined the stellar and baryonic mass of the galaxy by fitting empirical

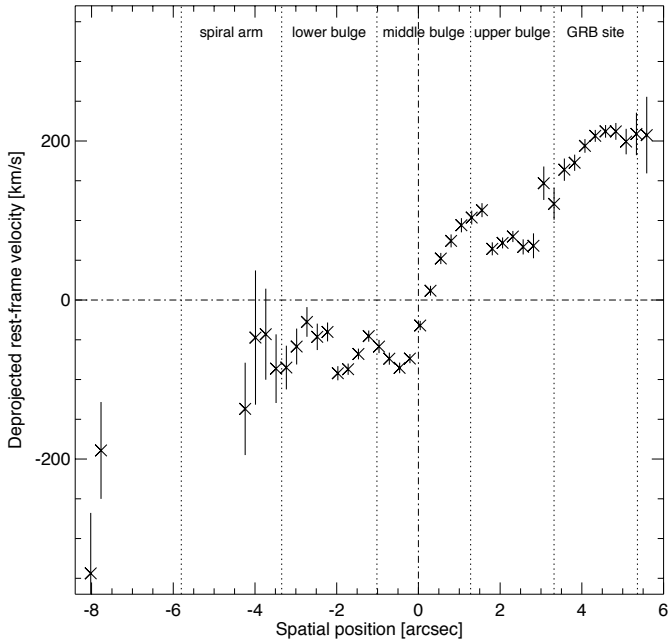

Figure 7.3: *Rotation curve using the weighted mean of the center of the emission lines [O II], Hβ, [O III] and Hα over the spatially resolved host galaxy spectrum. The curve shows the true rotation curve of the galaxy, corrected for the inclination of 49 deg.*

models for GRB host galaxies to the spectral energy distribution (SED) of the galaxy according to Michałowski et al. (2008). This method is based on the radiative transfer code GRASIL developed by Silva et al. (1998) which models the spectrum of the galaxy taking the stellar UV output and its absorption and redistribution by dust. The best fitting model was found to be similar to the SED of the GRB 000210 host galaxy which then gives a total stellar mass of $(7.9 \pm 0.4)\times10^9$ $M_\odot$ and a total baryonic mass of two times the stellar mass. The error quoted comes only from the errors of the model fitting, the total error from the model itself is around a factor of two. The measurement of the rotation curve which flattens at a value of 212 km/s[1] (considering the inclination) allows an estimate of the dynamical mass to 1.14×10^{11} $M_\odot$ within a radius of 11 kpc.

7.4 SPATIALLY RESOLVED PROPERTIES

Fig. 7.4 shows the different regions selected for the analysis of the properties in different parts of the galaxy. The three peaks in Hα within the bulge seem to come from the nucleus of the galaxy and the innermost regions of the two spiral arms as can be seen in Fig. 7.2. The region in the upper spiral arm around the site where the GRB occurred is a large HII region, representing a clear peak in the Hα spatial profile. A second HII region is to the west of the GRB position, just outside the slit. The spiral arm below the bulge only has a very weak peak in Hα, which indicates a low star formation rate in this region.

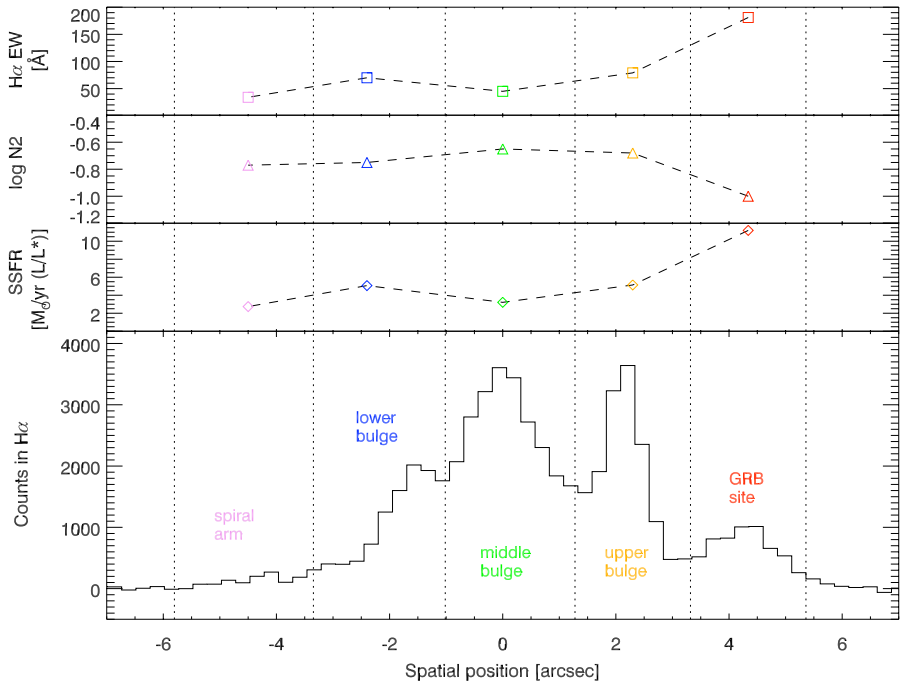

Figure 7.4: *Lower panel: Cut through the spectrum along the Hα line and indication of the regions selected for the individual spectra (see also Fig.7.2). The upper three panels show the metallicity proxy using the N2 parameter N2=log([NII]/Hα) as described in Chapter. 7.4, the specific star formation rate (SFR) per luminosity and the Hα EW as a proxy for the maximum age of the youngest stellar population in the five parts of the spectrum (the higher the EW, the younger the population). All three panels show that the GRB site is considerably different from the rest of the host galaxy.*

We analyze the properties of the ISM in the individual regions by comparing the emission line fluxes from the different regions (see Table 7.2). The Balmer lines Hα, Hβ and Hγ were found in emission in all regions, except that Hγ was not detected in the faint spectrum of the lower spiral arm. We also detect the forbidden lines [O II] $\lambda\lambda$3727,3729 and [O III] $\lambda\lambda$5007,4959 as well as [N II] λ6568 and the [S II] $\lambda\lambda$6716,6731 doublet. We measured the line properties (see Table 7.2) using the `splot` task in IRAF which fits Gaussian to the lines. The lines are unresolved within the resolution of the instrument. The continuum has been corrected for the Galactic extinction of E(B$-$V)$=$ 0.021 mag, measured fluxes were then both corrected for the underlying stellar absorption and extinction in the host galaxy.

7.4.1 Burst location

The accurate location within the host galaxy could be determined for only a small number of bursts. For XRF 020903 it was shown that the GRB occurred close, but not inside, a massive, star-forming supercluster (Bersier et al., 2006; Le Floc'h et al., 2006; Soderberg et al., 2004). GRB 980425 was coincident with a smaller star forming region (Fynbo et al., 2000; Sollerman et al., 2002). GRB 990705 whose spiral host could be resolved in *HST* images also occurred close to a star-forming region within a spiral arm (Le Floc'h et al., 2002). GRB 020819 lies close to a brighter "blob", possibly a star-forming region, next to a face-on spiral galaxy, whose connection to the spiral galaxy has yet to be proven spectroscopically (Jakobsson et al., 2005).

Line	Site	λ_{obs} [Å]	EW [Å]	Flux [10^{-17}erg/cm^2/s/Å]
[O II] 3727/29	GRB	4064.6	−152.3	11.2 ± 0.2
	Bu	4063.2	−97.9	12.7 ± 0.3
	Bm	4062.9	−48.91	16.8 ± 0.4
	Bl	4061.8	−56.38	13.4 ± 0.4
	lS	4061.5	−43.83	2.87 ± 0.08
Hγ 4340	GRB	4731.6	−9.82	1.12 ± 0.02
	Bu	4730.5	−6.85	1.45 ± 0.03
	Bm	4731.0	−1.796	0.99 ± 0.03
	Bl	4729.4	−2.598	0.86 ± 0.03
	lS	—	—	—
Hβ 4861	GRB	5299.9	−39.20	2.98 ± 0.02
	Bu	5298.3	−27.22	4.53 ± 0.02
	Bm	5297.1	−8.064	4.27 ± 0.03
	Bl	5296.3	−12.60	3.35 ± 0.02
	lS	5297.9	−8.917	0.65 ± 0.02
[O III] 4959	GRB	5406.4	−36.31	2.84 ± 0.18
	Bu	5404.4	−11.32	2.27 ± 0.20
	Bm	5402.9	−4.016	2.19 ± 0.13
	Bl	5402.8	−5.758	1.64 ± 0.12
	lS	5403.4	−6.004	0.43 ± 0.03
[O III] 5007	GRB	5458.6	−92.80	7.20 ± 0.06
	Bu	5456.4	−40.46	7.84 ± 0.14
	Bm	5456.3	−9.709	5.17 ± 0.13
	Bl	5455.1	−17.70	4.85 ± 0.13
	lS	5454.2	−21.75	1.43 ± 0.08
Hα 6567	GRB	7154.2	−181.8	9.73 ± 0.03
	Bu	7152.6	−79.32	12.1 ± 0.06
	Bm	7150.6	−45.71	21.9 ± 0.09
	Bl	7149.6	−70.33	12.9 ± 0.04
	lS	7150.1	−34.70	1.59 ± 0.02
[N II] 6586	GRB	7175.8	−19.44	0.96 ± 0.03
	Bu	7174.5	−16.45	2.53 ± 0.06
	Bm	7172.7	−10.62	4.97 ± 0.09
	Bl	7172.3	−13.08	2.28 ± 0.04
	lS	7175.4	−6.142	0.27 ± 0.03
[S II] 6716	GRB	7321.1	−50.81	1.60 ± 0.04
	Bu	7319.3	−23.04	3.04 ± 0.05
	Bm	7318.1	−10.55	4.58 ± 0.03
	Bl	7317.4	−14.57	2.34 ± 0.03
	lS	7316.2	−29.42	0.77 ± 0.12
[S II] 6731	GRB	7335.6	−36.25	1.09 ± 0.04
	Bu	7334.4	−20.25	2.64 ± 0.05
	Bm	7332.7	−7.164	3.10 ± 0.03
	Bl	7331.9	−9.370	1.48 ± 0.03
	lS	7334.5	−36.05	0.91 ± 0.12

Table 7.2: *Emission line fluxes in the five different parts studied. Abbreviations for the different parts along the slit: "GRB" = GRB explosion site, "bu" = upper part of the bulge, "bm" = middle part, "bl" = lower part, "ls"= lower spiral arm. Observed wavelengths are not corrected for the zero point error of around 4 Å mentioned in Chapter 7.3.2. The fluxes are only corrected for the Galactic extinction of E(B−V) = 0.021 mag before measuring the fluxes, no extinction correction in the host galaxy has been applied due to its uncertainty (see Chapter 7.4.2) The errors in the fluxes do not include the overall error from the flux calibration which is around 10%.*

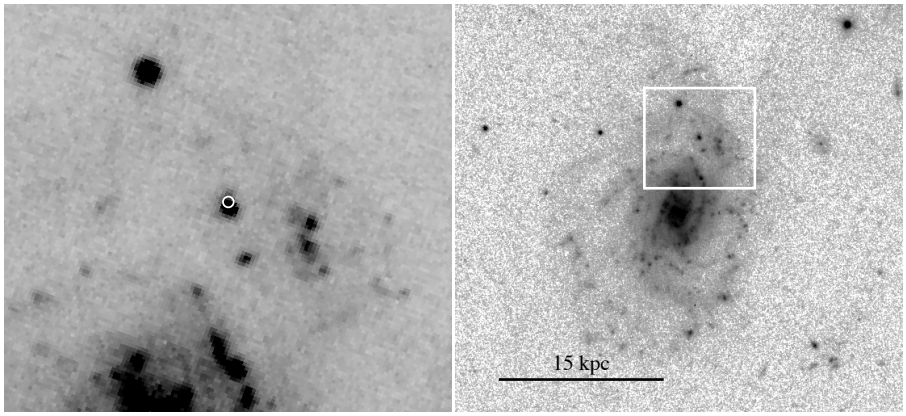

Figure 7.5: *HST image of the host galaxy of GRB 060505 (right panel) and a smaller region showing the HII region at the position of the GRB (left panel), the optical afterglow position from ground based observations is indicated by the white circle.*

HST images of the host galaxy (Ofek et al., 2007) show clearly that the burst lies at the edge of an HII region with a size of 400 pc. We have re-analysed these *HST* images, which are now public, taken in the F475W filter on May 19th, 2006 (*HST* program 10551, PI Kulkarni). Performing astrometry relative to the VLT observations taken on May 5th, we find that our position (see Fig. 7.5) differs slightly from that of Ofek et al. (2007), but is consistent within the errors on each measurement. Following the method of Fruchter et al. (2006), we determine that the burst occurred at the 80th percentile of the host galaxy light (i.e. 80% of the light of the host galaxy is contained in pixels of lower surface brightness than that containing the burst) which is close to the median observed for LGRBs. The difference in the values obtained by us and Ofek et al. (2007) comes from the slightly differing astrometry and the application of a small convolution to the image to allow for the positional uncertainty in our analysis. We note however that both our and Ofek's positions are consistent with the peak of the nearby HII region, which is one of the brightest regions of the galaxy. The peak of the light of this region lies at the 96th percentile of the galaxy light distribution. The absolute magnitude (-19.6 mag) and physical size of the galaxy (R_{80}) are slightly larger and brighter than the mean of LGRB hosts studied by Fruchter et al. (2006), but fit comfortably within the observed range.

The position of GRB 060505 within the host makes it unlikely that the GRB was a chance superposition with the galaxy and in fact occurred at a higher redshift, which could have been an explanation for the lack of the detection of a SN. This clear association of the OT position with a star forming region also supports the suggestion that GRB 060505 was due to the collapse of a massive star that originated in this star forming region. Short bursts have also been found in star forming galaxies (Berger et al., 2007), but a clear association with a star forming region has not been possible so far.

7.4.2 Extinction

Another issue in the discussion about the absent SN in the lightcurve of GRB 060505 is the question of extinction along the line of sight. The Galactic extinction along the line of sight of the GRB determined from the sky maps of Schlegel et al. (1998) is very low with E(B$-$V)$= 0.021$ mag. Determining the extinction in the individual parts in the host galaxy is difficult because of the incertainty in the possible Balmer absorption by an underlying older population which might especially play a role in the innermost parts of the host galaxy. For the following analysis

Filter	GRB site [mag]	HII region [mag]
B	24.31 ± 0.13	24.50 ± 0.08
V	23.99 ± 0.09	24.10 ± 0.08
R	23.84 ± 0.07	24.15 ± 0.16
I	23.53 ± 0.15	23.45 ± 0.08
K_S	21.95 ± 0.30	—

Table 7.3: *Photometry of the GRB site and the nearby HII region west of the GRB site*

of the properties in the different parts, we mainly used emission line ratios so that extinction correction plays a minor role.

For the GRB region, we determined the extinction from the broad-band afterglow photometry using the values of the afterglow from the series of observations in the B, V, R and I bands from the first night with the contribution of the galaxy subtracted (D. Xu et al. in preparation). The SED gives no indication of additional reddening along the line of sight through the galaxy and the slope is consistent, within errors, with X-ray data from *Swift* XRT observations. This rules out the possibility that GRB060505 was obscured by dust which would have prevented the detection of a SN. Furthermore, this argues against the suggestion that GRB 060505 took place at a higher redshift and just happened to lie by chance behind this star forming region, as this would probably have added additional extinction to the SED.

7.4.3 STELLAR POPULATION MODELING OF THE GRB SITE

The age of the stellar population at the GRB site is an important key to understand the progenitor nature of this SN-less GRB. We analyze the burst region with photometry for the HII region of the GRB using an aperture of radius 0."4 and a sky annulus from 0."6 to 1."0. The small aperture was necessary since the GRB occurred in the spiral arm of the galaxy. All the images had similar seeing except for the I and K_S bands which were smoothed to the resolution of the BVR images before the photometry was extracted. Aperture corrections were determined from isolated well exposed but non-saturated stars in the science images. The photometry was corrected for Galactic extinction. We did a similar analysis for the other HII region to the west of the GRB site in the same spiral arm which was outside the slit in order to investigate a possible connection between the two regions in terms of their ages. The photometry of these two HII regions is presented in Table 7.3. For the second HII region, the signal in the K_S band was too low to derive any magnitude.

The photometric results were then compared to predictions from the spectral evolutionary synthesis models of Zackrisson et al. (2001). These models include a realistic treatment of the nebular line and continuum emission, which has been found to be important for modelling photometric data of young stellar populations Östlin et al. (2003, 2007) where the nebular component may significantly affect the broadband colors. We have redshifted the spectra from the Zackrisson et al. (2001) model, integrated over the instrument throughput curve and fitted these to the observed photometry. We adopted an instantaneous burst with Salpeter IMF from 0.08 to 120 $M_\odot$ and two different metallicities for the stars and gas of Z=0.004 (12+log(O/H) $\sim$ 8.0 of 0.2 $Z_\odot$) and Z=0.008 (12+log(O/H)$\sim$8.3 or 0.4 $Z_\odot$). For the extinction we used a Galactic extinction law (Cardelli et al., 1989). One degree of freedom, namely the dust reddening can be removed from the fit as both Hα and Hβ are available from the spectrum. In order to correct for the underlying Balmer absorption before deriving the extinction, we use the models of Gonzalez Delgado et al. (1997).

The best fits were obtained with a metallicity of Z=0.008 giving an age of 9 Myr and a reddening of E(B-V)=0.07 mag. It should be noted, however, that in addition to an interval around 9 Myr (7–14 Myr), the 1σ uncertainties also allow solutions in the range of 25–100 Myr. A lower metallicity of Z=0.004 gives a worse fit and the only allowed interval within the 1σ limit is 25–65 Myr. In conclusion, although favouring a young progenitor, the broadband photometry in this case does not provide very tight constraints on the stellar population age. The modeling for the HII region west of the GRB site gave an even lower age of $3-5$ Myr applying an extinction of E(B-V)=0.25 mag. Here the extinction was left as a free parameter since no spectrum covering this region was available. Even though we lack a more robust measurement of the age of this region from for example spectroscopic measurements of the Hα-EW, our data suggest that these two HII regions are different from the rest of the galaxy and that their onset of star formation might indeed have been triggered at approximately the same time by a minor merging event as suggested in Chapter 7.3.1.

An important indicator for the age of a population, especially when it is very young, is the predicted evolution of the Hα EW derived from the spectra. Assuming again an Salpeter IMF from 0.08 to 120 $M_\odot$ and a metallicity of Z=0.008, the EW of $\sim$ 192 Å indicates an age of 6 ± 1 Myr or less at the GRB site based on the evolution of the EW derived by Zackrisson et al. (2001). This value has to be interpreted as an upper limit due to the HI covering factor leading to a possible Lyman continuum leak which could lower the strengths of the Hα line. The measurement of the Hα-EW is not affected by calibration errors and very reliable in terms of its physical origin as it is directly related to the percentage of very young, blue stars in the region. In order to illustrate the relative difference of the stellar population age throughout the galaxy, we plot the Hα-EW in Fig. 7.4 which is inversely proportional to the age of the population as a proxy for the maximum age of the youngest stellar population.

The different methods applied for the GRB region agree in a young age for the underlying population. The age derived from the Hα-EW is most reliable from the calibration point of view as photometry of the GRB region is always affected by contamination from neighbouring regions. Both methods point to a very low age of the progenitor star of about 6 Myr which corresponds to the lifetime of a 32 $M_\odot$ star. A further determination of a young age of the GRB region could be done by directly detecting the presence of Wolf-Rayet (WR) stars (Wiersema et al., 2007). Unfortunately the continuum flux of our spectrum is not high enough to detect WR star lines. The young ages found for this region, however, connect well with predictions from the latest stellar evolution models for the lifetimes of massive, rapidly rotating, chemically homogeneous single star progenitors (Yoon & Langer, 2005; Woosley & Heger, 2005).

7.4.4 METALLICITY

In order to determine the metallicity, we used the R_{23} parameter (first proposed by Pagel et al., 1979) which is a two-valued function of the metallicity. The degeneracy between the two solutions can be broken by using the ratio [N II]/Hα (Lilly et al., 2003) which indicates some preference for the lower branch solution for the GRB site with [N II]/Hα=0.10 and likely a preference for the upper branch in the other parts of the galaxy, however, an upper branch solution for all regions cannot be excluded.

In the last years, a number of recalibrations of the R_{23} parameter have been done. Most of the recent metallicites of GRB host galaxies have been determined using the parametrization of Kewley & Dopita (2002) for the two branches which takes into account the oxygen ionization state. Using a first guess for the metallicity and a decision for the upper or lower branch

solution, the metallicity then can be determined iteratively which usually converges very fast. Recently, a new recalibration has been done by Kewley et al. (2007) which corrects for the known overestimation of the metallicity from the R_{23} parameter using metallicity calibrations based on measurement of the electron temperature T_e. In Tab.7.4, we only give the values from the recent Kewley et al. (2007) calibration and the solution from both branches.

An independent estimate for the metallicity comes from the so-called $O3N2$ method using the ratio $O3N2$=log((O III/Hβ)/(N II/Hα)) (e.g. Pettini & Pagel, 2004), which is empirically calibrated on a sample of H II regions with electron temperature (T_e) determined metallicities. This parameter is less sensitive to extinction compared to the R_{23} parameter as both line ratios lie very close to each other and are therefore very little affected by extinction. Adopting the metallicities determined through the $O3N2$ parameter as 12+log(O/H)=8.73$-$0.32 x $O3N2$, the gradient throughout the host galaxy is slightly less pronounced compared to the estimate through the R_{23} method, but the tendency is consistent with the values derived from R_{23}.

A final relative metallicity estimator is the N2 parameter, which is simply log([NII]/Hα) (Pettini & Pagel, 2004). This ratio is insensitive to underlying extinction due to the small wavelength difference between the two lines. The calibrations by Pettini & Pagel (2004) allow to transform this ratio into an oxygen abundance. The N2 parameter and the derived metallicity show a picture consistent with the metallicity derived with the R_{23} and $O3N2$ parameter. Again, we find a relatively low metallicity in the GRB region and a higher one in the other parts of the galaxy. In Fig. 7.4 we therefore plot the N2 parameter as a proxy for the relative metallicity.

Consistently for all methods, we find that the metallicity varies over the different regions in the host galaxy (see Table 7.4 and Fig. 7.4 for the [NII]/Hα proxy). The star forming region at the GRB site has a relatively low value of (0.19 to 0.40 $Z_\odot$ for the different calibrations and taking 8.69 as value for the solar metallicity, Asplund et al., 2004) whereas in the other regions covered by the slit the metallicity ranges from 0.49 solar at lower spiral arm to 0.65 solar in the middle bulge region. Here, we also have a much older stellar population which could be responsible for the enrichment of the ISM in that part of the galaxy. From the O3N2 and N2 calibrations, we can infer a (O/H) metallicity gradient throughout the galaxy of -0.03 dex/kpc[1]. For the R_{23} parameter, we cannot determine the gradient as the decision for the upper or lower branch solution in the different regions remains unclear. For comparison in the local universe, for the Milky Way, M33 and M51 gradients of -0.07 (Smartt & Rolleston, 1997), -0.05 (Magrini et al., 2007) and -0.02 dex/kpc[1] (Bresolin et al., 2004) have been derived.

Site	R_{23} K07 (lb/ub)	O3N2	N2/metal.
GRB	7.96/8.20	8.29	-1.00/8.28
Upper Bulge	7.69/8.44	8.44	-0.68/8.47
Middle Bulge	7.84/8.36	8.50	-0.65/8.50
Lower Bulge	7.87/8.34	8.44	-0.75/8.42
Lower Spiral arm	8.00/8.18	8.38	-0.77/8.41Ê

Table 7.4: *Metallicities in the different parts in 12+log(O/H). K07 refers to Kewley et al. (2007), "ub" and "lb" stand for upper and lower branch solution of the two valued R_{23} parameter. The last column states the N2 parameter and the metallicity derived from it according to Pettini & Pagel (2004)*

7.4.5 LUMINOSITY WEIGHTED STAR FORMATION RATE

The instantaneous star formation rate (SFR) can be obtained from the Hα emission flux as HI is excited by UV light mainly coming from young, blue O stars which have their peak lumi-

Site	SFR/8 pix. [$M_\odot$/yr]	M_B	lum. weighted SFR [$M_\odot$/yr/(L/L_*)]
GRB	0.015	−13.82	11.2
Upper Bulge	0.018	−14.86	5.14
Middle Bulge	0.033	−16.03	3.21
Lower Bulge	0.020	−14.99	5.07
Lower Spiral arm	0.003	−13.60	2.74

Table 7.5: *Star formation rate in the different parts. M_B is the absolute magnitude of the corresponding region in B band (observer frame).*

nosity in the UV. The conversion formula for Hα is then SFR[$M_\odot yr^{-1}$] = 7.9 $\times 10^{-42}$ $\times$ 4π F [erg/cm^2/s^1] d_L^2 Kennicutt (1998) where d_L the luminosity distance and F the Hα line flux.

As we only cover a part of the galaxy by the slit, we cannot make a statement about the global SFR in this spiral galaxy, but only about the relative SFR between the different parts that we extracted from the spectrum. Table 7.5 lists the SFR per 8 $\times$ 5 pixels along the slit (the area covered by the individual parts of the 2D spectrum) which corresponds to an area of 3.28 $\times$ 2.05 kpc^2. We then scale the SFR to the B-band luminosity fraction compared to the luminosity of a "standard" galaxy of M_B = −21 mag (Christensen et al., 2004) to get the luminosity weighted SFR for the individual regions. For the B-band magnitudes of the parts corresponding to the individual spectra, we determine the magnitude in a rectangular aperture of 8×5 pixels (9×5 for the lower spiral arm) from the VLT host image at the same position as the spectrum pieces (see Table 7.5 and Fig. 7.4). The luminosity weighted SFR is a factor of 2 to 3 higher in the star forming region around the GRB site with 11 $M_\odot/yr/(L/L_*)$, compared to the value in the bulge of around 3 to 5 $M_\odot/yr/(L/L_*)$. The latter value is higher than in an average spiral galaxy (Kennicutt, 1998) and a factor of 8 higher than in the spiral arm at the opposite side of the galaxy which has 2.7 $M_\odot/yr/(L/L_*)$. The luminosity weighted SFR at the GRB site, however, fits very well into the average value found in GRB host galaxies of 9.7 $M_\odot/yr/(L/L_*)$ (Christensen et al., 2004). To determine an absolute value for the SFR is, however, difficult as the absolute flux calibration might not be fully reliable. In addition, the B-band of our galaxy is shifted slightly towards the V-band, so the absolute magnitude in rest frame B-band would be smaller and therefore the luminosity weighted SFR slightly lower.

7.5 Spatially resolved echelle spectra of the host of GRB 060505

7.5.1 Observations

On July 16, 2007, we obtained 2×1200s spectra with HIRES and Keck I at the Keck Observatory on Mauna Kea, Hawaii. Using a 0.″8 slit, HIRES provides a resolution of 45,000 or $\sim$ 7 km/s. With the red setting used, the orders almost overlap in the blue between 3990 and 4100 Å.

The HIRES slit has a length of 7 arcsec and was positioned at two different angles on the host galaxy of GRB 060505 to cover the HII region at the GRB site, the center of the galaxy and another nearby HII region. The first position was chosen at the same angle (17 deg) as for the low-resolution spectra presented in the previous part of this Chapter, the second slit was positioned at zero degrees or North-South to cover the other large HII region west of the GRB position. The data were reduced using the IDL based HIRES pipeline. This pipeline has as an output one two-dimensional array containing the counts along the echelle traces and one file

containing the wavelengths and also provides a counts to flux conversion. In Fig. 7.6, we show the 2D spectra around some of the strongest lines. The center of the galaxy is to the top left.

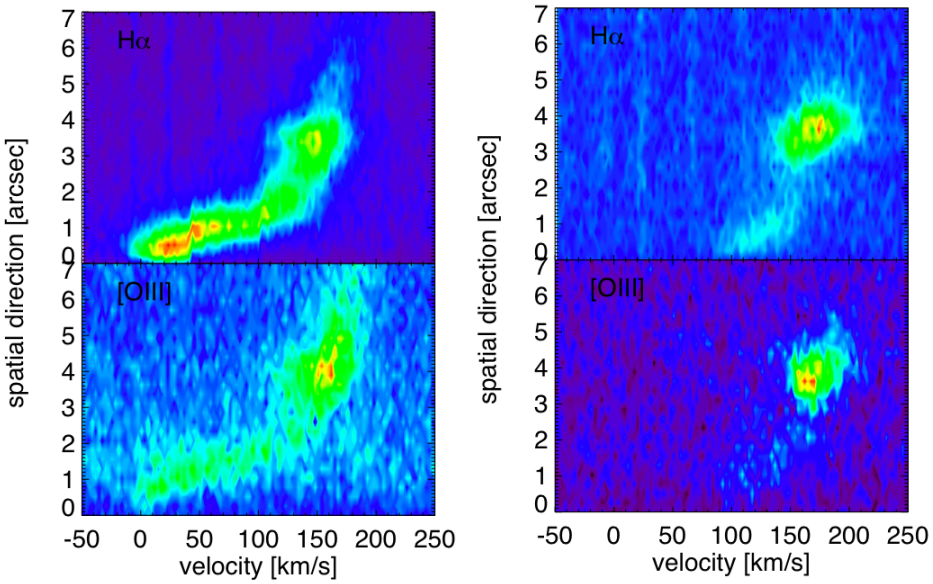

Figure 7.6: *Contour plots for Hα and [O III] along the two slitpositions (left: along the major axis, right: through the HII region next to the GRB site). v=0 km/s corresponds roughly to the center of the galaxy.*

7.5.2 ROTATION CURVE - REFINED

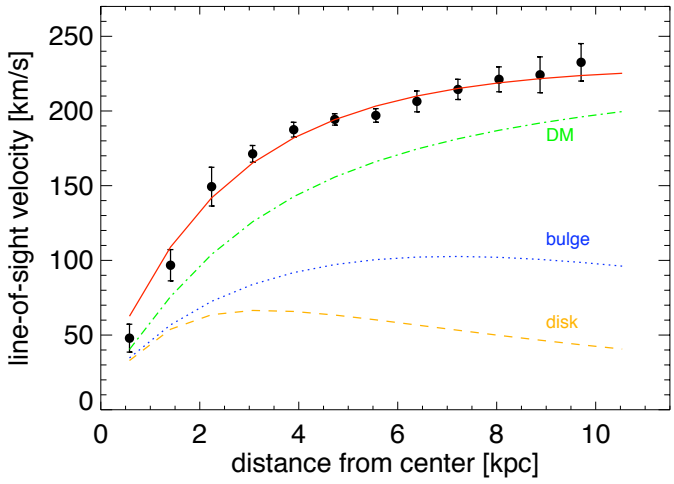

Figure 7.7: *Rotation curve for one half of the GRB 060505 host using high-resolution spectra and a fit with disk, bulge and a DM halo component.*

We extract the emission line profiles of the Hα line for each bin along the spatial direction where one bin corresponds to one row in the spectrum which is 0.25 arcsec or 0.4 kpc. These profiles are then fit by Gaussians and the centers are plotted in Fig. 7.7. For the inner part of the rotation curve, we rebinned the 2D spectrum in the spatial direction to half the resolution.

We then fit this rotation curve with contributions from the disk, the bulge and a dark matter (DM) halo where we take the profile corresponding to an isothermal sphere. Other DM profiles would only be different in the outermost regions which we cannot probe with the strong emission lines from SF regions. We get a best fit with the following values (χ^2 = 9.4 with 6 d.o.f): a disk scale length of 8.3 kpc, a mass-to-light ratio of 7.0 (solar units), a central luminosity density of $62.1\times10^{-3}M_\odot/pc^3$, a DM core radius of 3 kpc and a central density of the DM halo of 134×10^{-3} $M_\odot/pc^3$ and a bulge radius of 2.3 kpc. The rotation curve does not show any obvious particularities, only the fit in the innermost few kpc is not very good as the rotation curve rises steeper than expected. A steep rise has been observed in a number of spiral galaxies, especially when they have massive bulges (e.g. Sofue & Rubin, 2001, and references therein). The data quality, however, is too poor make any firm conclusion on a possible additional component or a high mass concentration in the center.

7.5.3 KINEMATIC PROPERTIES OF THE HOST OF GRB 060505

We also investigate the evolution of the velocity dispersion of the two strongest emission lines, Hα and [O III] from the center of the galaxy to the GRB HII region. Both lines trace each other and the observed changes are therefore likely real. The width is rather high in the center and drops quickly to a rather constant value throughout the disk with the exception of some "wiggles" of which one is conincident with the GRB HII region. The velocity dispersion along the second slit also shows a higher value at the HII regions, especially the one next to the GRB region. Also here the two lines trace each other except for the innermost part of the slit which is likely due to low S/N of [O III].

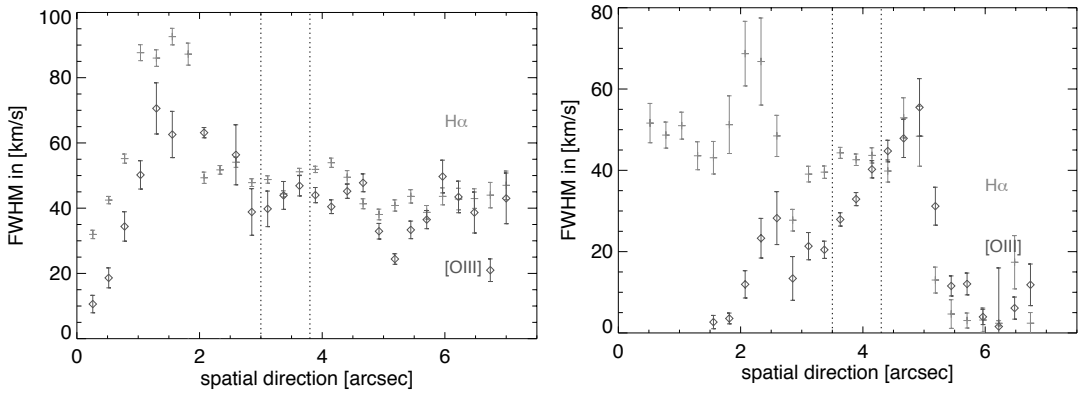

Figure 7.8: *Velocity dispersion along the two slits for Hα and [OIII] (left panel: major axis, right panel: second slit). The dashed lines indicate the position of the two large HII regions, for the slit along the major axis this is coincident with the position of the GRB.*

An enhancement in the central velocity dispersion is an indication for gas infall forming a bulge whereas very young disk galaxies show essentially a flat velocity dispersion along the axis (for a small overview over spiral galaxy rotation curves and velocity dispersions see Beckman et al., 2004). The dispersion falls rapidly and remains constant at about the same distance from the center where the rotation curve starts to flatten which is also what we observe here. However, the difference between the center and the outer parts is not as large as usually observed for spirals with large bulges.

We also refined our analysis on the radial dependence of the metallicity and SSFR along the major axis and include the information from the second slit with another large HII region.

From Fig. 7.9 we see that there is indeed a smooth metallicity gradient from the center to the GRB region and the metallicity in the neighbouring HII region (slit 2) is also rather low. The conversions from Pettini et al. (2002) give values of 12+log(O/H)= 8.28 and 8.20 for the GRB and the second HII region respectively.

In order to determine the SSFR, we fitted the values for the conversion factor between SFR and SSFR from the absolute B-band magnitude given in Table 7.5 between the lower bulge and the GRB region with a second order polynomial and multiplied the SFR with the fitcurve. The value found for the GRB region agrees very well with the one found from the FORS spectra. For the other slit we applied a similar fitcurve. From this refined analysis, it is even more obvious that the SSFR at the GRB site and its neighbouring HII region in slit 2 is clearly enhanced compared to the other regions of the galaxy.

7.6 THE LARGE SCALE STRUCTURE AROUND THE GRB HOST GALAXY

The fact that the field of GRB 060505 is covered by the 2dF survey (Colless et al., 2001) allows us to study the large scale structure around it.

The galactic environments of GRBs have so far not been studied much. At low redshifts Foley et al. (2006) studied the field of the host galaxy of GRB 980425, which was reported to be member of a group. However, based on redshift measurements of the proposed group members, Foley et al. (2006) could establish that the host of GRB 980425 is an isolated dwarf galaxy. Levan et al. (2006) also proposed GRB 030115 to be connected to a cluster around z $\sim$ 2.5 based on photometric redshifts. At redshifts $z \gtrsim 2$ a few GRB fields have been studied using narrow band Lyα imaging (Fynbo et al., 2002, 2003a; Jakobsson et al., 2005). In all cases several other galaxies at the same redshift as the GRB host were identified, but it is not sure whether the galaxy densities in these fields are higher than in blank fields as no blank field studies have been carried out at similar redshifts. However, the density of Lyα emitters was found to be as high as in the fields around powerful radio sources that have been proposed to be forming proto-clusters, which would suggest that GRBs could reside in overdense fields at $z \gtrsim 2$ (but note also that Bornancini et al. 2004 argue for a low galaxy density in GRB host galaxy environments).

To study the environment of the GRB 060505 host galaxy we searched the 2dF database for

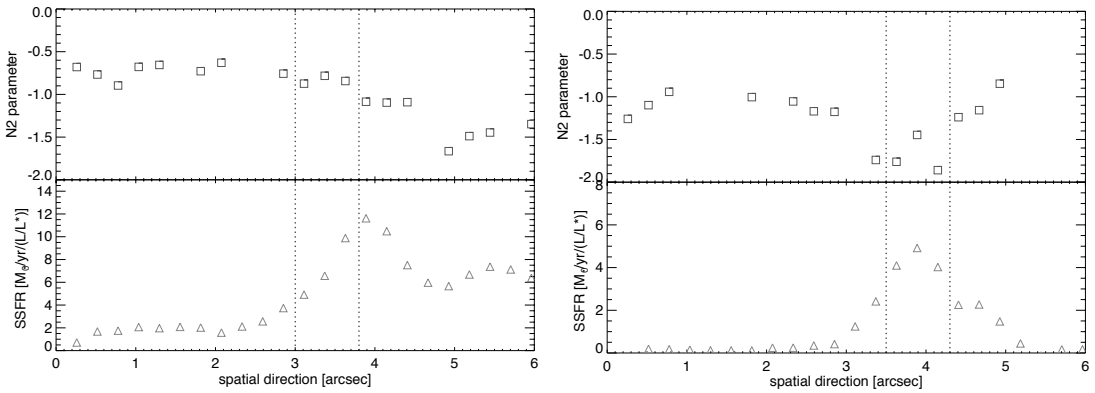

Figure 7.9: *Metallicities expressed through the N2 parameter and SSFR along the two HIRES slitpositions.*

all redshift measurements within a $2^\circ \times 2^\circ$ field around the GRB 060505 host and with redshifts within $\Delta z = 0.004$ (about ± 1000 km/s at the host galaxy redshift $z_{\rm host} = 0.089$). In Fig. 7.10 we show the field and the result is striking. In the GRB field there is a large filamentary overdensity of galaxies with redshifts in the range $0.089-0.093$. The filament extends towards the south west from the galaxy cluster Abell 3837 at $z = 0.0896$ located at a distance of 40 arcmin on the sky (4 Mpc in projection) from the host. This suggests that the host galaxy of GRB 060505 lies in the foreground of the galaxy cluster and that it may be falling into the overdense region defined by the cluster and the filament extending out from it.

7.7 Discussion and conclusions

The low redshift of the host galaxy of GRB 060505 puts us in the rare fortunate situation of allowing us to study the properties in the different parts of the galaxy in a spatially resolved longslit spectrum, including the star forming region around the GRB site. The spatially resolved spectrum also enables us to determine for the first time the rotation curve of a GRB host galaxy for which we find a maximum velocity of 212 km/s.

The star forming region around the burst site is shown to be different in its properties from the rest of the galaxy. Of all the parts of the galaxy traced by the slit the burst region has the highest Hα EW, the youngest (luminosity weighted) age and the highest luminosity weighted star-formation rate and lies near the peak of the surface brightness distribution. Furthermore, the metallicity of the burst site is relatively low with only $1/5$ $Z_\odot$ according to the most recent calibrations. A low metallicity is assumed to be important for a massive star to produce a GRB (see e.g. Woosley & Heger, 2005). Also, a generally higher metallicity has been found for the environments of SN Ic that did not produce a GRB compared to the environment of long-duration GRBs that were accompagnied by a SN Ic Modjaz et al. (2008a).

Connected to the nondetection of a SN in the lightcurve of GRB 060505, there has been some discussions about the classification of the burst as a long-duration GRB (Ofek et al., 2007). In addition, some concerns were put forward that the association between the GRB and the low-redshift 2dF galaxy might be due to a chance superposition (Schaefer & Xiao, 2006). The clear association of the OT position with a star-forming region with a size of 400pc, however, disfavours this possibility and strengthens the suggestion that GRB 060505 was due to the collapse of a massive star that originated in this star-forming region. Using the size of the star forming region measured from the *HST* data of the host galaxy and assuming that GRB 060505 was due to a merger event, Ofek et al. (2007) derive a maximum age of 10 Myr for the progenitor system assuming the lowest possible kick-off velocity from their birth site which is consistent with the shortest time-delays of a merging system (Belczynski et al., 2006).

Ofek et al. (2007) argue that the properties of the host galaxy and the location of the burst within its host provide evidence that GRB 060505 is of a different nature than other long GRBs, in particular in comparison with the sample in Fruchter et al. (2006). As shown in this paper, the properties of the host and of the birth range fall well within the range of other long GRB hosts and birth sites in the sample of Fruchter et al. (2006). In particular, similar hosts and burst locations have been found for other nearby long GRBs. The long-duration bursts GRB 980425 (Fynbo et al., 2000), GRB 990705 (Le Floc'h et al., 2002) and GRB 020819 (Jakobsson et al., 2005) were also located in the outer parts of spiral hosts. Fruchter et al. (2006) also argue that even though most GRB hosts are young, metal poor dwarfs, long GRBs that are found in spiral galaxies would lie on the outskirts of those, preferring metal poor, star-forming regions which is exactly the case for GRB 060505.

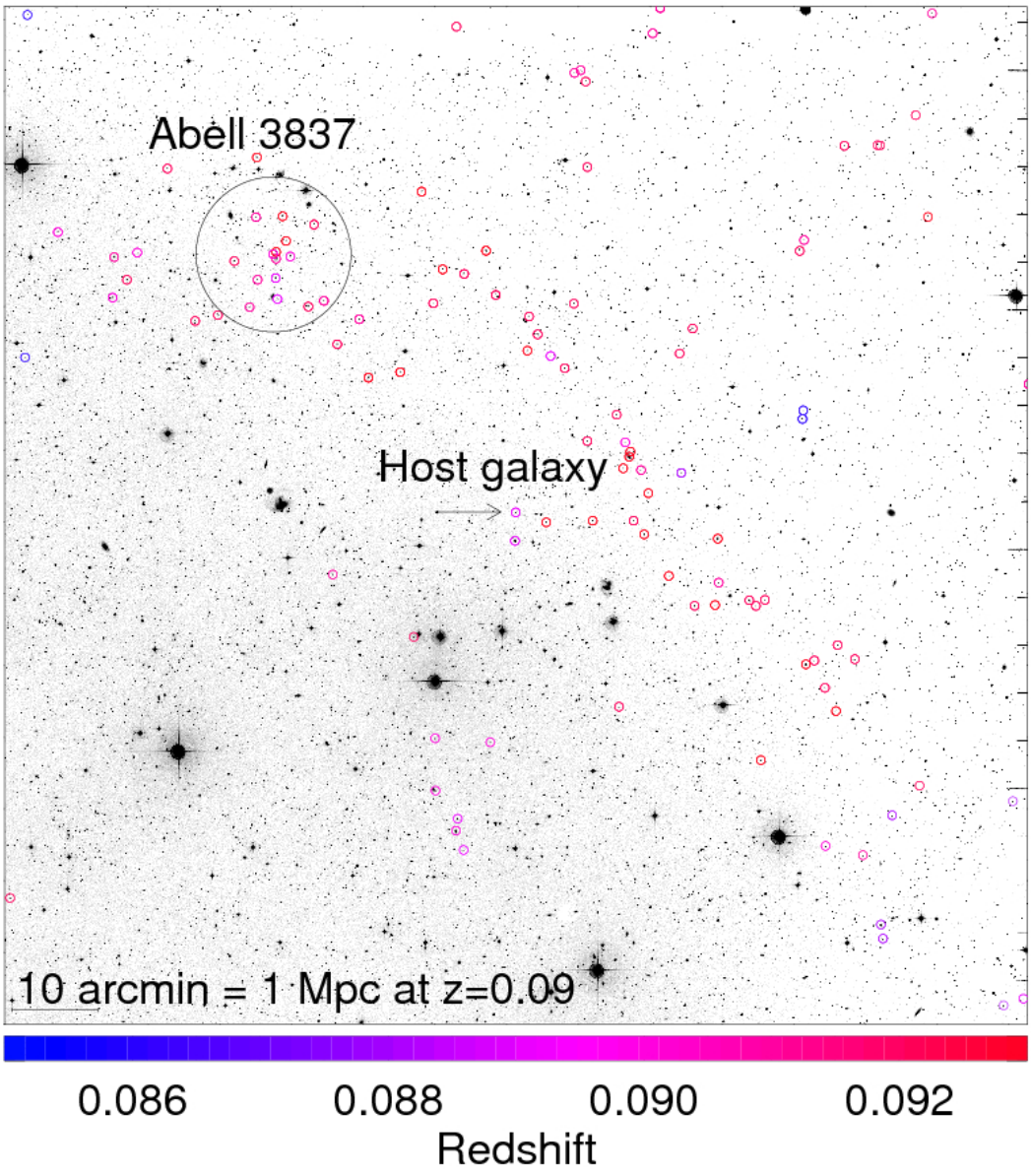

Figure 7.10: *The large scale structure around the host galaxy of GRB 060505 shown in a field of a size of 2° × 2°. The colored circles indicate the galaxies with redshifts known from the 2dF galaxy survey. Blue indicates galaxies with a lower redshift compared to the host galaxy, red a higher redshift. Most galaxies in the field lie on a filament at slightly higher redshift than the host galaxy, stretching out from the Abell 3837 cluster to the North-East of the host.*

Further support for the death of a massive star as the origin for this burst comes from the remarkably young age of the stellar population at the GRB site of less than 6 Myr, which is just barely consistent with even the shortest timescales needed for a binary compact object system to merge (Belczynski et al., 2006). Also, there should be no reason to expect a low metallicity for a merging system. Even though some short-duration GRBs have occurred in star-forming galaxies (e.g. Fox et al., 2005; Covino et al., 2006; Soderberg et al., 2006a; Berger et al., 2007;

Berger, 2008) the specific star formation of the GRB 060505 HII region is significantly larger than that inferred for these events.

Levesque & Kewley (2007) claim that the properties of the GRB region are similar to short GRB hosts in star formation rate and metallicity derived from emission lines. Several points in their analysis, however, are highly debatable. Instead of applying a luminosity or stellar mass-weighted specific star formation rate they compare the uncorrected star formation rate with the one of entire short and long burst host galaxies. Furthermore, they take a "sample" of only two short GRB hosts, as their analysis requires emission lines to be able to derive metallicities for the hosts using the R_{23} parameter. This leaves out a part of the short GRB host sample, namely the ones that have been claimed to reside in early type galaxies without ongoing star formation that are therefore inaccessible for metallicity measurements using R_{23} or similar emission line calibrations (for a summary on the properties of early type short GRB hosts see Prochaska et al., 2006a). In addition, one of the two bursts used in their sample is X-ray flash (XRF) 050416A, where evidence for a supernova component at late times has been found, making this burst likely to be a collapsar event (Soderberg et al., 2007). Considering the still very small sample available for a detailed study of their properties and the large variety of short GRB hosts, a comparison between the hosts of the two types of GRBs should be taken with caution.

In our opinion, the evidence from the properties of the GRB region strongly suggests that GRB 060505 was the result of the death of a massive star that died without producing a SN. Several theoretical works have developed models to explain models of GRBs that do not produce a bright or no SN at all (Fryer et al., 2006; Tominaga et al., 2007). Our toy-model of determining the nature of a GRB according to a (missing) SN connection seems to have to undergo a revision and be improved with additional information from the environment in order to draw conclusions concerning the GRB progenitor.

Acknowledgements

We thank the Paranal staff for performing the observations reported in this paper. G. Ö. thanks E. Zackrisson for integrating his model spectra over the relevant filter at the observed redshift and making these models available to us. B. M.-J. wants to thank Steven Bamford for valuable discussions about rotation curve fitting of well resolved galaxies. Based on ESO-ToO proposal 077.D-0661 and ESO-LP proposal 177.A-0591.

Published as: Christina C. Thöne, Michał J. Michałowski, Nick L. J. Cox, Johan P. U. Fynbo, Jens Hjorth, Jesper Sollerman & Paul M. Vreeswijk– *"NGC 2770 - a supernova Ib factory?"* submitted to the Astrophysical Journal, preprint:astro-ph/0807.0473

8

NGC 2770 - A SUPERNOVA IB FACTORY?

ABSTRACT – *NGC 2770 has been the host of three supernovae of Type Ib during the last 10 years, SN 1999eh, SN 2007uy and SN 2008D. SN 2008D attracted special attention due to the serendipitous discovery of an associated X-ray transient. In this paper, we study the properties of NGC 2770 and specifically the three SN sites to investigate whether this galaxy is in any way peculiar to cause a high frequency of SNe Ib. We model the global SED of the galaxy from broadband data and derive a star-formation and SN rate comparable to the values of the Milky Way. We further study the galaxy using longslit spectroscopy covering the major axis and the three SN sites. From the spectroscopic study we find subsolar metallicities for the SN sites, a high extinction and a moderate star-formation rate. In a high resolution spectrum, we also detect diffuse interstellar bands in the line-of-sight towards SN 2008. A comparison of NGC 2770 to the global properties of a galaxy sample with high SN occurance ($\geq$ 3 SN in the last 100 years) suggests that NGC 2770 is not particularly destined to produce such an enhancement of observed SNe observed. Its properties are also very different from gamma-ray burst host galaxies. Statistical considerations on SN Ib detection rates give a probability of $\sim$ 1.5% to find a galaxy with three Ib SNe detected in 10 years. The high number of rare Ib SNe in this galaxy is therefore likely to be a coincidence rather than special properties of the galaxy itself. NGC 2770 has a small irregular companion, NGC 2770B, which is highly starforming, has a very low mass and one of the lowest metallicities detected in the nearby universe as derived from longslit spectroscopy. In the most metal poor part, we even detect Wolf-Rayet features, against the current models of WR stars which require high metallicities.*

8.1 INTRODUCTION

In this Chapter, we analyse the local and global properties of NGC 2770 at z=0.007 which hosted 3 Type Ib SNe detected within only ten years, SN 1999eh, SN 2007uy and SN 2008D, the last one was connected to XRF 080109 which likely marked the onset of the explosion. For the global properties, we model the spectral energy distribution with broad band data from UV to radio and searched the literature on observations of NGC 2770. We then compare it to a sample of other spiral galaxies and conclude that the only exceptional property is a relatively high HI mass but that the SFR and SNR are fully within the average of the sample (which includes both galaxies with and without SNe detected). Furthermore, we study the galaxy with four longslit spectra placed along the major axis of the galaxy and through the positions of all three SNe. From emission line meaurements, we determine a range of properties at different HII regions in the galaxy including metallicity, extinction, star formation rate and some kinematical studies from a UVES high resolution spectrum of SN 2008D.

In the second part, we establish a sample of galaxies with frequent (3 or more) SNe detected,

compare their properties with those of NGC 2770 as well as GRB hosts and investigate a possible correlation between the SN type and the galaxy type and the frequency of a certain SN type in a certain galaxy. We also estimate the probability of finding three SNe Ib in one galaxy in only 10 years by considering all current and past SN searches. Finally, we analyse a spectrum of the companion galaxy NGC 2770B which is highly star forming and very metal poor and looks more like the galaxy where one would expect a high number of SNe.

8.2 OBSERVATIONS

We carried out optical spectroscopy using the FORS2 spectrograph at the VLT on Jan. 11.31, 2008 and grims 300V. A 1.″0 arcsec wide slit together with the 300V grism provided a resolution of 11 Å. The slit covered the site of SN 2008D as well as some outer parts of the galaxy. We obtained further spectra with ALFOSC at the NOT on Jan. 13, 15 and on Feb. 03 using grism 4. These observations were also part of the observations reported in Malesani et al. (2008a). While Malesani et al. (2008a) used these data to study the supernova itself, we instead concentrate on the host galaxy. The three NOT spectra were obtained at three different slit positions (see also Fig. 8.4). The first included the positions of SNe 2008D and 2007uy which were also detected in the spectrum. The second one was placed along the major axis of the galaxy and the last one included the positions of SNe 2008D and 1999eh, where the latter one had already faded. On Jan. 15.21, we also obtained one 600s spectrum of the nearby galaxy NGC 2770B with ALFOSC (Fynbo et al., 2008a). Reduction and flux calibration of the spectra were done using standard tasks in IRAF. For the flux calibration we used the standard stars HD 19445, BD+75325 and BD+332642 for the ALFOSC spectra and GD 108 for the FORS2 spectrum. From the longslit spectra we then extracted traces of equal sizes at the positions of the SNe and other HII regions in the galaxy (see Section 8.4)

Furthermore, we obtained high-resolution echelle spectra of SN 2008D with UVES (Dekker et al., 2000) at the VLT on Jan. 18, 2008. We used the DIC1 (390+564) setting together with a 1.″0 wide slit. This set-up covers a wavelength range from 3300 to 6650Å at a resolution of 6–8 km s^{-1}. The UVES data have been reduced and extracted using the ESO CPL pipeline [1] and flux-calibrated with the master response curves provided by ESO [2].

We also obtained imaging data with FORS1 at the VLT on March 16 using an Hα filter shifted to z= 0.007 with a central wavelength of 6604 Å and a width of 64 Å as well as an offband filter for which we used the Hα filter at z=0 with $\lambda_{\rm center} = 6563$ Å and $\Delta\lambda = 61$ Å. In order to flux calibrate the Hα image we determined the flux within the Hα line from one of the traces extracted from the FORS spectra. We compared this flux with the counts within several rectangular apertures of the same size as for the extraction of the spectrum (1 $\times$ 3 arcsec) at the same positions along the slit by accounting for the different continuum levels from the galaxy and the varying strength of the [N II] line which is included in the Hα narrowband filter.

For a log of the observations see Table 8.1. Fig. 8.1 shows a color composite of I band observations taken with FORS1 (Malesani et al., 2008a) and the Hα and Hα offband images used in this Section. At z = 0.007 one arcsec corresponds to 0.13 kpc and we use a distance of 27 Mpc to NGC 2770.

[1] http://www.eso.org/sci/data-processing/software/pipelines/ uves/uves-pipe-recipes.html
[2] http://www.eso.org/observing/dfo/quality/UVES/qc/re- sponse.html

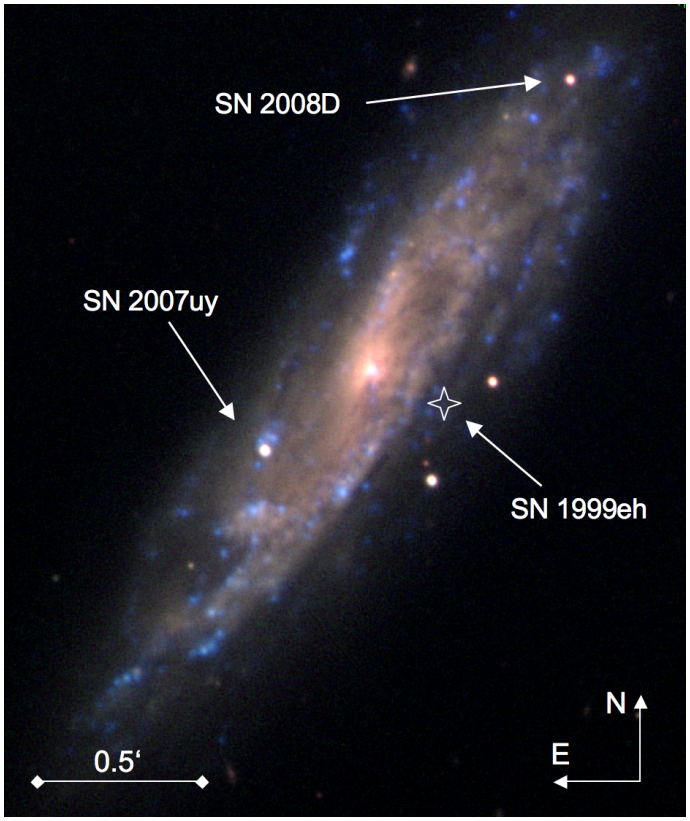

Figure 8.1: *Image of NGC 2770 from I (red color), Hα (blue) and Hα offband (green) filters. The field of view is about 2×2.5 arcmin. Blue indicates Hα emission which nicely show the SF regions in the spiral arms of the galaxy. The positions of the 3 SNe are shown of which two are still visible in the image.*

Date [**UT**]	**telescope/instrument**	**grism/filter**	λ, $\lambda_c/\Delta\lambda$ [**Å**]	**exptime** [**s**]
Jan. 11.31	VLT/FORS2	grism 300V	3000–9600	600
Jan. 13.07	NOT/ALFOSC	grism 4	2950–9050	3600
Jan. 15.21	NOT/ALFOSC	grism 4	2950–9050	600
Jan. 15.95	NOT/ALFOSC	grism 4	2950–9050	3600
Jan. 18.22	VLT/UVES	DIC1	3300–6650	3600
Feb. 03.15	NOT/ALFOSC	grism 4	2950–9050	1800
Mar. 16.11	VLT/FORS1	Hα at z=0.007	6604 / 64	120
Mar. 16.11	VLT/FORS1	Hα at z=0	6563 / 61	120

Table 8.1: *Log of the spectroscopic and narrowband imaging observations.*

8.3 Global properties of NGC 2770

8.3.1 Modelling of the spectral energy distribution

Extensive data are available in the literature on the emission of NGC 2770 at various wavelengths. We performed photometry on the archival *GALEX* (Martin et al., 2003, 2005) UV images and Sloan Digital Sky Survey (SDSS) *ugriz* images. Furthermore, we obtained the infrared and radio fluxes from Cutri et al. (2003); Moshir & et al. (1990); Dressel & Condon (1978) and Condon et al. (1998) reported in the NASA Extragalactic Database (NED). These data were used

to fit the broad band spectral energy distribution (SED) with templates from the GRASIL code (Silva et al., 1998).

In the GRASIL code each SED template is calculated by the following procedure. At the first stage an initial gas reservoir, infalling gas rate and star formation history are assumed and then at given time the emission of the resulting stellar population is summed up. Finally, the total galaxy spectrum is calculated by means of a two-dimensional radiative transfer method, applied to photons reprocessed by dust. After we found the best-fitting template we derived several galaxy properties from the SED (as in Michałowski et al., 2008). SFR, SN rate, stellar, dust, gas and total baryonic masses are given as output from GRASIL for the best-fiting template. The Infrared luminosity was obtained by integrating the SED over the range of $8 - 1000\,\mu$m. The average extinction (outside of the molecular clouds) was calculated as: $A_V = 2.5 \log(V$-band starlight extinguished by molecular clouds only / V-band starlight observed, see Silva et al. (1998)). This parameter describes the extinction averaged throughout the galaxy as opposed to the line-of-sight extinction derived from optical GRB afterglows. R_V was calculated comparing the extinction in the V- and B-bands: $R_V = A_V/E(B-V)$.

The spectral energy distribution (SED) of NGC 2770 is well represented by an average model composed of the spiral Sc (NGC 6946) and Sb galaxies, taken from Silva et al. (1998). From the SED fit (see Fig. 8.2) we derive a star-formation rate (SFR) of $\sim 1.1 M_\odot$ yr^{-1} and a stellar mass of 2.1×10^{10} M$_\odot$ (see Michałowski et al., 2008, for details on how these are derived from the SEDs). The resulting specific star-formation rate (SSFR) is 0.05 Gyr^{-1}. The SFRs derived from different methods (radio, IR, UV, SED modelling) differ by about a factor of 2. This is not surprising since the UV SFR estimate is affected by extinction and the different methods trace different parts of SF in the galaxy. Still, the values indicate that the SFR is not particularly high in NGC 2770. The SFR in radio is also directly connected to the supernova rate (SNR) as the nonthermal radio flux is produced by relativistic electrons accelerated in the SN shocks. Also the supernova rate (SNR) both from radio data and the SED modelling is therefore rather low with 0.01–0.02 SNe yr^{-1} which is comparable to the SNR of the Milky Way (MW). In addition to the SED fit, we also searched the literature for global measurements and properties of NGC 2770. Those, together with the SED outputs, are presented in Table 8.2.

8.3.2 NGC 2770 IN THE CONTEXT OF OTHER SPIRAL GALAXIES

In order to quantify to what extent the properties of NGC 2770 are similar to other galaxies we compare the global properties of NGC 2770 with a sample of more than 100 nearby spiral galaxies from Broeils & Rhee (1997) which also includes NGC 2770. This sample is based on two HI surveys of spiral and irregular galaxies with the Westerbork Synthesis Radio Telescope. We then determine the median and mean values of a number of properties and compare that with the values derived for NGC 2770. The mean in this sample is dominated by a few extreme outliers in the sample, therefore, we prefer to take the median value for comparison. We then conclude the following:

- The HI surface density is one of the highest in the sample (median: 3.65 M$_\odot$/pc^2, maximum: 8.05 M$_\odot$/pc^2, NGC 2770: 4.99 M$_\odot$/pc^2).
- The HI mass is also above average (median: 3.5 $\times10^9$ M$_\odot$, NGC 2770: 7×10^9 M$_\odot$).
- The total mass is above the median but slightly below the mean, however this is dominated by some very massive galaxies (median: log M$_{\rm tot}$ = 7.8 M$_\odot$, NGC 2770: log M$_{\rm tot}$ = 11.38 M$_\odot$).

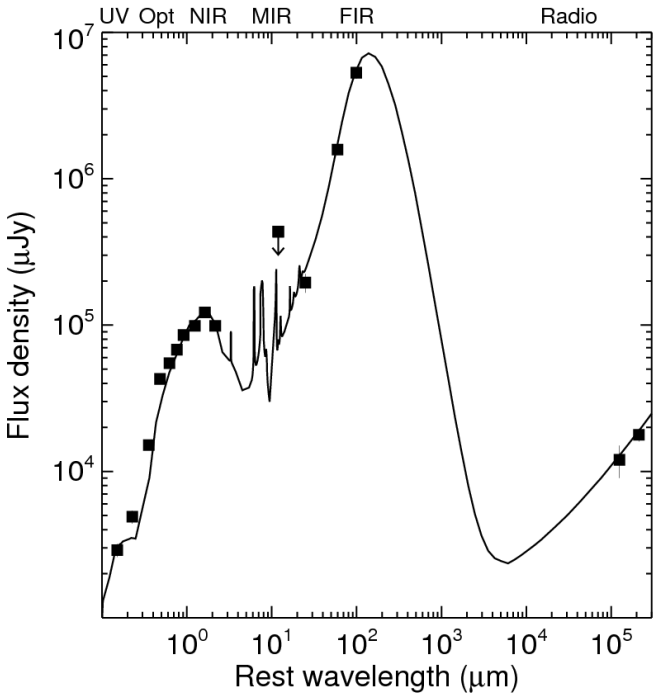

Figure 8.2: *Modelling of the broad-band SED of NGC 2770 from UV to radio wavelength using archival data compiled from the NASA Extragalactic Database (NED) and publicly available optical and ultraviolet data from the SDSS and GALEX archives. Error bars are mostly smaller than the symbols. The solid line shows the best-fit model from the GRASIL code (Silva et al., 1998), which is the average of Sb and Sc templates (based on NGC 6946).*

- The ratio of the gas mass to the blue (B-band) luminosity is close to average (median: 0.26 $M_\odot/L_{B\odot}$, NGC 2770: 0.24 $M_\odot/L_{B\odot}$).

- The ratio of the gas mass to the near-IR (H-band) luminosity is slightly above average (median: 0.31 $M_\odot/L_{H\odot}$, NGC 2770: 0.44 $M_\odot/L_{H\odot}$).

- The ratio of the gas mass to the total mass is slightly above average (median: 0.05, NGC 2770: 0.06).

This comparison shows that NGC 2770 has more or less average properties within this sample, except for the HI mass. The rather high gas mass and HI surface density indicate that there is a lot of material present to produce stars. However, the current and past SFRs as derived from different datasets (see also Section 8.4.3) are not at all exceptionally high. Soderberg et al. (2008) suggested that the companion galaxy NGC 2770B could be interacting with NGC 2770 and cause the enhancement in SF. No obvious perturbations are visible in the optical images of NGC 2770. It would be interesting to investigate possible perturbations in the HI velocity field, but the available data from VLA do not provide a good enough resolution. Wainwright et al. (2007) conclude from *HST* imaging of GRB host galaxies that about 30–50% show evidence for interaction. However, the host of GRB 980425/SN 1998bw was found to be an isolated galaxy (Foley et al., 2006) and the SF history is also consistent with a constant SFR over a few Gyrs (Sollerman et al., 2005b).

Property	Value	Notes	Reference
SFR (SED)	1.1 $M_\odot$ yr^{-1}		this work
SFR (radio)	0.6 $M_\odot$ yr^{-1}	using Yun & Carilli (2002)	this work
LIR	1.4×10^{10} $L_\odot$		this work
SFR (IR)	1.22 $M_\odot$ yr^{-1}	using Kennicutt (1992a, eq. 4)	this work
SFR (UV)	0.50 $M_\odot$ yr^{-1}	using Kennicutt (1992a, eq. 1)	this work
v_{rot}^{max}	152 km s^{-1}	21cm emission	(Rhee & van Albada, 1996)
M_{gas}	1.9×10^9 $M_\odot$		this work
N_{HI}	1.6×10^{20} atom cm^{-2}		(Staveley-Smith & Davies, 1988)
M_{HI}	7×10^9 $M_\odot$		(Broeils & Rhee, 1997)
M_{star}	2.1×10^{10} $M_\odot$	SED	this work
M_{tot}	2.6×10^{10} $M_\odot$	SED	this work
M_{tot}	1.1×10^{11} $M_\odot$	including DM; from v_{rot}	(Broeils & Rhee, 1997)
M_{dust}	1.9×10^7 $M_\odot$	SED	this work
M_{BH}	1.3×10^6 $M_\odot$		(Dong & De Robertis, 2006)
SN rate SED	0.02 SN yr^{-1}		this work
SN rate radio	0.01 SN yr^{-1}	using Condon (eq. 18 in 1992)	this work
A_V	0.15 mag	SED	this work
A_B	0.19 mag	SED	this work
A_B	0.14 mag	from N_{HI}	(Staveley-Smith & Davies, 1988)
E(B–V)	0.03 mag	SED	this work
E(B–V)	0.84 mag	Balmer decrement, global	(Ho et al., 1997)
R_V	4.3	SED	this work
n_e	54 cm^{-3}	(electron density)	(Ho et al., 1997)

Table 8.2: *Global properties of NGC 2770 derived from the literature and the SED fitting.*

8.4 SPATIALLY RESOLVED OPTICAL SPECTROSCOPY OF NGC 2770

From the four 2-dimensional longslit spectra, we extracted traces at all positions along the slit that showed emission in Hα. We chose equally large extraction windows in all the spectra with a width of 3 arcsec, corresponding to 0.43 kpc. The spectra were then extracted using the strong and well defined SN traces as templates. For the slit containing SNe 2008D and 2007uy we took the SN trace closest to the region we wanted to extract. The relative distortions along the spatial axis are however only within one to two pixels and even for spectra with only one template trace, we are confident that we extracted the same region along the entire dispersion axis. We note here that the FORS spectrograph has an atmospheric dispersion corrector while ALFOSC has none. This implies that the ALFOSC slit do not necessarily trace the same physical region in the blue and in the red part of the spectra. However, the airmass at the time of the observations was very low and the expected refraction should be negligible.

For the wavelength calibration, we extracted several traces from the arc spectrum with the SN trace as a template and shifted to different positions along the spatial axis. In each of these traces we identified the arc lines and wavelength calibrated the different parts along the slit with the nearest arc spectrum trace. Fortunately, the distortion of the arclines along the entire chip is also within a few pixels. The maximum deviation between the arclines at the extracted trace and the position taken for the arcspectrum should be less than 1 pixel which corresponds to an accuracy of 0.3 Å comparable to the accuracy from the wavelength calibration itself. Finally, we flux calibrated the individual spectra using the corresponding standard stars observed at the same night and the same setting. We note that the flux of an extraction window is different from the one of a pointsource as the point spread functions from the neighbouring pixels in the

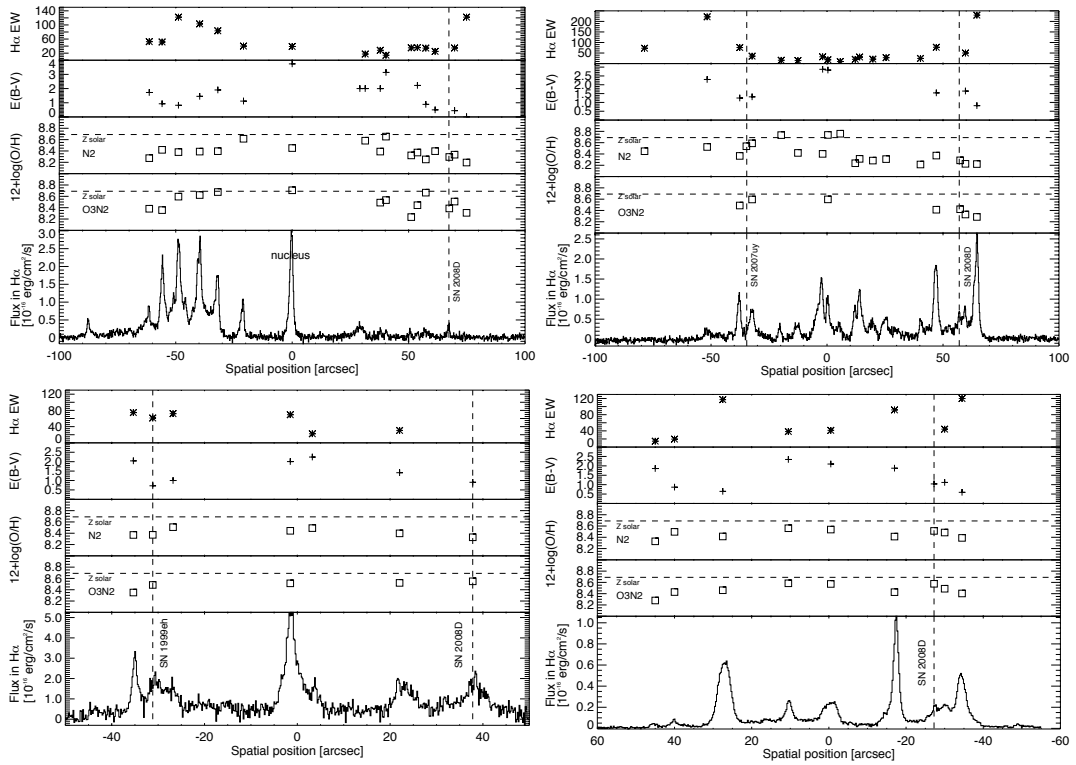

Figure 8.3: *Cut through the Hα line and the properties at the different HII regions (see Fig. 8.4 for the slitpositions on the galaxy). We plot two calibrations for the metallicity (errors are 0.2 dex for both methods), the extinction E(B–V) in [mag] and the Hα EW in [Å]. The four panels are: upper left: ALFOSC slitposition covering the major axis of the galaxy (slit1), upper right: the slit going through the sites of SN 2008D and SN 2007uy (slit2), lower left: position including SN 2008D and 1999eh (slit3) and lower right: the FORS slitposition (slit4). For the slit along the major axis, spatial position = 0 arcsec indicates the center of the galaxy, for the other positions, for the other slits, 0 kpc was chosen randomly.*

spatial direction extend into the extracted part.

We then fitted the emission lines present in the spectra with Gaussians and measured the fluxes and, where possible, the equivalent widths (EW) of the Hα line. For the SN regions, the latter is prevented by the contamination from the SN continuum. In a few cases, deblending the [N II] and Hα lines in the ALFOSC spectra proved to be difficult at this low resolution. In some regions, it seems that the part covered by the slit actually contains two kinematically different regions as the Hα lines shows a double peak which then blends with the bluer component of the corresponding [N II] double peak. This is not surprising since we observe NGC 2770 at a small inclination. Regions with heavily blended lines were discarded from the analysis. The properties in the different regions derived from the emission line analysis as present in the next sections are listed in Tab. 8.3 and plotted in Fig. 8.3.

8.4.1 METALLICITY

For the different regions along the slits we estimated the metallicity using the N2 parameter. This is the ratio between [N II]/Hα and is calibrated as 12+log(O/H)=9.37 + 2.03×N2 + 1.26×N2^2 + 0.32×N2^3 (Pettini & Pagel, 2004). In the regions with significant detection of [O III],

Position [arcsec]	12+log(O/H) (O3N2)	(N2)	E(B-V) [mag]	Hα EW [Å]	SFR [10^{-2}M$_\odot$/yr/kpc^2]
74.86	8.31	8.20	0.01	122.1	5.2
69.73	8.50	8.33	0.44	34.70	4.9
67.45 (08D)	8.38	8.30	—	—	2.7
61.37	—	8.40	—	25.04	2.1
57.38	8.66	8.25	0.89	34.32	5.1
53.77	8.44	8.37	2.22	35.75	5.3
51.11	8.23	8.32	4.20	35.09	4.9
40.28	8.53	8.65	3.12	14.21	3.1
37.81	8.49	8.40	2.00	28.19	6.7
31.35	—	8.58	—	17.55	3.6
0.0	8.71	8.45	3.74	38.85	38.2
–20.90	—	8.61	1.12	40.08	4.0
–31.92	8.67	8.40	1.90	83.27	14.7
–39.71	8.62	8.39	1.62	102.9	15.6
–48.83	8.59	8.38	0.82	122.1	18.2
–55.86	8.36	8.41	0.93	51.63	10.2
–51.37	8.38	8.28	1.72	52.52	5.8
64.60	8.28	8.22	0.82	229.8	15.8
59.66	8.32	8.23	1.64	50.07	4.9
57.38 (08D)	8.42	8.29	—	—	3.9
47.12	8.41	8.37	1.27	77.29	9.7
40.28	—	8.21	—	24.31	3.1
25.46	—	8.31	—	27.85	4.9
19.76	—	8.29	—	21.16	4.4
14.06	—	8.31	—	31.13	8.0
12.16	—	8.24	—	20.14	4.5
5.70	—	8.76	—	9.743	3.7
0.38	8.60	8.74	2.91	17.89	7.3
–1.90	—	8.40	2.88	32.19	12.0
–12.54	—	8.42	—	14.37	3.9
–19.76	—	8.73	—	15.95	2.8
–32.30	8.59	8.59	1.41	35.29	10.9
–34.77(07uy)	—	8.53	—	—	8.1
–37.62	8.49	8.37	1.37	76.20	15.1
–51.68	—	8.52	2.23	221.6	3.6
–78.66	—	8.45	—	72.64	3.5
37.81 (08D)	—	8.33	—	—	10.7
22.04	8.52	8.40	1.41	30.53	10.2
3.23	—	8.49	2.25	22.36	9.8
–1.52	8.51	8.44	2.00	69.33	32.9
–26.79	—	8.51	—	71.93	11.1
–31.16 (99eh) ...	8.48	8.37	0.72	61.23	11.8
–35.34	8.35	8.37	2.04	74.66	11.2
34.50	8.40	8.39	0.59	119.9	2.8
30.00	8.49	8.48	1.12	44.25	1.2
27.25 (08D)	8.57	8.51	0.95	5.014	1.1
17.00	8.43	8.41	1.88	91.78	4.1
0.500	8.57	8.54	2.10	41.34	1.4
–10.50	8.58	8.56	2.34	38.31	1.1
–27.50	8.46	8.41	0.64	117.2	3.7
–40.00	8.43	8.50	0.87	19.61	0.3
–45.00	8.28	8.33	1.86	14.56	0.2

Table 8.3: *Measurements from the optical spectra, from top to bottom: slit through the major axis (slit1), slit through SN 2007uy and SN 2008D (slit2), slit through SN 2008D and SN 1999eh (slit3) and FORS spectra through SN 2008D (slit4). Metallicities and SFRs were calculated from the fluxes not corrected for the extinction. The error in the metallicities are around 0.2 dex.*

we also use the O3N2 parameter, $O3N2$=log[(O III λ 5007 /Hβ)/(N II/Hα)], to derive metallicities with 12+log(O/H)=8.73 – 0.32 O3N2 (Pettini & Pagel, 2004).

The O3N2 parameter has been calibrated against oxygen abundances derived directly by determining the electron temperature T_e from the temperature sensitive [O III] λ 4363 line (e.g. Izotov et al., 2006b). The O3N2 parameter is also considered as the most reliable method by Kewley & Dopita (2002), if the spectra could be corrected for dust extinction. However, for low metallicities, the [O III] λ 5007 line becomes very weak. We were not able to use it for deriving metallicities everywhere, since in some parts of the spectra it was only detected with very low significance. For consistency, we therefore use the N2 estimate throughout this article. The N2 parameter does, however, saturate at about solar metallicity and even turns around at higher metallicities (about twice solar). This is not a problem in our data as we do not have regions where the O3N2 parameter gives supersolar metallicities while the N2 metallicity gives a subsolar value.

We find that the N2 and the O3N2 methods give rather consistent results at the sites where both are determined. The error of the O3N2 parameter is about 0.2 dex in the ALFOSC spectra and 0.10–0.15 in the FORS slit. The metallicities from the O3N2 and N2 parameters have systematic errors of 0.14 dex for O3N2 and 0.18 for N2. We therefore estimate the total error of each metallicity value to be 0.2 dex for both O3N2 and N2. In Fig. 8.3 we plot the results from both methods where available. Figure 8.4 visualizes the 2D distribution of the N2 metallicities in the different parts of the galaxy as probed by the four slits.

The metallicity at the SN sites derived from N2 are 12+log(O/H) $\sim$ 8.4, 8.5 and 8.4 for SNe 2008D, 2007uy and 1999eh respectively, which corresponds to 0.55–0.70 $Z_\odot$ [when using 8.66 for the Sun Asplund et al. (2004)]. The metallicities derived at the position of SN 2008D differ between the ALFOSC and the FORS slits, but still agree within the errors. We therefore adopt an average metallicity of 8.4 for SN 2008D. The other regions in the outer spiral arms on both sides of the galaxy give similar values for the metalicity for different slits. The nucleus and the central regions have solar or supersolar metallicity. From this we derive a metallicity gradient of -0.06 dex per kpc. The average metallicity computed from the values along the major axis of the galaxy is 8.4.

It is interesting to note that the metallicities at the SN Ib sites in NGC 2770 lie between the low values found for GRB connected broadline SNe Ic and those of broadline SNe Ic not connected to GRBs (Modjaz et al., 2008a). They are also slightly higher than the metallicity of the HII region which hosted SN 1998bw, a broadlined SN Ic connected to GRB 980425, as determined from IFU observations of the host (Christensen et al., 2008). Also the site of the SN-less GRB 060505 (Thöne et al., 2008a) had a lower metallicity as the SN Ib sites in NGC 2770. It seems, GRB related SNe have a rather low metallicity while SNe Ib have about half solar to solar metallicities whereas (broadline) SNe Ic require solar to slightly above solar metallicities. This result seems consistent with the suggestion that in nonrotating stars, the mass loss scales with the metallicity (e.g Crowther et al., 2002) and SN Ic progenitors are likely experiencing larger mass loss than SNe Ib. Fast rotating stars, however, as required by the collapsar model (MacFadyen & Woosley, 1999), should preferentially have low metallicities and less mass loss in order to keep the high angular momentum, which is required to produce a GRB.

8.4.2 EXTINCTION

The extinction throughout the galaxy is estimated from the Balmer decrement. Since Hγ is not detected, we can only use the Hα/Hβ ratio (Osterbrock, 1989). The derived extinction is

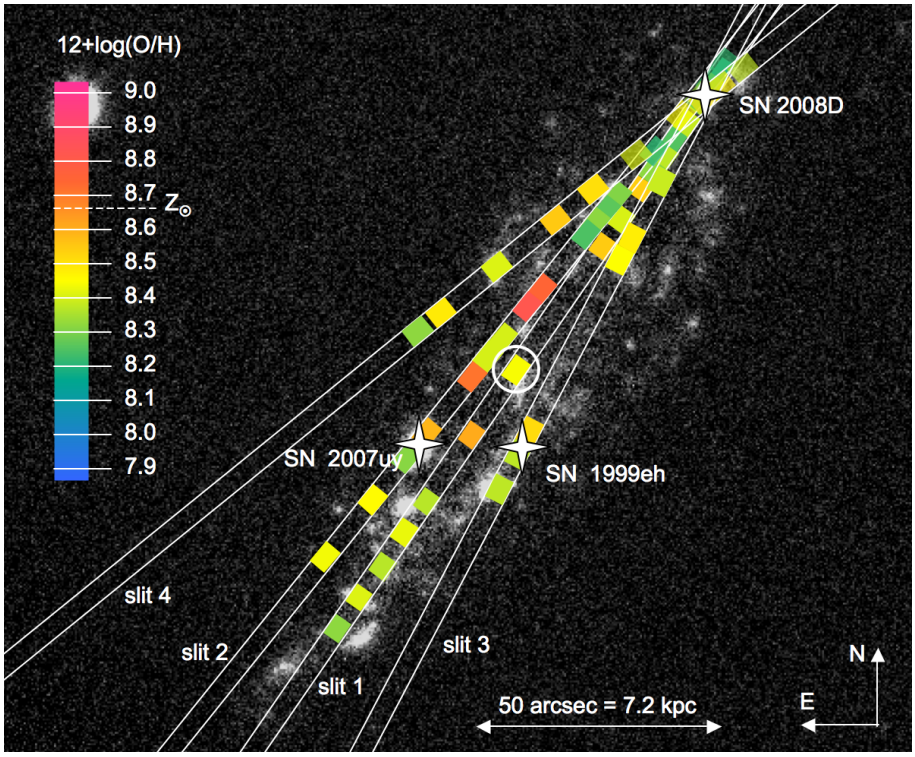

Figure 8.4: *Metallicities in NGC 2770 along the 4 slitpositions as described in Fig. 8.3 including the 3 SN sites derived from the [N II]/Hα ratio. The image of the galaxy was taken with the Hα filter in order to highlight the starforming regions. The circle indicates the center of the galaxy.*

generally high with values for E(B–V) between 0.4 and 3.7 mag with most of the regions having E(B–V) $\sim$ 1 mag. The extinction at the SN sites is considerable with E(B–V)=0.9 mag for SN 2008D, 1.4 mag for SN 2007uy and 0.7 mag for SN 1999eh. Malesani et al. (2008a) get a value of E(B–V)=0.8 mag from fitting the SN SED, while (Modjaz et al., 2008b) adopt 0.6$\pm$0.1 from the SN broadband fit. The Galactic extinction towards NGC 2770 is negligible with E(B–V)= 0.02 mag (Schlegel et al., 1998).

Further evidence for dust extinction along the line of sight towards SN 2008D comes from the detection of NaD absorption in the UVES high resolution spectra, the EWs measured are listed in Tab. 8.4. For unsaturated and mildly saturated lines, there is a direct relation between the strength of the Na D absorption and the extinction (Munari & Zwitter, 1997) which have been calibrated towards stars in the LMC. Taking the EW for the two components together, we get an extinction of E(B–V)=1.1 mag. However, Munari & Zwitter (1997) note that systems with such high EWs are usually consisting of several components and the extinction of different components is additive so it is more appropriate to add the extinction of the resolved subcomponents which are on the linear part of the EW–E(B–V) relation. The two components then give $E(B-V)_1$ = 0.14 and $E(B-V)_2$ = 0.18 mag and therefore $E(B-V)_{\rm tot}$ = 0.32 mag. There is also a high N_H column derived from the X-ray spectra (Soderberg et al., 2008) of $N_H = (7\pm1)\times10^{21}$ cm^{-2}, assuming Galactic abundances. The corresponding gas-to-dust ratio of 2.8×10^{21} cm^{-2}mag^{-1} is low (close to the Galactic ratio N_H = 1.7 10^{21} cm^{-2}mag^{-1}) compared to the ratios observed in GRB host galaxies that are typically an order of magnitude higher, suggesting that NGC 2770 is dust-rich compared to those hosts.

line id	$\lambda_{\rm rest}$ [Å]	$\lambda_{\rm obs}$ [Å]	EW [Å]	b [km/s]	log N [cm^{-2}]
Ca II K	3933.66	3961.00	0.55±0.03	14.1±7.1	12.92±0.07
		3961.20		18.3±2.4	12.78±0.07
Ca II H	3968.47	3996.05	0.42±0.03	14.1±7.1	12.92±0.07
		3996.25		18.3±2.4	12.78±0.07
Na I D2	5889.95	5930.92	0.33±0.02	7.3±0.3	12.96±0.05
		5931.21	0.38±0.02	8.1±0.3	12.71±0.02
Na I D1	5895.92	5936.94	0.26±0.02	7.3±0.3	12.96±0.05
		5937.23	0.36±0.02	8.1±0.3	12.71±0.02
DIB	5780.37	5821.5	0.245±0.04	—	—
DIB	5796.99	5837.4	0.850±0.05	—	—
DIB	6283.85	6328.0	0.090±0.02	—	—

Table 8.4: *Equivalent width measurements, b parameters and column densities (where applicable) of interstellar absorption lines in NGC 2770 along the line of sight to SN 2008D, all wavelengths are in air. EWs are given for both components in the Ca II and Na I absorption systems. Galactic rest DIB wavelengths are from Galazutdinov et al. (2000)*

We also detect a number of diffuse interstellar bands (DIBs) at $\lambda\lambda$ 5821.5 Å, 5837.4 Å and 6328.0 Å in the UVES spectra which indicates the presence of dust at the site of SN 2008D. DIBs are speculated to be produced by large carbon molecules, possibly related to the polycyclic aromatic hydrocarbons (PAHs) that produce strong fluorescence lines in the mid-infrared. It is interesting to note that DIBs have never been detected in the afterglow spectra of GRBs suggesting a harder radiation field and younger stars in those galaxies compared to NGC 2770. We fit the observed spectra (rebinned to 0.09Å) with template DIB profiles obtained from high-resolution high-S/N spectra of DIBs in the diffuse cloud toward HD 144217. We keep the width of the feature fixed but leave the continuum, the central wavelength and the depth scaling as free parameters. Doppler broadening due to the different velocity components as fitted from the NaD and Ca II absorption in the UVES spectra (see Section 8.4.4) is negligible for the broad λ 6283 and λ 5780 DIBs (FWHM $\sim$ 100 and $\sim$ 200 km/s). For the narrow λ 5797 DIB (FWHM $\sim$ 40 km/s) we assume that DIBs are present in similar abundance in both cloud components as is the case for the Ca II absorption strenghts. Taking into account the two components increases the derived λ 5797 DIB strength by about 10-15%.

Diffuse interstellar bands can provide an important measure, just as Na I and K I, for the amount of dust in line-of-sights probing the diffuse interstellar medium. Additionally, the behavior of different DIBs (or DIB ratios) in the Milky Way can be used to gain insight in the local physical conditions of extra-galactic diffuse clouds. The λ 5780 DIB carrier is sensitive to UV radiation and becomes stronger when exposed to sufficient UV (at which time for example the λ 5797 DIB carrier is already being destroyed by this radiation). For example, the DIB strengths (strong λ 5780 and λ 6283 DIBs) toward SN2001el in NGC 1448 suggest a strong local UV field (Sollerman et al., 2005a). On the other hand, observations of the ISM toward SN2006X in M100 (Cox & Patat, 2008) indicate a dense environment protected from strong UV radiation as it shows a very weak λ 6283 DIB and the presence of di-atomic molecules. The λ 6283 DIB towards SN2008D in NGC2770 is slightly stronger (EW λ 6283/E(B–V) = 1200 mÅ) than the Galactic average (EW λ 6283/E(B–V) = 900 mÅ(Luna et al., 2008)), while the λ 5780 DIB is a little weaker (EW λ 5780)/E(B–V) $\sim$ 350 mÅ) than the Galactic average (EW(5780)/E(B-V) = 460 mÅ). For single clouds the λ 5780 and λ 6283 DIB strengths show a reasonable correlation though variations in their ratios are common. Together with a slightly above average λ 5797/λ 5780 ratio and the presence of multiple cloud components in the atomic lines this indicates that

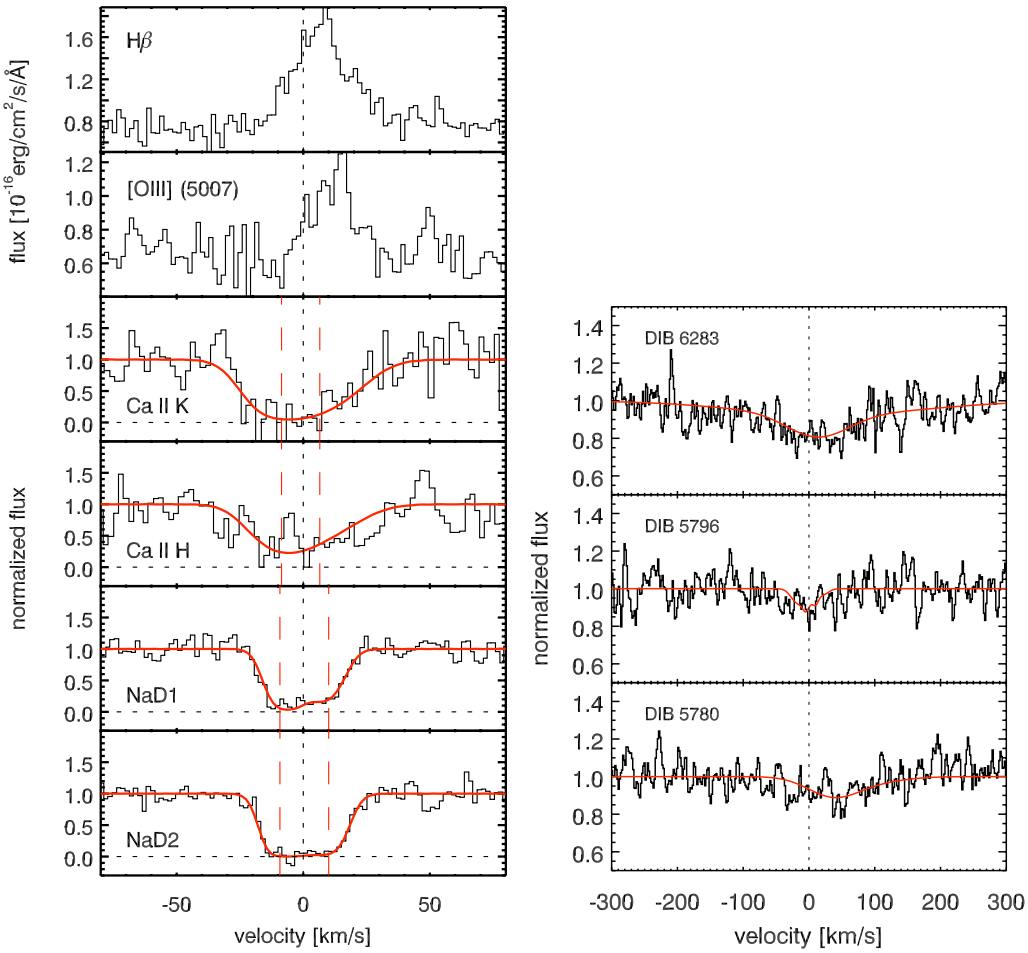

Figure 8.5: *Left panel: Fits to the Calcium and Sodium absorption lines in the UVES spectra and comparison to Hβ and [O III] emission lines. The dashed horizontal lines indicate the continuum level. Zero velocity corresponds to the center of the galaxy. Right panel: Fits to the DIBs detected in the UVES spectra of SN 2008D.*

with SN2008D we probe an ensemble of diffuse clouds with varying local conditions.

For example, SN2006X probes a compact dense interstellar cloud with E(B–V) $\sim$ 1 mag and shows a relative weak λ 6283 DIB of 177 mÅ (compared to the Galactic average of 900 mÅ per E(B–V)) (Cox & Patat, 2008; Luna et al., 2008). The line-of-sight toward SN2008D instead probes at least two diffuse components and shows a relative strong λ 6283 DIB (EW = 850 mÅ or EW/E(B–V) = 1200 mÅ) even slightly stronger than the Galactic "average" relation EW(5780)/E(B-V) $\sim$ 350 mÅ for SN2008D, and 460 mÅ for MW, and 189 mÅ (EW/E(B–V) = 630 mÅ) for SN2001el (Sollerman et al., 2005a). The λ 5780 DIB carrier is sensitive to UV radiation and becomes stronger when exposed to UV radiation. The λ 5780 is relatively weak with respect to the Galactic average, while the 6283 is stronger. Although generally these two DIBs show some correlation ratios that clearly differ between different sightlines.

8.4.3 STAR FORMATION RATES AND AGES OF THE STELLAR POPULATION

The local as well as the global SFR in NGC 2770 was determined by using the Hα flux and the conversion by Kennicutt (1992a). The SFRs at the four different slit positions are given in Table 8.3 as SFR/kpc^2. We did the same for a range of regions within NGC 2770 by using the image taken with the Hα filter with the continuum subtracted using the offband filter as described in Section 8.2. The SFR at the sites of SNe 2008D and 1999eh are comparable but not especially high. SN 2007uy lies a few arcsec from two sites with higher SF. The local SFRs elsewhere in NGC 2770 vary from 2×10^{-3} to 4×10^{-1} M$_\odot$/yr/kpc^2. The total SFR from the Hα image taking an elliptic aperture to include the entire galaxy yields a flux of 6.1×10^{-12} erg/cm^2/s^{-1} or a SFR of 0.42 M$_\odot$/yr which is consistent with other measurements from the UV, IR and radio fluxes.

The Hα EW is further correlated with the age of the underlying population at least in the first 10^6 to 10^7yr (see e.g. Zackrisson et al., 2001). Table 8.3 also lists the Hα EW at the different parts within the four slits. We cannot determine the EW at the sites of SN 2008D and SN 2007uy as the continuum is strongly affected by the presence of the SNe and we can only measure the EW of the nearby sites. We find that the stellar populations close to the SN sites are not among the youngest ones. This is a bit surprising since the progenitors of SNe Ib are expected to be stars with masses $>$ 30–40 M$_\odot$ whose lifetimes are $<$ 6–7 Myr corresponding to a Hα EW of $>$ 100 Å (see e.g. Sollerman et al., 2005b). There seems to be a strong gradient (see Fig. 8.3) in NGC 2770 towards high EWs in the outskirts of the galaxy whereas the center has rather low EWs corresponding to an older population. However, the EWs near all three SN sites are not particularly high which does not suggest particularily young populations.

8.4.4 KINEMATICS

The UVES high resolution data allow us to study the kinematics in the sightline towards SN 2008D. We use the FITLYMAN program in MIDAS (Fontana & Ballester, 1995) to fit different components to the Na I D1 and D2 as well as the Ca II H & K lines and to determine column densities (see Table 8.4). The absorption lines are best fitted with two components which are at velocities of -9.21 and 10.01 km/s for the Na I lines and -8.60 and 6.54 km/s for the Ca II lines. As v = 0 km/s, we take the redshift of the center of the galaxy for which we adopt $z = 0.007$ as determined from the ALFOSC spectra probing the center of the galaxy. The two components are very narrow and have Doppler b parameters of 7.3 and 8.1 km/s for Na I D and 14.1 and 18.3 km/s for Ca II, the turbulent b parameter is very small and was fixed to 1 km/s.

We compare the position of the absorption with the emission lines which are likely to originate in the SF regions where the SN reside. The emission lines have a width of around 30 km/s which is most likely due to the turbulence in the SF region. There is no velocity shift between the hydrogen and oxygen emission lines suggesting a common origin for both elements. The redder component of all absorption lines is coincident with the position of the emission lines while the blue component is slightly shifted. This indicates that the absorbing material is most likely in front of the H II region of the SN. The position of the λ 5797 and λ 6283 DIBs are coincident with the other absorption lines whereas the λ 5780 DIB is offset by about 40 km/s. A fit with fixing the center of the line to v= 0 km/s gives almost the same χ^2 and a slightly lower line strength of 230 mÅ. There is also an intrinsic scatter of the rest wavelength of DIBs from different surveys which vary by 10–20 km/s. Due to the low line strengths and their intrinsically broad profile, it is not possible to distinguish different velocity components in the DIBs.

8.5 NGC 2770 IN THE CONTEXT OF OTHER GRB AND SN HOSTS

8.5.1 OTHER GALAXIES WITH HIGH SN RATE

A number of galaxies exist that have had more than one SN detected in the optical. The record until today is for NGC 6946 with 9 SNe detected, and where all that could be classified were SNe II. NGC 6236 (M 83) had 6 SNe and there are 3 galaxies with 5 SNe: NGC 4303 (M61), NGC 4321 (M100) and NGC 2276 (Arp 25). Furthermore, there are 9 galaxies with 4 SNe detected and 26 with 3 SNe of which one is NGC 2770 (complete up to May 30, 2008). We compiled this information from the CfA database including only galaxies with a catalogue name. We also include in our sample of frequent SN galaxies 4 galaxies that had 2 stripped-envelope SNe (to date NGC 2770 is the only one with 3). This sample is clearly biased but may still be useful for the comparison between frequent SN galaxies.

In Table 8.6 we list the SFRs, SNRs and specific SFRs weighted by the mass represented by the K-band luminosity for this sample. The radio SFRs are derived from Yun & Carilli (2002, eq. 15), the UV SFRs from Kennicutt (1992a). For most galaxies, there is a good agreement between the UV and radio SFR except for NGC 2276 and NGC 3670. Usually, radio SFRs are higher than UV SFRs as the UV is affected by extinction in the host galaxy, which plays a larger role in edge on galaxies. In our sample, we do not to account for the extinction correction and this was not done either for the GRB sample we use for comparison in Section 8.8. The SNRs were calculated from the nonthermal radio flux according to Condon (1992, eq. 18) which are based on the assumption that the radio flux comes from synchrotron radiation from electrons accelerated in the SN remnants.

It may appear surprising that the galaxies with the highest number of observed SNe do not necessarily have the highest (expected) SNRs as derived from radio data. However, most galaxies with 4 or more SN detected have an expected SNR between 1–4 in 10 yrs. This is consistent with the number of actually detected SNe considering the small numbers and that SN observations in most of these galaxies have only been possible for the last few tens of years. NGC 2770 has a SSFR and SNR among the lowest in our sample and does not reflect the detected SN rate which could, however, be a statistical fluctuation (see Chapter 8.5.3).

An important bias in SN detections is the inclination of the galaxy observed as noted by several authors (e.g. Cappellaro et al., 1999). In our sample, the average number of SNe detected per galaxy drops towards higher inclinations, however, the distribution peaks around 30 deg inclination, most likely due to the low number of systems with lower inclinations. All of the galaxies with 5 and more SNe detected are seen nearly face-on. If we would have seen them edge-on, parts of the SNe might have been missed due to dust extinction or superposition with the bright central regions. Both issues are currently being addressed with SN searches in the IR (e.g. Mattila et al., 2007; Maiolino et al., 2002; Mannucci et al., 2003) and continuous monitoring of galaxies to perform image subtraction or observations in the radio (e.g. Cram et al., 1998)

It is interesting to note that many of the galaxies with frequent SN Ib/c occurrence are classified as starbursts, irregular or interacting with a neighboring galaxy whereas the galaxies with mainly SNe II or Ia are more "ordinary" spirals. This result is not surprising as SN Ib/c progenitors are likely more massive than those of SNe II and should therefore come from a younger population. Interaction between galaxies is considered as a possible trigger for star formation. In Fig. 8.7, we display the fraction of each SN type which occurred in the same type of galaxy. For the galaxy classification we adopted the values from de Vaucouleurs et al. (1991) which attributes values from –6 to 11 with –6 to 0 for elliptical galaxies, 1–9 spirals of increasing Hubble type and 10, 11 for irregular galaxies. SNe Ibc seem to be more frequently detected in later type

galaxy	incl. [°]	SNe	SN types	gal. type	SFR (rad.) [$M_\odot$/yr]	SFR (UV) [$M_\odot$/yr]	SNR [/yr]	$M_{stellar}$ [$M_\odot$]	SSFR [/Gyr]
MW	—	4	—	SBc	1	1	0.0100	$5\,10^{10}$	0.02
NGC 6946	29	9	II (6)	.SXT6..[4]	3.125	3.143	0.074	2.725×10^{10}	0.115
NGC 5236 (M83)	21	6	Ia (1)	.SXS5..[4]	7.002	0.278	0.167	6.506×10^{10}	0.108
NGC 4303 (M61)	25	5	II (4)	.SXT4..	11.17	10.09	0.265	7.828×10^{10}	0.143
NGC 4321 (M100)	36	5	Ia (4), II (1)	.SXS4..	6.655	4.569	0.158	9.942×10^{10}	0.067
NGC 2276 (Arp25)	21	5	II (2)	.SXT5..[4]	17.55	—	0.416	2.374×10^{10}	0.739
NGC 1316 (FornaxA)	56	4	Ia (3)	PLXS0P[1]	—	1.764	—	3.146×10^{10}	15.93
NGC 4038	65	4	Ia (1), Ib/c (1)	.SBS9P.[2,4]	16.00	—	0.387	—	
NGC 3367	13	4	Ia, Ib/c, II	.SBT5..[1]	11.30	—	0.267	5.092×10^{10}	0.222
NGC 6754	60	4	II (1), Ia (1)	.SBT3..	2.551	—	0.058	5.317×10^{11}	0.048
NGC 5468	24	4	II (1), Ia (2)	.SXT6..	—	—	—	—	—
NGC 4725	49	4	uncl.	.SXR2P.	0.393	1.475	0.009	8.632×10^{11}	0.005
NGC 3184	15	4	uncl.	.SXT6..	0.275	—	0.007	7.864×10^{11}	0.035
NGC 2841	65	4	Ia-p (2)	.SAR3*.[1]	<0.343	0.287	<0.008	2.668×10^{11}	0.013
NGC 3690	40	4	Ib (2), II (2)	.IB9P..[2,5]	67.10	0.679	1.587	7.283×10^{11}	0.921
NGC 521	—	3	II(1)	.SBR4..	0.819	—	0.019	1.630×10^{11}	0.006
NGC 664	—	3	II(3)	.S..3*.	3.777	—	0.089	3.938×10^{10}	0.096
NGC 735	—	3	II(1),Ic(1)	.S..3	0.830	—	0.019	3.044×10^{11}	0.027
NGC 1058	21	3	Ib/c(1), II(1)	.SAT5..	0.019	—	0.001	1.142×10^{9}	0.017
NGC 1084	56	3	II(2)	.SAS5..	8.110	—	0.193	2.324×10^{10}	0.349
NGC 1097	47	3	II(3)	.SBS3..[6]	7.180	0.172	0.171	8.872×10^{10}	0.081
NGC 1365	58	3	II(2)	.SBS3..	15.23	—	0.362	1.316×10^{11}	0.116
NGC 1448	79	3	Ia(1), II(2)	.SA.6*/	1.394	—	0.033	2.051×10^{10}	0.068
NGC 1559	56	3	II(2), Ia(1)	.SBS6..	8.049	—	0.191	1.841×10^{10}	0.437
UGC 1993	—	3	Ia, II	.S..3..	—	—	—	—	—
NGC 2207	54	3	Ib(1), Ib/c(1)	.SXT4P.[2]	29.69	—	0.704	6.953×10^{10}	0.427
NGC 2770	72	3	Ib(3)	.SAS5*.	0.586	0.638	0.014	9.821×10^{9}	0.059
NGC 3147	31	3	Ia, Ib	.SAT4..[6]	7.393	—	0.175	1.512×10^{11}	0.049
NGC 3627 (M66)	67	3	Ia, II(2)	.SXS3..[1,6]	2.441	1.111	0.058	4.086×10^{10}	0.060
NGC 3631	28	3	II (1)	.SAS5..	1.148	—	0.028	1.492×10^{10}	0.077
NGC 3938	14	3	Ic,II	.SAS5..	0.426	0.816	0.010	8.586×10^{9}	0.050
NGC 3947	31	3	Ia(1), IIn(1)	RSBT3..	2.070	—	0.049	5.592×10^{10}	0.037
NGC 4157	90	3	II, uncl.(2)	.SXS3$/	1.162	—	0.028	1.184×10^{10}	0.098
NGC 4254 (M99)	—	3	II(1)	.SAS5..	25.09	12.29	0.594	1.715×10^{10}	0.146
NGC 4374 (M84)	—	3	Ia(2)	.E.1...[1,3,6]	—	0.064	—	6.344×10^{10}	1.104
NGC 4527	71	3	Ia(1)	.SXS4..[1]	5.817	—	0.138	8.834×10^{10}	0.066
NGC 4939	—	3	II(1)	.SAS4..[6]	4.971	—	0.118	7.156×10^{10}	0.069
NGC 5033	70	3	II(2)	.SAS5..[6]	2.775	0.393	0.066	2.201×10^{10}	0.126
NGC 5253	90	3	I(1)	.I..9P*[4]	0.148	0.079	0.004	1.445×10^{9}	0.102
NGC 5457 (M101)	7	3	II(1)	.SXT6..	0.443	0.270	0.011	6.307×10^{9}	0.070
NGC 5668	22	3	Ia, II	.SAS7..	0.603	—	0.014	9.036×10^{8}	0.668
NGC 3810	—	2	Ib(1), Ic (1)	.SAT5..	1.249	—	0.029	1.134×10^{10}	0.110
NGC 7714	42	2	Ib/c(2)	.SBS3*P[1,4,5]	1.258	0.952	0.029	1.704×10^{10}	0.074
NGC 4568	65	2	Ib(1), Ic (1)	(SAbc)[2]	6.391	1.128	0.151	8.751×10^{10}	0.073
NGC 3464	50	2	Ib(1), Ic(1)	.SBT5..	—	—	—	—	—

Table 8.5: *Complete sample of all galaxies with $\geq$ 3 SNe and 5 galaxies with 2 stripped envelope SNe, compiled from the CfA SN database. The classifications are adopted from RC3 [a], for those galaxies without RC3 classifications, we use the classification from NED. The adopted T value is the number in the classification code for spirals, the only elliptical galaxy, NGC 1316 has T=–2. Radio data, UV flux and K-band luminosity are taken from NED where available. SNRs are derived from radio data according to Condon (1992, eq. 18), SFRs are from Yun & Carilli (2002, eq. 15) for radio and Kennicutt (1992a) for UV SFRs.*

[1] low ionization nuclear emission line region (LINER)

[2] interacting galaxy

[3] low excitation radio galaxy (LERG)

[4] starburst

[5] Wolf-Rayet galaxy

[6] Seyfert galaxy

[7] 1st column: R = outer ring; P = pseudo outer ring; C = compact; D = dwarf, 2nd column: E, S, I, P: elliptical, spiral, irregular, peculiar, 3rd column: X = transition between A (no bar) and B (barred galaxy). "+": transition between elliptical and lenticular galaxies (E/S0); 4th column: T = transition between s (no inner ring) and r (strong inner ring), number = ellipticity for an elliptical galaxy: 0 = round, 6, 7 = edge-on; 0 = I0 galaxies; 5th column: lenticulars: -, 0, or + (lenticular stages), spirals: Hubble stage: 0 for 0/a, 1 for a, ... 9 for m, for Magellanic irregulars, always 9; 6th column: Uncertainty (* or $), P (minor peculiarity), or / = sp (spindle; an edgewise galaxy); 7th column: same as 6th, if needed.

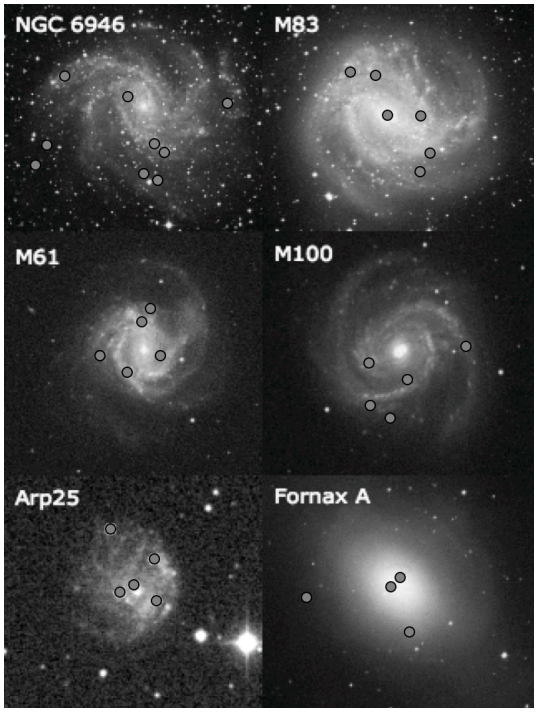

Figure 8.6: *Images of the top 5 SN galaxies and Fornax A (only Ia SNe) with the positions of the SNe indicated.*

spirals compared to SN Type II, whereas SN Ia are rather evenly distributed over all galaxy types. van den Bergh et al. (2005) investigated the complete sample of SNe detected with the LOSS SN search and their hosts up to 2005 and do not find a significant different between the Hubble Type of SN Type Ib/c and SN Type II. For our sample, we do only consider frequent SN hosts which introduces some bias in the sample. Panel I in Fig. 8.7, however, shows that, at least in our sample, there is a tendency of a higher fraction of SNe Ib/c over SNe II for spirals of later Hubble type.

Furthermore, some galaxies seem to produce only a certain type of SNe. In order to investigate this notion, we calculated the fraction of galaxies that only had one SN type detected from our sample of 44 frequent SN galaxies. 29 of those had SNe II out of which 51% had only SNe II, 13 had SNe Ib/c with 46% only having SNe Ib/c and 17 with SNe Ia of which only 29% had uniquely SNe Ia. In these numbers, we only include the classified SNe. It seems that indeed, galaxies with SNe II and Ib/c often only have one type of SN whereas this is less pronounced for SNe Ia. This result suggests that the SF history in those galaxies is rather uniform in the sense that SF has a common onset in time and first produces mainly SNe Ibc expected to come from the most massive stars, whereas later on, when the dominant population has become older, mainly SNe II are produced.

8.5.2 Comparison to other GRB and SN hosts

We now compare our sample of frequent SN galaxies to the hosts of long GRBs that are known to be connected to broadlined SNe Ic. For the GRB hosts, we take the sample from Castro Cerón et al. (2008) which lists the UV SFRs derived from the relations of Kennicutt (1992a) as well as the stellar masses derived from the restframe K band luminosity. GRB hosts have generally

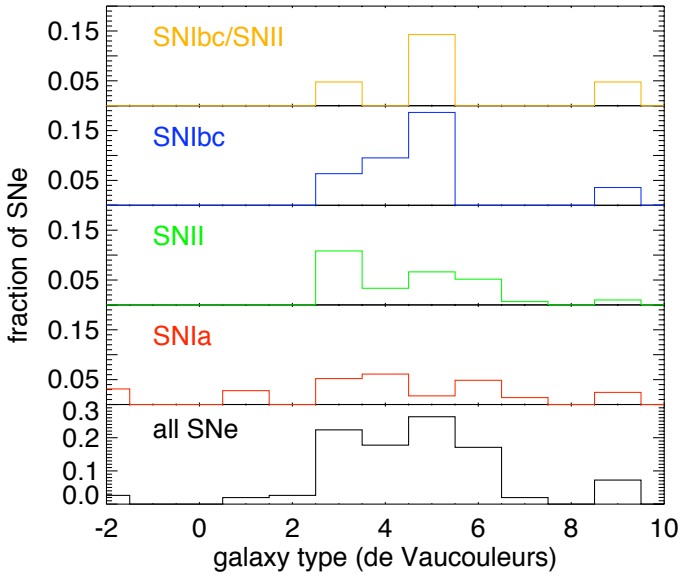

Figure 8.7: *Fraction of detected SNe sorted according to the de Vaucouleurs classification (de Vaucouleurs et al., 1991) of their host galaxies. SNe Ib/c seem to be more concentrated towards later type spirals whereas SNe II seem to prefer earlier type spirals which are also expected to have an older stellar population. In general, most SNe are detected in spiral galaxies.*

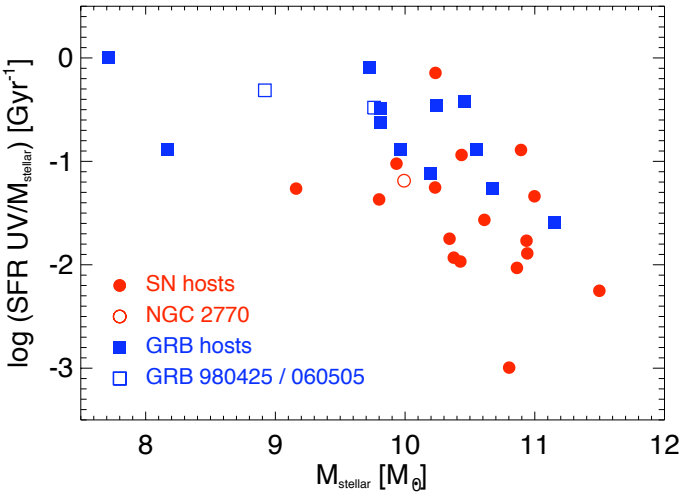

Figure 8.8: *Specific SFR from the UV versus stellar mass derived from the K-band luminosity for GRB hosts (blue squares) and the sample of frequent SN galaxies (red dots) presented in Tab.8.5. The GRB hosts specifically mentioned in Sec. 8.5.2 and NGC 2770 are plotted as empty symbols.*

lower masses (log $M_{*,SN}$ =10.71 $M_\odot$, log $M_{*,GRB}$ =10.36 $M_\odot$) and higher SFRs (SFR_{GRB} =2.9 $M_\odot$/yr, SFR_{SN} = 2.0 $M_\odot$/yr) than the frequent SN hosts from our sample. This leads to a higher SSFR for GRB hosts (0.075 and 0.32 Gyr^{-1} for SN and GRB hosts respectively) even though the two samples overlap partially. We note that the masses derived in Castro Cerón et al. (2008) are about two times higher than the masses in the sample Savaglio et al. (2008) which partially overlap with the sample of Castro Cerón et al. (2008). This difference is partly explained by the use of different assumptions for the ratio $M_{stellar}/L_K$ in both works. NGC 2770 has a SSFR close

to the average in the frequent SN host sample, but a somewhat lower mass, but the SSFR lies clearly in the lower end of the distribution of long GRB hosts.

The hosts of broadlined SNe Ic from the sample of Modjaz et al. (2008a) have SFRs comparable to those of GRB hosts, but most likely smaller SSFRs due to their higher masses. As mentioned above, hosts of broadlined SNe Ic have higher metallicities than nearby GRB hosts which always have subsolar metallicities, some of them even down to 1/10 solar (for a complete sample see Savaglio et al., 2008, and references therein). Modjaz et al. (2008a) also note that the properties of the hosts of broadlined SNe Ic are consistent with those of normal nearby starforming spiral galaxies.

Some nearby GRB hosts are also different from the usual picture of low mass, high SF GRB hosts. The host of GRB 980425, connected to SN 1998bw (broadlined SN Ic) is a spiral galaxy with not particularly high SF in most parts of the galaxy, 1/3 of the global SF derived from this galaxy comes from a very luminous Wolf-Rayet (WR) region close to the GRB site (Christensen et al., 2008). The host of GRB 060505, a long GRB without SN, is a spiral galaxy and displays relatively high SF and a low metallicity at the site of the GRB (Thöne et al., 2008a), but not in the galaxy in general, even though the SF is still higher than in NGC 2770. It is still an open question whether GRB hosts are a special population of star-forming galaxies or following the general trend of other galaxies with redshift.

8.5.3 SN DETECTION RATES AND THE PROBABILITY OF FINDING 3 SNE IN NGC 2770 IN 10 YEARS

NGC 2770 apparently has a high observed SN Ib rate with 3 explosions within ten years. Indeed, although 39 more galaxies are known to have had 3 or more SNe, no other galaxy has had more than two Ib/c SNe. Is this unexpected?

To date, no independent measurement of the SN rate of SNe Ib exists. In most cases (e.g. Dahlen et al., 2004; Cappellaro et al., 2005) rates in the literature are given for all Core Collapse Supernovae (CC SNe) together. Such results are, however, dominated by SNe II, which are the most frequent SNe. Some papers list at least SNe Ib/c and SNe II separately (e.g. Cappellaro et al., 1999; Mannucci et al., 2005).

The rate measurements are either volumetric in case of higher-z SN surveys (e.g. Dahlen et al., 2004; Neill et al., 2006), or galaxy monitoring type searches, i.e. searches that look repetitively with a given cadence at a sample of galaxies. This kind of search usually has a number of biases, such as the frequency of observations, the limiting magnitudes achieved, the techniques used for detection or the galaxy inclination, and are restricted to lower or intermediate redshift (Cappellaro et al., 1999; Botticella et al., 2008).

Unlike SNe Ia, where an accurate and complete volumetric SN rate at low redshift has been measured (Dilday et al., 2008), the most recent results for CC-SNe is still from Cappellaro et al. (1999). Making estimates to correct for a number of biases, (Cappellaro et al., 1997) combine the results of 5 different supernova searches (including pre-CCD data) and obtain a rate of $0.08 \pm 0.04 \times (\mathrm{H_o}/75)^2$ SNu for SNe Ib/c (1 SNu = 1 SN per 100 yr per $10^{10} L_{\odot}^{B}$). This rate increases to $0.14 \pm 0.07 \times (\mathrm{H_o}/75)^2$ if one only takes Sbc-Sd type galaxies. For NGC 2770, we find a B-band luminosity from NED of $1.1 \times 10^{10} L_{\odot}^{B}$. Assuming a Poissonian distribution for supernova events, the probability of NGC 2770 to have 3 SNe Ib/c in a decade is then 6.1×10^{-7}. The probability of getting 3 SN Ib events is even smaller.

We cross-check our expected number of SN events in NGC 2770 with Mannucci et al. (2005), who normalized the SN rate to the K-band luminosity (SNuK) by using the same sample of

SN host galaxies as Cappellaro et al. (1999). The K-band luminosity is a better indicator of the stellar mass than the B-band luminosity which traces mostly the young star population. With a K band magnitude of 9.57 for NGC 2770 and by comparing with their predicted rates for Sbc galaxies (Mannucci et al., 2005, Tab. 2) we calculate a probability of 1.5×10^{-6} for NGC 2770 to have 3 SN Ib/c events within a decade. The two probabilities derived differ by a factor of about two. However, the chance probability for the observed SN rate at NGC 2770 is overall very small. In addition, the B-K color of NGC 2770 is 3.20, a value that does not indicate an extreme CC SN production (Mannucci et al., 2005). We note that the values derived here are only the probability to detect a SN from statistical considerations and the luminosity of the galaxy and do not necessarily correlate with the expected SN rate from radio observations.

However, we also have to account for the number of observed galaxies to derive a number for the probability to find one such galaxy which produced 3 SNe Ib. SNe have been discovered in ~ 3500 local galaxies but the total number of *monitored* galaxies is difficult to estimate, due also to the lack of information and uncertainties in individual amateur efforts. The results from Cappellaro et al. (1999) and Mannucci et al. (2005) are based on samples of 9346 and 8450 galaxies respectively. The LOSS search (Filippenko et al., 2001), which is the most successful and systematic search in low-z, monitors around 5000 local galaxies. If we now assume ~ 10000 monitored galaxies, the chance of observing this high SN rate in any galaxy becomes $0.6 - 1.5\%$ which is still a fairly low probability but given the uncertainties it could be consistent with a chance coincidence. This would also support the conclusions derived in Chapter 8.3 and Chapter 8.5.1 that NGC 2770 has no extraordinary global properties.

As a curiosity we add here that the same method of calculating probabilities, can to some extent explain the observed SN rates in the top SN producing galaxies (those with more than 5 observed SNe) with probabilities in the range $10^{-3} - 10^{-1}$, except the top SN producing galaxy, NGC 6946, which has a SED very similar to NGC 2770 (chance probability lower than 10^{-4}).

8.6 NGC 2770B

We also obtained spectra of the neighboring galaxy, NGC 2770B, which has the same redshift as NGC 2770 (Fynbo et al., 2008a) and can therefore be considered as a companion of NGC 2770. The galaxy consists of two "blobs" and we divide the 2D spectrum in 3 parts of which two are part of the first "blob" but show a small spatial separation in the emission lines in the 2D spectrum. Both regions shows very strong emission lines which points to a very young population undergoing heavy star formation. In Table 8.6 we list the emission lines detected as well as their fluxes.

We detect a large range of emission lines not detected in the spectra of NGC 2770 including [Ne III], Hδ, Ca II, Na I, [O III] λ 4363, He I, He II, [S III] and [Ar III] where the western "blob" of the galaxy shows most emission lines. [Ne III] λ 3869 is exceptionally strong, especially in the western blob which indicates a large number of young stars. The spectrum resembles very much the nebular spectrum of young HII regions such as the Orion nebula in the MW. In this region, we also detect a clear Wolf-Rayet (WR) feature at 4640 Å (restframe). In Fig. 8.9, we show the spectrum of region one which has the strongest emission lines with an inset showing an enlargement of the WR feature.

The extinction as derived from the Balmer decrement using both Hα/Hβ as well as $H\beta$/Hγ is consistent with zero. In order to determine the metallicity for NGC 2770B we cannot use any of the measurements which require [N II] that is only barely detected. This might be both an effect of the low metallicitiy and probably also a high temperature in the HII regions. Instead,

Line/property	region 1	region 2	region 3
	flux [10^{-15}erg cm^{-2} s^{-1}]		
[O II] λ 3729	13.8	7.07	5.95
[Ne III] λ 3869	15.5	2.43	1.71
Hϵ	6.47	—	—
Ca II λ 3969	9.69	0.73	1.06
Hδ	7.34	1.16	1.17
Hγ	14.3	1.46	1.74
[O III] λ 4363	3.23	—	0.28
He I λ 4472	1.02	—	—
Hβ	29.6	4.37	4.04
EW[Å]	615	44.4	119
[O III] λ 4960	71.1	8.88	7.81
[O III] λ 5008	194	25.8	23.4
He I λ 5876	3.11	0.13	0.49
[S III] λ 6313	0.84	0.23	—
Hα	71.3	14.1	12.6
EW[Å]	2200	295	709
[N II] λ 6585	0.51	0.04	0.14
[S II] λ 6718	0.97	0.54	0.30
[S II] λ 6732	2.60	0.19	0.89
Ne I λ 7024	1.14	0.68	0.45
He I λ 7065	0.63	—	—
[Ar III] λ 7135	1.76	0.33	0.29
[O II] 7330	1.81	—	—
12+log(O/H)	7.19	7.29	7.26
E(B-V)	0	0	0
SFR arcsec^{-2}	0.025	0.0049	0.0043

Table 8.6: *Fluxes and properties for three regions in NGC 2770B. The metallicity has been derived from the R_{23} parameter, the extinction from the Balmer line decrement, the SFR from Hα and is listed as SFR/arcsec^2.*

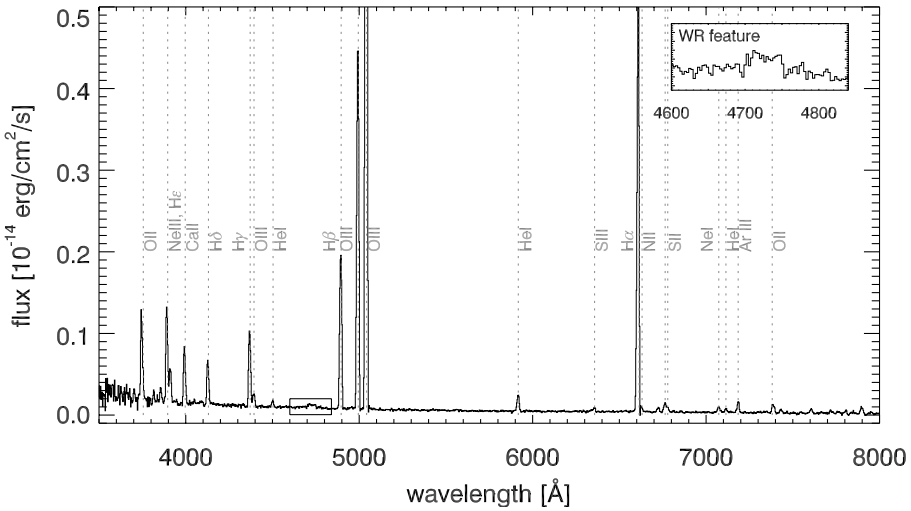

Figure 8.9: *Spectrum of region 1 in NGC 2770B which has the strongest emission lines. The emission lines of [O III] and Hα have been cutted in order to enlarge the scale to show the weaker emission lines.*

we use the R_{23} parameter (Kewley & Dopita, 2002) based on the line fluxes of Hα, Hβ, [O III] and [O II] which are all detected with high S/N in contrast to the spectra of NGC 2770. The metallicities we derive are among the lowest detected for nearby galaxies with 1/30 to 1/25

solar.

In two of the three spectra extracted from NGC 2770B, we also detected the [O III] λ 4363 line which allows us to determine the electron temperature. From the electron temperature, it is possible to derive directly the abundances of O^+/H and O^{++}/H by using the method described by Izotov et al. (2006b, eq. 1, 2, 4 and 5) and assuming that T_e(O II)=–0.577+T_e(O III)[2.065–0.498T_e(O III)] which Izotov et al. (2006b) suggests for low metallicities (eq. 14). We then get values of T_e(O II) = 1.4×10^4 K for region 1 and T_e(O II) = 1.2×10^4 K for region 3 which gives metallicities of 12+log(O/H)=7.1 and 7.6 respectively. The value for region 1 agrees very well with the one derived from R_{23} whereas the value for region 3 from the T_e method is higher. We note, however, that the [O III] λ 4363 line in region 3 was not detected with high significance.

The SFR in the eastern blob is comparable to the SFR in the nucleus of NGC 2770, however in the western part it is about an order of magnitude higher than in any region in NGC 2770. The very high EW of the Hα line also indicate a dominant stellar population of only a few Myrs. We also calculate the global SFR from collapsing the entire spectrum of NGC 2770B and obtain a SFR of 0.11 $M_\odot$ yr^{-1}. We obtained images from the 2MASS catalogue in K_s band and determined a magnitude of K_s = 15.3 mag for NGC 2770B. Assuming a mass-to-light ratio of 0.4, the median value adopted by Castro Cerón et al. (2008) for GRB host galaxies, and taking eq. 1 from Castro Cerón et al. (2008), we determine a mass of only log M_*=7.65 $M_\odot$. Together with the SFR derived from Hα, this gives a very high specific SFR of 0.39 Gyr^{-1}.

NGC 2770B is a rather unsual galaxy compared to its massive neighbour NGC 2770. The fact that no SN has been detected (yet) in this galaxy is likely only due to the fact that its total mass is very low and so the expected observed SN rate. It is also one of the most metal poor galaxies ever detected (see e.g. Izotov et al., 2006a) which further indicates a very young stellar population. What triggered this high SFR in NGC 2770B remains unclear. It is also interesting that the most metal poor region has a clear detection of a WR feature. WR stars do only occur in a very narrow time window after the onset of a starburst between 2 and 5×10^6 yr and are therefore a good tracer of the SF history. Models for WR stars predict a strong metallicity dependence on the wind which produces these features (e.g. Vink et al., 2001). However, there are a number of low metallicity galaxies with detected WR features which have challenged this model (e.g. Brinchmann et al., 2008). Possible explanations are that there are actually more WR stars produced than predicted from the models or that WR stars which are rapidly rotating can form at much lower metallicities. The latter has been suggested as progenitor for GRBs. In general, NGC 2770B seems to be a exceptional galaxy that might be interesting for future studies.

8.7 Conclusions

We have investigated the properties of the three SN sites in NGC 2770, the host of three SNe Ib, and the other regions in the host along 4 longslit positions. Previous observations in all wavelengths from UV to radio allow us to fit the SED of NGC 2770 and derive a range of global properties from it. We then set NGC 2770 in context to a sample of galaxies with frequent SN occurrence (3 or more SNe detected) and also compute the probability to detect three SNe Ib in a galaxy within only 10 years as it was the case for NGC 2770. From this analyses, we then conclude the following:

- NGC 2770 has global properties similar to the MW, even though it has a higher number of SNe observed. Its SFR and SNR are around the average of other nearby spiral galaxies and our sample of frequent SN galaxies.

- The only outstanding property of NGC 2770 is its high HI mass which indicates a large reservoir for forming stars.
- The metallicities at the SN sites in NGC 2770 are around 0.5 solar which is similar to the values observed for nearby GRB sites, but lower than for broadline SN Ic sites.
- Almost half of the galaxies with SNe II and Ib/c only have one type of SN which is likely connected to the age of the dominant stellar population. Galaxies producing SNe Ib/cs have a higher deVaucouleurs number than those producing SN II.
- SN and GRB hosts seem to be somewhat different in terms of SFRs and masses.
- The probability to detect 3 SNe Ib in a galaxy is 0.6 to 1.5 % assuming 10,000 monitored galaxies.

It therefore seems to be likely that observing 3 SNe Ib in NGC 2770 was only a chance coincidence. NGC 2770 is by no means a special galaxy that would be predestined to produce only stripped-envelope SNe. In fact its properties are not typical for galaxies with (frequent) SN Ib/c occurrence. However, it might also imply that the local properties at the SN sites are more important, at least in some galaxies, to produce a certain type of SN than its global properties.

Acknowledgments

CT and PMV want to thank Cédric Ledoux for the reduction of the UVES spectra. We thank the staff and the NOT and the VLT to perform the observations. In this work we made use of the NASA Extragalactic Database (NED). NED is operated by the Jet Propulsion Laboratory, California Institute of Technology, under contract with the National Aeronautics and Space Administration. Based on ESO program 080.D-0526.

CONCLUSIONS AND OUTLOOK

The last 150 pages have shown that the claim that GRBs can be used as lighthouses to study the high redshift universe is not just an empty phrase but a true fact. In addition, they are themselves one of the most puzzling events ever observed and we are just starting to understand what exactly happens when a GRB goes off. This thesis has covered observations from the low to the high redshift universe from z=0.007 to z=4.04 while it tried to contribute to both aspects.

GRBs at low redshift allow us to get a closer look on the actual explosion site. It seems that for most of them, they are somewhat special places in their galaxy (e.g. GRB 060505), but there are also counterexamples (e.g. GRB 980425) where the GRB region is not the most exceptional one. However, all GRB sites seem to agree in their overall properties with high star formation rate and moderate to low metallicity. This is in good agreement with the current progenitor models for long GRBs which require Wolf-Rayet stars with high angular momentum that can possibly only be sustained at low metallicity and therefore low mass loss. The progenitors of stripped-envelope supernovae, which have also been found connected to GRBs, might as well be such Wolf-Rayet stars that have lost parts of their envelope depending on their metallicity. Our investigations on the sites of three SNe Ib compared to broadline Ic SNe support this metallicity dependence, but we need larger samples and better resolved spectroscopy to ultimately confirm this suggestion.

GRBs at higher redshifts are better suited to probe the interstellar medium in the line of sight inside their hosts through absorption lines. We have presented three examples for afterglow spectra (GRB 060526, GRB 030329 and GRB 060206) also spanning a large range in redshifts from z=0.16 to 4.04. Whether the abundances were different for the lowest and the highest redshift burst we cannot determine as we only detected Mg in the one with the lowest redshift, but the kinematics in both galaxies might not be so different after all. Both show several velocity components spanning 300–400 km/s which could be interpreted as galactic outflows as observed for some nearby galaxies. Finestructure lines in the z=4.04 burst furthermore allowed us to get some additional information on the distance from the burst, supporting the outflow suggestion. As GRB hosts are assumed to be highly star forming, otherwise, the probability that a massive star required to form a GRB is very small, this scenario seems very likely.

The fact that long GRBs are connected to the death of massive stars have lead to the suggestion that they might trace the star-formation history throughout the universe. Due to their brightness, selecting star forming galaxies from the detection of a GRB seems quite appealing as such a selection might suffer from less biases than other surveys which are either magnitude limited or select only a special type of galaxy. In the last years, a sample of GRB host galaxy observations at different wavelengths have been built up. They all seem to get to a similar conclusion, namely that GRB hosts themselves are not particularly different from how the "average" star forming galaxy looks like at the corresponding redshift. At high redshifts, most galaxies

might have been actively star forming, but GRBs are also detected at lower redshifts and their hosts seem to be blue, small, compact galaxies. The required star-formation rates cannot have been sustained over such a long time. What was it then that triggered this star-formation? Interactions between neighboring galaxies possibly? *HST* observations suggest that many GRB hosts show indications for mergers. It would be worth looking at the large scale environment to see if long GRB hosts do have close neighbours or reside in denser regions.

Surprisingly, the metallicity evolution of GRB hosts as probed by absorption line spectroscopy seems to be very shallow and higher than galaxies probed by QSO sightlines. It is unknown which of the two samples is closer to the "average" metallicity at the corresponding redshifts. GRB hosts might have been enriched already very early on due to heavy star formation, so the higher metallicity would be an intrinsic property of GRB hosts. Or they might simply be more massive than QSO absorbers and just follow the luminosity-metallicity relation. Simulations suggest the latter, but the observed sample is still small. The kinematics from absorption lines in high resolution spectra and possible correlations with abundances, HI column density, extinction or other properties could possible solve this issue.

Forgetting about the issues with the host galaxies, GRBs could also be used as pure, powerful lightsources to probe the intergalactic medium, its density and metallicity evolution by studying the Ly α forest much like it is done already with quasar spectra. One would not suspect any differences compared to using quasar spectra, but you never know. The sample of high resolution spectra of GRBs which would be needed for those investigations is still small and statistical studies of the Lyman α forest not possible, but individual sightlines might reveal some interesting structures in the intergalactic medium.

Also in the field of GRB progenitors, there is still a large gap which is so far unknown: the short GRBs. Despite some attempts, no one has so far succeeded to get a decent spectrum of a short GRB afterglow and to determine its redshift directly from absorption lines. Some suggest that the surrounding medium of a short burst is expected to be much less dense than for a long GRB because they are found further out from their actual hosts and birthsites. Or it might have been just bad luck so far. Very low density environment have, however, now also been found for a few long GRBs. The comparison between the afterglow luminosity of short and long GRBs compared to their total energy might also imply that there is not so much difference. And again, the definition of "short" and "long" is still under discussion. Are short GRBs a truly different phenomenon or are short and long bursts not so different after all? Some, or even better, a large sample of short GRB afterglow spectra could contribute to that issue. But short GRB follow-up remains a tough business, even in the days of 8–10m telescopes.

At least for some long duration GRBs we now start to get a more detailed picture of the stellar population they were born into. We will maybe never be able to see the progenitor of a GRB as it is possible for some nearby SNe, but its environment might as well give us some useful hints. The first IFU study of a GRB host remained puzzling, but more will follow. The host of GRB 060505 will be investigated with a similar dataset using VIMOS at the IFU and data will come in this summer. Then we can hopefully answer the question if the GRB site was a unique site in that galaxy. Another proposal that just got accepted will do another study of NGC 2770, also with the VIMOS IFU. The galaxy itself seems not to be special, but maybe the solution to the mystery does not lie in the galaxy itself but in the properties at the supernova sites. Even though GRB research remains difficult, has to rely on fortunate circumstances, favorable time allocation committees and on small samples, the future looks promising.

Coauthorstatements

Paper I

ISM studies of GRB 030329 with high resolution spectroscopy

Christina C. Thöne, Jochen Greiner, Sandra Savaglio & Emmanël Jehin
The Astrophysical Journal, vol. **671**, pp. 628–636, 2007

Chapter 4 is based on this paper. Christina Thöne wrote the paper, did the entire analysis and made all the figures. Sandra Savaglio helped with the fitting program FITLYMAN, the structuring of the paper and made important contributions to the discussion of the absorption line fitting and flux calibration. Jochen Greiner was the PI of the data on which the paper is based, had the idea for the paper and also contributed to the discussion. Emmanuël Jehin did the reduction and preliminary flux calibration of the UVES data, which was refined with photometric data by Christina Thöne.

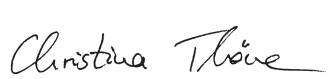

Christina Thöne

Sandra Savaglio

Paper II

Spatially resolved properties of GRB 060505 - implications to the nature of the progenitor

Christina C. Thöne, Johan P. U. Fynbo, Göran Östlin, Bo Milvang-Jensen, Klaas Wiersema, Daniele Malesani, Desiree Della Monica Ferreira, Javier Gorosabel, D. Alexander Kann, Darach Watson, Michał Michałowski, Andrew S. Fruchter, Andrew J. Levan, Jens Hjorth & Jesper Sollerman

The Astrophysical Journal, vol. **677**, pp. 1151–1161, 2008

Chapter 7 is based on this paper. Christina Thöne and Johan Fynbo jointly had the ideas that went into the paper. Christina Thöne did the analysis of the spectra, wrote the paper and made Fig. 2a and 4. Johan Fynbo did the analysis of the large scale structure around the host galaxy, wrote Section 5 and made Fig. 1, 2a and 6. Göran Östlin did the analysis of the stellar population age that went into Section 4.3. Bo Milvang-Jensen did the analysis of the rotation curve and made Fig. 3, which was later improved by Christina Thöne using HIRES data that will go into a future paper. Desiree Della Monica Ferrera and Javier Gorosabel did the global photometry of the host galaxy, Michał Michałowski did the SED modelling, Andrew Levan did the astrometry of the archival HST images, Alexander Kann provided the extinction measurement from the SED of the GRB region. Other authors contributed in various ways to the analysis and conclusions.

Christina Thöne

Johan Fynbo

Göran Östlin

Paper III

The host of GRB 060206 - kinematics of a distant galaxy

Christina C. Thöne, Klaas Wiersema, Cédric Ledoux, Rhaana L. C. Starling, Antonio de Ugarte Postigo, Andrew J. Levan, Johan P. U. Fynbo, Peter A. Curran, Javier Gorosabel, Alexander J. van der Horst, Alvaro Llorente, Evert Rol, Nial R. Tanvir, Paul M. Vreeswijk, Ralph A. M. J. Wijers & Lisa J. Kewley
Astronomy & Astrophysics 2008 in press, preprint: astro-ph/0708.3448

Chapter 5 is based on this paper. Christina Thöne wrote the text, did the analysis and made Fig. 1–4 and Fig. 7. Klaas Wiersema did independently the analysis on the implications of the ratio between fine-structure and ground-state in the different velocity components. Christina Thöne and Klaas Wiersema jointly wrote Sect. 5.1, 5.3 and 7. Cédric Ledoux made crucial contributions and suggestions to the absorption line fitting. Rhaana Starling did the extinction measurement from the afterglow SED. Antonio de Ugarte Postigo did the final analysis of the equivalent widths in the intervening system from different datasets and made Fig. 6. Andrew Levan provided the analysis of the HST data on the host field. Johan Fynbo had the idea for the paper which was the follow-up paper of a A&A letter by Johan Fynbo on the same dataset to provide a more thorough analysis. He also did the comparison with QSO-DLAs (Sect. 5.4) and made Fig. 5. The other authors contributed in various ways to the analysis, data reduction and discussion.

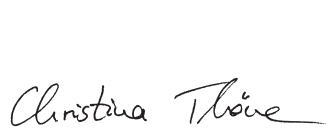

Christina Thöne

Klaas Wiersema

Paper IV

Photometry and Spectroscopy of GRB 060526: A detailed study of the afterglow and host of a high-redshift gamma-ray burst

C. C. Thöne, D. A. Kann, G. Jóhannesson, J. H. Selj, A. Jaunsen, J. P. U. Fynbo, K. S. Baliyan, C. Bartolini, I. F. Bikmaev, J. S. Bloom, R. A. Burenin, B. E. Cobb, S. Covino, P. A. Curran, H. Dahle, J. French, S. Ganesh, G. Greco, A. Guarnieri, L. Hanlon, J. Hjorth, M. Ibrahimov, G. L. Israel, P. Jakobsson, B. L. Jensen, U. G. Jørgensen, I. M. Khamitov, D. Malesani, N. Masetti, J. Näränen, E. Pakstiene, M. N. Pavlinsky, D. A. Perley, A. Piccioni, G. Pizzichini, A. Pozanenko, D. Nanni, V. Rumyantsev, D. Sharapov, D. Starr, R. A. Sunyaev, F. Terra, P. M. VreeswijkÊ& A. C. Wilson
submitted to Astronomy & Astrophysics, preprint: astro-ph/0806.1182

Chapter 3 is based on this paper. Christina Thöne had the idea for the paper and wrote most of the text excluding the light curve fitting and modelling of the light curve with multiple energy injections. The analytical modelling of the lightcurve was done by Alexander Kann who also made Fig. 1 to 5 and wrote part of the introduction and conclusions. The numerical modelling was done by Guðlaugur Jóhannesson who also wrote Section 2.5. Christina Thöne did the spectroscopic analysis, Fig. 7 and 8, and most of the photometry that went into the light curve modelling. Daniele Malesani did the analysis of the ESO-large program data on the host of GRB 060526 and provided Fig. 6. Other authors contributed in various ways to the analysis and commented on the paper. The data used for this paper come from a large range of observatories and most of coauthors were responsible in obtaining these observations and providing the reduced images.

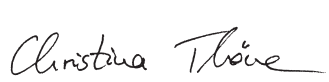
Christina Thöne


Alexander Kann


Guðlaugur Jóhannesson

Paper V

NGC 2770 - A SN Ib factory?

Christina C. Thöne, Michał Michałowski, Giorgos Leloudas, Nick Cox, Johan P. U. Fynbo, Jens Hjorth, Jesper Sollerman & Paul M. Vreeswijk

submitted to The Astrophysical Journal, preprint: astro-ph/0807.0437

Chapter 8 is based on this paper. Christina Thöne had the idea for the paper, did the spectroscopic analysis, wrote most of the text and did all Figures except Fig. 2. Michał Michałowski did the SED modelling including Fig. 2 and the literature search on properties of NGC 2770 as well as the data from which the star-formation rate, supernova rate and mass of the sample of frequent SN galaxies were derived. Giorgos Leloudas contributed the statistical analysis of detecting 3 Ib SNe in a galaxy like NGC 2770. Nick Cox contributed the fitting, analysis and discussion of the DIBs in the UVES spectra. Other authors contributed in various ways to the analysis and made suggestions for further analysis, comparisons and the discussion.

Christina Thöne | Michał Michałowski | Giorgos Leloudas

PUBLICATIONS

First author papers

- *NGC 2770: a SN Ib factory?*
  C. C. Thöne, M. J. Michalowski, G. Leloudas, N. L. J. Cox, J. P. U. Fynbo, J. Hjorth & J. Sollerman, ApJ under revision (preprint: astro-ph/0807.0347)

- *Photometry and Spectroscopy of GRB 060526: A detailed study of the afterglow and host of a high-redshift Gamma-ray burst*
  C. C. Thöne, D. A. Kann, G. Jóhannesson, J. H. Selj, A. Jaunsen, J. P. U. Fynbo, K. S. Baliyan, C. Bartolini, I. F. Bikmaev, J. S. Bloom, R. A. Burenin, B. E. Cobb, P. A. Curran, S. Covino, H. Dahle, J. French, S. Ganesh, G. Greco, A. Guarnieri, L. Hanlon, J. Hjorth, M. Ibrahimov, G. L. Israel, P. Jakobsson, B. L. Jensen, U. G. Jørgensen, I. M. Khamitov, D. Malesani, N. Masetti, J. Näränen, E. Pakstiene, M. N. Pavlinsky, D. A. Perley, A. Piccioni, G. Pizzichini, A. Pozanenko, D. Nanni, V. Rumyantsev, D. Sharapov, D. Starr, R. A. Sunyaev, F. Terra, P. M. Vreeswijk & A. C. Wilson, A&A under revision (preprint: astro-ph/0806.1182)

- *The host of GRB 060206: kinematics of a distant galaxy*
  C.C. Thöne, K. Wiersema, C. Ledoux, R. L. C. Starling, A. de Ugarte Postigo, A. J. Levan, J. P. U. Fynbo, P. Curran, J. Gorosabel, A. van der Horst, A. Llorente, E. Rol, N. R. Tanvir , P. M. Vreeswijk, R. A. M. J. Wijers & L. Kewley, A&A in press (preprint: astro-ph/0708.3448)

- *Spatially resolved properties of the GRB060505 host: implications for the nature of the progenitor*
  C. C. Thöne; J. P. U. Fynbo; G. Östlin; B. Milvang-Jensen; K. Wiersema; D. Malesani; D. Della Monica Ferreira; J. Gorosabel; D. A. Kann, D. Watson; M. J. Michałowski, J. Hjorth, A. S. Fruchter & J. Sollerman, ApJ, 676, 1151 (2008)

- *ISM studies of GRB030329 with high resolution spectroscopy*
  C. C. Thöne; J. Greiner; S. Savaglio & E. Jehin, ApJ, 671, 628 (2007)

Contribution to other papers

- *Early spectroscopic identification of SN 2008D*
  D. Malesani, J. P. U. Fynbo, J. Hjorth, G. Leloudas, J. Sollerman, M. D. Stritzinger, P. M. Vreeswijk, D. J. Watson, J. Gorosabel, M. Michałowski, **C. C. Thöne**, T. Augustijn, D. Bersier, P. Jakobsson, A. O. Jaunsen, C. Ledoux, A. J. Levan, B. Milvang-Jensen, E. Rol, N. R. Tanvir, K. Wiersema, D. Xu, L. Albert, M. Bayliss, C. Gall, L. F. Grove, B. P. Koester, E. Leitet, T. Pursimo & I. Skillen, ApJL, under revision (preprint: astro-ph/0805.1188)

- *IFU observations of the GRB 980425/SN 1998bw host galaxy: Unusual emission line ratios in GRB regions*
  L. Christensen, P. Vreeswijk, J. Sollerman, **C. C. Thöne**, E. Le Floc' h & K. Wiersema, A&A accepted (preprint: astro-ph/0807.3554)

- *GROND - a 7 channel imager*
  J. Greiner, W. Bornemann, C. Clemens, M. Deuter, G. Hasinger, M. Honsberg, H. Huber, S. Huber, M. Krauss, T. Krühler, A. Küpçü Yoldaş, H. Mayer-Hasselwander, B. Mican, N. Primak, F. Schrey, I. Steiner, G. Szokoly, **C. C. Thöne**, A. Yoldaş, S. Klose, U. Laux, & J. Winkler, PASP 120, 405 (2008)

- *Detection of GRB 060927 at z = 5.47: Implications for the Use of Gamma Ray Bursts as Probes of the End of the Dark Ages*
  A. E. Ruiz-Velasco; H. Swan; E. Troja; D. Malesani; J. P. U. Fynbo; R. L. C. Starling; D. Xu; F. Aharonian; C. Akerlof; M. I. Andersen; M. C. B. Ashley; S. Barthelmy; D. Bersier; J. M. Castro Cerón; A. J. Castro-Tirado; N. Gehrels; E. Gögüş, J. Gorosabel; C. Guidorzi; T. Güver; J. Hjorth; D. Horns; P. Jakobsson; B. L. Jensen; U. Kızıloglu; H. Krimm; C. Ledoux; A. J. Levan; T. McKay; A. Melandri; B. Milvang-Jensen; C. G. Mundell; P. T. OÕBrien; M. Özel; A. Phillips; R. Quimby; E. Rol; G. Rowell; W. Rujopakarn; E. Rykoff; B. E. Schaefer; J. Sollerman; N. R. Tanvir; **C. C. Thöne**; W. Vestrand; P. M. Vreeswijk; D. Watson; J. C. Wheeler; R. A. M. J. Wijers; J. Wren; S. Yost, S. & F. Yuan ApJ 669, 1 (2007)

- *Photospheric and chromospheric activity on EY Dra*
  H. Korhonen; K. Brogaard; K. Holhjem; S. Ramstedt; J. Rantala; **C. C. Thöne** & K. Vida, AN, 328, 897 (2007)

- *A search for host galaxies of 24 Gamma Ray Bursts*
  J.-E. Ovaldsen; A. O. Jaunsen; J. P. U. Fynbo; J. Hjorth; **C. C. Thöne**; C. Féron; D. Xu; J. H. Selj & J. Teuber, ApJ, 662, 294 (2007)

- *The nature of the X-ray flash of August 24 2005. Photometric evidence for an on-axis z = 0.83 burst with continuous energy injection and an associated supernova?*
  J. Sollerman; J. P. U. Fynbo; J. Gorosabel; J. P. Halpern; J. Hjorth; P. Jakobsson; N. Mirabal; D. Watson; D. Xu; A. J. Castro-Tirado; C. Féron; A. O. Jaunsen; M. Jelinek; B. L. Jensen; D. A. Kann; J.-E. Ovaldsen; A. Pozanenko; M. Stritzinger; **C. C. Thöne**; A. de Ugarte Postigo; S. Guziy; M. Ibrahimov; S. P. Jaervinen; A. Levan; V. Rumyantsev & N. Tanvir, N., A&A, 466, 839-846 (2007)

- *A new type of massive stellar death: no supernovae from two nearby long gamma ray bursts*
  J. P. U. Fynbo; D. Watson; **C. C. Thöne**, J. Sollerman; J. S. Bloom; T. M. Davis; J. Hjorth; P. Jakobsson; U. G. Jørgensen; J. F. Graham; A. S. Fruchter; D. Bersier; L. Kewley; A. Cassan; J. M. Castro Ceron; S. Foley; J. Gorosabel; T. C. Hinse; K. D. Horne; B. L. Jensen; S. Klose; D. Kocevski; J.-B. Marquette; D. Perley; E. Ramirez-Ruiz; M. D. Stritzinger; P. M. Vreeswijk; R. A. M. Wijers; K. G. Woller; D. Xu & M. Zub, Nature 444, 1047-1049 (2006)

- *HI column densities of z>2 Swift gamma-ray bursts*
  P. Jakobsson; J. P. U. Fynbo; C. Ledoux; P. Vreeswijk; D. A. Kann; J. Hjorth; N. R. Tanvir; D. Reichart; J. Gorosabel; S. Klose; R. S. Priddey; D. Watson; J. Sollerman; A. S. Fruchter; A. de Ugarte Postigo; K. Wiersema; G. Björnsson; **C. C. Thöne**; K. Pedersen & B. L. Jensen, A&A 460, L13-L16 (2006)

- *Are short γ-ray bursts collimated? GRB 050709, a flare but no break*
  D. Watson; J. Hjorth; P. Jakobsson; D. Xu; J. P. U. Fynbo; J. Sollerman; **C. C. Thöne** & K. Pedersen, A&A 454, L123-L126 (2006)

- *Supernova 2006aj and the associated X-Ray Flash 060218*
  J. Sollerman; A. O. Jaunsen; J. P. U. Fynbo; J. Hjorth; P. Jakobsson; M. Stritzinger; C. Féron; P. Laursen; J.-E. Ovaldsen; J. Selj; **C. C. Thöne**; D. Xu; T. Davis; J. Gorosabel; D. Watson; R. Duro; I. Ilyin; B. L. Jensen; N. Lysfjord; T. Marquart; T. B. Nielsen; J. Näränen; H. E. Schwarz; S. Walch; M. Wold & G. Östlin, A&A 454, 503-509 (2006)

- *Probing cosmic chemical evolution with gamma-ray bursts: GRB 060206 at z = 4.048*
  J. P. U. Fynbo; R. L. C. Starling; C. Ledoux; K. Wiersema; **C. C. Thöne**; J. Sollerman; P. Jakobsson; J. Hjorth; D. Watson; P. M. Vreeswijk; P. Møller; E. Rol; J. Gorosabel; J. Näränen; R. A. M. J. Wijers; G. Björnsson; J. M. Castro Cerón; P. Curran; D. H. Hartmann; S. T. Holland; B. L. Jensen; A. J. Levan; M. Limousin; C. Kouveliotou; G. Nelemans; K. Pedersen; R. S. Priddey & N. R. Tanvir, A&A 451, L47-L50 (2006)

Conference proceedings and non refereed publications

- *Unraveling the dynamics and kinematics of GRB hosts with high resolution spectroscopy*
  C. C. Thöne; J. P. U. Fynbo; L. Christensen; K. Wiersema & J. S. Bloom, Proceedings of *Gamma Ray Bursts 2007*, Santa Fe, New Mexico, November 5–9, AIP Conference Proceedings, Vol. 1000, pp. 492 – 495 (2008)

- *Gamma-Ray Bursts as Cosmological Probes: from Concept to Reality*
  J. Fynbo; P. Vreeswijk; P. Jakobsson; A. Jaunsen; C. Ledoux; D. Malesani; **C. Thöne**; S. Ellison; J. Gorosabel; J. Hjorth; B. Jensen; C. Kouveliotou; A. Levan; P. Møller; E. Rol; A. Smette; J. Sollerman; R. Starling; N. Tanvir; D. Watson; K. Wiersema; R. Wijers & D. Xu, The Messenger Vol. 130, p. 43 (2007)

- *GROND Commissioned at the 2.2-m MPI Telescope on La Silla*
  J. Greiner; W. Bornemann; C. Clemens; M. Deuter; G. Hasinger; M. Honsberg; H. Huber; S. Huber; M. Krauss; T. Krühler; A. Küpçü Yoldaş; H. Mayer-Hasselwander; B. Mican; N. Primak; F. Schrey; I. Steiner; G. Szokoly; **C. C. Thöne**; A. Yoldaş; S. Klose; U. Laux & J. Winkler, The Messenger vol. 130. p. 12 (2007)

- *The spatially resolved host of GRB 060505 and implications for the nature of the progenitor*
  C. C. Thöne & J. P. U. Fynbo, Proceedings of the Amsterdam conference, 10 years of GRB afterglows, March 19-23, 2007, to appear in New Astronomy Reviews (preprint: astro-ph/0706.0674)

- *No supernovae detected in two long-duration gamma-ray bursts*
  Watson, D., Fynbo, J. P. U., **Thöne, C. C.** & Sollerman, J., proceedings to the discussion meeting *Gamma-ray bursts* by the Royal Society, London, September 2006, Phil. Trans. R. Soc. A 365, 1269 (2007), (astro-ph/0703678)

- *The short gamma-ray burst revolution*
  J. Hjorth; A. Levan; N. Tanvir; R. Starling; S. Klose; C. Kouveliotou; C. Féron; P. Ferrero; A. Fruchter; J. Fynbo; J. Gorosabel; P. Jakobsson; D. A. Kann; K. Pedersen; E. Ramirez-Ruiz; J. Sollerman; **C. Thöne**; D. Watson; K. Wiersema & D. Xu, The Messenger Vol. 126, p.16 (2006)

- *The Peculiar Type Ia Supernova 2005hk*
  V. Stanishev; S. Taubenberger; G. Blanc; G. C. Anupama; S. Benetti; E. Cappellaro; N. Elias-Rosa; C. Féron; A. Goobar; K. Krisciunas; A. Pastorello; D. K. Sahu; M. E. Salvo; B. P. Schmidt; J. Sollerman; **C. C. Thöne**; M. Turatto & W. Hillebrandt, Proceedings of the conference*The Multicoloured Landscape of Compact Objects and their Explosive Origins*, 2006 June 11–24, Cefalu, Sicily, AIP Conference Proceedings, Vol. 924, pp. 336-341 (2007)

Popular science articles

- *Stjerner som ville dø i fred afsløres ved gamma-stråling*
  C. C. Thöne, D. Malesani & D. Xu, Kvant Nr. 1 (2007)

GRB coordinates network circulars

1. *GRB 051117B: r and I observations of possible host galaxy*, C. Thoene; C. Feron; P. Jakobsson; B. L. Jensen; J. P. U. Fynbo; J. Sollerman; H. Pedersen; D. Watson & J. Hjorth, GCN circular # 4291 (2005)

2. *GRB060130: further R-band imaging*, J. Nielsen; C. Thoene; C. Feron; J. P. U. Fynbo; B. L. Jensen; J. Hjorth & C. Karoff, GCN circular # 4625 (2006)

3. *GRB060218: optical brightening in V and r*, J.-E. Ovaldsen; D. Xu; J. H.Selj; A.O. Jaunsen; C. Feron; C. Thoene; J. P. U. Fynbo & J. Hjorth, GCN circular #4816 (2006)

4. *GRB060313: optical observations of the afterglow candidate*, C. Thoene; C. Feron; J. Hjorth & B. L. Jensen, GCN circular # 4871 (2006)

5. *GRB060424: optical afterglow detection*, C. C. Thoene; K. Nilsson; B. L. Jensen & J. Fynbo, GCN circular #5003 (2006)

6. *GRB060507: optical afterglow detection*, C. C. Thoene; B. L. Jensen; J. Fynbo & J.-E. Solheim, GCN circular # 5094 (2006)

7. *VLT optical spectroscopy of GRB 060512*, R. Starling; C. C. Thoene; J. P. U. Fynbo; P. Vreeswijk & J. Hjorth, GCN circular # 5131 and correction 5149 (2006)

8. *GRB060505: VLT observations of the optical afterglow*, C. C. Thoene; J. P. U. Fynbo; J. Sollerman; B. L. Jensen; J. Hjorth; P. Jakobsson & S. Klose, GCN circular # 5161 (2006)

9. *GRB060526: possible break in the optical light curve*, C. C. Thoene; J. P. U. Fynbo & U. G. Joergensen, GCN circular #5179 (2006)

10. *GRB060526: afterglow fitting and probable jet break*, D. A. Kann & C. C. Thoene, GCN circular # 5187 (2006)

11. *GRB060614: optical observations*, C. C. Thoene; J. P. U. Fynbo; B. L. Jensen; J. Hjorth; D. Xu; U. G. Joergensen & K. Woller, GCN circular # 5272 (2006)

12. *GRB060614: detection of the host galaxy but no supernova emission*, J. P. U. Fynbo; C. C. Thoene; B. L. Jensen; J. Hjorth; J. Sollerman; D. Watson; D. Xu; J.-E. Ovaldsen; U. G. Joergensen; T. Hinse & K. Woller, GCN circular # 5277 (2006)

13. *GRB 060729 redshift*, C. C. Thoene; A. Levan; P. Jakobsson; E. Rol; J. Gorosabel; J. P. U. Fynbo; B. L. Jensen; J. Hjorth & P. Vreeswijk, GCN circular # 5373 (2006)

14. *GRB060901: optical observations*, K. Wiersema & C. C. Thoene, GCN circular # 5501 (2006)

15. *VLT redshift of GRB 060906*, P. Vreeswijk; P. Jakobsson; C. Ledoux; C. Thoene, C & J. Fynbo, GCN circular # 5535 (2006)

16. *GRB 060908: Danish/DFOSC optical observations*, K. Wiersema; C. C. Thoene & E. Rol, GCN circular # 5552 (2006)

17. *GRB 060807: Detection of the possible host galaxy*, C. C. Thoene; C. Henriksen & K. Wiersema, GCN circular # 5672 (2006)

18. *GRB060908: Detection of the possible host*, C. C. Thoene; C. Henriksen & K. Wiersema, GCN circular # 5674 (2006)

19. *GRB 061021: VLT spectrum with no lines*, C. C. Thoene; Fynbo, J. P. U. & P. Jakobsson, GCN circular # 5747 (2006)

20. *GRB 061110: NOT observations*, C. C. Thoene; D. Malesani; J. P. U. Fynbo; C. Henriksen & D. Sharapov, GCN circular # 5799 (2006)

21. *GRB 061110B: NOT optical observations*, C. C. Thoene; D. Malesani; J. P. U. Fynbo; C. Henriksen & D. Sharapov, GCN circular # 5807 (2006)

22. *GRB 061110B: VLT redshift*, J. P. U. Fynbo; D. Malesani.; C. C. Thoene; P. M. Vreeswijk; J. Hjorth & C. Henriksen, GCN circular # 5809 (2006)

23. *GRB 061110A: VLT tentative redshift*, C. C. Thoene; J. P. U. Fynbo; P. Jakobsson; P. M. Vreeswijk & J. Hjorth, GCN circular # 5812 (2006)

24. *GRB 061110A: refined R-band analysis*, C. C. Thoene & J. P. U. Fynbo, GCN circular # 5817 and correction 5818 (2006)

25. *GRB 070224: optical afterglow candidate* C. C. Thoene; D. A. Kann & T. Augusteijn, GCN circular # 6142 (2007)

26. *GRB 070224: optical afterglow confirmation*, C. C. Thoene; D. A. Kann, T. Augusteijn & C. Reyle-Laffont, GCN circular # 6154 (2007)

27. *GRB 070306: NOT observations*, D. Malesani; Jaunsen, A. O.; C. C. Thoene; J. Hjorth; D. Paraficz; E. Leitet & B. Caldwell, GCN circular # 6178 (2007)

28. *GRB060901: Candidate optical afterglow*, K. Wiersema; E. Rol & C. C. Thoene, GCN circular # 6188 (2007)

29. *GRB 070306: possible emission-line redshift*, A. O. Jaunsen; C. C. Thoene; J. P. U. Fynbo; J. Hjorth & P. Vreeswijk, GCN circular # 6202 (2007)

30. *GRB 070406: NOT observations*, D. Malesani; H. Uthas; C. C. Thoene; J. P. U. Fynbo; J. Hjorth & M. I. Andersen, GCN circular # 6254 (2007)

31. *GRB 070406: further analysis of NOT images*, D. Malesani; H. Uthas; J. Hjorth; C. C. Thoene; J. P. U. Fynbo & M. I. Andersen, GCN circular # 6257 (2007)

32. *GRB 070411: OA redshift*, P. Jakobsson; D. Malesani; C. C. Thoene; J. P. U. Fynbo; J. Hjorth; A. O. Jaunsen; M. I. Andersen & Vreeswijk, P. M., GCN circular # 6283 (2007)

33. *GRB 070411: break in the optical light curve*, D. Malesani; E. Rol; L. A. Antonelli; J. P. U. Fynbo; P. A. Curran; K. Wiersema; A. J. Levan; N. R. Tanvir; V. Testa; E. Palazzi; A. O. Jaunsen; C. C. Thoene; J. Hjorth & P. M. Vreeswijk, GCN circular # 6343 (2007)

34. *GRB 070506: VLT redshift*, C. C. Thoene; A. O. Jaunsen; J. P. U. Fynbo; P. Jakobsson & P. M. Vreeswijk, GCN circular # 6379 (2007)

35. *GRB 070508: Multicolor optical observations and possible redshift limit*, C. C. Thoene; J. P. U. Fynbo & A. Williams, GCN circular # 6389 (2007)

36. *GRB 070509: objects inside XRT error circle*, D. Malesani; C. C. Thoene; A. Williams; J. P. U. Fynbo; A. O. Jaunsen & P.M. Vreeswijk, GCN circular # 6410 (2007)

37. *GROND upper limits of GRB 070521*, J. Greiner; C. Clemens; T. Kruehler, A. Kuepcue-Yoldas, N. Primak; G. Szokoly; A. Yoldas; S. Klose; U. Laux & C. C. Thoene, GCN circular # 6449 (2007)

38. *GRB 070611: VLT redshift*, C. C. Thoene; P. Jakobsson; J. P. U. Fynbo; D. Malesani; J. Hjorth & P. M. Vreeswijk, GCN circular # 6499 (2007)

39. *GRB 070621: NOT observations*, D. Malesani; C. C. Thoene; J. P. U. Fynbo; N. R. Tanvir & A. Tziamtzis, GCN circular # 6565 (2007)

40. *GRB 070611: VLT observations*, P. Jakobsson; D. Malesani; D. Xu; J. P. U. Fynbo; J. Hjorth & C. C.Thoene, GCN circular # 6601 (2007)

41. *GRB 070714B: Keck observations*, D. A. Perley; J. S. Bloom; C. C. Thoene & N. R. Butler, GCN circular # 6652 (2007)

42. *GRB 060814: Keck host detection and redshift*, C. C. Thoene; D. A. Perley & J. S. Bloom, GCN circular # 6663 (2007)

43. *GRB 070802: VLT redshift*, J. X. Prochaska, C. C. Thoene, D. Malesani, J. P. U. Fynbo & P. M. Vreeswijk, GCN circular # 6698 (2007)

44. *GRB 070809: Keck imaging*, D. A. Perley, C. C. Thoene, J. Cooke, J. S. Bloom & E. Barton, GCN circular # 6739 (2007)

45. *GRB 070810: Keck redshift and photometry*, C. C. Thoene, D. A. Perley, J. Cooke, J. S. Bloom, H.-W. Chen & E. Barton, GCN circular # 6741 (2007)

46. *GRB 070810B: Keck spectroscopy of possible host galaxies*, C. C. Thoene, J. S. Bloom, N. R. Butler & P. Nugent, GCN circular # 6756 (2007)

47. *GRB 070810A: Continued Keck Imaging*, D. A. Perley, J. S. Bloom & C. C. Thoene, GCN circular # 6757 (2007)

48. *GRB 061110A: redshift confirmed*, J. P. U. Fynbo, C. C. Thoene, D. Malesani, J. Hjorth, P. M. Vreeswijk & P. Jakobsson, GCN circular # 6759 (2007)

49. *GRB 070810B: Image Subtraction of Multiple Keck Observations*, D. Kocevski, J. S. Bloom, C. C. Thoene & J. X. Prochaska, GCN circular # 6771 (2007)

50. *GRB 070809: Confirmation of optical transient*, D. A. Perley, C. C. Thoene & J. S. Bloom, GCN circular # 6774 (2007)

51. *GRB 070917: Confirmation of optical afterglow*, J. P. U. Fynbo, M. D. Stritzinger, C. Gall, A. O. Jaunsen, C. C. Thoene, D. Malesani, P. Vreeswijk, J. Hjorth & J. Sollerman, GCN circular # 6803 (2007)

52. *GRB 071010B: Keck/LRIS Spectroscopy*, J. X. Prochaska, D. A. Perley, M. Modjaz, J. S. Bloom, D. Poznanski & C. C. Thoene, GCN circular # 6890 (2007)

53. *GRB 071020: VLT spectroscopy*, P. Jakobsson, P. M. Vreeswijk, J. Hjorth, D. Malesani, J. P. U. Fynbo & C. C. Thoene, GCN circular # 6952 (2007)

54. *GRB 071031: VLT high resolution spectroscopy*, C. Ledoux, P. Jakobsson, A.O. Jaunsen, C.C. Thoene, P. M. Vreeswijk, D. Malesani, J. P. U. Fynbo & J. Hjorth, GCN circular # 7023 (2007)

55. *GRB 070429B: Probable host galaxy and redshift* D. A. Perley, J. S. Bloom, M. Modjaz, D. Poznanski & C. C. Thoene, GCN circular # 7140 (2007)

56. *Possible XRF in NGC 2770 - NOT observations of the optical counterpart*, C. C. Thoene, D. Malesani, J. Hjorth, J. P. U. Fynbo, P. Jakobsson, M. Bayliss & B. Koester, GCN circular # 7161 (2008)

57. *Transient in NGC 2770: spectroscopic evidence for a SN*, D. Malesani, J. Hjorth, P. Jakobsson, P. M. Vreeswijk, C.C. Thoene, J.P.U. Fynbo, D. J. Watson, J. Sollerman, N.R. Tanvir & T. Stanke, GCN circular # 7169 (2008)

58. *XRF 080109 / SN 2008D: spectroscopic evolution*, D. Malesani, J. Sollerman, J. P. U. Fynbo, C. C. Thoene, D. Xu, J. Hjorth, G. Leloudas, P.M. Vreeswijk, D.J. Watson, P. Jakobsson, T. Augusteijn, C. Villforth & S.-M. Niemi, GCN circular # 7184 (2008)

59. *GRB 080411: VLT redshift*, C. C. Thoene, A. De Cia, D. Malesani & P. M. Vreeswijk, GCN circular # 7587 (2008)

60. *GRB 080413B: VLT redshift*, P. M. Vreeswijk, C. C. Thoene, D. Malesani, J. P. U. Fynbo, J. Hjorth, P. Jakobsson, N. R. Tanvir & A. J. Levan, GCN circular # 7601 (2008)

61. *GRB 080413A: VLT/UVES redshift*, C. C. Thoene, D. Malesani, P. M. Vreeswijk, J. P. U. Fynbo, P. Jakobsson, C. Ledoux & A. Smette, GCN circular # 7602 (2008)

62. *GRB 080430: Spectroscopy from CAHA*, A. de Ugarte Postigo, L. Christensen, J. Gorosabel, C. Thöne, D.A. Kann, A. Mora, T. Szeifert, M. Jelinek, A. J. Castro-Tirado, S. Pedraz, N. Cardiel & D. Montes GCN circular # 7650 (2008)

63. *GRB 080430 - multicolor observations of the afterglow*, C. C. Thoene, J. P. U. Fynbo, A. de Ugarte Postigo, D. A. Kann, N. E. Groeneboom, Ø. Rudjord, J. R. Kristiansen & T. Purismo, GCN circular # 7658 (2008)

64. *GRB 080430: Shallow decay*, A. de Ugarte Postigo, C. C. Thöne, F. Aceituno, N. E. Groeneboom, Ø. Rudjord, J. R. Kristiansen & T. Purismo, GCN circular # 7662 (2008)

65. *GRB 080506: Observations from NOT*, A. de Ugarte Postigo, C. C. Thoene, J. P. U. Fynbo, E. Leitet & L. M. Trinchant, GCN circular # 7690 (2008)

66. *GRB080603B: NOT redshift*, J. Fynbo, P.-O. Quirion, D. Xu, D. Malesani, C. C. Thoene, J. Hjorth, B. Milvang-Jensen & P. Jakobsson, GCN circular, # 7797 (2008)

67. *GRB 080605: VLT redshift*, P. Jakobsson, P. M. Vreeswijk, D. Xu & C. C. Thoene, GCN circular, # 7832 (2008)

68. *GRB 080613B - NOT optical and IR nondetections*, C. C. Thoene, D. Malesani, J. P. U. Fynbo, L. Malo, R. J. Cardenes and A. A. Djupvik, GCN circular, # 7878 (2008)

69. *GRB 080804: UVES redshift*, C. C. Thoene, A. de Ugarte Postigo, P. M. Vreeswijk, D. Malesani & P. Jakobsson, GCN circular # 8058 (2008)

70. *GRB 080810: Observations from NOT*, A. de Ugarte Postigo, C. C. Thoene, J. P. U. Fynbo, J. Hjorth, P. Jakobsson, Z. Banhidi, F. Grundahl & T. Arentoft, GCN circular # 8089 (2008)

71. *GRB 080810 - optical observations*, C. C. Thoene, A. de Ugarte Postigo & C. Liebig, GCN circular # 8106 (2008)

72. *GRB 080825B - optical counterpart candidate*, C. C. Thoene, A. de Ugarte Postigo & D. Ricci, GCN circular # 8135 (2008)

73. *GRB 080825: Afterglow confirmation and redshift estimate*, A. de Ugarte Postigo, C. C. Thoene & D. Ricci, GCN circular # 8137 (2008)

74. *GRB 080905A: NOT and VLT observations*, D. Malesani, A. de Ugarte Postigo, J. P. U. Fynbo, A. J. Levan, E. Rol, N. R. Tanvir , C. C. Thoene, J. Telting & A. Baran, GCN circular # 8190 (2008)

Other circulars

- *Supernova 2007cn in UGC 11953*, R. J. Foley; J. S. Bloom; A. V. Filippenko; C. C. Thoene, CBET # 1032 (2007)

BIBLIOGRAPHY

Abraham, R. G., Ellis, R. S., Fabian, A. C., Tanvir, N. R., & Glazebrook, K. 1999, MNRAS, 303, 641

Adelberger, K. L., Steidel, C. C., Shapley, A. E., & Pettini, M. 2003, ApJ, 584, 45

Akerlof, C., Balsano, R., Barthelmy, S., Bloch, J., Butterworth, P., Casperson, D., Cline, T., Fletcher, S., Frontera, F., Gisler, G., Heise, J., Hills, J., Kehoe, R., Lee, B., Marshall, S., McKay, T., Miller, R., Piro, L., Priedhorsky, W., Szymanski, J., & Wren, J. 1999, Nature, 398, 400

Alloin, D., Collin-Souffrin, S., Joly, M., & Vigroux, L. 1979, A&A, 78, 200

Amati, L., Frontera, F., Tavani, M., in't Zand, J. J. M., Antonelli, A., Costa, E., Feroci, M., Guidorzi, C., Heise, J., Masetti, N., Montanari, E., Nicastro, L., Palazzi, E., Pian, E., Piro, L., & Soffitta, P. 2002, A&A, 390, 81

Asplund, M., Grevesse, N., Sauval, A. J., Allende Prieto, C., & Kiselman, D. 2004, A&A, 417, 751

Baba, H., Yasuda, N., Ichikawa, S.-I., Yagi, M., Iwamoto, N., Takata, T., Horaguchi, T., Taga, M., Watanabe, M., Okumura, S.-I., Ozawa, T., Yamamoto, N., & Hamabe, M. 2002, Report of the National Astronomical Observatory of Japan, 6, 23

Ballester, P., Dorigo, D., Disarò, A., Pizarro de La Iglesia, J. A., & Modigliani, A. 2000, in Astronomical Society of the Pacific Conference Series, Vol. 216, Astronomical Data Analysis Software and Systems IX, ed. N. Manset, C. Veillet, & D. Crabtree, 461

Band, D., Matteson, J., Ford, L., Schaefer, B., Palmer, D., Teegarden, B., Cline, T., Briggs, M., Paciesas, W., Pendleton, G., Fishman, G., Kouveliotou, C., Meegan, C., Wilson, R., & Lestrade, P. 1993, ApJ, 413, 281

Barth, A. J., Sari, R., Cohen, M. H., Goodrich, R. W., Price, P. A., Fox, D. W., Bloom, J. S., Soderberg, A. M., & Kulkarni, S. R. 2003, ApJ, 584, L47

Barthelmy, S. D., Butterworth, P., Cline, T. L., Gehrels, N., Fishman, G. J., Kouveliotou, C., & Meegan, C. A. 1995, Ap&SS, 231, 235

Beckman, J. E., Zurita, A., & Vega Beltrán, J. C. 2004, Lecture Notes and Essays in Astrophysics, vol. 1, p. 43-62., 1, 43

Belczynski, K., Perna, R., Bulik, T., Kalogera, V., Ivanova, N., & Lamb, D. Q. 2006, ApJ, 648, 1110

Berger, E. 2008, ArXiv: astro-ph/0805.0306, 1

Berger, E., Cowie, L. L., Kulkarni, S. R., Frail, D. A., Aussel, H., & Barger, A. J. 2003, ApJ, 588, 99

Berger, E., Fox, D. B., Price, P. A., Nakar, E., Gal-Yam, A., Holz, D. E., Schmidt, B. P., Cucchiara, A., Cenko, S. B., Kulkarni, S. R., Soderberg, A. M., Frail, D. A., Penprase, B. E., Rau, A., Ofek, E., Burnell, S. J. B., Cameron, P. B., Cowie, L. L., Dopita, M. A., Hook, I., Peterson, B. A., Podsiadlowski, P., Roth, K. C., Rutledge, R. E., Sheppard, S. S., & Songaila, A. 2007, ApJ, 664, 1000

Berger, E. & Gladders, M. 2006, GRB Coordinates Network, 5170

Berger, E., Kulkarni, S. R., Bloom, J. S., Price, P. A., Fox, D. W., Frail, D. A., Axelrod, T. S., Chevalier, R. A., Colbert, E., Costa, E., Djorgovski, S. G., Frontera, F., Galama, T. J., Halpern, J. P., Harrison, F. A., Holtzman, J., Hurley, K., Kimble, R. A., McCarthy, P. J., Piro, L., Reichart, D., Ricker, G. R., Sari, R., Schmidt, B. P., Wheeler, J. C., Vanderppek, R., & Yost, S. A. 2002, ApJ, 581, 981

Berger, E., Penprase, B. E., Cenko, S. B., Kulkarni, S. R., Fox, D. B., Steidel, C. C., & Reddy, N. A. 2006, ApJ, 642, 979

Berger, E., Price, P. A., Cenko, S. B., Gal-Yam, A., Soderberg, A. M., Kasliwal, M., Leonard, D. C., Cameron, P. B., Frail, D. A., Kulkarni, S. R., Murphy, D. C., Krzeminski, W., Piran, T., Lee, B. L., Roth, K. C., Moon, D.-S., Fox, D. B., Harrison, F. A., Persson, S. E., Schmidt, B. P., Penprase, B. E., Rich, J., Peterson, B. A., & Cowie, L. L. 2005, Nature, 438, 988

Bersier, D., Fruchter, A. S., Strolger, L.-G., Gorosabel, J., Levan, A., Burud, I., Rhoads, J. E., Becker, A. C., Cassan, A., Chornock, R., Covino, S., de Jong, R. S., Dominis, D., Filippenko, A. V., Hjorth, J., Holmberg, J., Malesani, D., Mobasher, B., Olsen, K. A. G., Stefanon, M., Castro Cerón, J. M., Fynbo, J. P. U., Holland, S. T., Kouveliotou, C., Pedersen, H., Tanvir, N. R., & Woosley, S. E. 2006, ApJ, 643, 284

Bertin, E. & Arnouts, S. 1996, A&AS, 117, 393

Beuermann, K., Hessman, F. V., Reinsch, K., Nicklas, H., Vreeswijk, P. M., Galama, T. J., Rol, E., van Paradijs, J., Kouveliotou, C., Frontera, F., Masetti, N., Palazzi, E., & Pian, E. 1999, A&A, 352, L26

Blake, C. H., Bloom, J. S., Starr, D. L., Falco, E. E., Skrutskie, M., Fenimore, E. E., Duchêne, G., Szentgyorgyi, A., Hornstein, S., Prochaska, J. X., McCabe, C., Ghez, A., Konopacky, Q., Stapelfeldt, K., Hurley, K., Campbell, R., Kassis, M., Chaffee, F., Gehrels, N., Barthelmy, S., Cummings, J. R., Hullinger, D., Krimm, H. A., Markwardt, C. B., Palmer, D., Parsons, A., McLean, K., & Tueller, J. 2005, Nature, 435, 181

Blanton, M. R., Dalcanton, J., Eisenstein, D., Loveday, J., Strauss, M. A., SubbaRao, M., Weinberg, D. H., Anderson, Jr., J. E., Annis, J., Bahcall, N. A., Bernardi, M., Brinkmann, J., Brunner, R. J., Burles, S., Carey, L., Castander, F. J., Connolly, A. J., Csabai, I., Doi, M., Finkbeiner, D., Friedman, S., Frieman, J. A., Fukugita, M., Gunn, J. E., Hennessy, G. S., Hindsley, R. B., Hogg, D. W., Ichikawa, T., Ivezić, Ž., Kent, S., Knapp, G. R., Lamb, D. Q., Leger, R. F., Long, D. C., Lupton, R. H., McKay, T. A., Meiksin, A., Merelli, A., Munn, J. A., Narayanan, V., Newcomb, M., Nichol, R. C., Okamura, S., Owen, R., Pier, J. R., Pope, A., Postman, M., Quinn, T., Rockosi, C. M., Schlegel, D. J., Schneider, D. P., Shimasaku, K., Siegmund, W. A., Smee, S., Snir, Y., Stoughton, C., Stubbs, C., Szalay, A. S., Szokoly, G. P., Thakar, A. R., Tremonti, C., Tucker, D. L., Uomoto, A., Vanden Berk, D., Vogeley, M. S., Waddell, P., Yanny, B., Yasuda, N., & York, D. G. 2001, AJ, 121, 2358

Bloom, J. S., Berger, E., Kulkarni, S. R., Djorgovski, S. G., & Frail, D. A. 2003, AJ, 125, 999

Bloom, J. S., Kulkarni, S. R., & Djorgovski, S. G. 2002, AJ, 123, 1111

Bloom, J. S., Prochaska, J. X., Pooley, D., Blake, C. H., Foley, R. J., Jha, S., Ramirez-Ruiz, E., Granot, J., Filippenko, A. V., Sigurdsson, S., Barth, A. J., Chen, H.-W., Cooper, M. C., Falco, E. E., Gal, R. R., Gerke, B. F., Gladders, M. D., Greene, J. E., Hennanwi, J., Ho, L. C., Hurley, K., Koester, B. P., Li, W., Lubin, L., Newman, J., Perley, D. A., Squires, G. K., & Wood-Vasey, W. M. 2006, ApJ, 638, 354

Boella, G., Butler, R. C., Perola, G. C., Piro, L., Scarsi, L., & Bleeker, J. A. M. 1997, A&AS, 122, 299

Boksenberg, A., Sargent, W. L. W., & Rauch, M. 2003, ArXiv:astro-ph/0307557

Bond, N. A., Churchill, C. W., Charlton, J. C., & Vogt, S. S. 2001, ApJ, 562, 641

Bornancini, C. G., Martínez, H. J., Lambas, D. G., Le Floc'h, E., Mirabel, I. F., & Minniti, D. 2004, ApJ, 614, 84

Botticella, M. T., Riello, M., Cappellaro, E., Benetti, S., Altavilla, G., Pastorello, A., Turatto, M., Greggio, L., Patat, F., Valenti, S., Zampieri, L., Harutyunyan, A., Pignata, G., & Taubenberger, S. 2008, A&A, 479, 49

Bouché, N., Murphy, M. T., Péroux, C., Csabai, I., & Wild, V. 2006, MNRAS, 371, 495

Bregman, J. N. 1980, ApJ, 236, 577

Bresolin, F., Garnett, D. R., & Kennicutt, Jr., R. C. 2004, ApJ, 615, 228

Briggs, M. S., Paciesas, W. S., Pendleton, G. N., Meegan, C. A., Fishman, G. J., Horack, J. M., Brock, M. N., Kouveliotou, C., Hartmann, D. H., & Hakkila, J. 1996, ApJ, 459, 40

Brinchmann, J., Kunth, D., & Durret, F. 2008, A&A, 485, 657

Broeils, A. H. & Rhee, M.-H. 1997, A&A, 324, 877

Bromm, V. & Loeb, A. 2002, ApJ, 575, 111

Brown, P. J., Campana, S., & Boyd, P. T. 2006, GRB Coordinates Network, 5172

Bruzual, G. & Charlot, S. 2003, MNRAS, 344, 1000

Burrows, D. N., Hill, J. E., Nousek, J. A., Kennea, J. A., Wells, A., Osborne, J. P., Abbey, A. F., Beardmore, A., Mukerjee, K., Short, A. D. T., Chincarini, G., Campana, S., Citterio, O., Moretti, A., Pagani, C., Tagliaferri, G., Giommi, P., Capalbi, M., Tamburelli, F., Angelini, L., Cusumano, G., Bräuninger, H. W., Burkert, W., & Hartner, G. D. 2005a, Space Science Reviews, 120, 165

Burrows, D. N., Romano, P., Falcone, A., Kobayashi, S., Zhang, B., Moretti, A., O'Brien, P. T., Goad, M. R., Campana, S., Page, K. L., Angelini, L., Barthelmy, S., Beardmore, A. P., Capalbi, M., Chincarini, G., Cummings, J., Cusumano, G., Fox, D., Giommi, P., Hill, J. E., Kennea, J. A., Krimm, H., Mangano, V., Marshall, F., Mészáros, P., Morris, D. C., Nousek, J. A., Osborne, J. P., Pagani, C., Perri, M., Tagliaferri, G., Wells, A. A., Woosley, S., & Gehrels, N. 2005b, Science, 309, 1833

Campana, S., Barthelmy, S. D., Boyd, P. T., Brown, P. J., Burrows, D. N., Cummings, J. R., Guidorzi, C. G., Holland, S. T., Kennea, J. A., Markwardt, C. B., Marshall, F. E., Moretti, A., Page, K. L., Stamatikos, M., Tagliaferri, G., & van den Berk, D. E. 2006, GRB Coordinates Network, 5162

Campana, S., Barthelmy, S. D., Burrows, D. N., Gehrels, N., Guidorzi, C., Kennea, J. A., Marshall, F. E., McLean, K. M., Moretti, A., Stamatikos, M., Tagliaferri, G., & vanden Berk, D. E. 2016, GRB Coordinates Network, 5163

Campana, S., Moretti, A., Guidorzi, C., Chincarini, G., & Burrows, D. N. 2007, GRB Coordinates Network, 5168

Cappellaro, E., Evans, R., & Turatto, M. 1999, A&A, 351, 459

Cappellaro, E., Riello, M., Altavilla, G., Botticella, M. T., Benetti, S., Clocchiatti, A., Danziger, J. I., Mazzali, P., Pastorello, A., Patat, F., Salvo, M., Turatto, M., & Valenti, S. 2005, A&A, 430, 83

Cappellaro, E., Turatto, M., Tsvetkov, D. Y., Bartunov, O. S., Pollas, C., Evans, R., & Hamuy, M. 1997, A&A, 322, 431

Cardelli, J. A., Clayton, G. C., & Mathis, J. S. 1989, ApJ, 345, 245

Castro, S., Galama, T. J., Harrison, F. A., Holtzman, J. A., Bloom, J. S., Djorgovski, S. G., & Kulkarni, S. R. 2003, ApJ, 586, 128

Castro Cerón, J. M. 2008, PhD thesis, http://www.astro.ku.dk/%7Ejosemari/DISSERTATION/

Castro Cerón, J. M., Michałowski, M. J., Hjorth, J., Malesani, D., Gorosabel, J., Watson, D., & Fynbo, J. P. U. 2008, ArXiv:astro-ph/0803.2235, 1

Castro Cerón, J. M., Michałowski, M. J., Hjorth, J., Watson, D., Fynbo, J. P. U., & Gorosabel, J. 2006, ApJ, 653, L85

Caulet, A. & Newell, R. 1996, ApJ, 465, 205

Cenko, S. B., Berger, E., Djorgovski, S. G., Mahabal, A. A., & Fox, D. B. 2006, GRB Coordinates Network, 5155

Chen, H.-W., Prochaska, J. X., Bloom, J. S., & Thompson, I. B. 2005, ApJ, 634, L25

Chen, H.-W., Prochaska, J. X., Ramirez-Ruiz, E., Bloom, J. S., Dessauges-Zavadsky, M., & Foley, R. J. 2007, ApJ, 663, 420

Chincarini, G., Moretti, A., Romano, P., Falcone, A. D., Morris, D., Racusin, J., Campana, S., Covino, S., Guidorzi, C., Tagliaferri, G., Burrows, D. N., Pagani, C., Stroh, M., Grupe, D., Capalbi, M., Cusumano, G., Gehrels, N., Giommi, P., La Parola, V., Mangano, V., Mineo, T., Nousek, J. A., O'Brien, P. T., Page, K. L., Perri, M., Troja, E., Willingale, R., & Zhang, B. 2007, ApJ, 671, 1903

Christensen, L., Hjorth, J., & Gorosabel, J. 2004, A&A, 425, 913

Christensen, L., Vreeswijk, P. M., Sollerman, J., Thöne, C. C., Le Floc´h, E., & Wiersema, K. 2008, A&A, in press

Churchill, C., Steidel, C., & Kacprzak, G. 2005, in Astronomical Society of the Pacific Conference Series, Vol. 331, Extra-Planar Gas, ed. R. Braun, 387

Churchill, C. W., Mellon, R. R., Charlton, J. C., Jannuzi, B. T., Kirhakos, S., Steidel, C. C., & Schneider, D. P. 2000, ApJ, 543, 577

Churchill, C. W., Vogt, S. S., & Charlton, J. C. 2003, AJ, 125, 98

Ciardi, B. & Loeb, A. 2000, ApJ, 540, 687

Cobb, B. E., Bailyn, C. D., van Dokkum, P. G., Buxton, M. M., & Bloom, J. S. 2004, ApJ, 608, L93

Colgate, S. A. 1968, Canadian Journal of Physics, 46, 476

Colless, M., Dalton, G., Maddox, S., Sutherland, W., Norberg, P., Cole, S., Bland-Hawthorn, J., Bridges, T., Cannon, R., Collins, C., Couch, W., Cross, N., Deeley, K., De Propris, R., Driver, S. P., Efstathiou, G., Ellis, R. S., Frenk, C. S., Glazebrook, K., Jackson, C., Lahav, O., Lewis, I., Lumsden, S., Madgwick, D., Peacock, J. A., Peterson, B. A., Price, I., Seaborne, M., & Taylor, K. 2001, MNRAS, 328, 1039

Conciatore, M. L., Capalbi, M., Vetere, L., Palmer, D., & Burrows, D. 2006, GRB Coordinates Network, 5114

Condon, J. J. 1992, ARA&A, 30, 575

Condon, J. J., Cotton, W. D., Greisen, E. W., Yin, Q. F., Perley, R. A., Taylor, G. B., & Broderick, J. J. 1998, AJ, 115, 1693

Cool, R. J., Eisenstein, D. J., Hogg, D. W., Blanton, M. R., Schlegel, D. J., Brinkmann, J., Schneider, D. P., & vanden Berk, D. E. 2006, GRB Coordinates Network, 4695

Costa, E., Frontera, F., Heise, J., Feroci, M., in't Zand, J., Fiore, F., Cinti, M. N., Dal Fiume, D., Nicastro, L., Orlandini, M., Palazzi, E., Rapisarda#, M., Zavattini, G., Jager, R., Parmar, A., Owens, A., Molendi, S., Cusumano, G., Maccarone, M. C., Giarrusso, S., Coletta, A., Antonelli, L. A., Giommi, P., Muller, J. M., Piro, L., & Butler, R. C. 1997, Nature, 387, 783

Covino, S., D'Avanzo, P., Klotz, A., Perley, D. A., Amati, L., Campana, S., Chincarini, G., Cucchiara, A., D'Elia, V., Guetta, D., Guidorzi, C., Kann, D. A., Küpcü Yoldaş, A., Misra, K., Olofsson, G., Tagliaferri, G., Antonelli, L. A., Berger, E., Bloom, J. S., Böer, M., Clemens, C., D'Alessio, F., Della Valle, M., di Serego Alighieri, S., Filippenko, A. V., Foley, R. J., Fox, D. B., Fugazza, D., Fynbo, J., Gendre, B., Goldoni, P., Greiner, J., Kocevksi, D., Maiorano, E., Masetti, N., Meurs, E., Modjaz, M., Molinari, E., Moretti, A., Palazzi, E., Pandey, S. B., Piranomonte, S., Poznanski, D., Primak, N., Romano, P., Rossi, E., Roy, R., Silverman, J. M., Stella, L., Stratta, G., Testa, V., Vergani, S. D., Vitali, F., & Zerbi, F. 2008, MNRAS, 699

Covino, S., Malesani, D., Israel, G. L., D'Avanzo, P., Antonelli, L. A., Chincarini, G., Fugazza, D., Conciatore, M. L., Della Valle, M., Fiore, F., Guetta, D., Hurley, K., Lazzati, D., Stella, L., Tagliaferri, G., Vietri, M., Campana, S., Burrows, D. N., D'Elia, V., Filliatre, P., Gehrels, N., Goldoni, P., Melandri, A., Mereghetti, S., Mirabel, I. F., Moretti, A., Nousek, J., O'Brien, P. T., Pellizza, L. J., Perna, R., Piranomonte, S., Romano, P., & Zerbi, F. M. 2006, A&A, 447, L5

Cox, N. L. J. & Patat, F. 2008, A&A, 485, L9

Cram, L., Hopkins, A., Mobasher, B., & Rowan-Robinson, M. 1998, ApJ, 507, 155

Crockett, R. M., Maund, J. R., Smartt, S. J., Mattila, S., Pastorello, A., Smoker, J., Stephens, A. W., Fynbo, J., Eldridge, J. J., Danziger, I. J., & Benn, C. R. 2008, ApJ, 672, L99

Crockett, R. M., Smartt, S. J., Eldridge, J. J., Mattila, S., Young, D. R., Pastorello, A., Maund, J. R., Benn, C. R., & Skillen, I. 2007, MNRAS, 381, 835

Crowther, P. A. 2007, ARA&A, 45, 177

Crowther, P. A., Dessart, L., Hillier, D. J., Abbott, J. B., & Fullerton, A. W. 2002, A&A, 392, 653

Curran, P. A., van der Horst, A. J., Wijers, R. A. M. J., Starling, R. L. C., Castro-Tirado, A. J., Fynbo, J. P. U., Gorosabel, J., Järvinen, A. S., Malesani, D., Rol, E., Tanvir, N. R., Wiersema, K., Burleigh, M. R., Casewell, S. L., Dobbie, P. D., Guziy, S., Jakobsson, P., Jelínek, M., Laursen, P., Levan, A. J., Mundell, C. G., Näränen, J., & Piranomonte, S. 2007, MNRAS, 381, L65

Cutri, R. M., Skrutskie, M. F., van Dyk, S., Beichman, C. A., Carpenter, J. M., Chester, T., Cambresy, L., Evans, T., Fowler, J., Gizis, J., Howard, E., Huchra, J., Jarrett, T., Kopan, E. L., Kirkpatrick, J. D., Light, R. M., Marsh, K. A., McCallon, H., Schneider, S., Stiening, R., Sykes, M., Weinberg, M., Wheaton, W. A., Wheelock, S., & Zacarias, N. 2003, 2MASS All Sky Catalog of point sources. (The IRSA 2MASS All-Sky Point Source Catalog, NASA/IPAC Infrared Science Archive. http://irsa.ipac.caltech.edu/applications/Gator/)

Dahlen, T., Strolger, L.-G., Riess, A. G., Mobasher, B., Chary, R.-R., Conselice, C. J., Ferguson, H. C., Fruchter, A. S., Giavalisco, M., Livio, M., Madau, P., Panagia, N., & Tonry, J. L. 2004, ApJ, 613, 189

Dai, X., Halpern, J. P., Morgan, N. D., Armstrong, E., Mirabal, N., Haislip, J. B., Reichart, D. E., & Stanek, K. Z. 2007, ApJ, 658, 509

Dai, Z. G. & Lu, T. 1998, MNRAS, 298, 87

de Ugarte Postigo, A., Castro-Tirado, A. J., Gorosabel, J., Jóhannesson, G., Björnsson, G., Gudmundsson, E. H., Bremer, M., Pak, S., Tanvir, N., Castro Cerón, J. M., Guzyi, S., Jelínek, M., Klose, S., Pérez-Ramírez, D., Aceituno, J., Campo Bagatín, A., Covino, S., Cardiel, N., Fathkullin, T., Henden, A. A., Huferath, S.,

Kurata, Y., Malesani, D., Mannucci, F., Ruiz-Lapuente, P., Sokolov, V., Thiele, U., Wisotzki, L., Antonelli, L. A., Bartolini, C., Boattini, A., Guarnieri, A., Piccioni, A., Pizzichini, G., del Principe, M., di Paola, A., Fugazza, D., Ghisellini, G., Hunt, L., Konstantinova, T., Masetti, N., Palazzi, E., Pian, E., Stefanon, M., Testa, V., & Tristram, P. J. 2005, A&A, 443, 841

de Vaucouleurs, G., de Vaucouleurs, A., Corwin, Jr., H. G., Buta, R. J., Paturel, G., & Fouque, P. 1991, Third Reference Catalogue of Bright Galaxies (Volume 1-3, XII, 2069 pp. 7 figs.. Springer-Verlag Berlin Heidelberg New York)

Dekker, H., D'Odorico, S., Kaufer, A., Delabre, B., & Kotzlowski, H. 2000, in Presented at the Society of Photo-Optical Instrumentation Engineers (SPIE) Conference, Vol. 4008, Proc. SPIE Vol. 4008, p. 534-545, Optical and IR Telescope Instrumentation and Detectors, Masanori Iye; Alan F. Moorwood; Eds., ed. M. Iye & A. F. Moorwood, 534–545

D'Elia, V., Fiore, F., Meurs, E. J. A., Chincarini, G., Melandri, A., Norci, L., Pellizza, L., Perna, R., Piranomonte, S., Sbordone, L., Stella, L., Tagliaferri, G., Vergani, S. D., Ward, P., Angelini, L., Antonelli, L. A., Burrows, D. N., Campana, S., Capalbi, M., Cimatti, A., Costa, E., Cusumano, G., Della Valle, M., Filliatre, P., Fontana, A., Frontera, F., Fugazza, D., Gehrels, N., Giannini, T., Giommi, P., Goldoni, P., Guetta, D., Israel, G., Lazzati, D., Malesani, D., Marconi, G., Mason, K., Mereghetti, S., Mirabel, F., Molinari, E., Moretti, A., Nousek, J., Perri, M., Piro, L., Stratta, G., Testa, V., & Vietri, M. 2007, A&A, 467, 629

Deng, J. & Zhu, Y. 2008, GRB Coordinates Network, 7160, 1

Denicoló, G., Terlevich, R., & Terlevich, E. 2002, MNRAS, 330, 69

Dessauges-Zavadsky, M., Prochaska, J. X., & D'Odorico, S. 2002, A&A, 391, 801

Dey, A., Soifer, B. T., Desai, V., Brand, K., Le Floc'h, E., Brown, M. J. I., Jannuzi, B. T., Armus, L., Bussmann, S., Brodwin, M., Bian, C., Eisenhardt, P., Higdon, S. J., Weedman, D., & Willner, S. P. 2008, ApJ, 677, 943

Dickey, J. M. & Lockman, F. J. 1990, ARA&A, 28, 215

Dilday, B., Kessler, R., Frieman, J. A., Holtzman, J., Marriner, J., Miknaitis, G., Nichol, R. C., Romani, R., Sako, M., Bassett, B., Becker, A., Cinabro, D., DeJongh, F., Depoy, D. L., Doi, M., Garnavich, P. M., Hogan, C. J., Jha, S., Konishi, K., Lampeitl, H., Marshall, J. L., McGinnis, D., Prieto, J. L., Riess, A. G., Richmond, M. W., Schneider, D. P., Smith, M., Takanashi, N., Tokita, K., van der Heyden, K., Zheng, N. Y. C., Barentine, J., Brewington, H., Choi, C., Crotts, A., Dembicky, J., Harvanek, M., Im, M., Ketzeback, W., Kleinman, S. J., Krzesiński, J., Long, D. C., Malanushenko, E., Malanushenko, V., McMillan, R. J., Nitta, A., Pan, K., Saurage, G., Snedden, S. A., Watters, S., Wheeler, J. C., & York, D. 2008, ArXiv: astro-ph/0801.3297, 1

Dong, X. Y. & De Robertis, M. M. 2006, AJ, 131, 1236

Dressel, L. L. & Condon, J. J. 1978, ApJS, 36, 53

Ellison, S. L. 2006, MNRAS, 368, 335

Ellison, S. L., Mallén-Ornelas, G., & Sawicki, M. 2003, ApJ, 589, 709

Ellison, S. L., Vreeswijk, P., Ledoux, C., Willis, J. P., Jaunsen, A., Wijers, R. A. M. J., Smette, A., Fynbo, J. P. U., Møller, P., Hjorth, J., & Kaufer, A. 2006, MNRAS, 372, L38

Erb, D. K., Shapley, A. E., Pettini, M., Steidel, C. C., Reddy, N. A., & Adelberger, K. L. 2006, ApJ, 644, 813

Evans, P. A., Beardmore, A. P., Page, K. L., Tyler, L. G., Osborne, J. P., Goad, M. R., O'Brien, P. T., Vetere, L., Racusin, J., Morris, D., Burrows, D. N., Capalbi, M., Perri, M., Gehrels, N., & Romano, P. 2007, A&A, 469, 379

Ferrero, P., Klose, S., Kann, D. A., Savaglio, S., Palazzi, E., Maiorano, E., Böhm, P., Schulze, S., Grupe, D., Oates, S. R., Sánchez, S. F., Amati, L., Greiner, J., Hjorth, J., Malesani, D., Barthelmy, S. D., Gorosabel, J., Masetti, N., & Roth, M. M. 2008, ArXiv:astro-ph/0804.2457, 1

Filippenko, A. V., Li, W. D., Treffers, R. R., & Modjaz, M. 2001, in Astronomical Society of the Pacific Conference Series, Vol. 246, IAU Colloq. 183: Small Telescope Astronomy on Global Scales, ed. B. Paczynski, W.-P. Chen, & C. Lemme, 121–+

Fiore, F., D'Elia, V., Lazzati, D., Perna, R., Sbordone, L., Stratta, G., Meurs, E. J. A., Ward, P., Antonelli, L. A., Chincarini, G., Covino, S., Di Paola, A., Fontana, A., Ghisellini, G., Israel, G., Frontera, F., Marconi, G., Stella, L., Vietri, M., & Zerbi, F. 2005, ApJ, 624, 853

Fishman, G. J., Meegan, C. A., Wilson, R. B., & et al. 1989, in Goddard Space Flight Center, Greenbelt, MD, USA, Vol. 353, Proc. GRO Science Workshop, April 10 - 12, 1989, ed. W. N. Johnson, 2–39

Foley, S., Watson, D., Gorosabel, J., Fynbo, J. P. U., Sollerman, J., McGlynn, S., McBreen, B., & Hjorth, J. 2006, A&A, 447, 891

Fontana, A. & Ballester, P. 1995, The Messenger, 80, 37

Förster Schreiber, N. M., Genzel, R., Lehnert, M. D., Bouché, N., Verma, A., Erb, D. K., Shapley, A. E., Steidel, C. C., Davies, R., Lutz, D., Nesvadba, N., Tacconi, L. J., Eisenhauer, F., Abuter, R., Gilbert, A., Gillessen, S., & Sternberg, A. 2006, ApJ, 645, 1062

Fox, D. B., Frail, D. A., Price, P. A., Kulkarni, S. R., Berger, E., Piran, T., Soderberg, A. M., Cenko, S. B., Cameron, P. B., Gal-Yam, A., Kasliwal, M. M., Moon, D.-S., Harrison, F. A., Nakar, E., Schmidt, B. P., Penprase, B., Chevalier, R. A., Kumar, P., Roth, K., Watson, D., Lee, B. L., Shectman, S., Phillips, M. M., Roth, M., McCarthy, P. J., Rauch, M., Cowie, L., Peterson, B. A., Rich, J., Kawai, N., Aoki, K., Kosugi, G., Totani, T., Park, H.-S., MacFadyen, A., & Hurley, K. C. 2005, Nature, 437, 845

Frail, D. A., Cameron, P. B., Kasliwal, M., Nakar, E., Price, P. A., Berger, E., Gal-Yam, A., Kulkarni, S. R., Fox, D. B., Soderberg, A. M., Schmidt, B. P., Ofek, E., & Cenko, S. B. 2006, ApJ, 646, L99

Frail, D. A., Kulkarni, S. R., Nicastro, L., Feroci, M., & Taylor, G. B. 1997, Nature, 389, 261

Frail, D. A., Kulkarni, S. R., Sari, R., Djorgovski, S. G., Bloom, J. S., Galama, T. J., Reichart, D. E., Berger, E., Harrison, F. A., Price, P. A., Yost, S. A., Diercks, A., Goodrich, R. W., & Chaffee, F. 2001, ApJ, 562, L55

French, J. & Jelinek, M. 2006, GRB Coordinates Network, 5165

Fruchter, A. S., Levan, A. J., Strolger, L., Vreeswijk, P. M., Thorsett, S. E., Bersier, D., Burud, I., Castro Cerón, J. M., Castro-Tirado, A. J., Conselice, C., Dahlen, T., Ferguson, H. C., Fynbo, J. P. U., Garnavich, P. M., Gibbons, R. A., Gorosabel, J., Gull, T. R., Hjorth, J., Holland, S. T., Kouveliotou, C., Levay, Z., Livio, M., Metzger, M. R., Nugent, P. E., Petro, L., Pian, E., Rhoads, J. E., Riess, A. G., Sahu, K. C., Smette, A., Tanvir, N. R., Wijers, R. A. M. J., & Woosley, S. E. 2006, Nature, 441, 463

Fryer, C. L., Mazzali, P. A., Prochaska, J., Cappellaro, E., Panaitescu, A., Berger, E., van Putten, M., van den Heuvel, E. P. J., Young, P., Hungerford, A., Rockefeller, G., Yoon, S.-C., Podsiadlowski, P., Nomoto, K., Chevalier, R., Schmidt, B., & Kulkarni, S. 2007, PASP, 119, 1211

Fryer, C. L., Young, P. A., & Hungerford, A. L. 2006, ApJ, 650, 1028

Fukugita, M., Shimasaku, K., & Ichikawa, T. 1995, PASP, 107, 945

Fynbo, J. P. U., Jakobsson, P., Möller, P., Hjorth, J., Thomsen, B., Andersen, M. I., Fruchter, A. S., Gorosabel, J., Holland, S. T., Ledoux, C., Pedersen, H., Rhoads, J., Weidinger, M., & Wijers, R. A. M. J. 2003a, A&A, 406, L63

Fynbo, J. P. U., Ledoux, C., Möller, P., Thomsen, B., & Burud, I. 2003b, A&A, 407, 147

Fynbo, J. P. U., Malesani, D., Augusteijn, T., & Niemi, S.-M. 2008a, GRB Coordinates Network, 7186

Fynbo, J. P. U., Möller, P., Thomsen, B., Hjorth, J., Gorosabel, J., Andersen, M. I., Egholm, M. P., Holland, S., Jensen, B. L., Pedersen, H., & Weidinger, M. 2002, A&A, 388, 425

Fynbo, J. P. U., Prochaska, J. X., Sommer-Larsen, J., Dessauges-Zavadsky, M., & Moller, P. 2008b, ArXiv:astro-ph/0801.3273, 801

Fynbo, J. P. U., Starling, R. L. C., Ledoux, C., Wiersema, K., Thöne, C. C., Sollerman, J., Jakobsson, P., Hjorth, J., Watson, D., Vreeswijk, P. M., Møller, P., Rol, E., Gorosabel, J., Näränen, J., Wijers, R. A. M. J., Björnsson, G., Castro Cerón, J. M., Curran, P., Hartmann, D. H., Holland, S. T., Jensen, B. L., Levan, A. J., Limousin, M., Kouveliotou, C., Nelemans, G., Pedersen, K., Priddey, R. S., & Tanvir, N. R. 2006a, A&A, 451, L47

Fynbo, J. P. U., Watson, D., Thöne, C. C., Sollerman, J., Bloom, J. S., Davis, T. M., Hjorth, J., Jakobsson, P., Jørgensen, U. G., Graham, J. F., Fruchter, A. S., Bersier, D., Kewley, L., Cassan, A., Castro Cerón, J. M., Foley, S., Gorosabel, J., Hinse, T. C., Horne, K. D., Jensen, B. L., Klose, S., Kocevski, D., Marquette, J.-B., Perley, D., Ramirez-Ruiz, E., Stritzinger, M. D., Vreeswijk, P. M., Wijers, R. A. M., Woller, K. G., Xu, D., & Zub, M. 2006b, Nature, 444, 1047

Fynbo, J. U., Holland, S., Andersen, M. I., Thomsen, B., Hjorth, J., Björnsson, G., Jaunsen, A. O., Natarajan, P., & Tanvir, N. 2000, ApJ, 542, L89

Gal-Yam, A., Leonard, D. C., Fox, D. B., Cenko, S. B., Soderberg, A. M., Moon, D.-S., Sand, D. J., Li, W., Filippenko, A. V., Aldering, G., & Copin, Y. 2007, ApJ, 656, 372

Gal-Yam, A., Moon, D.-S., Fox, D. B., Soderberg, A. M., Kulkarni, S. R., Berger, E., Cenko, S. B., Yost, S., Frail, D. A., Sako, M., Freedman, W. L., Persson, S. E., Wyatt, P., Murphy, D. C., Phillips, M. M., Suntzeff, N. B., Mazzali, P. A., & Nomoto, K. 2004, ApJ, 609, L59

Galama, T. J., Vreeswijk, P. M., van Paradijs, J., Kouveliotou, C., Augusteijn, T., Böhnhardt, H., Brewer, J. P., Doublier, V., Gonzalez, J.-F., Leibundgut, B., Lidman, C., Hainaut, O. R., Patat, F., Heise, J., in't Zand, J., Hurley, K., Groot, P. J., Strom, R. G., Mazzali, P. A., Iwamoto, K., Nomoto, K., Umeda, H., Nakamura, T., Young, T. R., Suzuki, T., Shigeyama, T., Koshut, T., Kippen, M., Robinson, C., de Wildt, P., Wijers, R. A. M. J., Tanvir, N., Greiner, J., Pian, E., Palazzi, E., Frontera, F., Masetti, N., Nicastro, L., Feroci, M., Costa, E., Piro, L., Peterson, B. A., Tinney, C., Boyle, B., Cannon, R., Stathakis, R., Sadler, E., Begam, M. C., & Ianna, P. 1998, Nature, 395, 670

Gehrels, N., Chincarini, G., Giommi, P., Mason, K. O., Nousek, J. A., Wells, A. A., White, N. E., Barthelmy, S. D., Burrows, D. N., Cominsky, L. R., Hurley, K. C., Marshall, F. E., Mészáros, P., Roming, P. W. A., Angelini, L., Barbier, L. M., Belloni, T., Campana, S., Caraveo, P. A., Chester, M. M., Citterio, O., Cline, T. L., Cropper, M. S., Cummings, J. R., Dean, A. J., Feigelson, E. D., Fenimore, E. E., Frail, D. A., Fruchter, A. S., Garmire, G. P., Gendreau, K., Ghisellini, G., Greiner, J., Hill, J. E., Hunsberger, S. D., Krimm, H. A., Kulkarni, S. R., Kumar, P., Lebrun, F., Lloyd-Ronning, N. M., Markwardt, C. B., Mattson, B. J., Mushotzky, R. F., Norris, J. P., Osborne, J., Paczyński, B., Palmer, D. M., Park, H.-S., Parsons, A. M., Paul, J., Rees, M. J., Reynolds, C. S., Rhoads, J. E., Sasseen, T. P., Schaefer, B. E., Short, A. T., Smale, A. P., Smith, I. A., Stella, L., Tagliaferri, G., Takahashi, T., Tashiro, M., Townsley, L. K., Tueller, J., Turner, M. J. L., Vietri, M., Voges, W., Ward, M. J., Willingale, R., Zerbi, F. M., & Zhang, W. W. 2004, ApJ, 611, 1005

Gezari, S., Dessart, L., Basa, S., Martin, D. C., Neill, J. D., Woosley, S. E., Hillier, D. J., Bazin, G., Forster, K., Friedman, P. G., Le Du, J., Mazure, A., Morrissey, P., Neff, S. G., Schiminovich, D., & Wyder, T. K. 2008, ArXiv:astro-ph/0804.1123, 804

Ghirlanda, G., Ghisellini, G., & Lazzati, D. 2004, ApJ, 616, 331

Gilmozzi, R., Cassatella, A., Clavel, J., Fransson, C., Gonzalez, R., Gry, C., Panagia, N., Talavera, A., & Wamsteker, W. 1987, Nature, 328, 318

Gladders, M., Berger, E., Morrell, N., & Roth, M. 2005, GRB Coordinates Network, 3798

Gonzalez Delgado, R. M., Leitherer, C., & Heckman, T. 1997, ApJ, 489, 601

Gorosabel, J., Castro-Tirado, A. J., Ramirez-Ruiz, E., Granot, J., Caon, N., Cairós, L. M., Rubio-Herrera, E., Guziy, S., de Ugarte Postigo, A., & Jelínek, M. 2006, ApJ, 641, L13

Gorosabel, J., Pérez-Ramírez, D., Sollerman, J., de Ugarte Postigo, A., Fynbo, J. P. U., Castro-Tirado, A. J., Jakobsson, P., Christensen, L., Hjorth, J., Jóhannesson, G., Guziy, S., Castro Cerón, J. M., Björnsson, G., Sokolov, V. V., Fatkhullin, T. A., & Nilsson, K. 2005, A&A, 444, 711

Greiner, J., Klose, S., Reinsch, K., Martin Schmid, H., Sari, R., Hartmann, D. H., Kouveliotou, C., Rau, A., Palazzi, E., Straubmeier, C., Stecklum, B., Zharikov, S., Tovmassian, G., Bärnbantner, O., Ries, C., Jehin, E., Henden, A., Kaas, A. A., Grav, T., Hjorth, J., Pedersen, H., Wijers, R. A. M. J., Kaufer, A., Park, H.-S., Williams, G., & Reimer, O. 2003a, Nature, 426, 157

Greiner, J., Peimbert, M., Estaban, C., Kaufer, A., Jaunsen, A., Smoke, J., Klose, S., & Reimer, O. 2003b, GRB Coordinates Network, 2020

Grupe, D., Gronwall, C., Wang, X.-Y., Roming, P. W. A., Cummings, J., Zhang, B., Mészáros, P., Trigo, M. D., O'Brien, P. T., Page, K. L., Beardmore, A., Godet, O., vanden Berk, D. E., Brown, P. J., Koch, S., Morris, D., Stroh, M., Burrows, D. N., Nousek, J. A., McMath Chester, M., Immler, S., Mangano, V., Romano, P., Chincarini, G., Osborne, J., Sakamoto, T., & Gehrels, N. 2007, ApJ, 662, 443

Gull, T. R., Vieira, G., Bruhweiler, F., Nielsen, K. E., Verner, E., & Danks, A. 2005, ApJ, 620, 442

Haislip, J. B., Nysewander, M. C., Reichart, D. E., Levan, A., Tanvir, N., Cenko, S. B., Fox, D. B., Price, P. A., Castro-Tirado, A. J., Gorosabel, J., Evans, C. R., Figueredo, E., MacLeod, C. L., Kirschbrown, J. R., Jelinek, M., Guziy, S., Postigo, A. D. U., Cypriano, E. S., Lacluyze, A., Graham, J., Priddey, R., Chapman, R., Rhoads, J., Fruchter, A. S., Lamb, D. Q., Kouveliotou, C., Wijers, R. A. M. J., Bayliss, M. B., Schmidt, B. P., Soderberg, A. M., Kulkarni, S. R., Harrison, F. A., Moon, D. S., Gal-Yam, A., Kasliwal, M. M., Hudec, R., Vitek, S., Kubanek, P., Crain, J. A., Foster, A. C., Clemens, J. C., Bartelme, J. W., Canterna, R., Hartmann, D. H., Henden, A. A., Klose, S., Park, H.-S., Williams, G. G., Rol, E., O'Brien, P., Bersier, D., Prada, F., Pizarro, S., Maturana, D., Ugarte, P., Alvarez, A., Fernandez, A. J. M., Jarvis, M. J., Moles, M., Alfaro, E., Ivarsen, K. M., Kumar, N. D., Mack, C. E., Zdarowicz, C. M., Gehrels, N., Barthelmy, S., & Burrows, D. N. 2006, Nature, 440, 181

Hall, P. B., Anderson, S. F., Strauss, M. A., York, D. G., Richards, G. T., Fan, X., Knapp, G. R., Schneider, D. P., Vanden Berk, D. E., Geballe, T. R., Bauer, A. E., Becker, R. H., Davis, M., Rix, H.-W., Nichol, R. C., Bahcall, N. A., Brinkmann, J., Brunner, R., Connolly, A. J., Csabai, I., Doi, M., Fukugita, M., Gunn, J. E., Haiman, Z., Harvanek, M., Heckman, T. M., Hennessy, G. S., Inada, N., Ivezić, Ž., Johnston, D., Kleinman, S., Krolik, J. H., Krzesinski, J., Kunszt, P. Z., Lamb, D. Q., Long, D. C., Lupton, R. H., Miknaitis, G., Munn, J. A., Narayanan, V. K., Neilsen, E., Newman, P. R., Nitta, A., Okamura, S., Pentericci, L., Pier, J. R., Schlegel, D. J., Snedden, S., Szalay, A. S., Thakar, A. R., Tsvetanov, Z., White, R. L., & Zheng, W. 2002, ApJS, 141, 267

Halpern, J. P., Armstrong, E., Campana, S., & Mirabal, N. 2006a, GRB Coordinates Network, 5176

Halpern, J. P., Armstrong, E., & Mirabal, N. 2006b, GRB Coordinates Network, 5188

Hammer, F., Flores, H., Schaerer, D., Dessauges-Zavadsky, M., Le Floc'h, E., & Puech, M. 2006, A&A, 454, 103

Hanuschik, R. W. 2003, A&A, 407, 1157

Hao, H., Stanek, K. Z., Dobrzycki, A., Matheson, T., Bentz, M. C., Kuraszkiewicz, J., Garnavich, P. M., Howk, J. C., Calkins, M. L., Worthey, G., Modjaz, M., & Serven, J. 2007, ApJ, 659, L99

Heavens, A., Panter, B., Jimenez, R., & Dunlop, J. 2004, Nature, 428, 625

Heckman, T. M., Lehnert, M. D., Strickland, D. K., & Armus, L. 2000, ApJS, 129, 493

Heckman, T. M., Sembach, K. R., Meurer, G. R., Strickland, D. K., Martin, C. L., Calzetti, D., & Leitherer, C. 2001, ApJ, 554, 1021

Heger, A., Fryer, C. L., Woosley, S. E., Langer, N., & Hartmann, D. H. 2003, ApJ, 591, 288

Hendry, M. A., Smartt, S. J., Crockett, R. M., Maund, J. R., Gal-Yam, A., Moon, D.-S., Cenko, S. B., Fox, D. W., Kudritzki, R. P., Benn, C. R., & Østensen, R. 2006, MNRAS, 369, 1303

Hjorth, J., Sollerman, J., Gorosabel, J., Granot, J., Klose, S., Kouveliotou, C., Melinder, J., Ramirez-Ruiz, E., Starling, R., Thomsen, B., Andersen, M. I., Fynbo, J. P. U., Jensen, B. L., Vreeswijk, P. M., Castro Cerón, J. M., Jakobsson, P., Levan, A., Pedersen, K., Rhoads, J. E., Tanvir, N. R., Watson, D., & Wijers, R. A. M. J. 2005a, ApJ, 630, L117

Hjorth, J., Sollerman, J., Møller, P., Fynbo, J. P. U., Woosley, S. E., Kouveliotou, C., Tanvir, N. R., Greiner, J., Andersen, M. I., Castro-Tirado, A. J., Castro Cerón, J. M., Fruchter, A. S., Gorosabel, J., Jakobsson, P., Kaper, L., Klose, S., Masetti, N., Pedersen, H., Pedersen, K., Pian, E., Palazzi, E., Rhoads, J. E., Rol, E., van den Heuvel, E. P. J., Vreeswijk, P. M., Watson, D., & Wijers, R. A. M. J. 2003, Nature, 423, 847

Hjorth, J., Watson, D., Fynbo, J. P. U., Price, P. A., Jensen, B. L., Jørgensen, U. G., Kubas, D., Gorosabel, J., Jakobsson, P., Sollerman, J., Pedersen, K., & Kouveliotou, C. 2005b, Nature, 437, 859

Ho, L. C., Filippenko, A. V., & Sargent, W. L. W. 1997, ApJS, 112, 315

Huang, Y. F., Cheng, K. S., & Gao, T. T. 2006, ApJ, 637, 873

Hullinger, D., Barbier, L., Barthelmy, S., Cummings, J., Fenimore, E., Gehrels, N., Krimm, H., Koss, M., Markwardt, C., Palmer, D., Parsons, A., Sakamoto, T., Sato, G., Stamatikos, M., & Tueller, J. 2006, GRB Coordinates Network, 5142

Hurley, K., Dingus, B. L., Mukherjee, R., Sreekumar, P., Kouveliotou, C., Meegan, C., Fishman, G. J., Band, D., Ford, L., Bertsch, D., Cline, T., Fichtel, C., Hartman, R., Hunter, S., Thompson, D. J., Kanbach, G., Mayer-Hasselwander, H., von Montigny, C., Sommer, M., Lin, Y., Nolan, P., Michelson, P., Kniffen, D., Mattox, J., Schneid, E., Boer, M., & Niel, M. 1994, Nature, 372, 652

Hurley, K., Mitrofanov, I., Kozyrev, A., Litvak, M., Grinkov, A. S. V., Charyshnikov, S., Boynton, W., Fellows, C., Harshman, K., Hamara, D., Shinohara, C., Starr, R., & Cline, T. 2006, ApJS, 164, 124

Izotov, Y. I., Papaderos, P., Guseva, N. G., Fricke, K. J., & Thuan, T. X. 2006a, A&A, 454, 137

Izotov, Y. I., Stasińska, G., Meynet, G., Guseva, N. G., & Thuan, T. X. 2006b, A&A, 448, 955

Jakobsson, P., Björnsson, G., Fynbo, J. P. U., Jóhannesson, G., Hjorth, J., Thomsen, B., Møller, P., Watson, D., Jensen, B. L., Östlin, G., Gorosabel, J., & Gudmundsson, E. H. 2005, MNRAS, 362, 245

Jakobsson, P., Fynbo, J. P. U., Ledoux, C., Vreeswijk, P., Kann, D. A., Hjorth, J., Priddey, R. S., Tanvir, N. R., Reichart, D., Gorosabel, J., Klose, S., Watson, D., Sollerman, J., Fruchter, A. S., de Ugarte Postigo, A., Wiersema, K., Björnsson, G., Chapman, R., Thöne, C. C., Pedersen, K., & Jensen, B. L. 2006a, A&A, 460, L13

Jakobsson, P., Hjorth, J., Fynbo, J. P. U., Watson, D., Pedersen, K., Björnsson, G., & Gorosabel, J. 2004a, ApJ, 617, L21

Jakobsson, P., Hjorth, J., Fynbo, J. P. U., Weidinger, M., Gorosabel, J., Ledoux, C., Watson, D., Björnsson, G., Gudmundsson, E. H., Wijers, R. A. M. J., Möller, P., Pedersen, K., Sollerman, J., Henden, A. A., Jensen, B. L., Gilmore, A., Kilmartin, P., Levan, A., Castro Cerón, J. M., Castro-Tirado, A. J., Fruchter, A., Kouveliotou, C., Masetti, N., & Tanvir, N. 2004b, A&A, 427, 785

Jakobsson, P., Levan, A., Fynbo, J. P. U., Priddey, R., Hjorth, J., Tanvir, N., Watson, D., Jensen, B. L., Sollerman, J., Natarajan, P., Gorosabel, J., Castro Cerón, J. M., Pedersen, K., Pursimo, T., Árnadóttir, A. S., Castro-Tirado, A. J., Davis, C. J., Deeg, H. J., Fiuza, D. A., Mykolaitis, S., & Sousa, S. G. 2006b, A&A, 447, 897

Jester, S., Schneider, D. P., Richards, G. T., Green, R. F., Schmidt, M., Hall, P. B., Strauss, M. A., Vanden Berk, D. E., Stoughton, C., Gunn, J. E., Brinkmann, J., Kent, S. M., Smith, J. A., Tucker, D. L., & Yanny, B. 2005, AJ, 130, 873

Jóhannesson, G., Björnsson, G., & Gudmundsson, E. H. 2006, ApJ, 647, 1238

Juneau, S., Glazebrook, K., Crampton, D., McCarthy, P. J., Savaglio, S., Abraham, R., Carlberg, R. G., Chen, H.-W., Le Borgne, D., Marzke, R. O., Roth, K., Jørgensen, I., Hook, I., & Murowinski, R. 2005, ApJ, 619, L135

Kann, D. A. 2007, GRB Coordinates Network, 6209

Kann, D. A., Klose, S., & Zeh, A. 2006, ApJ, 641, 993

Kann, D. A., Klose, S., Zhang, B., Malesani, D., Nakar, E., Wilson, A. C., Butler, N. R., Antonelli, L. A., Chincarini, G., Cobb, B. E., Covino, S., D'Avanzo, P., D'Elia, V., Della Valle, M., Ferrero, P., Fugazza, D., Gorosabel, J., Israel, G. L., Mannucci, F., Piranomonte, S., Schulze, S., Stella, L., Tagliaferri, G., & Wiersema, K. 2007, ArXiv:astro-ph/0712.2186, 712

Kann, D. A., Klose, S., Zhang, B., Wilson, A. C., Butler, N. R., Malesani, D., Nakar, E., Antonelli, L. A., Chincarini, G., Cobb, B. E., Covino, S., D'Avanzo, P., D'Elia, V., Della Valle, M., Ferrero, P., Fugazza, D., Gorosabel, J., Israel, . L., Mannucci, F., Piranomonte, S., Schulze, S., Stella, L., Tagliaferri, G., & Wiersema, K. 2008, ArXiv:astro-ph/0804.1959, 804

Kasliwal, M. M., Cenko, S. B., Kulkarni, S. R., Cameron, P. B., Nakar, E., Ofek, E. O., Rau, A., Soderberg, A. M., Campana, S., Bloom, J. S., Perley, D. A., Pollack, L. K., Barthelmy, S., Cummings, J., Gehrels, N., Krimm, H. A., Markwardt, C. B., Sato, G., Chandra, P., Frail, D., Fox, D. B., Price, P. A., Berger, E., Grebenev, S. A., Krivonos, R. A., & Sunyaev, R. A. 2008, ApJ, 678, 1127

Kawai, N., Kosugi, G., Aoki, K., Yamada, T., Totani, T., Ohta, K., Iye, M., Hattori, T., Aoki, W., Furusawa, H., Hurley, K., Kawabata, K. S., Kobayashi, N., Komiyama, Y., Mizumoto, Y., Nomoto, K., Noumaru, J., Ogasawara, R., Sato, R., Sekiguchi, K., Shirasaki, Y., Suzuki, M., Takata, T., Tamagawa, T., Terada, H., Watanabe, J., Yatsu, Y., & Yoshida, A. 2006, Nature, 440, 184

Kelly, P. L., Kirshner, R. P., & Pahre, M. 2007, ArXiv:astro-ph/0712.0430, 712

Kennicutt, Jr., R. C. 1992a, ApJS, 79, 255

—. 1992b, ApJ, 388, 310

—. 1998, ARA&A, 36, 189

Kewley, L. J., Brown, W. R., Geller, M. J., Kenyon, S. J., & Kurtz, M. J. 2007, AJ, 133, 882

Kewley, L. J. & Dopita, M. A. 2002, ApJS, 142, 35

Khamitov, I. M., Burenin, R. A., Bikmaev, I. F., Sakhibullin, N. A., Pavlinsky, M. N., Sunyaev, R. A., & Aslan, Z. 2007, Astronomy Letters, 33, 797

King, A., Olsson, E., & Davies, M. B. 2007, MNRAS, 374, L34

Klebesadel, R. W., Strong, I. B., & Olson, R. A. 1973, ApJ, 182, L85

Klose, S., Greiner, J., Rau, A., Henden, A. A., Hartmann, D. H., Zeh, A., Ries, C., Masetti, N., Malesani, D., Guenther, E., Gorosabel, J., Stecklum, B., Antonelli, L. A., Brinkworth, C., Castro Cerón, J. M., Castro-Tirado, A. J., Covino, S., Fruchter, A., Fynbo, J. P. U., Ghisellini, G., Hjorth, J., Hudec, R., Jelínek, M., Kaper, L., Kouveliotou, C., Lindsay, K., Maiorano, E., Mannucci, F., Nysewander, M., Palazzi, E., Pedersen, K., Pian, E., Reichart, D. E., Rhoads, J., Rol, E., Smail, I., Tanvir, N. R., de Ugarte Postigo, A., Vreeswijk, P. M., Wijers, R. A. M. J., & van den Heuvel, E. P. J. 2004, AJ, 128, 1942

Kobulnicky, H. A., Kennicutt, Jr., R. C., & Pizagno, J. L. 1999, ApJ, 514, 544

Kobulnicky, H. A. & Kewley, L. J. 2004, ApJ, 617, 240

Kocevski, D. & Butler, N. 2008, ApJ, 680, 531

Kouveliotou, C., Meegan, C. A., Fishman, G. J., Bhat, N. P., Briggs, M. S., Koshut, T. M., Paciesas, W. S., & Pendleton, G. N. 1993, ApJ, 413, L101

Krimm, H. A., Granot, J., Marshall, F. E., Perri, M., Barthelmy, S. D., Burrows, D. N., Gehrels, N., Mészáros, P., & Morris, D. 2007, ApJ, 665, 554

Krühler, T., Küpcü Yoldaş, A., Greiner, J., Clemens, C., McBreen, S., Primak, N., Savaglio, S., Yoldaş, A., & Szokoly, G. P. 2008, ArXiv:astro-ph/0805.2824, 1

Kulkarni, S. R. 2005, ArXiv:astro-ph/0510256

Kulkarni, S. R., Djorgovski, S. G., Ramaprakash, A. N., Goodrich, R., Bloom, J. S., Adelberger, K. L., Kundic, T., Lubin, L., Frail, D. A., Frontera, F., Feroci, M., Nicastro, L., Barth, A. J., Davis, M., Filippenko, A. V., & Newman, J. 1998, Nature, 393, 35

Laursen, P. & Sommer-Larsen, J. 2007, ApJ, 657, L69

Le Floc'h, E., Charmandaris, V., Forrest, W. J., Mirabel, I. F., Armus, L., & Devost, D. 2006, ApJ, 642, 636

Le Floc'h, E., Duc, P.-A., Mirabel, I. F., Sanders, D. B., Bosch, G., Rodrigues, I., Courvoisier, T. J.-L., Mereghetti, S., & Melnick, J. 2002, ApJ, 581, L81

Ledoux, C., Petitjean, P., Fynbo, J. P. U., Møller, P., & Srianand, R. 2006, A&A, 457, 71

Ledoux, C., Petitjean, P., & Srianand, R. 2003, MNRAS, 346, 209

Lee, W. H. & Ramirez-Ruiz, E. 2007, New Journal of Physics, 9, 17

Leitherer, C., Schaerer, D., Goldader, J. D., Delgado, R. M. G., Robert, C., Kune, D. F., de Mello, D. F., Devost, D., & Heckman, T. M. 1999, ApJS, 123, 3

Levan, A., Fruchter, A., Rhoads, J., Mobasher, B., Tanvir, N., Gorosabel, J., Rol, E., Kouveliotou, C., Dell'Antonio, I., Merrill, M., Bergeron, E., Castro Cerón, J. M., Masetti, N., Vreeswijk, P., Antonelli, A., Bersier, D., Castro-Tirado, A., Fynbo, J., Garnavich, P., Holland, S., Hjorth, J., Nugent, P., Pian, E., Smette, A., Thomsen, B., Thorsett, S. E., & Wijers, R. 2006, ApJ, 647, 471

Levesque, E. M. & Kewley, L. J. 2007, ApJ, 667, L121

Li, L.-X. & Paczyński, B. 1998, ApJ, 507, L59

Li, W., Wang, X., Van Dyk, S. D., Cuillandre, J.-C., Foley, R. J., & Filippenko, A. V. 2007, ApJ, 661, 1013

Lilly, S. J., Carollo, C. M., & Stockton, A. N. 2003, ApJ, 597, 730

Lipkin, Y. M., Ofek, E. O., Gal-Yam, A., Leibowitz, E. M., Poznanski, D., Kaspi, S., Polishook, D., Kulkarni, S. R., Fox, D. W., Berger, E., Mirabal, N., Halpern, J., Bureau, M., Fathi, K., Price, P. A., Peterson, B. A., Frebel, A., Schmidt, B., Orosz, J. A., Fitzgerald, J. B., Bloom, J. S., van Dokkum, P. G., Bailyn, C. D., Buxton, M. M., & Barsony, M. 2004, ApJ, 606, 381

Luna, R., Cox, N. L. J., Satorre, M. A., García Hernández, D. A., Suárez, O., & García Lario, P. 2008, A&A, 480, 133

Lynds, C. R. & Sandage, A. R. 1963, ApJ, 137, 1005

MacFadyen, A. I. & Woosley, S. E. 1999, ApJ, 524, 262

Madau, P., Ferguson, H. C., Dickinson, M. E., Giavalisco, M., Steidel, C. C., & Fruchter, A. 1996, MNRAS, 283, 1388

Magrini, L., Vílchez, J. M., Mampaso, A., Corradi, R. L. M., & Leisy, P. 2007, A&A, 470, 865

Maiolino, R., Vanzi, L., Mannucci, F., Cresci, G., Ghinassi, F., & Della Valle, M. 2002, A&A, 389, 84

Malesani, D., Covino, S., D'Avanzo, P., D'Elia, V., Fugazza, D., Piranomonte, S., Ballo, L., Campana, S., Stella, L., Tagliaferri, G., Antonelli, L. A., Chincarini, G., Della Valle, M., Goldoni, P., Guidorzi, C., Israel, G. L., Lazzati, D., Melandri, A., Pellizza, L. J., Romano, P., Stratta, G., & Vergani, S. D. 2007, A&A, 473, 77

Malesani, D., Fynbo, J. P. U., Hjorth, J., Leloudas, G., Sollerman, J., Stritzinger, M. D., Vreeswijk, P. M., Watson, D. J., Gorosabel, J., Michałowski, M. J., Thöne, C. C., Augusteijn, T., Bersier, D., Jakobsson, P., Jaunsen, A. O., Ledoux, C., Levan, A. J., Milvang-Jensen, B., Rol, E., Tanvir, N. R., Wiersema, K., Xu, D., Albert, L., Bayliss, M., Gall, C., Grove, L. F., Koester, B. P., Leitet, E., Pursimo, T., & Skillen, I. 2008a, ArXiv:astro-ph/0805.1188, 805

Malesani, D., Hjorth, J., Jakobsson, P., Vreeswijk, P. M., Thöne, C. C., Fynbo, J. P. U., Watson, D. J., Sollerman, J., Tanvir, N. R., & Stanke, T. 2008b, GRB Coordinates Network, 7169

Malesani, D., Tagliaferri, G., Chincarini, G., Covino, S., Della Valle, M., Fugazza, D., Mazzali, P. A., Zerbi, F. M., D'Avanzo, P., Kalogerakos, S., Simoncelli, A., Antonelli, L. A., Burderi, L., Campana, S., Cucchiara, A., Fiore, F., Ghirlanda, G., Goldoni, P., Götz, D., Mereghetti, S., Mirabel, I. F., Romano, P., Stella, L., Minezaki, T., Yoshii, Y., & Nomoto, K. 2004, ApJ, 609, L5

Mangano, V., La Parola, V., Cusumano, G., Mineo, T., Malesani, D., Dyks, J., Campana, S., Capalbi, M., Chincarini, G., Giommi, P., Moretti, A., Perri, M., Romano, P., Tagliaferri, G., Burrows, D. N., Gehrels, N., Godet, O., Holland, S. T., Kennea, J. A., Page, K. L., Racusin, J. L., Roming, P. W. A., & Zhang, B. 2007, ApJ, 654, 403

Mannucci, F., Della Valle, M., Panagia, N., Cappellaro, E., Cresci, G., Maiolino, R., Petrosian, A., & Turatto, M. 2005, A&A, 433, 807

Mannucci, F., Maiolino, R., Cresci, G., Della Valle, M., Vanzi, L., Ghinassi, F., Ivanov, V. D., Nagar, N. M., & Alonso-Herrero, A. 2003, A&A, 401, 519

Markwardt, C., Barbier, L., Barthelmy, S., Cummings, J., Fenimore, E., Gehrels, N., Hullinger, D., Krimm, H., Koss, M., Palmer, D., Parsons, A., Sakamoto, T., Sato, G., Stamatikos, M., & Tueller, J. 2006, GRB Coordinates Network, 5174

Martin, C., Barlow, T., Barnhart, W., Bianchi, L., Blakkolb, B. K., Bruno, D., Bushman, J., Byun, Y.-I., Chiville, M., Conrow, T., Cooke, B., Donas, J., Fanson, J. L., Forster, K., Friedman, P. G., Grange, R., Griffiths, D., Heckman, T., Lee, J., Jelinsky, P. N., Kim, S.-W., Lee, S.-C., Lee, Y.-W., Liu, D., Madore, B. F., Malina, R., Mazer, A., McLean, R., Milliard, B., Mitchell, W., Morais, M., Morrissey, P. F., Neff, S. G., Raison, F., Randall, D., Rich, M., Schiminovich, D., Schmitigal, W., Sen, A., Siegmund, O. H. W., Small, T., Stock, J. M., Surber, F., Szalay, A., Vaughan, A. H., Weigand, T., Welsh, B. Y., Wu, P., Wyder, T., Xu, C. K., & Zsoldas, J. 2003, in Presented at the Society of Photo-Optical Instrumentation Engineers (SPIE) Conference, Vol. 4854, Future EUV/UV and Visible Space Astrophysics Missions and Instrumentation. Edited by J. Chris Blades, Oswald H. W. Siegmund. Proceedings of the SPIE, Volume 4854, pp. 336-350 (2003)., ed. J. C. Blades & O. H. W. Siegmund, 336–350

Martin, D. C., Fanson, J., Schiminovich, D., Morrissey, P., Friedman, P. G., Barlow, T. A., Conrow, T., Grange, R., Jelinsky, P. N., Milliard, B., Siegmund, O. H. W., Bianchi, L., Byun, Y.-I., Donas, J., Forster, K., Heckman, T. M., Lee, Y.-W., Madore, B. F., Malina, R. F., Neff, S. G., Rich, R. M., Small, T., Surber, F., Szalay, A. S., Welsh, B., & Wyder, T. K. 2005, ApJ, 619, L1

Masetti, N., Bartolini, C., Bernabei, S., Guarnieri, A., Palazzi, E., Pian, E., Piccioni, A., Castro-Tirado, A. J., Castro Cerón, J. M., Verdes-Montenegro, L., Sagar, R., Mohan, V., Pandey, A. K., Pandey, S. B., Bock, H., Greiner, J., Benetti, S., Wijers, R. A. M. J., Beskin, G. M., & Gorosabel, J. 2000, A&A, 359, L23

Masetti, N., Palazzi, E., Pian, E., Simoncelli, A., Hunt, L. K., Maiorano, E., Levan, A., Christensen, L., Rol, E., Savaglio, S., Falomo, R., Castro-Tirado, A. J., Hjorth, J., Delsanti, A., Pannella, M., Mohan, V., Pandey, S. B., Sagar, R., Amati, L., Burud, I., Castro Cerón, J. M., Frontera, F., Fruchter, A. S., Fynbo, J. P. U., Gorosabel, J., Kaper, L., Klose, S., Kouveliotou, C., Nicastro, L., Pedersen, H., Rhoads, J., Salamanca, I., Tanvir, N., Vreeswijk, P. M., Wijers, R. A. M. J., & van den Heuvel, E. P. J. 2003, A&A, 404, 465

Matheson, T., Garnavich, P. M., Stanek, K. Z., Bersier, D., Holland, S. T., Krisciunas, K., Caldwell, N., Berlind, P., Bloom, J. S., Bolte, M., Bonanos, A. Z., Brown, M. J. I., Brown, W. R., Calkins, M. L., Challis, P., Chornock, R., Echevarria, L., Eisenstein, D. J., Everett, M. E., Filippenko, A. V., Flint, K., Foley, R. J., Freedman, D. L., Hamuy, M., Harding, P., Hathi, N. P., Hicken, M., Hoopes, C., Impey, C., Jannuzi, B. T., Jansen, R. A., Jha, S., Kaluzny, J., Kannappan, S., Kirshner, R. P., Latham, D. W., Lee, J. C., Leonard, D. C., Li, W., Luhman, K. L., Martini, P., Mathis, H., Maza, J., Megeath, S. T., Miller, L. R., Minniti, D., Olszewski, E. W., Papenkova, M., Phillips, M. M., Pindor, B., Sasselov, D. D., Schild, R., Schweiker, H., Spahr, T., Thomas-Osip, J., Thompson, I., Weisz, D., Windhorst, R., & Zaritsky, D. 2003, ApJ, 599, 394

Mattila, S., Väisänen, P., Farrah, D., Efstathiou, A., Meikle, W. P. S., Dahlen, T., Fransson, C., Lira, P., Lundqvist, P., Östlin, G., Ryder, S., & Sollerman, J. 2007, ApJ, 659, L9

Maund, J. R. & Smartt, S. J. 2005, MNRAS, 360, 288

Maund, J. R., Smartt, S. J., & Schweizer, F. 2005, ApJ, 630, L33

McBreen, S., Foley, S., Watson, D., Hanlon, L., Malesani, D., Fynbo, J. P. U., Kann, D. A., Gehrels, N., McGlynn, S., & Palmer, D. 2008, ApJ, 677, L85

McGaugh, S. S. 1991, ApJ, 380, 140

Mereghetti, S., Götz, D., Borkowski, J., Walter, R., & Pedersen, H. 2003, A&A, 411, L291

Meszaros, P. 2006, Reports of Progress in Physics, 69, 2259

Meszaros, P. & Rees, M. J. 1997, ApJ, 476, 232

Metzger, M. R., Djorgovski, S. G., Kulkarni, S. R., Steidel, C. C., Adelberger, K. L., Frail, D. A., Costa, E., & Frontera, F. 1997, Nature, 387, 878

Meynet, G., Maeder, A., Schaller, G., Schaerer, D., & Charbonnel, C. 1994, A&AS, 103, 97

Michałowski, M. J., Hjorth, J., Castro Cerón, J. M., & Watson, D. 2008, ApJ, 672, 817

Mirabal, N., Halpern, J. P., An, D., Thorstensen, J. R., & Terndrup, D. M. 2006, ApJ, 643, L99

Mirabal, N., Halpern, J. P., Kulkarni, S. R., Castro, S., Bloom, J. S., Djorgovski, S. G., Galama, T. J., Harrison, F. A., Frail, D. A., Price, P. A., Reichart, D. E., Ebeling, H., Bunker, A., Dawson, S., Dey, A., Spinrad, H., & Stern, D. 2002, ApJ, 578, 818

Modjaz, M., Kewley, L., Kirshner, R. P., Stanek, K. Z., Challis, P., Garnavich, P. M., Greene, J. E., Kelly, P. L., & Prieto, J. L. 2008a, AJ, 135, 1136

Modjaz, M., Li, W., Butler, N., Chornock, R., Perley, D., Blondin, S., Bloom, J. S., Filippenko, A. V., Kirshner, R. P., Kocevski, D., Poznanski, D., Hicken, M., Foley, R. J., Stringfellow, G. S., Berlind, P., Barrado y Navascues, D., Blake, C. H., Bouy, H., Brown, W., Challis, P., Chen, H., de Vries, W. H., Dufour, P., Falco, E., Friedman, A., Ganeshalingam, M., Garnavich, P., Holden, B., Illingworth, G., Liebert, J., Marion, G. H., Lee, N., Olivier, S. S., Olszewski, E., Prochaska, J. X., Silverman, J. M., Smith, N., Starr, D., Steele, T. N., Stockton, A., Williams, G. G., & Wood-Vasey, W. M. 2008b, ArXiv:astro-ph/0805.2201, 805

Modjaz, M., Stanek, K. Z., Garnavich, P. M., Berlind, P., Blondin, S., Brown, W., Calkins, M., Challis, P., Diamond-Stanic, A. M., Hao, H., Hicken, M., Kirshner, R. P., & Prieto, J. L. 2006, ApJ, 645, L21

Molinari, E., Vergani, S. D., Malesani, D., Covino, S., D'Avanzo, P., Chincarini, G., Zerbi, F. M., Antonelli, L. A., Conconi, P., Testa, V., Tosti, G., Vitali, F., D'Alessio, F., Malaspina, G., Nicastro, L., Palazzi, E., Guetta, D., Campana, S., Goldoni, P., Masetti, N., Meurs, E. J. A., Monfardini, A., Norci, L., Pian, E., Piranomonte, S., Rizzuto, D., Stefanon, M., Stella, L., Tagliaferri, G., Ward, P. A., Ihle, G., Gonzalez, L., Pizarro, A., Sinclaire, P., & Valenzuela, J. 2007, A&A, 469, L13

Monet, D. G., Levine, S. E., Canzian, B., Ables, H. D., Bird, A. R., Dahn, C. C., Guetter, H. H., Harris, H. C., Henden, A. A., Leggett, S. K., Levison, H. F., Luginbuhl, C. B., Martini, J., Monet, A. K. B., Munn, J. A., Pier, J. R., Rhodes, A. R., Riepe, B., Sell, S., Stone, R. C., Vrba, F. J., Walker, R. L., Westerhout, G., Brucato, R. J., Reid, I. N., Schoening, W., Hartley, M., Read, M. A., & Tritton, S. B. 2003, AJ, 125, 984

Monfardini, A., Kobayashi, S., Guidorzi, C., Carter, D., Mundell, C. G., Bersier, D. F., Gomboc, A., Melandri, A., Mottram, C. J., Smith, R. J., & Steele, I. A. 2006, ApJ, 648, 1125

Morton, D. C. 2003, ApJS, 149, 205

Moshir, M. & et al. 1990, in IRAS Faint Source Catalogue, version 2.0 (1990)

Munari, U. & Zwitter, T. 1997, A&A, 318, 269

Nakar, E. & Granot, J. 2007, MNRAS, 380, 1744

Nakar, E., Piran, T., & Granot, J. 2003, New Astronomy, 8, 495

Neill, J. D., Sullivan, M., Balam, D., Pritchet, C. J., Howell, D. A., Perrett, K., Astier, P., Aubourg, E., Basa, S., Carlberg, R. G., Conley, A., Fabbro, S., Fouchez, D., Guy, J., Hook, I., Pain, R., Palanque-Delabrouille, N., Regnault, N., Rich, J., Taillet, R., Aldering, G., Antilogus, P., Arsenijevic, V., Balland, C., Baumont, S., Bronder, J., Ellis, R. S., Filiol, M., Gonçalves, A. C., Hardin, D., Kowalski, M., Lidman, C., Lusset, V., Mouchet, M., Mourao, A., Perlmutter, S., Ripoche, P., Schlegel, D., & Tao, C. 2006, AJ, 132, 1126

Nestor, D. B., Turnshek, D. A., & Rao, S. M. 2005, ApJ, 628, 637

Nesvadba, N. P. H., Lehnert, M. D., Davies, R. I., Verma, A., & Eisenhauer, F. 2008, A&A, 479, 67

Nilsson, K. K., Orsi, A., Lacey, C. G., Baugh, C. M., & Thommes, E. 2007, A&A, 474, 385

Norris, J. P. 2002, ApJ, 579, 386

Noterdaeme, P., Ledoux, C., Petitjean, P., & Srianand, R. 2008, A&A, 481, 327

Nysewander, M., Fruchter, A. S., & Pe'er, A. 2008, ArXiv:astro-ph/0806.3607, 1

Oates, S. R., de Pasquale, M., Page, M. J., Blustin, A. J., Zane, S., McGowan, K., Mason, K. O., Poole, T. S., Schady, P., Roming, P. W. A., Page, K. L., Falcone, A., & Gehrels, N. 2007, MNRAS, 380, 270

Ofek, E. O., Cenko, S. B., Gal-Yam, A., Fox, D. B., Nakar, E., Rau, A., Frail, D. A., Kulkarni, S. R., Price, P. A., Schmidt, B. P., Soderberg, A. M., Peterson, B., Berger, E., Sharon, K., Shemmer, O., Penprase, B. E., Chevalier, R. A., Brown, P. J., Burrows, D. N., Gehrels, N., Harrison, F., Holland, S. T., Mangano, V., McCarthy, P. J., Moon, D.-S., Nousek, J. A., Persson, S. E., Piran, T., & Sari, R. 2007, ApJ, 662, 1129

Ofek, E. O., Cenko, S. B., Gal-Yam, A., Peterson, B., Schmidt, B. P., Fox, D. B., & Price, P. A. 2006, GRB Coordinates Network, 5123

Osterbrock, D. E. 1989, Astrophysics of gaseous nebulae and active galactic nuclei (Research supported by the University of California, John Simon Guggenheim Memorial Foundation, University of Minnesota, et al. Mill Valley, CA, University Science Books, 1989, 422 p.)

Östlin, G., Cumming, R. J., & Bergvall, N. 2007, A&A, 461, 471

Östlin, G., Zackrisson, E., Bergvall, N., & Rönnback, J. 2003, A&A, 408, 887

Östlin, G., Zackrisson, E., Sollerman, J., Mattila, S., & Hayes, M. 2008, MNRAS, 387, 1227

Ovaldsen, J.-E., Jaunsen, A. O., Fynbo, J. P. U., Hjorth, J., Thöne, C. C., Féron, C., Xu, D., Selj, J. H., & Teuber, J. 2007, ApJ, 662, 294

Paczyński, B. & Rhoads, J. E. 1993, ApJ, 418, L5

Pagel, B. E. J., Edmunds, M. G., Blackwell, D. E., Chun, M. S., & Smith, G. 1979, MNRAS, 189, 95

Palmer, D., Cummings, J., Stamatikos, M., Markwardt, C., & Sakamoto, T. 2006, GRB Coordinates Network, 5076

Panaitescu, A. & Kumar, P. 2001, ApJ, 554, 667

Panaitescu, A., Mészáros, P., Burrows, D., Nousek, J., Gehrels, N., O'Brien, P., & Willingale, R. 2006, MNRAS, 369, 2059

Pastorello, A., Smartt, S. J., Mattila, S., Eldridge, J. J., Young, D., Itagaki, K., Yamaoka, H., Navasardyan, H., Valenti, S., Patat, F., Agnoletto, I., Augusteijn, T., Benetti, S., Cappellaro, E., Boles, T., Bonnet-Bidaud, J.-M., Botticella, M. T., Bufano, F., Cao, C., Deng, J., Dennefeld, M., Elias-Rosa, N., Harutyunyan, A., Keenan, F. P., Iijima, T., Lorenzi, V., Mazzali, P. A., Meng, X., Nakano, S., Nielsen, T. B., Smoker, J. V., Stanishev, V., Turatto, M., Xu, D., & Zampieri, L. 2007, Nature, 447, 829

Pei, Y. C. 1992, ApJ, 395, 130

Penprase, B. E., Berger, E., Fox, D. B., Kulkarni, S. R., Kadish, S., Kerber, L., Ofek, E., Kasliwal, M., Hill, G., Schaefer, B., & Reed, M. 2006, ApJ, 646, 358

Perna, R. & Loeb, A. 1998, ApJ, 501, 467

Péroux, C., Dessauges-Zavadsky, M., D'Odorico, S., Kim, T.-S., & McMahon, R. G. 2007, MNRAS, 382, 177

Petitjean, P., Ledoux, C., Noterdaeme, P., & Srianand, R. 2006, A&A, 456, L9

Pettini, M. & Pagel, B. E. J. 2004, MNRAS, 348, L59

Pettini, M., Rix, S. A., Steidel, C. C., Hunt, M. P., Shapley, A. E., & Adelberger, K. L. 2002, Ap&SS, 281, 461

Pettini, M., Shapley, A. E., Steidel, C. C., Cuby, J.-G., Dickinson, M., Moorwood, A. F. M., Adelberger, K. L., & Giavalisco, M. 2001, ApJ, 554, 981

Pettini, M., Smith, L. J., King, D. L., & Hunstead, R. W. 1997, ApJ, 486, 665

Pian, E., Mazzali, P. A., Masetti, N., Ferrero, P., Klose, S., Palazzi, E., Ramirez-Ruiz, E., Woosley, S. E., Kouveliotou, C., Deng, J., Filippenko, A. V., Foley, R. J., Fynbo, J. P. U., Kann, D. A., Li, W., Hjorth, J., Nomoto, K., Patat, F., Sauer, D. N., Sollerman, J., Vreeswijk, P. M., Guenther, E. W., Levan, A., O'Brien, P., Tanvir, N. R., Wijers, R. A. M. J., Dumas, C., Hainaut, O., Wong, D. S., Baade, D., Wang, L., Amati, L., Cappellaro, E., Castro-Tirado, A. J., Ellison, S., Frontera, F., Fruchter, A. S., Greiner, J., Kawabata, K., Ledoux, C., Maeda, K., Møller, P., Nicastro, L., Rol, E., & Starling, R. 2006, Nature, 442, 1011

Pilyugin, L. S. 2001, A&A, 369, 594

Piranomonte, S., D'Elia, V., Ward, P., Fiore, F., & Meurs, E. J. A. 2007, ArXiv:astro-ph/0701563

Price, P. A., Fox, D. W., Kulkarni, S. R., Peterson, B. A., Schmidt, B. P., Soderberg, A. M., Yost, S. A., Berger, E., Djorgovski, S. G., Frail, D. A., Harrison, F. A., Sari, R., Blain, A. W., & Chapman, S. C. 2003, Nature, 423, 844

Prochaska, J. X. 2006, ApJ, 650, 272

Prochaska, J. X., Bloom, J. S., Chen, H.-W., Foley, R. J., Perley, D. A., Ramirez-Ruiz, E., Granot, J., Lee, W. H., Pooley, D., Alatalo, K., Hurley, K., Cooper, M. C., Dupree, A. K., Gerke, B. F., Hansen, B. M. S., Kalirai, J. S., Newman, J. A., Rich, R. M., Richer, H., Stanford, S. A., Stern, D., & van Breugel, W. J. M. 2006a, ApJ, 642, 989

Prochaska, J. X., Chen, H.-W., & Bloom, J. S. 2006b, ApJ, 648, 95

Prochaska, J. X., Chen, H.-W., Dessauges-Zavadsky, M., & Bloom, J. S. 2007, ApJ, 666, 267

Prochaska, J. X., Chen, H.-W., Wolfe, A. M., Dessauges-Zavadsky, M., & Bloom, J. S. 2008a, ApJ, 672, 59

Prochaska, J. X., Dessauges-Zavadsky, M., Ramirez-Ruiz, E., & Chen, H.-W. 2008b, ArXiv:astro-ph/0806.0399, 1

Prochaska, J. X., Herbert-Fort, S., & Wolfe, A. M. 2005, ApJ, 635, 123

Prochter, G. E., Prochaska, J. X., Chen, H.-W., Bloom, J. S., Dessauges-Zavadsky, M., Foley, R. J., Lopez, S., Pettini, M., Dupree, A. K., & Guhathakurta, P. 2006, ApJ, 648, L93

Racusin, J. L., Karpov, S. V., Sokolowski, M., Granot, J., Wu, X. F., Pal'shin, V., Covino, S., van der Horst, A. J., Oates, S. R., Schady, P., Smith, R. J., Cummings, J., Starling, R. L. C., Piotrowski, L. W., Zhang, B., Evans, P. A., Holland, S. T., Malek, K., Page, M. T., Vetere, L., Margutti, R., Guidorzi, C., Kamble, A., Curran, P. A., Beardmore, A., Kouveliotou, C., Mankiewicz, L., Melandri, A., O'Brien, P. T., Page, K. L., Piran, T., Tanvir, N. R., Wrochna, G., Aptekar, R. L., Bartolini, C., Barthelmy, S., Beskin, G. M., Bondar, S., Campana, S., Cucchiara, A., Cwiok, M., D'Avanzo, P., D'Elia, V., Della Valle, M., Dominik, W., Falcone, A., Fiore, F., Fox, D. B., Frederiks, D. D., Fruchter, A. S., Fugazza, D., Garrett, M., Gehrels, N., Golenetskii, S., Gomboc, A., Greco, G., Guarnieri, A., Immler, S., Kasprowicz, G., Levan, A. J., Mazets, E. P., Molinari, E., Moretti, A., Nawrocki, K., Oleynik, P. P., Osborne, J. P., Pagani, C., Paragi, Z., Perri, M., Piccioni, A., Ramirez-Ruiz, E., Roming, P. W. A., Steele, I. A., Strom, R. G., Testa, V., Tosti, G., Ulanov, M. V., Wiersema, K., Wijers, R. A. M. J., Zarnecki, A. F., Zerbi, F., Meszaros, P., Chincarini, G., & Burrows, D. N. 2008, ArXiv:astro-ph/0805.1557, 805

Rao, S. M. & Turnshek, D. A. 2000, ApJS, 130, 1

Rauch, M. 1998, ARA&A, 36, 267

Reichart, D. E. 1998, ApJ, 495, L99

Rhee, M.-H. & van Albada, T. S. 1996, A&AS, 115, 407

Roming, P. W. A., Vanden Berk, D., Pal'shin, V., Pagani, C., Norris, J., Kumar, P., Krimm, H., Holland, S. T., Gronwall, C., Blustin, A. J., Zhang, B., Schady, P., Sakamoto, T., Osborne, J. P., Nousek, J. A., Marshall, F. E., Mészáros, P., Golenetskii, S. V., Gehrels, N., Frederiks, D. D., Campana, S., Burrows, D. N., Boyd, P. T., Barthelmy, S., & Aptekar, R. L. 2006, ApJ, 651, 985

Ruiz-Velasco, A. E., Swan, H., Troja, E., Malesani, D., Fynbo, J. P. U., Starling, R. L. C., Xu, D., Aharonian, F., Akerlof, C., Andersen, M. I., Ashley, M. C. B., Barthelmy, S. D., Bersier, D., Castro Cerón, J. M., Castro-Tirado, A. J., Gehrels, N., Göğüş, E., Gorosabel, J., Guidorzi, C., Güver, T., Hjorth, J., Horns, D., Huang, K. Y., Jakobsson, P., Jensen, B. L., Kızıloğlu, Ü., Kouveliotou, C., Krimm, H. A., Ledoux, C., Levan, A. J., Marsh, T., McKay, T., Melandri, A., Milvang-Jensen, B., Mundell, C. G., O'Brien, P. T., Özel, M., Phillips, A., Quimby, R., Rowell, G., Rujopakarn, W., Rykoff, E. S., Schaefer, B. E., Sollerman, J., Tanvir, N. R., Thöne, C. C., Urata, Y., Vestrand, W. T., Vreeswijk, P. M., Watson, D., Wheeler, J. C., Wijers, R. A. M. J., Wren, J., Yost, S. A., Yuan, F., Zhai, M., & Zheng, W. K. 2007, ApJ, 669, 1

Rykoff, E. S., Yost, S. A., Swan, H., & Rujopakarn, W. 2006, GRB Coordinates Network, 5166

Sari, R., Piran, T., & Halpern, J. P. 1999, ApJ, 519, L17

Sato, G., Yamazaki, R., Ioka, K., Sakamoto, T., Takahashi, T., Nakazawa, K., Nakamura, T., Toma, K., Hullinger, D., Tashiro, M., Parsons, A. M., Krimm, H. A., Barthelmy, S. D., Gehrels, N., Burrows, D. N., O'Brien, P. T., Osborne, J. P., Chincarini, G., & Lamb, D. Q. 2007, ApJ, 657, 359

Savage, B. D. & Sembach, K. R. 1991, ApJ, 379, 245

—. 1996, ARA&A, 34, 279

Savaglio, S. 2006, New Journal of Physics, 8, 195

Savaglio, S. & Fall, S. M. 2004, ApJ, 614, 293

Savaglio, S., Fall, S. M., & Fiore, F. 2003, ApJ, 585, 638

Savaglio, S., Glazebrook, K., & Le Borgne, D. 2008, ArXiv:astro-ph/0803.2718, 803

Savaglio, S., Panagia, N., & Padovani, P. 2002, ApJ, 567, 702

Schady, P., Mason, K. O., Page, M. J., de Pasquale, M., Morris, D. C., Romano, P., Roming, P. W. A., Immler, S., & vanden Berk, D. E. 2007, MNRAS, 377, 273

Schaefer, B. E. & Xiao, L. 2006, ArXiv:astro-ph/0608441

Schawinski, K., Justham, S., Wolf, C., Podsiadlowski, P., Sullivan, M., Steenbrugge, K. C., Bell, T., Roeser, H.-J., Walker, E., Astier, P., Balam, D., Balland, C., Carlberg, R., Conley, A., Fouchez, D., Guy, J., Hardin, D., Hook, I., Howell, A., Pain, R., Perrett, K., Pritchet, C., Regnault, N., & Yi, S. K. 2008, ArXiv:astro-ph/0803.3596, 1

Schlegel, D. J., Finkbeiner, D. P., & Davis, M. 1998, ApJ, 500, 525

Sembach, K. R., Howk, J. C., Savage, B. D., Shull, J. M., & Oegerle, W. R. 2001, ApJ, 561, 573

Shapley, A. E., Steidel, C. C., Pettini, M., & Adelberger, K. L. 2003, ApJ, 588, 65

Silva, L., Granato, G. L., Bressan, A., & Danese, L. 1998, ApJ, 509, 103

Skrutskie, M. F., Cutri, R. M., Stiening, R., Weinberg, M. D., Schneider, S., Carpenter, J. M., Beichman, C., Capps, R., Chester, T., Elias, J., Huchra, J., Liebert, J., Lonsdale, C., Monet, D. G., Price, S., Seitzer, P., Jarrett, T., Kirkpatrick, J. D., Gizis, J. E., Howard, E., Evans, T., Fowler, J., Fullmer, L., Hurt, R., Light, R., Kopan, E. L., Marsh, K. A., McCallon, H. L., Tam, R., Van Dyk, S., & Wheelock, S. 2006, AJ, 131, 1163

Slavin, J. D. 1989, ApJ, 346, 718

Smail, I., Ivison, R. J., Blain, A. W., & Kneib, J.-P. 2002, MNRAS, 331, 495

Smartt, S. J. & Rolleston, W. R. J. 1997, ApJ, 481, L47

Soderberg, A. M., Berger, E., Kasliwal, M., Frail, D. A., Price, P. A., Schmidt, B. P., Kulkarni, S. R., Fox, D. B., Cenko, S. B., Gal-Yam, A., Nakar, E., & Roth, K. C. 2006a, ApJ, 650, 261

Soderberg, A. M., Berger, E., Page, K. L., Schady, P., Parrent, J., Pooley, D., Wang, X.-Y., Ofek, E. O., Cucchiara, A., Rau, A., Waxman, E., Simon, J. D., Bock, D. C.-J., Milne, P. A., Page, M. J., Barentine, J. C., Barthelmy, S. D., Beardmore, A. P., Bietenholz, M. F., Brown, P., Burrows, A., Burrows, D. N., Byrngelson, G., Cenko, S. B., Chandra, P., Cummings, J. R., Fox, D. B., Gal-Yam, A., Gehrels, N., Immler, S., Kasliwal, M., Kong, A. K. H., Krimm, H. A., Kulkarni, S. R., Maccarone, T. J., Mészáros, P., Nakar, E., O'Brien, P. T., Overzier, R. A., de Pasquale, M., Racusin, J., Rea, N., & York, D. G. 2008, Nature, 453, 469

Soderberg, A. M., Kulkarni, S. R., Berger, E., Fox, D. B., Price, P. A., Yost, S. A., Hunt, M. P., Frail, D. A., Walker, R. C., Hamuy, M., Shectman, S. A., Halpern, J. P., & Mirabal, N. 2004, ApJ, 606, 994

Soderberg, A. M., Kulkarni, S. R., Nakar, E., Berger, E., Cameron, P. B., Fox, D. B., Frail, D., Gal-Yam, A., Sari, R., Cenko, S. B., Kasliwal, M., Chevalier, R. A., Piran, T., Price, P. A., Schmidt, B. P., Pooley, G., Moon, D.-S., Penprase, B. E., Ofek, E., Rau, A., Gehrels, N., Nousek, J. A., Burrows, D. N., Persson, S. E., & McCarthy, P. J. 2006b, Nature, 442, 1014

Soderberg, A. M., Nakar, E., Cenko, S. B., Cameron, P. B., Frail, D. A., Kulkarni, S. R., Fox, D. B., Berger, E., Gal-Yam, A., Moon, D.-S., Price, P. A., Anderson, G., Schmidt, B. P., Salvo, M., Rich, J., Rau, A., Ofek, E. O., Chevalier, R. A., Hamuy, M., Harrison, F. A., Kumar, P., MacFadyen, A., McCarthy, P. J., Park, H. S., Peterson, B. A., Phillips, M. M., Rauch, M., Roth, M., & Shectman, S. 2007, ApJ, 661, 982

Sofue, Y. & Rubin, V. 2001, ARA&A, 39, 137

Sollerman, J., Cox, N., Mattila, S., Ehrenfreund, P., Kaper, L., Leibundgut, B., & Lundqvist, P. 2005a, A&A, 429, 559

Sollerman, J., Holland, S. T., Challis, P., Fransson, C., Garnavich, P., Kirshner, R. P., Kozma, C., Leibundgut, B., Lundqvist, P., Patat, F., Filippenko, A. V., Panagia, N., & Wheeler, J. C. 2002, A&A, 386, 944

Sollerman, J., Jaunsen, A. O., Fynbo, J. P. U., Hjorth, J., Jakobsson, P., Stritzinger, M., Féron, C., Laursen, P., Ovaldsen, J.-E., Selj, J., Thöne, C. C., Xu, D., Davis, T., Gorosabel, J., Watson, D., Duro, R., Ilyin, I., Jensen, B. L., Lysfjord, N., Marquart, T., Nielsen, T. B., Näränen, J., Schwarz, H. E., Walch, S., Wold, M., & Östlin, G. 2006, A&A, 454, 503

Sollerman, J., Östlin, G., Fynbo, J. P. U., Hjorth, J., Fruchter, A., & Pedersen, K. 2005b, New Astronomy, 11, 103

Spitzer, L. 1978, Physical processes in the interstellar medium (New York Wiley-Interscience, 1978. 333 p.)

Stanek, K. Z., Dai, X., Prieto, J. L., An, D., Garnavich, P. M., Calkins, M. L., Serven, J., Worthey, G., Hao, H., Dobrzycki, A., Howk, C., & Matheson, T. 2007, ApJ, 654, L21

Stanek, K. Z., Matheson, T., Garnavich, P. M., Martini, P., Berlind, P., Caldwell, N., Challis, P., Brown, W. R., Schild, R., Krisciunas, K., Calkins, M. L., Lee, J. C., Hathi, N., Jansen, R. A., Windhorst, R., Echevarria, L., Eisenstein, D. J., Pindor, B., Olszewski, E. W., Harding, P., Holland, S. T., & Bersier, D. 2003, ApJ, 591, L17

Stark, D. P., Ellis, R. S., Richard, J., Kneib, J.-P., Smith, G. P., & Santos, M. R. 2007, ApJ, 663, 10

Starling, R. L. C., Vreeswijk, P. M., Ellison, S. L., Rol, E., Wiersema, K., Levan, A. J., Tanvir, N. R., Wijers, R. A. M. J., Tadhunter, C., Zaurin, J. R., Gonzalez Delgado, R. M., & Kouveliotou, C. 2005a, A&A, 442, L21

Starling, R. L. C., Wijers, R. A. M. J., Hughes, M. A., Tanvir, N. R., Vreeswijk, P. M., Rol, E., & Salamanca, I. 2005b, MNRAS, 360, 305

Starling, R. L. C., Wijers, R. A. M. J., Wiersema, K., Rol, E., Curran, P. A., Kouveliotou, C., van der Horst, A. J., & Heemskerk, M. H. M. 2007, ApJ, 661, 787

Stasińska, G. 1980, A&A, 84, 320

Staveley-Smith, L. & Davies, R. D. 1988, MNRAS, 231, 833

Steidel, C. C., Adelberger, K. L., Shapley, A. E., Pettini, M., Dickinson, M., & Giavalisco, M. 2003, ApJ, 592, 728

Steidel, C. C., Giavalisco, M., Pettini, M., Dickinson, M., & Adelberger, K. L. 1996, ApJ, 462, L17

Steidel, C. C., Kollmeier, J. A., Shapley, A. E., Churchill, C. W., Dickinson, M., & Pettini, M. 2002, ApJ, 570, 526

Steidel, C. C. & Sargent, W. L. W. 1992, ApJS, 80, 1

Sudilovsky, V., Savaglio, S., Vreeswijk, P., Ledoux, C., Smette, A., & Greiner, J. 2007, ApJ, 669, 741

Tanvir, N. R., Barnard, V. E., Blain, A. W., Fruchter, A. S., Kouveliotou, C., Natarajan, P., Ramirez-Ruiz, E., Rol, E., Smith, I. A., Tilanus, R. P. J., & Wijers, R. A. M. J. 2004, MNRAS, 352, 1073

Tavani, M. & et al. 2004, AGILE document AP 27, 1

Tejos, N., Lopez, S., Prochaska, J. X., Chen, H.-W., & Dessauges-Zavadsky, M. 2007, ApJ, 671, 622

Thomsen, B., Hjorth, J., Watson, D., Gorosabel, J., Fynbo, J. P. U., Jensen, B. L., Andersen, M. I., Dall, T. H., Rasmussen, J. R., Bruntt, H., Laurikainen, E., Augusteijn, T., Pursimo, T., Germany, L., Jakobsson, P., & Pedersen, K. 2004, A&A, 419, L21

Thöne, C. C., Fynbo, J. P. U., & Joergensen, U. G. 2006, GRB Coordinates Network, 5179

Thöne, C. C., Fynbo, J. P. U., Östlin, G., Milvang-Jensen, B., Wiersema, K., Malesani, D., Della Monica Ferreira, D., Gorosabel, J., Kann, D. A., Watson, D., Michałowski, M. J., Fruchter, A. S., Levan, A. J., Hjorth, J., & Sollerman, J. 2008a, ApJ, 676, 1151

Thöne, C. C., Fynbo, J. P. U., Sollerman, J., Jensen, B. L., Hjorth, J., Jakobsson, P., & Klose, S. 2006, GRB Coordinates Network, 5161

Thöne, C. C., Greiner, J., Savaglio, S., & Jehin, E. 2007a, ApJ, 671, 628

Thöne, C. C., Malesani, D., Hjorth, J., Jakobsson, P., Bayliss, M., & Koester, B. 2008b, GRB Coordinates Network, 7161

Thöne, C. C., Wiersema, K., Ledoux, C., Starling, R. L. C., de Ugarte Postigo, A., Levan, A. J., Fynbo, J. P. U., Curran, P. A., Gorosabel, J., van der Horst, A. J., LLorente, A., Rol, E., Tanvir, N. R., Vreeswijk, P. M., Wijers, R. A. M. J., & Kewley, L. J. 2007b, ArXiv:astro-ph/0708.3448, 1

Tominaga, N., Maeda, K., Umeda, H., Nomoto, K., Tanaka, M., Iwamoto, N., Suzuki, T., & Mazzali, P. A. 2007, ApJ, 657, L77

Tremonti, C. A., Heckman, T. M., Kauffmann, G., Brinchmann, J., Charlot, S., White, S. D. M., Seibert, M., Peng, E. W., Schlegel, D. J., Uomoto, A., Fukugita, M., & Brinkmann, J. 2004, ApJ, 613, 898

Tripp, T. M. & Bowen, D. V. 2005, in IAU Colloq. 199: Probing Galaxies through Quasar Absorption Lines, ed. P. Williams, C.-G. Shu, & B. Menard, 5–23

Tumlinson, J., Prochaska, J. X., Chen, H.-W., Dessauges-Zavadsky, M., & Bloom, J. S. 2007, ApJ, 668, 667

Uemura, M., Kato, T., Ishioka, R., Yamaoka, H., Monard, B., Nogami, D., Maehara, H., Sugie, A., & Takahashi, S. 2003, Nature, 423, 843

van den Bergh, S., Li, W., & Filippenko, A. V. 2005, PASP, 117, 773

van Dokkum, P. G. 2001, PASP, 113, 1420

van Marle, A. J., Langer, N., & García-Segura, G. 2005, A&A, 444, 837

van Paradijs, J., Groot, P. J., Galama, T., Kouveliotou, C., Strom, R. G., Telting, J., Rutten, R. G. M., Fishman, G. J., Meegan, C. A., Pettini, M., Tanvir, N., Bloom, J., Pedersen, H., Nørdgaard-Nielsen, H. U., Linden-Vørnle, M., Melnick, J., van der Steene, G., Bremer, M., Naber, R., Heise, J., in't Zand, J., Costa, E., Feroci, M., Piro, L., Frontera, F., Zavattini, G., Nicastro, L., Palazzi, E., Bennet, K., Hanlon, L., & Parmar, A. 1997, Nature, 386, 686

Vanderspek, R., Crew, G., Doty, J., Villasenor, J., Monnelly, G., Butler, N., Cline, T., Jernigan, J. G., Levine, A., Martel, F., Morgan, E., Prigozhin, G., Azzibrouck, G., Braga, J., Manchanda, R., Pizzichini, G., Ricker, G., Atteia, J.-L., Kawai, N., Lamb, D., Woosley, S., Donaghy, T., Suzuki, M., Shirasaki, Y., Graziani, C., Matsuoka, M., Tamagawa, T., Torii, K., Sakamoto, T., Yoshida, A., Fenimore, E., Galassi, M., Tavenner, T., Nakagawa, Y., Takahashi, D., Satoh, R., Urata, Y., Boer, M., Olive, J.-F., Dezalay, J.-P., Barraud, C., & Hurley, K. 2003, GRB Coordinates Network, 1997

Veilleux, S., Cecil, G., & Bland-Hawthorn, J. 2005, ARA&A, 43, 769

Vestrand, W. T., Wozniak, P. R., Wren, J. A., Fenimore, E. E., Sakamoto, T., White, R. R., Casperson, D., Davis, H., Evans, S., Galassi, M., McGowan, K. E., Schier, J. A., Asa, J. W., Barthelmy, S. D., Cummings, J. R., Gehrels, N., Hullinger, D., Krimm, H. A., Markwardt, C. B., McLean, K., Palmer, D., Parsons, A., & Tueller, J. 2005, Nature, 435, 178

Vestrand, W. T., Wren, J. A., Wozniak, P. R., Aptekar, R., Golentskii, S., Pal'Shin, V., Sakamoto, T., White, R. R., Evans, S., Casperson, D., & Fenimore, E. 2006, Nature, 442, 172

Vink, J. S., de Koter, A., & Lamers, H. J. G. L. M. 2001, A&A, 369, 574

Vreeswijk, P. M., Ellison, S. L., Ledoux, C., Wijers, R. A. M. J., Fynbo, J. P. U., Møller, P., Henden, A., Hjorth, J., Masi, G., Rol, E., Jensen, B. L., Tanvir, N., Levan, A., Castro Cerón, J. M., Gorosabel, J., Castro-Tirado, A. J., Fruchter, A. S., Kouveliotou, C., Burud, I., Rhoads, J., Masetti, N., Palazzi, E., Pian, E., Pedersen, H., Kaper, L., Gilmore, A., Kilmartin, P., Buckle, J. V., Seigar, M. S., Hartmann, D. H., Lindsay, K., & van den Heuvel, E. P. J. 2004, A&A, 419, 927

Vreeswijk, P. M., Fruchter, A., Kaper, L., Rol, E., Galama, T. J., van Paradijs, J., Kouveliotou, C., Wijers, R. A. M. J., Pian, E., Palazzi, E., Masetti, N., Frontera, F., Savaglio, S., Reinsch, K., Hessman, F. V., Beuermann, K., Nicklas, H., & van den Heuvel, E. P. J. 2001, ApJ, 546, 672

Vreeswijk, P. M., Ledoux, C., Smette, A., Ellison, S. L., Jaunsen, A. O., Andersen, M. I., Fruchter, A. S., Fynbo, J. P. U., Hjorth, J., Kaufer, A., Møller, P., Petitjean, P., Savaglio, S., & Wijers, R. A. M. J. 2007, A&A, 468, 83

Vreeswijk, P. M., Møller, P., & Fynbo, J. P. U. 2003, A&A, 409, L5

Vreeswijk, P. M., Smette, A., Fruchter, A. S., Palazzi, E., Rol, E., Wijers, R. A. M. J., Kouveliotou, C., Kaper, L., Pian, E., Masetti, N., Frontera, F., Hjorth, J., Gorosabel, J., Piro, L., Fynbo, J. P. U., Jakobsson, P., Watson, D., O'Brien, P. T., & Ledoux, C. 2006, A&A, 447, 145

Wainwright, C., Berger, E., & Penprase, B. E. 2007, ApJ, 657, 367

Warren, S. J., Møller, P., Fall, S. M., & Jakobsen, P. 2001, MNRAS, 326, 759

Watson, D., Fynbo, J. P. U., Ledoux, C., Vreeswijk, P., Hjorth, J., Smette, A., Andersen, A. C., Aoki, K., Augusteijn, T., Beardmore, A. P., Bersier, D., Castro Cerón, J. M., D'Avanzo, P., Diaz-Fraile, D., Gorosabel, J., Hirst, P., Jakobsson, P., Jensen, B. L., Kawai, N., Kosugi, G., Laursen, P., Levan, A., Masegosa, J., Näränen, J., Page, K. L., Pedersen, K., Pozanenko, A., Reeves, J. N., Rumyantsev, V., Shahbaz, T., Sharapov, D., Sollerman, J., Starling, R. L. C., Tanvir, N., Torstensson, K., & Wiersema, K. 2006, ApJ, 652, 1011

Watson, D., Hjorth, J., Fynbo, J. P. U., Jakobsson, P., Foley, S., Sollerman, J., & Wijers, R. A. M. J. 2007, ApJ, 660, L101

Waxman, E. & Draine, B. T. 2000, ApJ, 537, 796

Welsh, B. Y. & Lallement, R. 2005, A&A, 436, 615

Welty, D. E., Frisch, P. C., Sonneborn, G., & York, D. G. 1999, ApJ, 512, 636

Whalen, D., Prochaska, J. X., Heger, A., & Tumlinson, J. 2008, ArXiv:astro-ph/0802.0737, 1

Wiersema, K., Savaglio, S., Vreeswijk, P. M., Ellison, S. L., Ledoux, C., Yoon, S.-C., Møller, P., Sollerman, J., Fynbo, J. P. U., Pian, E., Starling, R. L. C., & Wijers, R. A. M. J. 2007, A&A, 464, 529

Wolfe, A. M., Gawiser, E., & Prochaska, J. X. 2005, ARA&A, 43, 861

Woosley, S. E. 1993, ApJ, 405, 273

Woosley, S. E. & Bloom, J. S. 2006, ARA&A, 44, 507

Woosley, S. E. & Heger, A. 2005, in Astronomical Society of the Pacific Conference Series, Vol. 332, The Fate of the Most Massive Stars, ed. R. Humphreys & K. Stanek, 395

Woosley, S. E. & Heger, A. 2006, ApJ, 637, 914

Woźniak, P. R., Vestrand, W. T., Wren, J. A., White, R. R., Evans, S. M., & Casperson, D. 2006, ApJ, 642, L99

Yamaoka, K., Sugita, S., Ohno, M., Takahashi, T., Fukazawa, Y., Terada, Y., Tamagawa, T., Abe, K., Endo, Y., Onda, K., Matsumura, S., Tashiro, M., Soojing, H., Sato, G., Nakazawa, K., Takahashi, T., Miyawaki, R., Enoto, T., Kokubun, M., Makishima, K., & Murakami, T. 2006, in Presented at the Society of Photo-Optical Instrumentation Engineers (SPIE) Conference, Vol. 6266, Space Telescopes and Instrumentation II: Ultraviolet to Gamma Ray. Edited by Turner, Martin J. L.; Hasinger, Günther. Proceedings of the SPIE, Volume 6266, pp. 626643 (2006).

Yoon, S.-C. & Langer, N. 2005, A&A, 443, 643

Yoon, S.-C., Langer, N., & Norman, C. 2006, A&A, 460, 199

Yun, M. S. & Carilli, C. L. 2002, ApJ, 568, 88

Zackrisson, E., Bergvall, N., Olofsson, K., & Siebert, A. 2001, A&A, 375, 814

Zeh, A., Klose, S., & Hartmann, D. H. 2004, ApJ, 609, 952

Zeh, A., Klose, S., & Kann, D. A. 2006, ApJ, 637, 889

Zhang, B. 2006, Nature, 444, 1010

Zhang, B., Zhang, B.-B., Liang, E.-W., Gehrels, N., Burrows, D. N., & Mészáros, P. 2007, ApJ, 655, L25

Zibetti, S., Ménard, B., Nestor, D. B., Quider, A. M., Rao, S. M., & Turnshek, D. A. 2007, ApJ, 658, 161

Zwaan, M. A., van der Hulst, J. M., Briggs, F. H., Verheijen, M. A. W., & Ryan-Weber, E. V. 2005, MNRAS, 364, 1467

Zwicky, F. 1937, ApJ, 86, 217